NUREG-1826

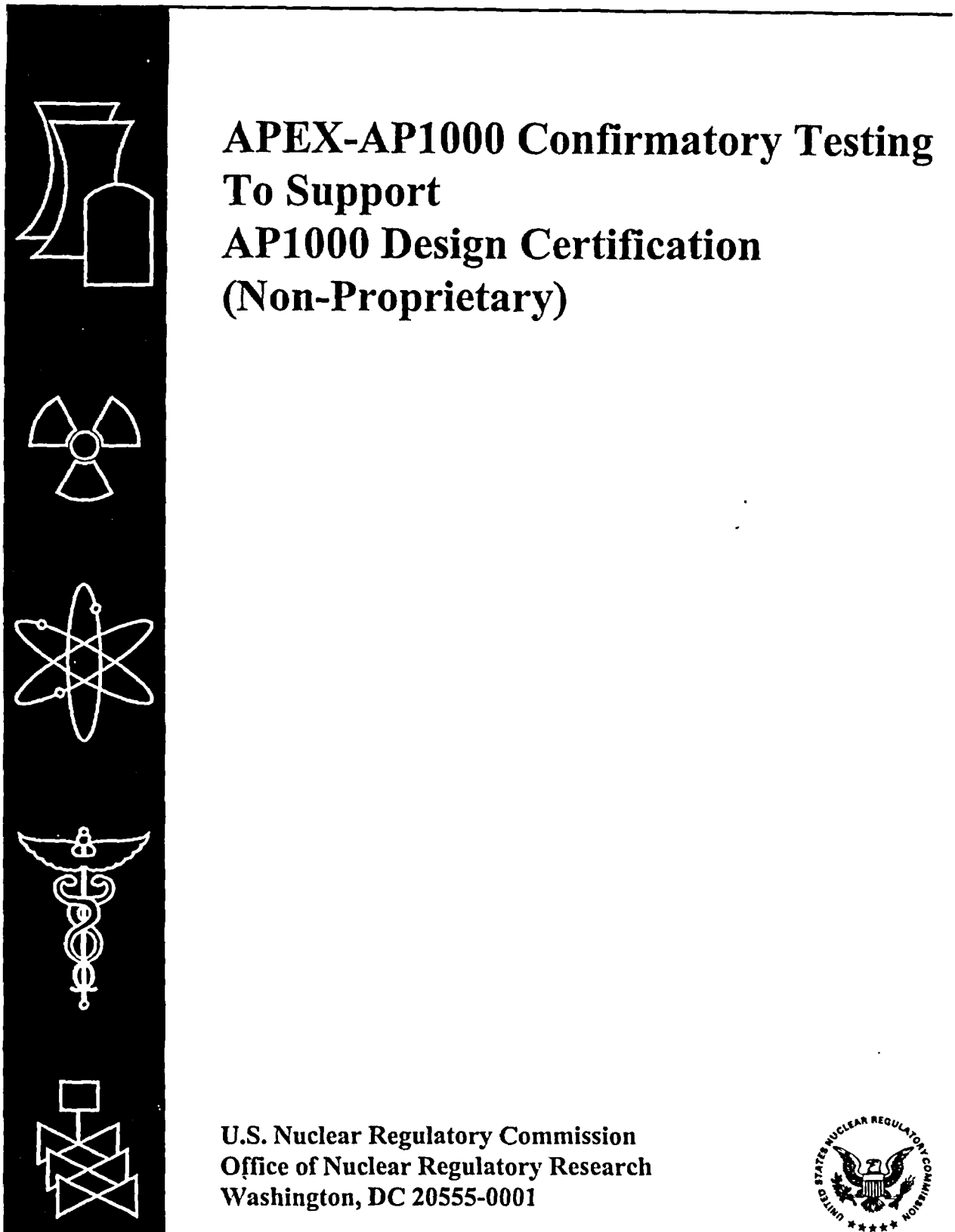

# APEX-AP1000 Confirmatory Testing To Support AP1000 Design Certification (Non-Proprietary)

U.S. Nuclear Regulatory Commission
Office of Nuclear Regulatory Research
Washington, DC 20555-0001

## AVAILABILITY OF REFERENCE MATERIALS IN NRC PUBLICATIONS

### NRC Reference Material

As of November 1999, you may electronically access NUREG-series publications and other NRC records at NRC's Public Electronic Reading Room at http://www.nrc.gov/reading-rm.html.
Publicly released records include, to name a few, NUREG-series publications; *Federal Register* notices; applicant, licensee, and vendor documents and correspondence; NRC correspondence and internal memoranda; bulletins and information notices; inspection and investigative reports; licensee event reports; and Commission papers and their attachments.

NRC publications in the NUREG series, NRC regulations, and *Title 10, Energy*, in the Code of *Federal Regulations* may also be purchased from one of these two sources.

1. The Superintendent of Documents
   U.S. Government Printing Office
   Mail Stop SSOP
   Washington, DC 20402–0001
   Internet: bookstore.gpo.gov
   Telephone: 202-512-1800
   Fax: 202-512-2250
2. The National Technical Information Service
   Springfield, VA 22161–0002
   www.ntis.gov
   1–800–553–6847 or, locally, 703–605–6000

A single copy of each NRC draft report for comment is available free, to the extent of supply, upon written request as follows:

Address: Office of the Chief Information Officer,
Reproduction and Distribution
Services Section
U.S. Nuclear Regulatory Commission
Washington, DC 20555-0001
E-mail: DISTRIBUTION@nrc.gov
Facsimile: 301–415–2289

Some publications in the NUREG series that are posted at NRC's Web site address http://www.nrc.gov/reading-rm/doc-collections/nuregs are updated periodically and may differ from the last printed version. Although references to material found on a Web site bear the date the material was accessed, the material available on the date cited may subsequently be removed from the site.

### Non-NRC Reference Material

Documents available from public and special technical libraries include all open literature items, such as books, journal articles, and transactions, *Federal Register* notices, Federal and State legislation, and congressional reports. Such documents as theses, dissertations, foreign reports and translations, and non-NRC conference proceedings may be purchased from their sponsoring organization.

Copies of industry codes and standards used in a substantive manner in the NRC regulatory process are maintained at—

The NRC Technical Library
Two White Flint North
11545 Rockville Pike
Rockville, MD 20852–2738

These standards are available in the library for reference use by the public. Codes and standards are usually copyrighted and may be purchased from the originating organization or, if they are American National Standards, from—

American National Standards Institute
11 West 42nd Street
New York, NY 10036–8002
www.ansi.org
212–642–4900

Legally binding regulatory requirements are stated only in laws; NRC regulations; licenses, including technical specifications; or orders, not in NUREG-series publications. The views expressed in contractor-prepared publications in this series are not necessarily those of the NRC.

The NUREG series comprises (1) technical and administrative reports and books prepared by the staff (NUREG–XXXX) or agency contractors (NUREG/CR–XXXX), (2) proceedings of conferences (NUREG/CP–XXXX), (3) reports resulting from international agreements (NUREG/IA–XXXX), (4) brochures (NUREG/BR–XXXX), and (5) compilations of legal decisions and orders of the Commission and Atomic and Safety Licensing Boards and of Directors' decisions under Section 2.206 of NRC's regulations (NUREG–0750).

NUREG-1826

# APEX-AP1000 Confirmatory Testing To Support AP1000 Design Certification (Non-Proprietary)

Manuscript Completed: June 2005
Date Published: August 2005

Prepared by
K.B. Welter and S.M. Bajorek
Advanced Reactors and Regulatory Effectiveness Branch
Division of Systems Analysis and Regulatory Effectiveness
Office of Nuclear Regulatory Research
U.S. Nuclear Regulatory Commission
Washington, DC 20555-0001

Jose' Reyes, Jr., Brian Woods, John Groome, John Hopson,
Eric Young, John DeNoma, and Kent Abel
Department of Nuclear Engineering
Institute of Thermal-Hydraulics
Oregon State University
Corvallis, OR 97601

Gene S. Rhee, NRC Project Manager

**Prepared for**
**Division of Systems Analysis and Regulatory Effectiveness**
**Office of Nuclear Regulatory Research**
**U.S. Nuclear Regulatory Commission**
**Washington, DC 20555-0001**

## PROPRIETARY INFORMATION NOTICE

This report does not contain any information that is proprietary to Westinghouse Electric Company. The U.S. Nuclear Regulatory Commission (NRC) has also prepared a proprietary version of this report for internal distribution.

In order to conform to the Commission's regulations concerning the protection of proprietary information so submitted to the NRC, as set forth in Title 10, Section 2.790, of the *Code of Federal Regulations* (10 CFR 2.790), the proprietary information in the proprietary version of this document is contained within brackets and, where the proprietary information has been deleted in the non-proprietary version, only the brackets remain (the information within the brackets in the proprietary version having been deleted). The justification for claiming the information as proprietary is indicated in both versions by means of lower case letters (a) through (f), located as a superscript immediately following the brackets enclosing each bracketed item of proprietary information, or in the margin opposite such information. These lower case letters refer to the types of information Westinghouse customarily holds in confidence, as identified in Sections (4)(ii)(a) through (4)(ii)(f) of the affidavit accompanying the transmittal of these documents pursuant to 10 CFR 2.790(b)(1).

**NUREG-1826 has been reproduced from the best available copy.**

# ABSTRACT

This report summarizes the confirmatory testing performed using the Advanced Plant Experiment (APEX) facility at Oregon State University (OSU). The APEX is a unique thermal-hydraulic integral system test facility, which is used to assess the performance of passive safety systems and was modified to accurately represent the design of the Westinghouse AP1000 advanced passive nuclear reactor. The U.S. Nuclear Regulatory Commission (NRC) sponsored eight beyond-design-basis accident (DBA) tests in the APEX facility, which were successfully completed from June 2003 through July 2004 and are discussed in detail in this report. Those eight beyond-DBA tests investigated scenarios with two or more simultaneous failures of the AP1000 passive safety systems during large- and small-break loss-of-coolant accidents, including station blackout and cold shutdown conditions. The experiments run in APEX-AP1000 confirm significant liquid entrainment and carryover of water to the automatic depressurization system (ADS) during and after actuation of the fourth-stage (ADS4) valves. These processes are important as thermal-hydraulic codes used to analyze the AP1000 design must adequately predict or bound upper plenum and hot leg entrainment. In addition, the tests show that failure of ADS4 valves on the non-pressurizer side of the plant results in a greater delay in in-containment refueling water storage tank (IRWST) injection than failure of ADS4 valves on the pressurizer side of the plant; while failure of two out of four ADS4 valves on the non-pressurizer side of the plant produces low two-phase mixture levels in the core during certain simulated vessel injection line and cold leg breaks.

# FOREWORD

The U.S. Nuclear Regulatory Commission (NRC) has reviewed Westinghouse Electric Company's request, dated March 28, 2002, for final design approval and standard design certification for the AP1000 advanced passive nuclear reactor. The AP1000 standard design is essentially an uprated version of Westinghouse's AP600 design, which the NRC certified on December 16, 1999.

Following receipt of an application for certification of a new nuclear power plant design, the NRC's standard design certification process involves an acceptance review, a technical review, and a rulemaking to certify the design. The AP1000 design certification review involved technical reviewers from the NRC's Offices of Nuclear Reactor Regulation, Nuclear Security and Incident Response, and Nuclear Regulatory Research. These reviewers carefully considered the AP1000 Design Control Document (DCD) and Probabilistic Risk Assessment in accordance with the applicable and technically relevant standards for reviewing design certification applications, as set forth in Title 10, Section 52.48, of the *Code of Federal Regulations* (10 CFR 52.48). In addition, the reviewers considered those standards that were modified by the exemptions identified in the final safety evaluation report (FSER) for the AP1000 design, which the NRC published as NUREG-1793 in September 2004.

In support of the NRC's design certification activities, this report documents the confirmatory integral testing conducted at Oregon State University's Advanced Plant Experiment (APEX) facility. Specifically, the NRC sponsored 8 beyond-design-basis accident (DBA) tests run in APEX, which is a one-quarter height, one-half time scale, reduced-pressure, integral test facility modified to represent AP1000 conditions. Those 8 beyond-DBA tests investigated scenarios with two or more simultaneous failures of the AP1000 passive safety system during large- and small-break loss-of-coolant accidents, including station blackout and cold shutdown conditions. The objectives of these beyond-DBA tests were to confirm AP1000 safety margins and provide a database to assess NRC's thermal-hydraulic computer codes. This report presents the results of these tests, along with a detailed scaling analysis and facility description.

Review of the APEX-AP1000 test results conclusively shows that the core remains cooled and did not experience heatup for most of the beyond-DBA scenarios. These test results were factored into the final evaluation of the AP1000 design and, on the basis of their independent analysis described in the FSER, the NRC staff concluded that Westinghouse's application for AP1000 design certification meets the applicable content requirements of 10 CFR 52.47, as well as the review standards of 10 CFR 52.48.

Carl J. Paperiello, Director
Office of Nuclear Regulatory Research

# CONTENTS

# APPENDICES

# Figures

## Tables

# EXECUTIVE SUMMARY

This report documents the confirmatory testing performed using the Advanced Plant Experiment (APEX) facility at Oregon State University (OSU). The APEX is a unique thermal-hydraulic integral system test facility, which is used to assess the performance of passive safety systems and was modified to accurately represent the designs of the Westinghouse AP600 and AP1000 advanced passive nuclear reactors. The U.S. Nuclear Regulatory Commission (NRC) sponsored eight beyond-design-basis accident (DBA) tests of the AP1000 design, which were successfully completed in the APEX facility from June 2003 through July 2004. This program had the following objectives:

- Conduct tests to assess the performance of the Westinghouse AP1000 passive safety systems for a select range of beyond-DBA scenarios.
- Generate data to confirm analyses that Westinghouse submitted for AP1000 design certification.
- Obtain experimental data to benchmark the NRC's thermal-hydraulic computer codes.

The NRC extensively used data from the APEX facility in the AP600 design certification process, drawing upon approximately 75 tests for use in code assessment and qualification of the AP600 safety margin. To address performance specific to the AP1000 design (essentially an uprated version of the AP600 design), the APEX facility underwent significant modifications in 2002 in order to more accurately represent the AP1000. That facility modification included an increase in the maximum core power; new pressurizer (PZR) and surge lines; larger core makeup tanks (CMTs); larger-diameter fourth-stage automatic depressurization system (ADS4) piping; and decreased line resistances for the CMTs, ADS4, and passive residual heat removal (PRHR) heat exchanger. In addition, Reyes performed a comprehensive scaling analysis (Appendix A) to guide the facility modifications to ensure that the APEX experiments preserved AP1000 conditions.

This study investigated several beyond-DBA scenarios, including 1- and 2-inch cold leg breaks, double-ended direction vessel injection (DEDVI) line breaks, Mode 5 operation with loss of residual normal heat removal system (RNS) cooling, and station blackout. Based on experience from analyzing previous AP600 tests, one of the main purposes of the APEX-AP1000 test program was to investigate the sensitivity of the failure of the automatic depressurization system (ADS) on core coolability.

Based on the experiments run in the APEX facility, we can draw the following conclusions:

(1) The APEX-AP1000 tests confirm significant liquid entrainment and carryover of water to the ADS4 system during and after ADS4 valve actuation. High liquid carryover to the ADS4 may occur in the AP1000 reactor. These data are appropriate for assessment of thermal-hydraulic codes used to analyze the AP1000.

(2) Test results from tests NRC-AP1000-03, 05, and DBA-02 show that failure of ADS4 valves on the non-pressurizer side of the plant results in a greater delay in in-containment refueling water storage tank (IRWST) injection than failure of ADS4 valves on the pressurizer side of the plant.

(3) Failure of two out of four ADS4 valves on the non-pressurizer side of the plant results in core uncovery (based on the two-phase mixture level) during simulated DEDVI line and cold leg breaks.

(4) Review of the APEX-AP1000 DBA test results and code calculations submitted by Westinghouse for design certification conclusively show that the core remains cooled, and heatup was not experienced for design-basis scenarios. In fact, core heatup was only experienced in select beyond-DBA tests (NRC-AP1000-05 and 06).

# ABBREVIATIONS

| | |
|---|---|
| ACC | Accumulator |
| ADS | Automatic Depressurization System |
| ADS4 | Fourth-Stage Automatic Depressurization System |
| AP600 | Advanced Passive 600-MWe Plant (Westinghouse) |
| AP1000 | Advanced Passive 1,000-MWe Plant (Westinghouse) |
| APEX | Advanced Plant Experiment (OSU Facility) |
| ASME | American Society of Mechanical Engineers |
| BAMS | Break and ADS Measurement System |
| CCFL | Counter-Current Flow Limitation |
| CFR | *Code of Federal Regulations* |
| CL | Cold Leg |
| CMT | Core Makeup Tank |
| CMT-PBL | Core Makeup Tank Pressure Balance Line |
| CRP | Condensate Return Pump |
| CRT | Condensate Return Tank |
| CVS | Chemical and Volume System |
| DAS | Data Acquisition System |
| DBA | Design-Basis Accident |
| DCD | Design Control Document (AP1000) |
| DEDVI | Double-Ended Direction Vessel Injection |
| DI | Demineralization System |
| DP | Differential Pressure |
| DVI | Direct Vessel Injection |
| FMM | Magnetic Flowmeter |
| FSER | Final Safety Evaluation Report |
| FST | Feedwater Storage Tank |
| FVM | Vortex Flowmeter |
| H2TS | Hierarchical Two-Tiered Scaling |
| HL | Hot Leg |

| | |
|---|---|
| HPS | Heated Phase Switch |
| HX | Heat Exchanger |
| IRWST | In-Containment Refueling Water Storage Tank |
| KW | Heater Power |
| LCT | Load Cell Transducer |
| LDP | Differential Pressure Level |
| LOCA | Loss-of-Coolant Accident |
| LT | Level Transducer |
| MFP | Main Feedwater Pump |
| NI | National Instruments |
| NRC | U.S. Nuclear Regulatory Commission |
| NSSS | Nuclear Steam Supply System |
| OSU | Oregon State University |
| P&ID | Piping and Instrumentation Drawings |
| PBL | Pressure Balance Line |
| PC | Process Controller |
| PIRT | Phenomena Identification and Ranking Table |
| PLC | Programmable Logic Controller |
| PORV | Power Operated Relief Valve |
| PRHR | Passive Residual Heat Removal |
| PT | Pressure Transducer |
| PZR | Pressurizer |
| RCP | Reactor Coolant Pumps |
| RCS | Reactor Coolant System |
| RNS | Residual Normal Heat Removal System |
| ROSA | Rig of Safety Assessment |
| RPV | Reactor Pressure Vessel |
| RSO | Return to Saturation Oscillation |
| Rx | Reactor Vessel |
| SB | Small Break |

| | |
|---|---|
| SBLOCA | Small-Break Loss-of-Coolant Accident |
| SCR | Silicon Control Rectifier |
| SG | Steam Generator |
| T/C | Thermocouple |
| TF | Fluid Temperature |
| TH | Heater Rod Temperature |
| TR | Thermocouple Rod |
| TW | Wall Temperature |

# 1. INTRODUCTION

This report documents the confirmatory testing performed using the Advanced Plant Experiment (APEX) facility at Oregon State University (OSU). The APEX is a unique thermal-hydraulic integral system test facility (Figure 1.1), which is used to assess the performance of passive safety systems and was modified to accurately represent the Westinghouse AP600 and AP1000 advanced passive nuclear reactor designs. The U.S. Nuclear Regulatory Commission (NRC) sponsored this research through Contract #NRC-04-03-049, which encompassed eight beyond-design-basis accident (DBA) tests of the AP1000 design. Testing began in June 2003, and the final test was completed in July 2004. This program had the following objectives:

- Conduct tests to assess the performance of the Westinghouse AP1000 passive safety systems for a select range of beyond-DBA scenarios.
- Generate data to confirm analyses that Westinghouse submitted for AP1000 design certification.
- Obtain experimental data to benchmark the NRC's thermal-hydraulic computer codes.

The NRC extensively used data from the APEX facility in the AP600 design certification process, drawing upon approximately 75 tests for use in code assessment and qualification of AP600 safety margin. To address performance specific to the AP1000 design (essentially an uprated version of the AP600 design), the APEX facility underwent significant modifications in 2002 in order to more accurately represent the AP1000. The facility modification included an increase in the maximum core power; new pressurizer (PZR) and surge lines; larger core makeup tanks (CMTs); larger-diameter fourth-stage automatic depressurization (ADS4) system piping; and decreased line resistances for the CMTs, ADS4, and passive residual heat removal (PRHR) heat exchanger (HX).

The study investigated several beyond-DBA scenarios, including 1- and 2-inch cold leg breaks, double-ended direction vessel injection (DEDVI) line breaks, Mode 5 operation with loss of residual normal heat removal system (RNS) cooling, and station blackout. Based on experience from analyzing previous AP600 tests, one of the main purposes of the APEX-AP1000 test program was to investigate the sensitivity of the failure of the automatic depressurization system (ADS) on core coolability. Therefore, for each accident scenario, one or more ADS valves were failed on demand or were unavailable for each test.

Chapter 1 includes this introduction, while Chapter 2 describes the results of the comprehensive scaling analysis (Appendix A) conducted by Reyes to guide the modifications to upgrade the APEX facility from AP600 to AP1000 geometries and test conditions. In Chapter 3, the reader can find a detailed facility description with component and instrument information (component dimensions can be found in Appendix B). Chapter 4 summarizes the APEX-AP1000 test results, while Appendix C contains more detailed instrument plots and sequence of events for each test. Readers should note that the non-proprietary version of this report the majority of the information in Appendices A, B, and C has been removed. In addition, a supplement to the proprietary version of this report includes three compact disks containing APEX facility drawings, test reports, and the APEX database.

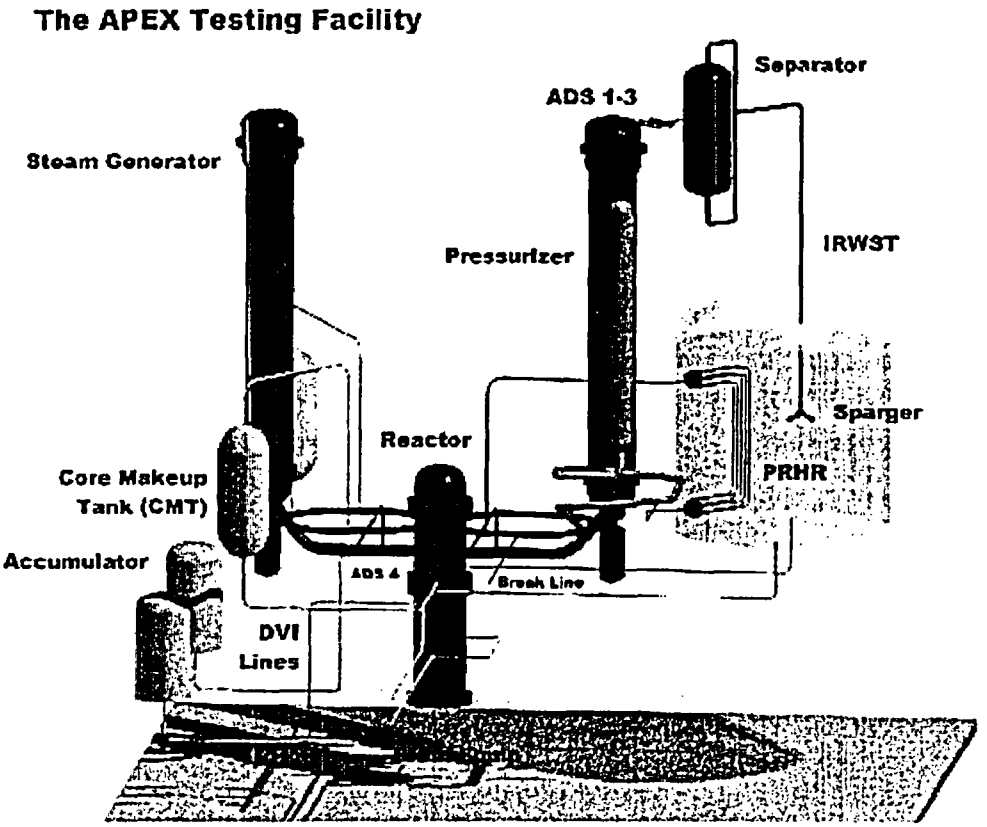


Figure 1.1. APEX Facility Layout

# 2. SCALING ANALYSIS RESULTS

The APEX-AP1000 scaling analysis by Reyes (Appendix A) provided the basis for modifying core decay power; CMT and PZR volumes; the in-containment refueling water storage tank (IRWST) and containment flood-up elevations; ADS4, IRWST, PRHR, and CMT line resistances; PZR surge line diameter; ADS4, upper core plate, and upper support plate flow areas; and upper plenum structures. The majority of the APEX-AP1000 scaling analysis was based on results from the original AP600 scaling analysis because the AP1000 is geometrically similar to the AP600, and the thermal-hydraulic phenomena studied fell within the scope of the original AP600 test program.

The purpose of the APEX-AP1000 confirmatory test program was to examine AP1000 passive safety system performance and provide high-quality benchmark data for the NRC's thermal-hydraulic computer codes used in reactor safety analysis. Previous testing in the APEX facility demonstrated that all of the thermal-hydraulic phenomena observed in large-scale AP600 facilities (such as ROSA-AP600 or SPES) were also observed in APEX and, consequently, provide a broad database for code assessment. However, the most faithful representation of the AP600 phenomena was for the very-long-term cooling phase, which occurs at low system pressure. The APEX-AP1000 test program was modified to include full-pressure ADS4 blowdown tests to investigate the transition period that leads to the onset of IRWST injection. The scaling analysis provided the basis for the plant modifications listed in Table 2.1.

Table 2.1. Modifications to APEX Components To Simulate AP1000 Conditions

| Component | Modification to APEX |
|---|---|
| Reactor Power | Increase core power by 67% |
| PZR | Increase PZR volume<br>Reduce PZR Surge Line Diameter |
| CMTs | Increase CMT volumes by 25%<br>Reduce line resistance to 64% of original value |
| IRWST | Increase IRWST liquid level |
| ADS4 | Increase ADS4 flow area by 76%<br>Reduce line resistance to 28% of original value |
| PRHR HX | Increase PRHR flow capacity by 74% by reducing line resistance<br>No change in surface area/tube number required for testing |
| Containment Sump Flood-Up Elevation | Change flood-up elevation in primary sump tank |

The following paragraphs briefly summarize the results of the scaling study.

(1) The original AP600 scaling analysis, WCAP-14270 [Ref. 1], which was conducted in support of the existing APEX facility design, was found to be applicable to the APEX-AP1000 design for two reasons. First, the thermal-hydraulic phenomena to be studied fell within the scope of the original AP600 test program, with the exception of upper plenum behavior. Second, the AP1000 design is geometrically similar to the AP600 design. As a result, all tank volumes, flow areas, and line resistance scaling ratios found in WCAP-14270 were used in the present study.

(2) An NRC PZR surge line study by Bessette and Di Marzo [Ref. 2] guided the modification of the APEX-AP1000 PZR surge line. The reduced line diameter is expected to produce a better simulation of the PZR draining behavior.

(3) The reactor coolant system (RCS) depressurization scaling analysis represents a more comprehensive approach than that implemented in the original AP600 study. Nonetheless, the derived similarity criteria resulted in scaling ratios that were identical to those in the original study. Thus, it was determined that the characteristic time ratios for the AP1000 reactor would be well-matched in APEX-AP1000. The greatest distortion (a factor of 2) was the result of pressure-scaled fluid properties.

(4) A scaling analysis was performed to design the APEX-AP1000 facility to simulate the important phenomena that occur during the transition from ADS4 blowdown to the onset of IRWST injection, as shown in Figure 2.1. The key phenomena have been identified and described, and the scaling analysis indicated that full-pressure ADS4 blowdown tests could be performed using the modified APEX-AP1000 test facility. The maximum decay power, at the time of ADS4 valve opening, was calculated for the DEDVI break. The AP1000 core axial void fraction profile and core averaged void fraction were also shown to be preserved in the APEX-AP1000 facility.

(5) A detailed pool entrainment scaling analysis was performed to design the upper plenum components in the APEX-AP1000 facility. The analysis indicated that well-scaled entrainment behavior is expected in the APEX facility to a depth of about 18.9 cm (0.55 in terms of dimensionless height) below the hot leg, as shown in Figure 2.2. Below this depth, the APEX facility is in the momentum-controlled region, whereas the AP1000 reactor would be in the deposition-controlled region at the equivalent scaled depth, as shown in Figure 2.2. It was also determined that the entrainment rates in the near-surface region are a factor of 150 times greater than those generated in the momentum-controlled region, which are a factor of 4 to 6 times greater than those generated in the deposition-controlled region. Thus the APEX facility will conservatively simulate the entrainment behavior when the level is below the midpoint of the upper plenum.

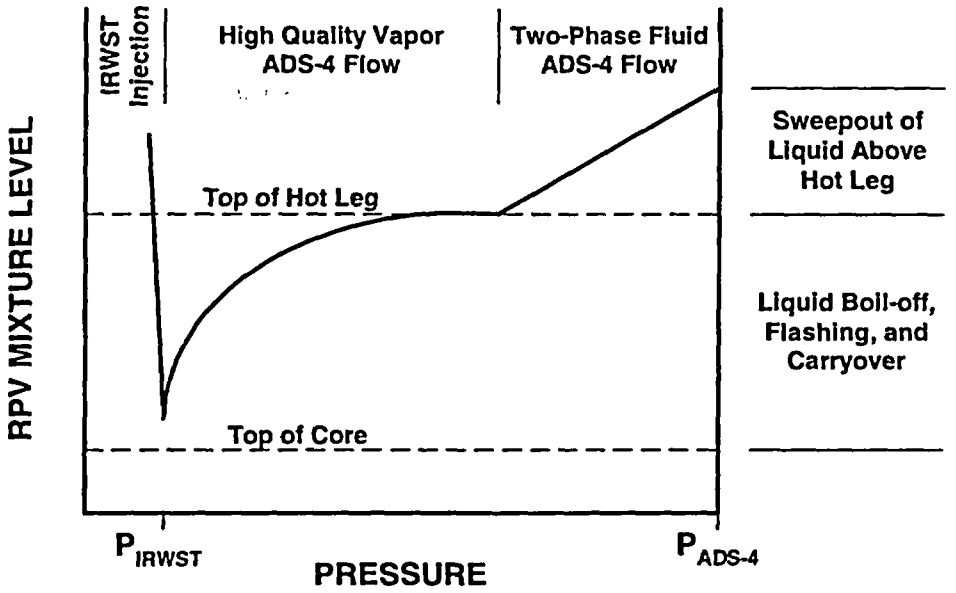


Figure 2.1. Important Phenomena During Transition from ADS4 Blowdown to IRWST Injection

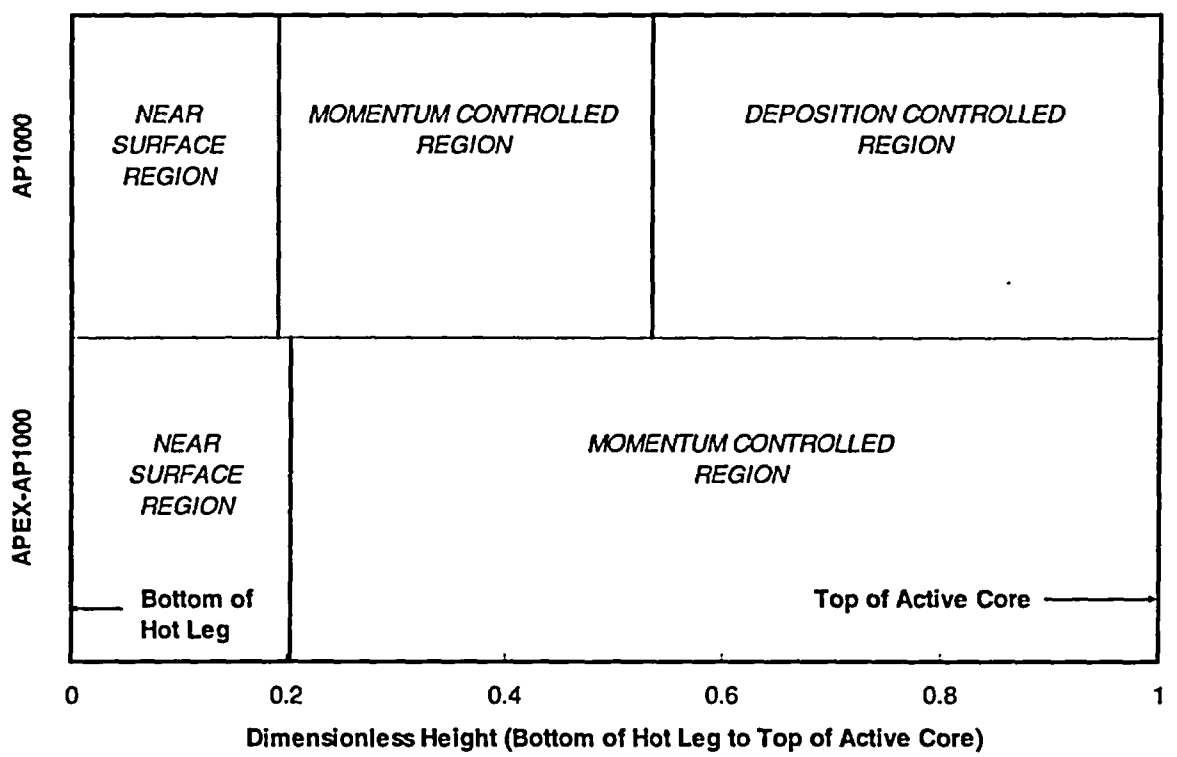


Figure 2.2. Upper Plenum Pool Entrainment Regions in AP1000 and APEX-AP1000

# 3. FACILITY DESCRIPTION

This chapter provides a comprehensive description of the APEX-AP1000 test facility, including the reactor coolant system (RCS); passive safety systems; instrumentation, controls, and power systems; and balance-of-plant components.

The OSU Department of Nuclear Engineering has modified its APEX facility to assess the performance of the AP1000 passive safety system. APEX is a unique, world-class, one-quarter height, one-half time scale, reduced-pressure, thermal-hydraulic, integral system test facility. In the past, the data obtained using the APEX facility formed an essential aspect of the AP600 design certification program. Modified to accurately represent the AP1000 reactor, the APEX facility is referred to as APEX-AP1000. Appendix B to this report presents information about the APEX-AP1000 facility, such as piping and component dimensions, setpoints, and control logic.

The APEX test facility, depicted in Figure 1.1, has been specifically designed and constructed to provide high-quality data for use in computer code benchmark calculations. Table 2.1 summarizes the significant modifications required to adapt the facility for AP1000 testing, which included new reactor heater rods to increase the maximum facility power from 600 kW to 1000 kW. In addition, the PZR and CMTs were increased in size, passive core cooling system injection line resistance was reduced, and the ADS4 valves and associated piping were increased in size to provide larger RCS depressurization capacity. In addition, a formal scaling analysis (Appendix A) was performed to ensure that the facility accurately represents the AP1000 reactor. The resulting APEX-AP1000 test facility includes the following systems:

- **Reactor Coolant System:** This includes an electrically heated 48-rod bundle core, a reactor vessel with internals, two hot legs (HLs), four cold legs (CLs), two 133 U-tube steam generators (SGs), one PZR, and four reactor coolant pumps (RCPs).
- **Passive Safety Systems:** This includes two CMTs, two accumulators (ACCs), a four-stage ADS, one PRHR HX, one IRWST, and portions of the lower containment compartments.
- **Balance of Plant:** This includes a feedwater system, non-safety grade chemical volume control system (CVS), and an active residual heat removal system. The geometry of the interconnecting pipe routings was also duplicated.

All of the RCS components are constructed of stainless steel and capable of consistent operation at 400 psia (2.76 MPa) while at saturation temperatures. All primary system components are insulated to minimize heat loss.

## 3.1 Reactor Coolant System (RCS)

The APEX facility RCS is a complete model of the AP1000 nuclear steam supply system (NSSS). As such, the RCS includes the reactor pressure vessel (RPV), one PZR, two SGs, four RCPs, and associated primary loop piping. See Figures 3.1 and 3.2 for elevation and plan views of the RCS, respectively.

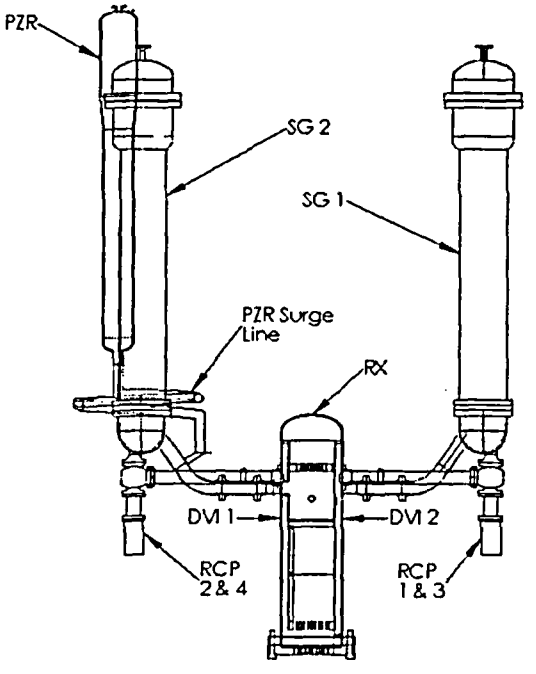


Figure 3.1. Elevation View of Reactor Coolant System

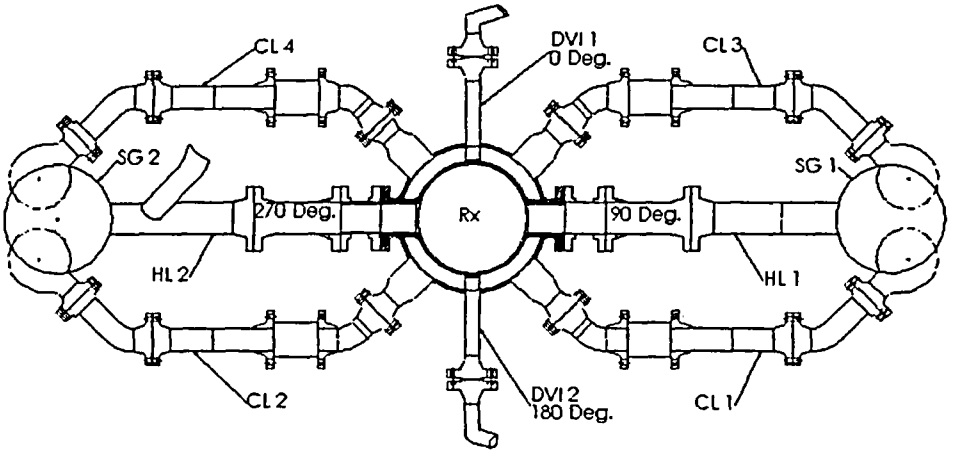


Figure 3.2. Plan View of Reactor Coolant System

## 3.2 Reactor Pressure Vessel (RPV)

The RPV models the upper and lower internals of the AP1000 reactor vessel, core barrel, downcomer, and core. The maximum core power is approximately 1000 kW, which can be distributed in two radial power zones and can be programmed to simulate time-dependent decay power. The RPV includes connections for the two HLs, four CLs, and two direct vessel injection (DVI) lines.

During normal operation, cold water enters through the four CLs into an annular downcomer region that is bounded by the inside surface of the reactor vessel shell and the outside surface of the core barrel. The cylindrical reactor vessel shell is fabricated from Stainless Steel (SS) 304 plate. The core barrel extends from the upper head flange down to the lower core plate and is made of SS 304.

The cold water in the downcomer flows into the lower plenum, a cylindrical fluid volume region bounded vertically by the lower core plate and the lower head plate. The lower head plate is bolted to the carbon-steel reactor vessel flange, which is welded to the cylindrical reactor vessel shell. The fluid changes direction in the lower plenum and travels upward through holes in the lower core plate into the core. The upper vessel head is a 2:1 elliptical head.

The heated zone of the core consists of 48 heater rods and 5 fluid thermocouple (T/C) rods. Six of the heater rods have a T/C located at the disc end (top) of the heater. In addition to the heater rod T/Cs and individual fluid T/Cs in the RPV, there are five T/C rods that measure the axial fluid temperature distribution in the core. All of the heater rods penetrate the lower head plate, lower plenum, and lower core plate to create a heated zone between the lower core plate and the upper core plate (see Figure 3.3). Two spacer grids are provided for support of the heaters, one at the mid-plane of the heaters and the other near the core exit. The heater bundle is surrounded by a reflector/baffle that directs the fluid through the core (see Figure 3.4). The reflector is filled with PUROCast™ (ceramic) to minimize the heat capacity of the core region.

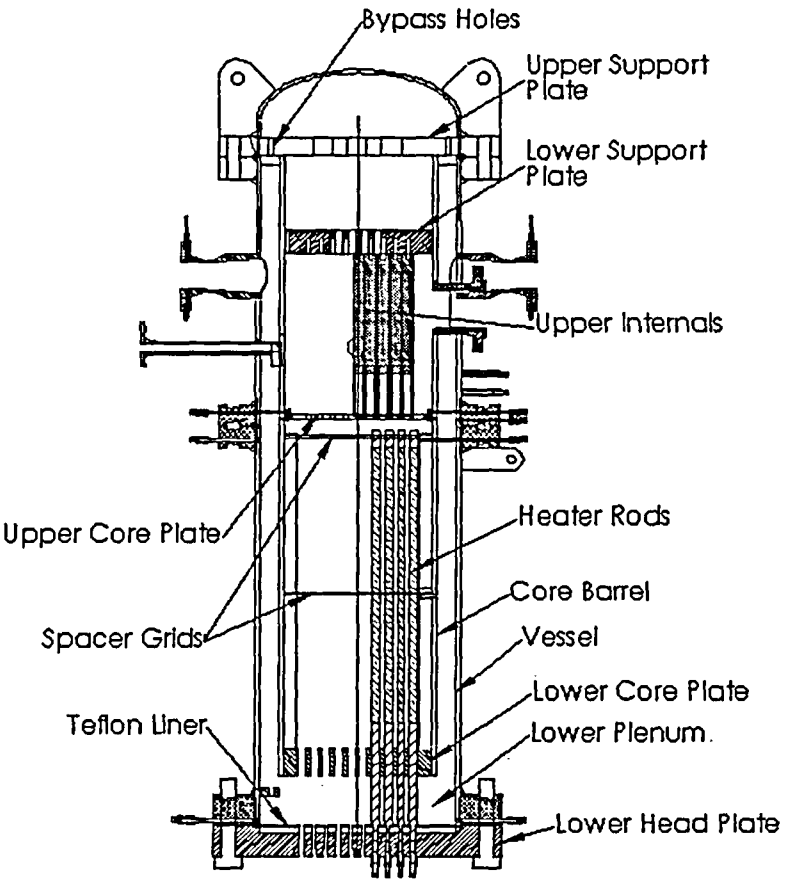


Figure 3.3. Reactor Cross-Section View

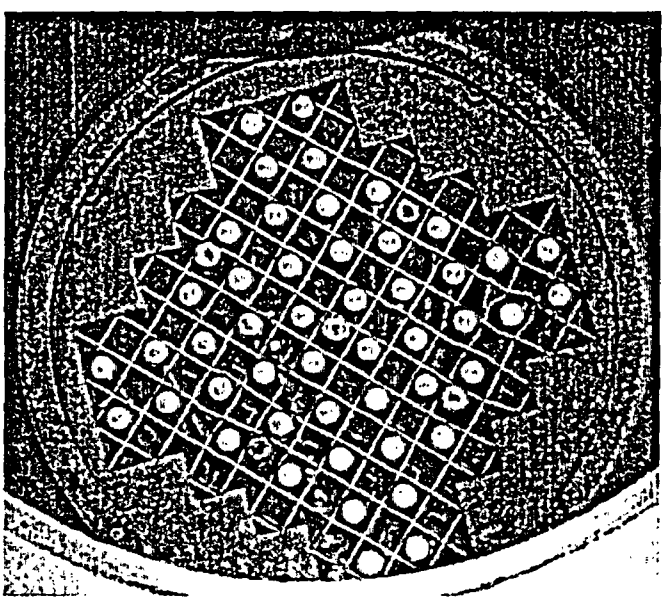

Figure 3.4. View of Reactor Core from Above

The heated water leaves the top of the core and flows upward through the upper core plate into the upper plenum. The upper plenum is bounded by the upper core plate and lower support plate (see Figure 3.3). The upper core plate supports the upper plenum internals that simulate the control rod guide tubes and other upper plenum structure. The heated water leaves the upper plenum via the two HL nozzles.

The volume above the upper support plate is the upper head region. It is connected to the upper plenum via 10 holes and a single hole in the upper support plate. The hole in the center of the upper support plate allows a capacitance level probe to penetrate to just above the upper core plate. The Drexelbrook Universal Lite™ capacitance probe provides a mixture level from the top of the upper core plate to the upper support plate. It is also connected to the downcomer via 10 bypass holes located at the top of the downcomer. The Universal LiteTM instrument is a capacitance-to-current transducer. A change in level produces a change in capacitance causing a corresponding change in current (4-20 mA). It is called a two-wire transmitter because the same two wires that are used to power the unit also indicate the change in level.

Table 3.1 lists the T/Cs located in the RPV, while Table 3.2 lists he pressure instrumentation in the RPV.

Table 3.1. Thermocouples in the Reactor Pressure Vessel

| Tag Name | Description | Tag Name | Description |
|---|---|---|---|
| TF-101 | CL-3/Reactor Flange @ Top | TF-163 | Lower Rx Vessel Layer A-A @ 135 degrees |
| TF-102 | CL-4/Reactor Flange @ Top | TF-164 | Upper Rx Vessel Layer H-H @ 0 degrees |
| TF-103 | CL-3/Reactor Flange @ Bottom | TF-165 | Upper Rx Vessel Layer H-H @ 6.2 degrees |
| TF-104 | CL-4/Reactor Flange @ Bottom | TF-166 | Upper Rx Vessel Layer I-I @ 0 degrees |
| TF-105 | CL-1/Reactor Flange @ Top | TF-167 | Heater Rod B2-319 @ 40.13" |
| TF-106 | CL-2/Reactor Flange @ Top | TF-168 | Upper Rx Vessel Layer K-K @ 270 degrees |
| TF-107 | CL-1/Reactor Flange @ Bottom | TF-169 | Upper Rx Vessel Layer M-M @ 90 degrees |
| TF-108 | CL-2/Reactor Flange @ Bottom | TF-170 | Upper Rx Vessel Layer M-M @ 270 degrees |
| TF-113 | DVI-1/Reactor Flange @ Top | TF-171 | Top of Reactor Down to within 0.50" of Upper Support Plate |
| TF-114 | DVI-2/Reactor Flange @ Bottom | TF-172 | Lower Rx Vessel Layer AA-AA @ 0 degrees |
| TF-115 | DVI-1/Reactor Flange @ Bottom | TF-173 | Lower Rx Vessel Layer AA-AA @ 270 degrees |
| TF-116 | DVI-2/Reactor Flange @ Top | TR-001-1 | Core Thermocouple Rod D-001 @ 10.50" |
| TF-118 | Lower Rx Vessel Layer Y-Y @ 30 degrees | TR-001-2 | Core Thermocouple Rod D-001 @ 19.13" |
| TF-120 | Top of Reactor @ 8.5" & 350 degrees | TR-001-3 | Core Thermocouple Rod D-001 @ 25.13" |

Table 3.1. Thermocouples in the Reactor Pressure Vessel

| Tag Name | Description | Tag Name | Description |
|---|---|---|---|
| TF-126 | Lower Rx Vessel Layer A-A @ 225 degrees | TR-001-4 | Core Thermocouple Rod D-001 @ 31.13" |
| TF-127 | Lower Rx Vessel Layer A-A @ 315 degrees | TR-001-5 | Core Thermocouple Rod D-001 @ 37.13" |
| TF-128 | Lower Rx Vessel Layer C-C @ 0 degrees | TR-001-6 | Core Thermocouple Rod D-001 @ 43.13" |
| TF-129 | Lower Rx Vessel Layer C-C @ 32 degrees | TR-303-1 | Core Thermocouple Rod D-303 @ 10.51" |
| TF-130 | Lower Rx Vessel Layer G-G @ 0 degrees | TR-303-2 | Core Thermocouple Rod D-303 @ 19.13" |
| TF-131 | Lower Rx Vessel Layer G-G @ 11.3 degrees | TR-303-3 | Core Thermocouple Rod D-303 @ 25.13" |
| TF-132 | Upper Rx Vessel Layer F-F @ 0 degrees | TR-303-4 | Core Thermocouple Rod D-303 @ 31.13" |
| TF-133 | Upper Rx Vessel Layer F-F @ 8 degrees | TR-303-5 | Core Thermocouple Rod D-303 @ 37.13" |
| TF-134 | Upper Rx Vessel Layer E-E @ 0 degrees | TR-303-6 | Core Thermocouple Rod D-303 @ 43.13" |
| TF-135 | Upper Rx Vessel Layer E-E @ 6.2 degrees | TR-308-1 | Core Thermocouple Rod E-308 @ 22.13" |
| TF-140 | HL-2/Reactor Flange @ Top | TR-308-2 | Core Thermocouple Rod E-308 @ 34.13" |
| TF-141 | HL-1/Reactor Flange @ Top | TR-308-3 | Core Thermocouple Rod E-308 @ 46.13" |
| TF-142 | HL-2/Reactor Flange @ Bottom | TR-308-4 | Core Thermocouple Rod D-001 @ 49.13" |
| TF-143 | HL-1/Reactor Flange @ Bottom | TR-308-5 | Core Thermocouple Rod D-001 @ 51.13" |
| TF-147 | Upper Rx Vessel Layer I-I @ 180 degrees | TR-308-6 | Core Thermocouple Rod D-303 @ 49.13" |
| TF-148 | Upper Rx Vessel Layer I-I @ 188 degrees | TR-313-1 | Core Thermocouple Rod D-313 @ 10.50" |
| TF-149 | Upper Rx Vessel Layer H-H @ 180 degrees | TR-313-2 | Core Thermocouple Rod D-313 @ 19.13" |
| TF-150 | Upper Rx Vessel Layer H-H @ 186.2 degrees | TR-313-3 | Core Thermocouple Rod D-313 @ 25.13" |

Table 3.1. Thermocouples in the Reactor Pressure Vessel

| Tag Name | Description | Tag Name | Description |
|---|---|---|---|
| TF-151 | Upper Rx Vessel Layer E-E @ 186.2 degrees | TR-313-4 | Core Thermocouple Rod D-313 @ 31.13" |
| TF-152 | Upper Rx Vessel Layer E-E @ 180 degrees | TR-313-5 | Core Thermocouple Rod D-313 @ 37.13" |
| TF-153 | Upper Rx Vessel Layer F-F @ 180 degrees | TR-313-6 | Core Thermocouple Rod D-313 @ 43.13" |
| TF-154 | Upper Rx Vessel Layer F-F @ 188 degrees | TR-318-1 | Core Thermocouple Rod F-318 @ 28.13" |
| TF-155 | Lower Rx Vessel Layer G-G @ 180 degrees | TR-318-2 | Core Thermocouple Rod F-318 @ 40.13" |
| TF-156 | Lower Rx Vessel Layer G-G @ 191.3 degrees | TR-318-3 | Core Thermocouple Rod F-318 @ 51.86" |
| TF-157 | Lower Rx Vessel Layer C-C @ 212 degrees | TR-318-4 | Core Thermocouple Rod D-303 @ 51.13" |
| TF-158 | Lower Rx Vessel Layer C-C @ 180 degrees | TR-318-5 | Core Thermocouple Rod D-313 @ 49.13" |
| TF-162 | Lower Rx Vessel Layer A-A @ 45 degrees | TR-318-6 | Core Thermocouple Rod D-313 @ 51.13" |

Table 3.2. Pressure Instrumentation in the Reactor Pressure Vessel

| Tag Name | Description |
|---|---|
| DP-111 | DP Across Upper Core Plate |
| DP-114 | DP Across Upper Support Plate |
| DP-121 | DVI-1/Cold Leg 1 Differential Pressure |
| DP-122 | DP Between DVI-2 and CL-2 |
| DP-123 | DP Between DVI-1 and CL-3 |
| DP-124 | DP Between DVI-2 and CL-4 |
| DP-125 | HL-1 Entrance Losses |
| DP-126 | HL-2 Entrance Losses |
| DP-128 | HL-2 Entrance Losses |
| LDP-101 | CL to Bypass Holes Uncompensated Water Level (270) |
| LDP-102 | CL to Bypass Holes Water Uncompensated Level (180) |
| LDP-103 | DVI to CL Uncompensated Water Level (270) |
| LDP-104 | DVI to CL Uncompensated Water Level (180) |
| LDP-105 | Upper Core Plate to DVI Uncompensated Water Level (270) |
| LDP-106 | Bottom of Core to Lower Core Plate Uncompensated Water Level (180) |
| LDP-107 | Bottom of Core to Lower Core Plate Uncompensated Water Level (270) |
| LDP-108 | Bottom of Core to Lower Core Plate Uncompensated Water Level (0) |
| LDP-109 | Lower Core Plate to Mid-Core Spacer Grid (0) Uncompensated Water Level |
| LDP-110 | Mid-Core Spacer Grid to Upper-Core Spacer Grid (0) Uncompensated Water Level |
| LDP-112 | Upper Core Plate to DVI Water Level (0) Uncompensated Water Level |
| LDP-113 | DVI to Bottom of Upper Support Plate (0) Uncompensated Water Level |
| LDP-115 | Upper Support Plate to Top of Reactor Uncompensated Water Level |
| LDP-116 | Bottom of Reactor to Bottom of Bypass Holes (270) Uncompensated Water Level |
| LDP-117 | Upper Core Spacer Grid to DVI Water Uncompensated Level (180) |
| LDP-118 | Lower Core Plate to Upper Core Plate (270) Uncompensated Water Level |
| LDP-119 | Lower Core Plate to Upper Core Support Grid (180) Uncompensated Water Level |
| LDP-127 | Reactor Wide Range Uncompensated Level |

Table 3.2. Pressure Instrumentation in the Reactor Pressure Vessel

| Tag Name | Description |
|---|---|
| LDP-138 | Upper Core Spacer Grid to Bottom of Upper Support Plate (180) Uncompensated Water Level |
| LDP-139 | Top of Lower Core Plate to Upper Core Spacer Grid Uncompensated Level |
| LDP-140 | Bottom of Reactor to Bottom of Flow Holes (180) Uncompensated Water Level |
| LDP-141 | Rx Vessel Upper Core Plate Uncompensated Level |
| PT-101 | CL-1 Pressure @ Reactor Flange |
| PT-102 | CL-2 Pressure @ Reactor Flange |
| PT-103 | CL-3 Pressure @ Reactor Flange |
| PT-104 | CL-4 Pressure @ Reactor Flange |
| PT-107 | Reactor Upper Head Pressure |
| PT-108 | Bottom of Reactor Pressure |
| PT-109 | DVI-1 Pressure @ Reactor Flange |
| PT-110 | DVI-2 Pressure @ Reactor Flange |
| PT-111 | Reactor Annular Pressure @ Flow Bypass Holes |
| PT-112 | Reactor Annular Pressure @ Bottom of Reactor |
| PT-113 | Reactor Pressure Below Mid-Core Spacer Grid |

## 3.3 Pressurizer (PZR)

A fully functional PZR, with internal heaters and a relief valve system capable of controlling the RCS pressure, has been included. The PZR is connected to HL-2 through the PZR surge line. The diameter of the PZR is not constant along its entire length. The larger diameter top was required for the APEX facility because there was not enough vertical space in the laboratory to accommodate the height of the PZR if the diameter remained constant (see Figure 3.5; note the notch in the beam to accommodate the taller PZR). The larger upper portion of the PZR is above the normal PZR water level, so only steam is present in the upper portion. The PZR in the APEX facility does not use a condensing spray for reduction of pressure; instead a vent is used to exhaust steam. A line from the first three stages of the ADS is connected to the top of the PZR for modeling the ADS depressurization of the primary system. The PZR has four heaters, and a T/C is installed in the disk end (top) of each heater. The PZR also has an air-operated valve to allow remote draining of the PZR. See Table 3.3 for a list of PZR-related instruments.

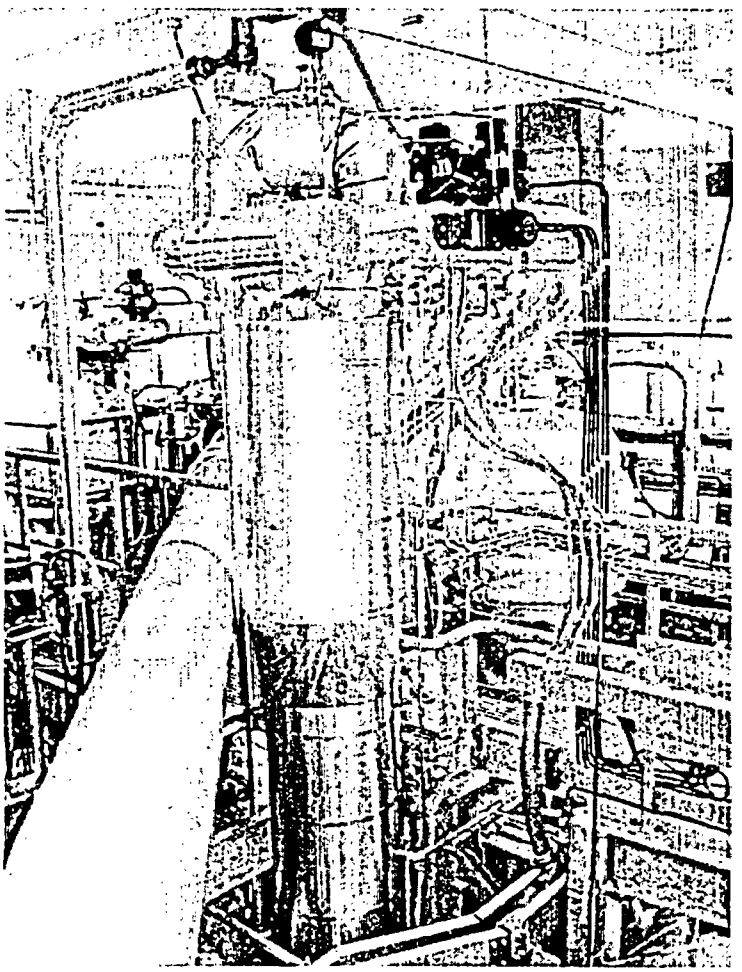

Figure 3.5. Photograph of Pressurizer in the APEX Facility

Table 3.3. Pressurizer Instrument Names and Locations

| LDP, HPS, DP, KW, and PT Cells | | Thermocouples | |
|---|---|---|---|
| **Tag Name** | **Description** | **Tag Name** | **Description** |
| DP-611 | PZR Surge Line DP | TF-601 | PZR Surge Line @ PZR Inlet |
| HPS-604-1 | Lower PZR Surge Line Heat Transfer Coefficient | TF-602 | ADS1–3 Common Line @ PZR |
| HPS-604-2 | Lower PZR Surge Line Heater dT above Fluid Temperature | TF-603 | PZR Surge Line @ HL-2 |
| HPS-604-3 | Lower PZR Surge Line Fluid Temperature | TF-605 | PZR Water Space Temperature |
| HPS-606-1 | ADS1–3 Common Inlet Heat Transfer Coefficient | TF-608 | PZR Fluid Temperature |
| HPS-606-2 | ADS1–3 Common Inlet Heater dT above Fluid Temperature | TF-614 | PZR Steam Vent Line Temperature |
| HPS-606-3 | ADS1–3 Common Inlet Fluid Temperature | TH-601 | PZR Heater Rod #1 |
| KW-601 | PZR Heater Power | TH-602 | PZR Heater Rod #2 |
| LDP-601 | PZR WR Uncompensated Water Level | TH-603 | PZR Heater Rod #3 |
| LDP-602 | PZR Surge Line Uncompensated Water Level | TH-604 | PZR Heater Rod #4 |
| LDP-605 | PZR Upper Surge Line Pipe Uncompensated Water Level | | |
| LDP-606 | PZR Surge Line Pipe Level @ PZR Inlet Uncompensated Water Level | | |
| LDP-607 | PZR Middle Surge Line Pipe Uncompensated Water Level | | |
| LDP-608 | PZR Lower Surge Line Pipe Uncompensated Water Level | | |
| LDP-609 | PZR Surge Line Pipe Uncompensated Water Level @ HL-2 | | |
| PT-602 | PZR NR Pressure | | |
| PT-603 | PZR NR Pressure | | |
| PT-604 | PZR Pressure | | |

## 3.4 Steam Generators (SGs)

Two SGs, one on each loop, have been included in the APEX facility. Each SG is instrumented and has a tube and shell made to simulate a Westinghouse Delta-75 Steam Generator (see Figure 2-8). The SG lower channel head includes connections for two RCPs and a single HL. SG2 contains a line from the PRHR HX located inside the IRWST. The T/Cs are attached to the outer surface and are embedded into the walls of selected SG tubes. Each SG contains 133 U-tubes. See Figures 3.6, 3.7, and 3.8 for images of the SG.

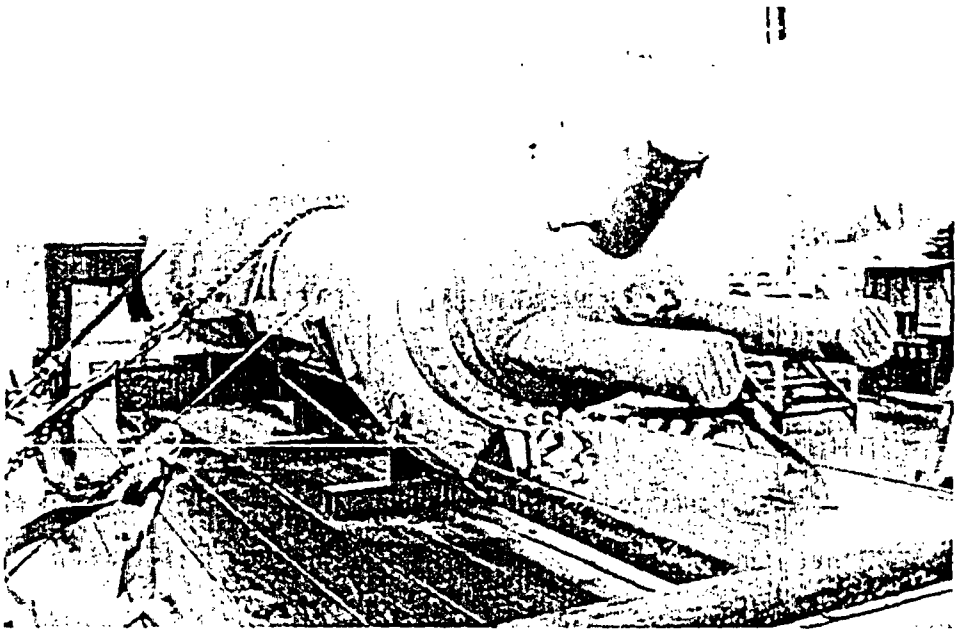

Figure 3.6. Steam Generator Being Delivered to the APEX Facility

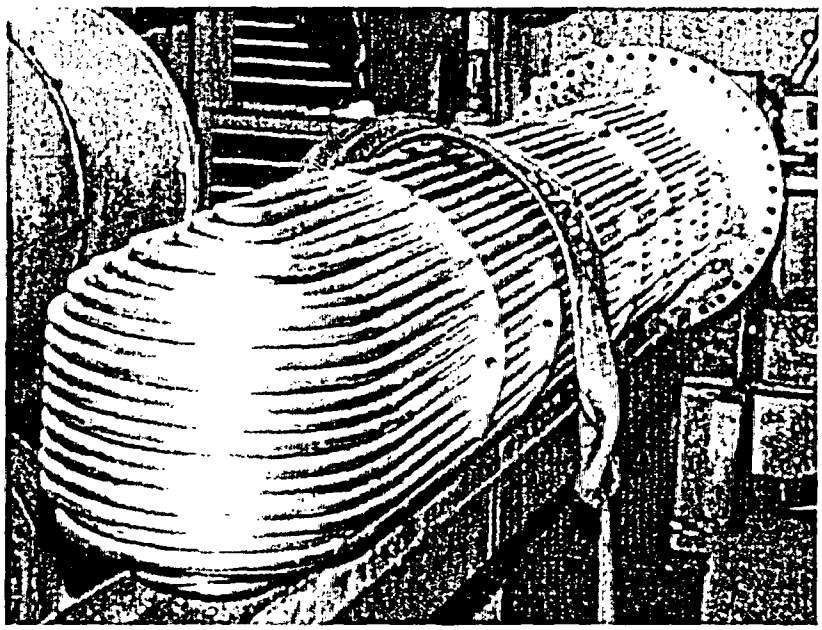

Figure 3.7. Steam Generator U-Tube Bundle

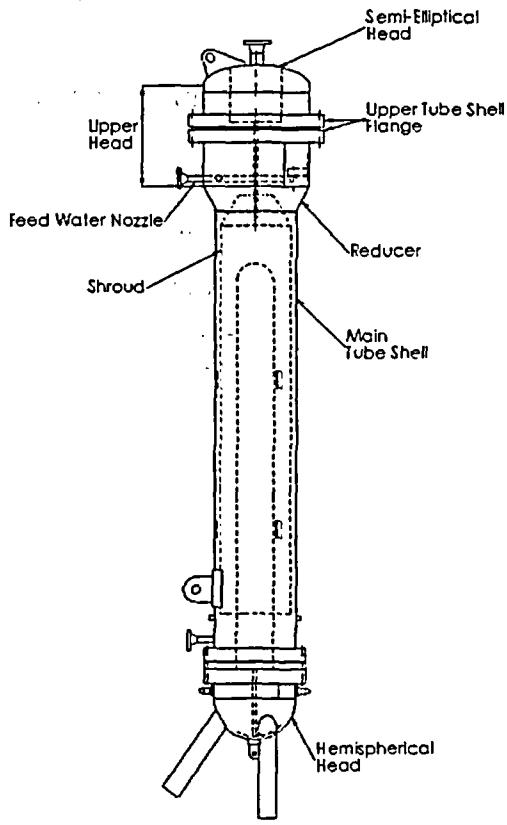


Figure 3.8. Steam Generator Components

A power-operated relief valve (PORV), and associated piping, is installed on both SGs and is connected to the exhaust header. An air-operated ball valve provides remote actuation. A flow orifice is installed in each line to limit steam flow. Each line includes a T/C, a pressure transmitter, and a Vortex flow meter. To provide flow measurement within the desired range, the PORV line was enlarged and a Vortex flow meter was installed. The PORV line discharges into a common steam line, which is then routed into the steam exhaust stack. Table 3.4 lists the instruments associated with the secondary side of the SGs, while Table 3.5 lists the instruments associated with the primary side of the SGs.

Table 3.4. Steam Generator Instrument Names and Locations (Secondary Side)

| LDP and PT Cells | | Thermocouples | |
|---|---|---|---|
| **Tag Name** | **Description** | **Tag Name** | **Description** |
| LDP-301 | SG1 WR Uncompensated Water Level | TF-301 | SG1 Steam Temperature |
| LDP-302 | SG2 WR Uncompensated Water Level | TF-305 | SG1 Downcomer HL Side Temperature |
| LDP-303 | SG1 NR Uncompensated Water Level | TF-306 | SG2 Downcomer HL Side Temperature |
| LDP-304 | SG2 NR Uncompensated Water Level | TF-307 | SG1 Downcomer CL Side Temperature |
| PT-301 | SG1 Pressure | TF-308 | SG2 Downcomer CL Side Temperature |
| PT-302 | SG2 Pressure | TF-310 | SG2 Steam Temperature |
| | | TF-311 | SG1 Feed Header Temperature |
| | | TF-312 | SG2 Feed Header Temperature |

Table 3.5. Steam Generator Instrument Names and Locations (Primary Side)

| LDP, DP, and PT Cells | | Thermocouples | |
|---|---|---|---|
| **Tag Name** | **Description** | **Tag Name** | **Description** |
| DP-211 | SG-1 Short Tube Entrance Losses | TF-207 | SG1 Short Tube @ Middle Outlet Side Temperature |
| DP-212 | SG2 Long Tube Exit Losses | TF-208 | SG2 Short Tube @ Middle Outlet Side Temperature |
| DP-213 | SG1 Long Tube Exit Losses | TF-209 | SG1 Short Tube @ Middle Inlet Side Temperature |
| DP-214 | SG2 Long Tube Entrance Losses | TF-210 | SG2 Short Tube @ Middle Inlet Side Temperature |
| LDP-207 | SG1 to HL1 Elbow Plenum Uncompensated Water Level | TF-211 | SG1 Long Tube @ Middle Outlet Temperature |
| LDP-208 | SG2 to HL2 Elbow Plenum Uncompensated Water Level | TF-212 | SG2 Long Tube @ Middle Outlet Temperature |
| LDP-209 | SG1 HL Plenum Uncompensated Water Level | TF-213 | SG1 Long Tube @ Middle Inlet Temperature |
| LDP-210 | SG2 CL4 Plenum Uncompensated Water Level | TF-214 | SG2 Long Tube @ Middle Inlet Temperature |
| LDP-211 | SG1 CL3 Plenum Uncompensated Water Level | TF-215 | SG1 Short Tube @ Top Temperature |
| LDP-212 | SG2 CL2 Plenum Uncompensated Water Level | TF-216 | SG2 Short Tube @ Top Temperature |
| LDP-213 | SG1 CL1 Plenum Uncompensated Water Level | TF-217 | SG1 Long Tube @ Top Temperature |
| LDP-214 | SG2 HL Plenum Uncompensated Water Level | TF-218 | SG2 Long Tube @ Top Temperature |
| LDP-215 | SG1 Long Tube HL Uncompensated Water Level | TW-201 | SG1 Short Tube Bottom Outlet |
| LDP-216 | SG2 Short Tube HL Uncompensated Water Level | TW-202 | SG2 Short Tube Bottom Outlet |
| LDP-217 | SG1 Short Tube HL Uncompensated Water Level | TW-203 | SG1 Short Tube Bottom Inlet |

Table 3.5. Steam Generator Instrument Names and Locations (Primary Side)

| LDP, DP, and PT Cells | | Thermocouples | |
|---|---|---|---|
| Tag Name | Description | Tag Name | Description |
| LDP-218 | SG2 Long Tube HL Uncompensated Water Level | TW-204 | SG2 Short Tube Bottom Inlet |
| LDP-219 | SG1 Long Tube CL Uncompensated Water Level | TW-205 | SG1 Long Tube Bottom Outlet |
| LDP-220 | SG2 Short Tube CL Uncompensated Water Level | TW-206 | SG2 Long Tube Bottom Outlet |
| LDP-221 | SG1 Short Tube CL Uncompensated Water Level | TW-208 | SG2 Long Tube Bottom Inlet |
| LDP-222 | SG2 Long Tube CL Uncompensated Water Level | TW-209 | SG1 Short Tube Top Outlet |
| PT-201 | SG1 Long Tube Pressure (Top) | TW-210 | SG2 Short Tube Top Outlet |
| PT-204 | SG2 Long Tube Pressure (Top) | | |

## 3.5 Reactor Coolant Pump (RCP)

Four variable-speed RCPs have been included as part of the RCS. The RCPs simulate the AP1000 canned motor pumps and are attached to the lower channel head of each SG. Each pump outlet is connected to a single CL. The pumps are fabricated from SS 304 and can be programmed to simulate RCP coastdown. Figure 3.9 shows two RCPs mounted on SG2, while Figure 3.10 shows the pump head curve of the RCPs. See Table 3.6 for a list of the instrumentation related to the RCPs.

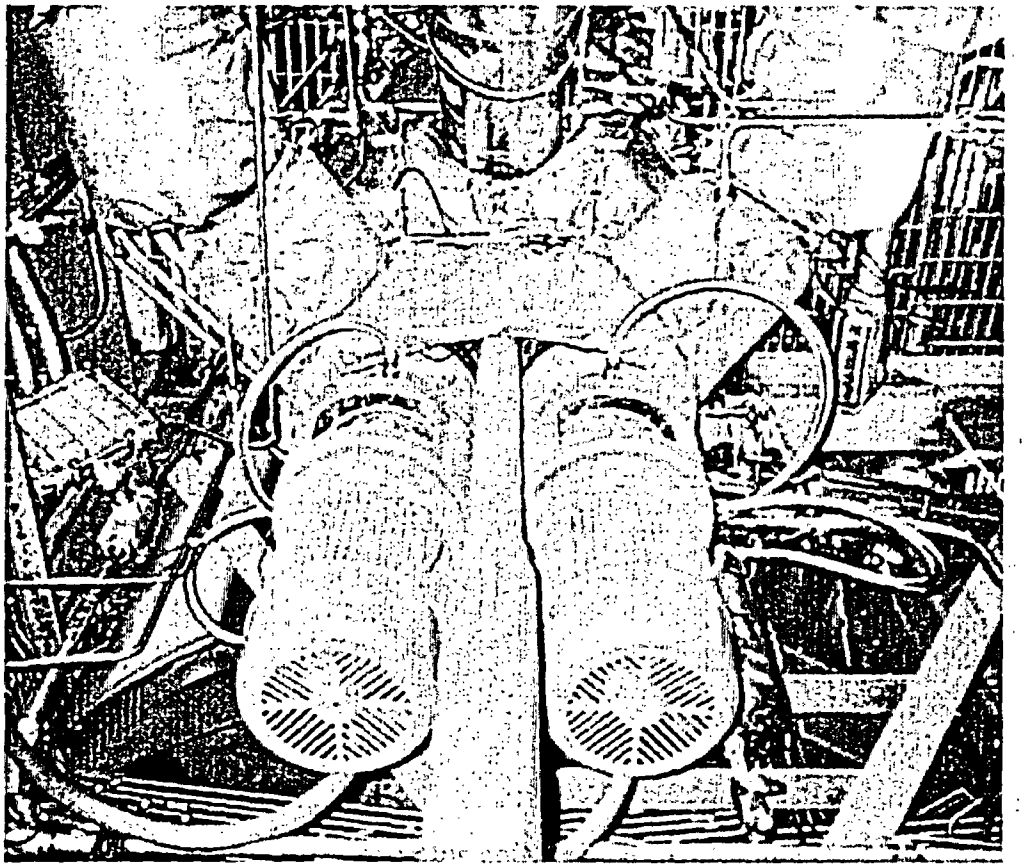

Figure 3.9. Image of Two Reactor Coolant Pumps from Bottom

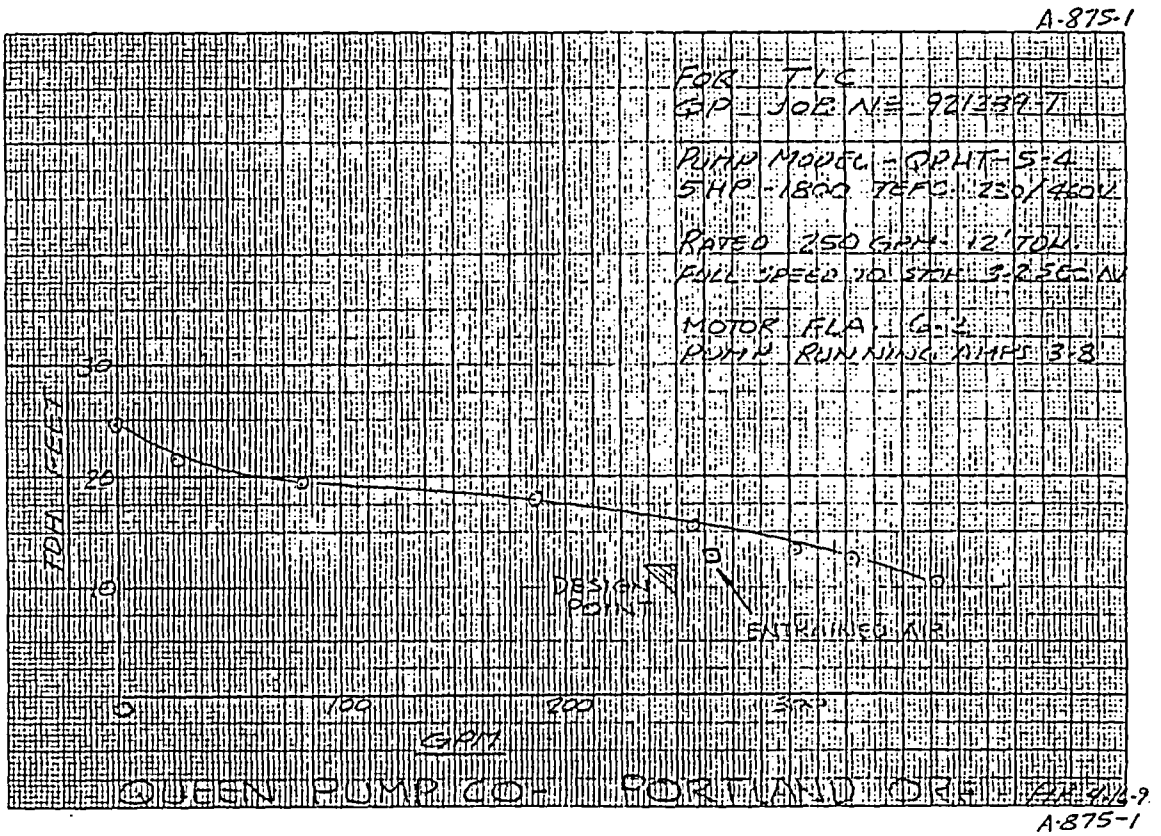


Figure 3.10. Reactor Coolant Pump Head Curve

Table 3.6. Reactor Coolant Pump Instrument Names and Locations

| Differential Pressure Cells | | Thermocouples | |
|---|---|---|---|
| **Tag Name** | **Description** | **Tag Name** | **Description** |
| DP-202 | RCP-2 DP | TF-201 | CL-1 @ RCP-1 Inlet Temperature |
| DP-203 | RCP-1 DP | TF-202 | CL-2 @ RCP-2 Inlet Temperature |
| DP-205 | RCP-3 DP | TF-203 | CL-3 @ RCP-3 Inlet Temperature |
| DP-206 | RCP-4 DP | TF-204 | CL-4 @ RCP-4 Inlet Temperature |

## 3.6 Primary Loop Piping

The primary loop piping models two primary loops, each consisting of a single HL and two CLs. Figure 3.11 shows the PZR side of the RCS.

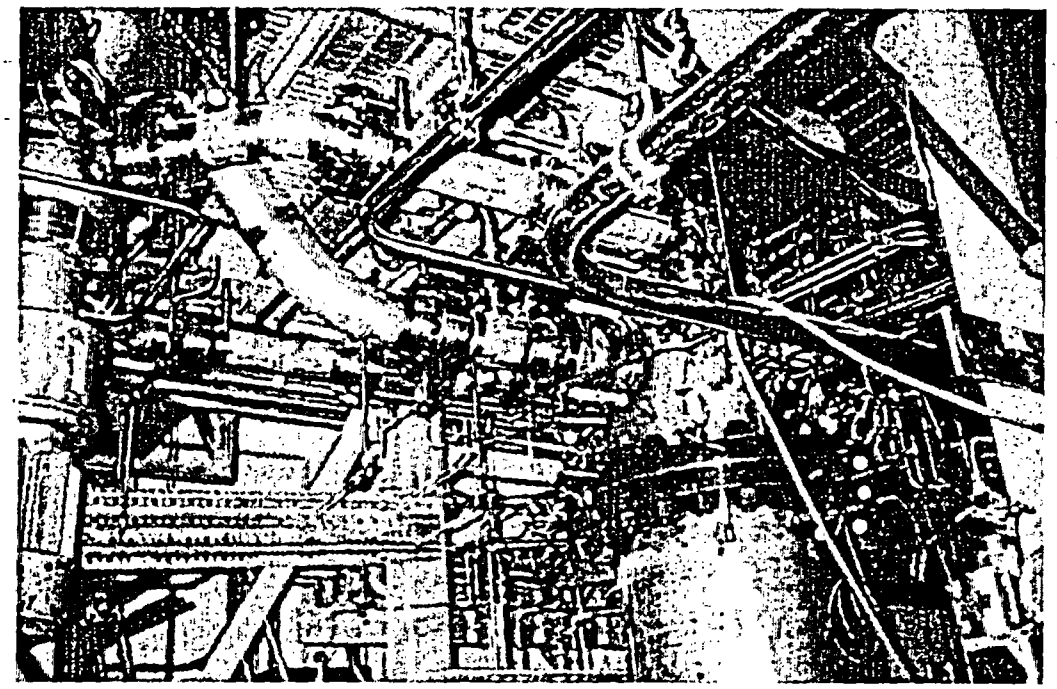

Figure 3.11. Primary Loop Piping in the Reactor Coolant System

Break spool pieces are installed on the HLs, CLs, DVI lines, and CMT pressure balance line (PBL) to simulate several pipe break scenarios. The APEX facility is able to simulate the following primary loop breaks:

- Top break on CL-3
- Bottom break on CL-3
- Bottom break on CL-4
- Bottom break on HL-2
- Single-ended DVI break
- Single-ended CMT balance line break
- Double-ended DVI break
- Double-ended CMT balance line break

Each of the primary loop breaks is initiated by pneumatic valves connected to the aforementioned locations. The break flow passes through an orifice plate, which is intended to set the size of the break, and may be changed out at anytime to simulate different break flow areas. The discharge from the break vents proceeds to the break and ADS measurement system (BAMS) to separate and measure the liquid and vapor components of the break flow rate.

### 3.6.1 Hot Legs (HLs)

In the primary side, each loop consists of a single pipe, which in turn, feeds the inverted U-tube SG mounted vertically on the bottom of each SG channel head. The HLs have connections for the fourth-stage ADS (ADS4). Refer to Table 3.7 for a list of instruments pertaining to the HL.

Table 3.7. Hot Leg Instrument Names and Locations

| Tag Name | Description |
|---|---|
| DP-209 | HL2 DP |
| DP-210 | HL2 DP |
| DP-216 | HL Break DP |
| DP-217 | HL1 to CL1 DP @ SG1 |
| DP-218 | HL2 to CL2 DP @ SG2 |
| DP-219 | HL1 to CL3 DP @ SG1 |
| DP-220 | HL2 to CL4 DP @ SG2 |
| DP-221 | HL1 to CL1 DP @ RX |
| DP-222 | HL2 to CL2 DP @ RX |
| DP-223 | HL1 to CL3 DP @ RX |
| DP-224 | HL2 to CL4 DP @ RX |
| HPS-205-1 | HL1 Heat Transfer Coefficient |
| HPS-205-2 | HL1 Heater dT above fluid temperature |
| HPS-205-3 | HL1 Fluid temperature |
| HPS-206-1 | HL2 Heat Transfer Coefficient |
| HPS-206-2 | HL2 Heater dT above fluid temperature |
| HPS-206-3 | HL2 Fluid Temperature |
| LDP-205 | HL1 Uncompensated Water Level |
| LDP-206 | HL2 Uncompensated Water Level |
| LDP-207 | SG1 to HL1 Elbow Plenum Uncompensated Water Level |
| LDP-208 | SG2 to HL2 Elbow Plenum Uncompensated Water Level |
| LDP-209 | SG1 HL Plenum Uncompensated Water Level |
| LDP-214 | SG2 HL Plenum Uncompensated Water Level |
| PT-202 | HL2 Pressure @ SG2 Flange |
| PT-205 | HL1 Pressure @ SG1 Flange |
| PT-206 | HL Break Pressure @ Break Valve |

### 3.6.2 Cold Legs (CLs)

In the primary side, each loop consists of two pipes, which in turn, feed the reactor vessel. The CL interconnects the reactor vessel and one of the two RCPs attached at the bottom of the SG. CL1 and CL3 have connections for the CMT-PBLs connected to the tops of CMT2 and CMT1, respectively. See Table 3.8 for a list of CL-related instrumentation.

Table 3.8. Cold Leg Instrument Names and Locations

| DP, LDP, HPS, FMM, and PT Cells | | Thermocouples | |
|---|---|---|---|
| **Tag Name** | **Description** | **Tag Name** | **Description** |
| DP-201 | CL1 DP | TF-201 | CL1 @ RCP1 Inlet Temperature |
| DP-204 | CL2 DP | TF-202 | CL2 @ RCP2 Inlet Temperature |
| DP-207 | CL3 DP | TF-203 | CL3 @ RCP3 Inlet Temperature |
| DP-208 | CL4 DP | TF-204 | CL4 @ RCP4 Inlet Temperature |
| DP-217 | HL1 to CL1 DP @ SG1 | TF-221 | CL3 T/C Rod @ 3.25 in. (8.26 cm) |
| DP-218 | HL2 to CL2 DP @ SG2 | TF-222 | CL4 T/C Rod @ 3.25 in. (8.26 cm) |
| DP-219 | HL1 to CL3 DP @ SG1 | TF-223 | CL3 T/C Rod @ 2.50 in. (6.35 cm) |
| DP-220 | HL2 to CL4 DP @ SG2 | TF-224 | CL4 T/C Rod @ 2.50 in. (6.35 cm) |
| DP-221 | HL1 to CL1 DP @ RX | TF-225 | CL3 T/C Rod @ 1.75 in. (4.45 cm) |
| DP-222 | HL2 to CL2 DP @ RX | TF-226 | CL4 T/C Rod @ 1.75 in. (4.45 cm) |
| DP-223 | HL1 to CL3 DP @ RX | TF-227 | CL3 T/C Rod @ 1.25 in. (3.18 cm) |
| DP-224 | HL2 to CL4 DP @ RX | TF-228 | CL4 T/C Rod @ 1.25 in. (3.18 cm) |
| FMM-201 | CL1 Loop Flow | TF-229 | CL3 T/C Rod @ 0.75 in. (1.91 cm) |
| FMM-202 | CL2 Loop Flow | TF-230 | CL4 T/C Rod @ 0.75 in. (1.91 cm) |
| FMM-203 | CL3 Loop Flow | TF-231 | CL3 T/C Rod @ 0.25 in. (0.64 cm) |
| FMM-204 | CL4 Loop Flow | TF-232 | CL4 T/C Rod @ 0.25 in. (0.64 cm) |
| HPS-201-1 | CL1 Heat Transfer Coefficient | TF-251-1 | CL1 Loop Seal Upper Temperature |
| HPS-201-2 | CL1 Heater dT Above Fluid Temperature | TF-251-2 | CL1 Loop Seal Middle Temperature |
| HPS-201-3 | CL1 Fluid Temperature | TF-251-3 | CL1 Loop Seal Lower Temperature |
| HPS-202-1 | CL2 Heat Transfer Coefficient | TF-252-1 | CL2 Loop Seal Upper Temperature |
| HPS-202-2 | CL2 Heater dT Above Fluid Temperature | TF-252-2 | CL2 Loop Seal Middle Temperature |
| HPS-202-3 | CL2 Fluid Temperature | TF-252-3 | CL2 Loop Seal Lower Temperature |
| HPS-203-1 | CL3 Heat Transfer Coefficient | TF-253-1 | CL3 Loop Seal Upper Temperature |
| HPS-203-2 | CL3 Heater dT Above Fluid Temperature | TF-253-2 | CL3 Loop Seal Middle Temperature |

Table 3.8. Cold Leg Instrument Names and Locations

| DP, LDP, HPS, FMM, and PT Cells | | Thermocouples | |
|---|---|---|---|
| **Tag Name** | **Description** | **Tag Name** | **Description** |
| HPS-203-3 | CL3 Fluid Temperature | TF-253-3 | CL3 Loop Seal Lower Temperature |
| HPS-204-1 | CL4 Heat Transfer Coefficient | TF-254-1 | CL4 Loop Seal Upper Temperature |
| HPS-204-2 | CL4 Heater dT Above Fluid Temperature | TF-254-2 | CL4 Loop Seal Middle Temperature |
| HPS-204-3 | CL4 Fluid Temperature | TF-254-3 | CL4 Loop Seal Lower Temperature |
| LDP-201 | CL1 Water Uncompensated Level | TF-255 | CL1 Safety Injection Nozzle Temperature |
| LDP-202 | CL2 Water Uncompensated Level | TF-256 | CL2 Safety Injection Nozzle Temperature |
| LDP-203 | CL3 Uncompensated Water Level | TF-257 | CL3 Safety Injection Nozzle Temperature |
| LDP-204 | CL4 Uncompensated Water Level | TF-258 | CL4 Safety Injection Nozzle Temperature |
| LDP-210 | SG2 CL4 Plenum Uncompensated Water Level | | |
| LDP-211 | SG1 CL3 Plenum Uncompensated Water Level | | |
| LDP-212 | SG2 CL2 Plenum Uncompensated Water Level | | |
| LDP-213 | SG1 CL1 Plenum Uncompensated Water Level | | |
| LDP-219 | SG1 Long Tube CL Uncompensated Water Level | | |
| LDP-220 | SG2 Short Tube CL Uncompensated Water Level | | |
| LDP-221 | SG1 Short Tube CL Uncompensated Water Level | | |
| LDP-222 | SG2 Long Tube CL Uncompensated Water Level | | |
| PT-203 | CL Break Pressure @ Break Valve | | |

### 3.6.3 Pressurizer Surge Line

The PZR surge line connects the bottom of the PZR to the top of HL2, near the SG end of the HL. The surge line enables continuous pressure adjustments between the RCS and the PZR. The PZR surge line spirals up from the HL to the PZR so that its geometry properly matches that of the AP1000 reactor (see Figure 3.12).

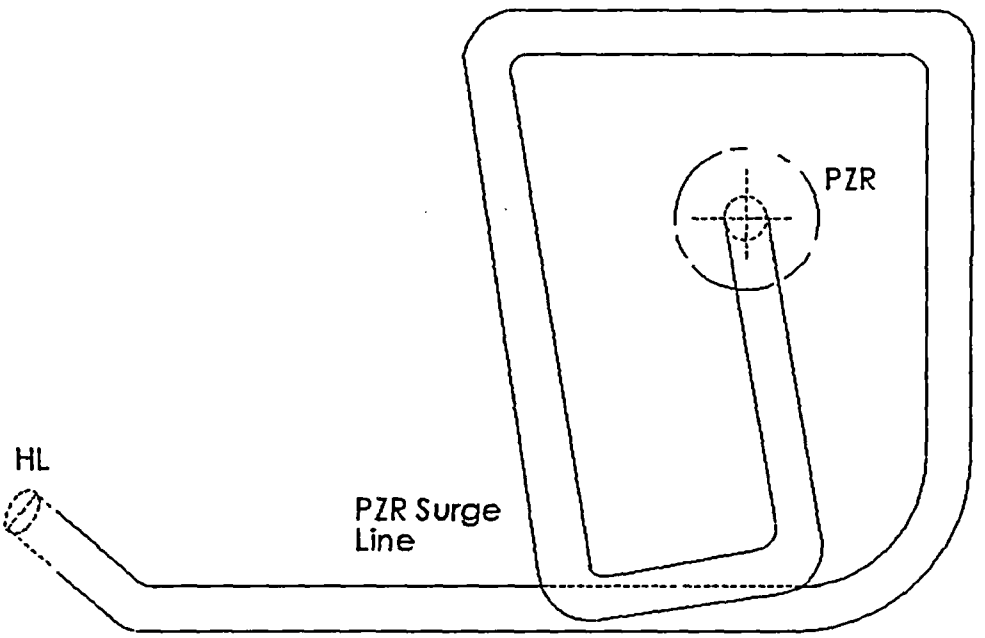


Figure 3.12. Pressurizer Surge Line Geometry (Top View)

## 3.7 Passive Safety Systems

### 3.7.1 Automatic Depressurization System (ADS) 1–4

The ADS1–3 valves in the APEX facility model two trains in the AP1000 reactor. Each valve is located after a flow orifice that models the scaled choked flow area of the AP1000. The ADS1–3 valve train discharges to the ADS1–3 separator, where the two-phase flow is separated and measured. All portions of the flow are recombined before dumping into the ADS1–3 sparger.

The ADS1–3 valves exit at the top of the PZR through a single section of pipe. The pipe then splits in three, and is reduced prior to the ADS1, 2, and 3 flow nozzles. After the valves, the piping is recombined into a common pipe, which is connected to the ADS1–3 separator. The fluid is separated into its steam and liquid components inside the ADS1–3 moisture separator. The steam flow and liquid flow are measured and then recombined and dumped though a sparger into the IRWST. The sparger consists of four separate legs (see Figure 3.13). The ADS1 valve is opened on "S" signal, "S" signal plus a time delay, or CMT low level, depending on the selected logic. The ADS2 and ADS3 valves open based on a time delay after actuation of ADS1.

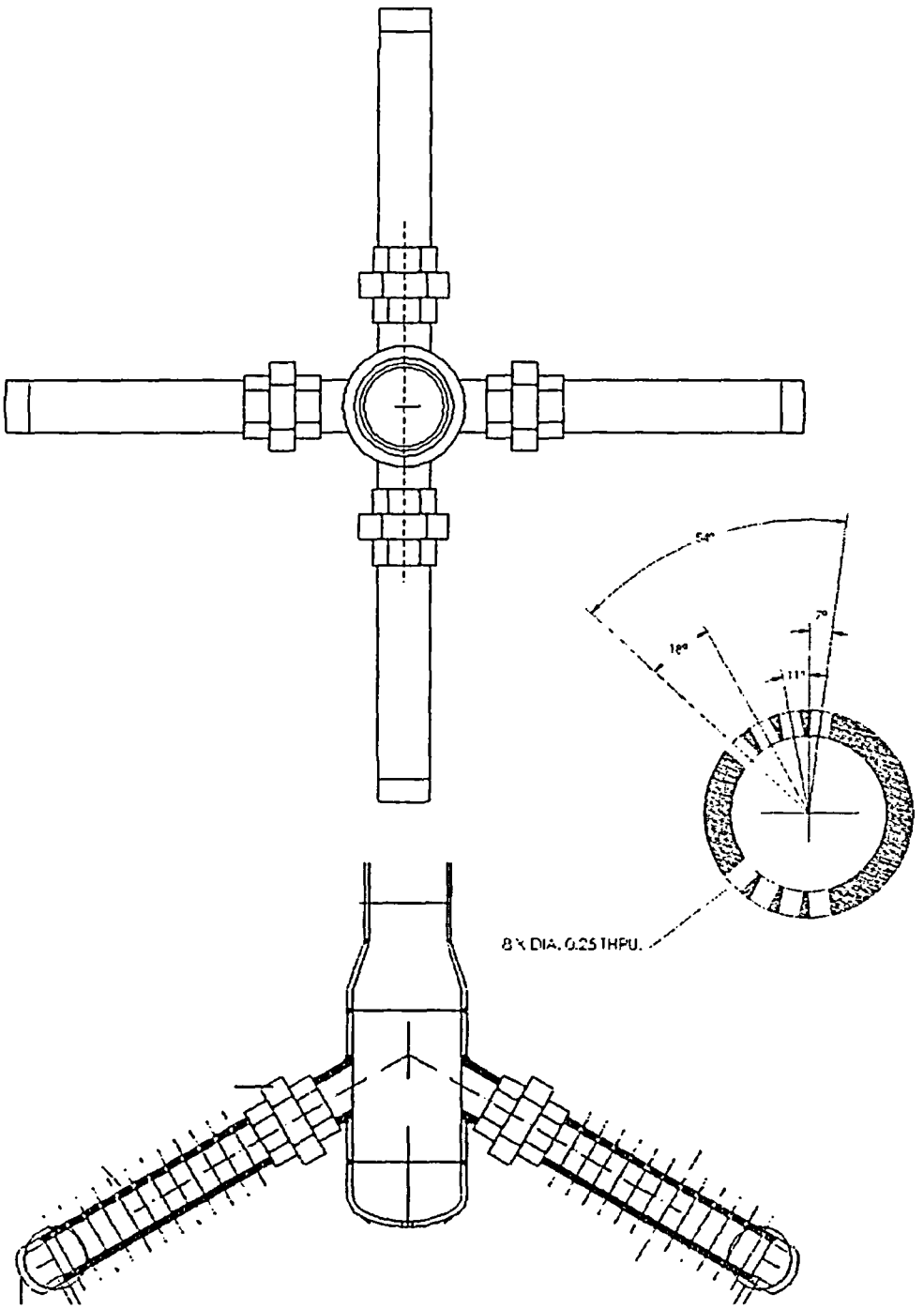


Figure 3.13. Illustration of Automatic Depressurization System 1–3 Sparger

Figure 3.14 shows the ADS1–3 sparger installed within the IRWST. Refer to Table 3.9 for a list of instrumentation pertaining to the ADS1–4 system.

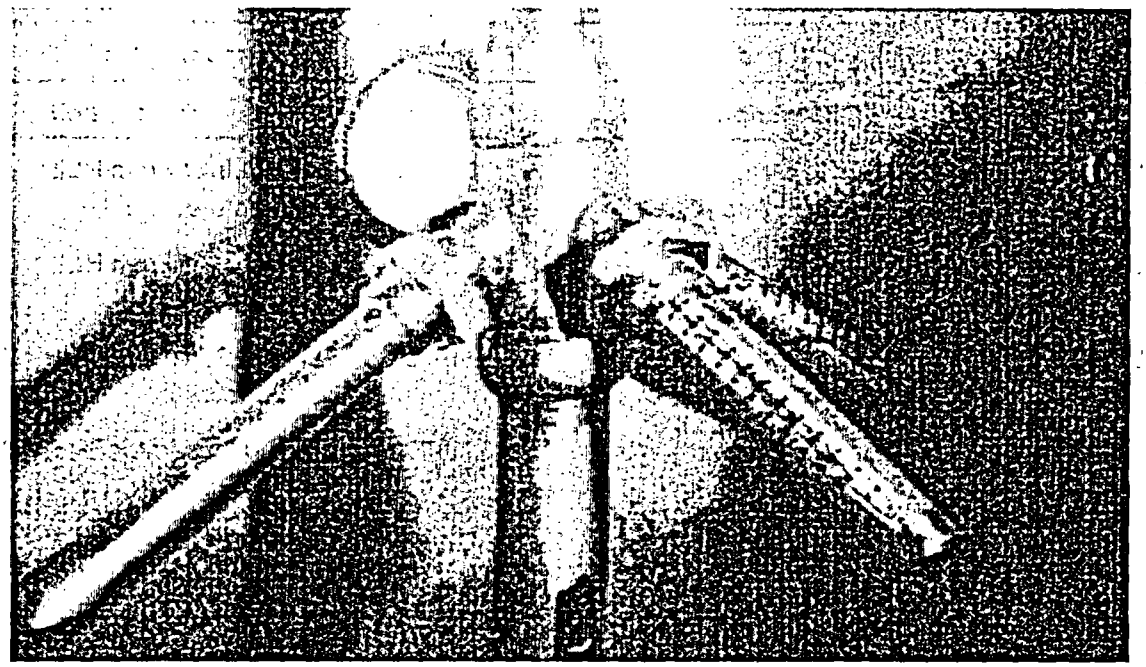

Figure 3.14. Photograph of Installed Sparger

Table 3.9. Automatic Depressurization System 1–4 Instrument Names and Locations

| LDP, FDP, HPS, FMM, and PT Cells | | Thermocouples | |
|---|---|---|---|
| **Tag Name** | **Description** | **Tag Name** | **Description** |
| FDP-604 | ADS2 Flow Differential Pressure | TF-602 | ADS1–3 Common Line @ PZR Temperature |
| FDP-605 | ADS1 Flow Differential Pressure | TF-609 | ADS4–1 Discharge Temperature |
| FDP-606 | ADS3 Flow Differential Pressure | TF-610 | ADS4–2 Discharge Temperature |
| FMM-601 | ADS1–3 Loop Seal Flow | TF-615 | ADS1–3 Common Line from PZR Temperature |
| FMM-602 | ADS4–2 Loop Seal Flow | TF-616 | ADS1–3 Separator Loop Seal Temperature |
| FMM-603 | ADS4–1 Loop Seal Flow | TF-617 | ADS1–3 Separator Steam Outlet Temperature |
| LDP-603 | ADS4A Vertical Exit Line Uncompensated Water Level | TF-618 | ADS4–2 Loop Seal Temperature |
| LDP-604 | ADS4B Vertical Exit Line Uncompensated Water Level | TF-619 | ADS4–1 Loop Seal Temperature |

Table 3.9. Automatic Depressurization System 1–4 Instrument Names and Locations

| LDP, FDP, HPS, FMM, and PT Cells | | Thermocouples | |
|---|---|---|---|
| **Tag Name** | **Description** | **Tag Name** | **Description** |
| LDP-610 | ADS1–3 Separator Uncompensated Water Level | TF-620 | ADS4–2 Inlet From HL2 Temperature |
| LDP-611 | ADS4–1 Separator Uncompensated Water Level | TF-621 | ADS4–1 Inlet From HL1 Temperature |
| LDP-612 | ADS4–2 Separator Uncompensated Water Level | TF-622 | ADS4–2 Separator Steam Outlet Temperature |
| PT-605 | ADS1–3 Separator Pressure | TF-623 | ADS4–1 Separator Steam Outlet Temperature |
| PT-606 | IRWST Sparger Line Pressure | TW-601 | ADS1–3 Separator Wall Temperature |
| PT-610 | ADS4–2 Separator Pressure | TW-602 | ADS4–2 Separator Wall Temperature |
| PT-611 | ADS4–1 Separator Pressure | TW-603 | ADS4–1 Separator Wall Temperature |
| HPS-606-1 | ADS1–3 Common Inlet Heat Transfer Coefficient | | |
| HPS-606-2 | ADS1–3 Common Inlet Heater dT Above Fluid Temperature | | |
| HPS-606-3 | ADS1–3 Common Inlet Fluid Temperature | | |

Two ADS4 valves are connected to the top of HL1 and HL2, respectively. Both ADS4 lines are similar, with the exception that ADS4–2 (PZR side) provides a tee connection for the PRHR HX system. Both ADS4 lines include valve flow area and line resistance. The flow from ADS4 is directed to a an orifice to match the separator, where the steam and liquid flows are separated and measured individually. The steam flow is routed through one of two lines depending on the expected flow rate and is then vented from the facility. The liquid flow is directed through a loop seal and into the primary sump.

### 3.7.2 In-Containment Refueling Water Storage Tank (IRWST)

The APEX IRWST is constructed of SS 304 and has four major connections, including the ADS1–3 sparger, DVI1 and 2, the primary sump, and the PRHR connections. Table 3.10 lists the pressure, weight, and flow rate instruments for the IRWST, while Table 3.11 lists the temperature measurement instrumentation. The temperature of the fluid in the IRWST is measured at several heights to determine stratification.

Table 3.10. IRWST LDP, LCT, FMM, DP, and PT Cells and Locations

| Tag Name | Description |
|---|---|
| DP-701 | IRWST-1 Injection Differential Pressure |
| DP-702 | IRWST-2 Injection Differential Pressure |
| FMM-701 | IRWST-1 Injection Flow |
| FMM-702 | IRWST-2 Injection Flow |
| FMM-703 | IRWST Overflow |
| LDP-701 | IRWST Uncompensated Water Level |
| PT-701 | IRWST Pressure |
| LCT-701 | IRWST Weight |

Table 3.11. IRWST Thermocouples and Location

| Tag Name | Description | Tag Name | Description |
|---|---|---|---|
| TF-701 | IRWST/PRHR T/C Rod @ Bottom Temperature | TF-713 | IRWST Discharge to DVI-01 @ IRWST Temperature |
| TF-702 | IRWST/PRHR T/C Rod @ 7.98 in. (20.27 cm) | TF-714 | IRWST Discharge to DVI-02 @ IRWST Temperature |
| TF-703 | IRWST/PRHR T/C Rod @ 15.97 in. (40.56 cm) | TF-715 | IRWST Sparger T/C Rod @ 8.97 in. (22.78 cm) |
| TF-704 | IRWST/PRHR T/C Rod @ 25.85 in. (65.67 cm) | TF-716 | IRWST Sparger Nozzle Temperature |
| TF-705 | IRWST/PRHR T/C Rod @ 35.73 in. (90.75 cm) | TF-717 | IRWST Sparger T/C Rod @ 66.34 in. (168.50 cm) |
| TF-706 | IRWST/PRHR T/C Rod @ 45.61 in. (115.85 cm) | TF-718 | IRWST Sparger T/C Rod @ 98.45 in. (250.06 cm) |
| TF-707 | IRWST/PRHR T/C Rod @ 55.49 in. (140.94 cm) | TF-719 | IRWST Sparger Outlet Temperature |
| TF-708 | IRWST/PRHR T/C Rod @ 65.36 in. (166.01 cm) | TF-720 | IRWST/DVI2 Injection Line Temperature |
| TF-709 | IRWST/PRHR T/C Rod @ 75.24 in. (191.11 cm) | TF-721 | IRWST/DVI1 Injection Line Temperature |
| TF-710 | IRWST/PRHR T/C Rod @ 86.36 in. (219.35 cm) | TF-722 | IRWST Steam Exhaust Line Temperature |
| TF-711 | IRWST/PRHR T/C Rod @ 97.47 in. (247.57 cm) | TF-723 | IRWST/Primary Sump Overflow Temperature |
| TF-712 | IRWST/PRHR T/C Rod @ 108.59 in. (275.82 cm) | | |

The two IRWST injection lines that connect into each DVI line start at the bottom of the IRWST, which in turn, connects to the SS 304 pipe connected to the DVI line. The IRWST injection lines are similar, with the exception that IRWST-1 provides a connection to the RNS pump suction. The IRWST injection line resistance is fine-tuned by an orifice plate installed in each line. The IRWST isolation valves (RCS-711/712) are opened on decreasing RCS pressure. See Figure 3.15 for an image of the IRWST.

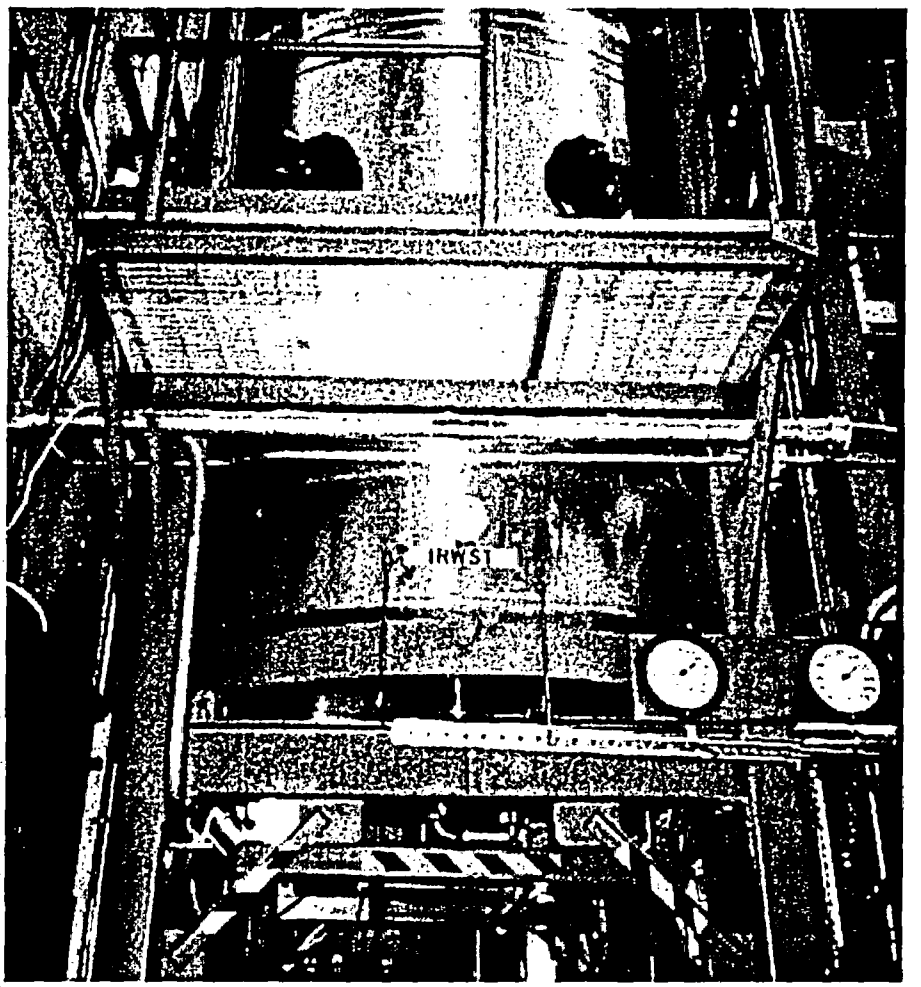


Figure 3.15. Photograph of the IRWST

### 3.7.3 Core Makeup Tanks (CMT)

The CMTs are constructed of SS 304, and each CMT is connected to a CL and a DVI line by SS 304 pipe. The CMT injection line isolation valves (RCS-529/530) open on "S" signal for the station blackout subroutine or "S" signal plus a time delay for all other routines. The line resistance of the CMT injection lines is fine-tuned through the use of an orifice. The isolation valves in the CMT balance line (RCS-535/536) have no automatic control and remain open during facility testing. See Figure 3.16 for an image of a CMT. Table 3.12 lists all CMT-related instruments and piping.

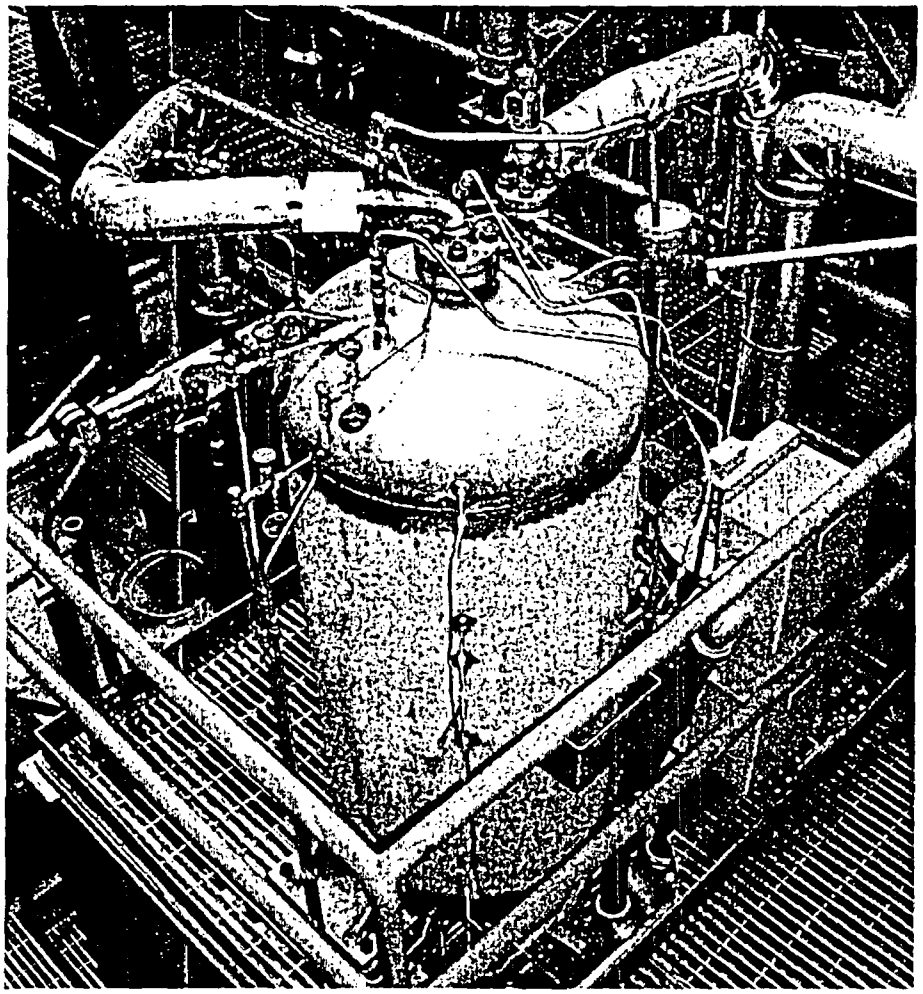

Figure 3.16. Photograph of a Core Makeup Tank

Table 3.12. Core Makeup Tank Instrument Names and Locations

| LDP, FMM, HPS, DP, and PT Cells | | Thermocouples | |
|---|---|---|---|
| Tag Name | Description | Tag Name | Description |
| DP-501 | CMT1 Injection Differential Pressure | TF-501 | CMT1 Long T/C Rod @ 0.30 in. (0.76 cm) Temperature |
| DP-502 | CMT2 Injection DP | TF-502 | CMT2 Injection Line Temperature |
| DP-503 | CMT1 Balance Line DP | TF-503 | CMT1 @ ½ Lower Head Height |
| DP-504 | CMT2 Balance Line DP | TF-504 | CMT2 Long T/C Rod @ 0.30 in. (0.76 cm) Temperature |
| FMM-501 | CMT1 Injection Flow | TF-505 | CMT1 @ 20% Volume-Height |
| FMM-502 | CMT2 CL Balance Line Flow | TF-506 | CMT2 @ ½ Lower Head Height |
| FMM-503 | CMT1 CL Balance Line Flow | TF-507 | CMT1 Long T/C Rod @ 20.87 in. (53.01 cm) Temperature |

Table 3.12. Core Makeup Tank Instrument Names and Locations

| LDP, FMM, HPS, DP, and PT Cells | | Thermocouples | |
|---|---|---|---|
| Tag Name | Description | Tag Name | Description |
| FMM-504 | CMT2 Injection Flow | TF-508 | CMT2 @ 20% Volume-Height |
| LDP-501 | CMT1 NR Uncompensated Water Level (Bottom) | TF-509 | CMT1 Long T/C Rod @ 36.89 in. (93.70 cm) Temperature |
| LDP-502 | CMT2 WR Uncompensated Water Level | TF-510 | CMT2 Long T/C Rod @ 20.87 in. (53.01 cm) Temperature |
| LDP-503 | CMT1 NR Uncompensated Water Level (Middle) | TF-511 | CMT1 @ 50% Volume-Height |
| LDP-504 | CMT2 NR Uncompensated Water Level (Bottom) | TF-512 | CMT2 Long T/C Rod @ 36.89 in. (93.70 cm) Temperature |
| LDP-505 | CMT1 NR Uncompensated Water Level (Top) | TF-513 | CMT1 Long T/C Rod @ 40.59 in. (103.10 cm) Temperature |
| LDP-506 | CMT2 NR Uncompensated Water Level (Middle) | TF-514 | CMT2 @ 50% Volume-Height |
| LDP-507 | CMT1 WR Uncompensated Water Level | TF-515 | CMT1 Long T/C Rod @ 43.41 in. (110.26 cm) Temperature |
| LDP-508 | CMT2 NR Uncompensated Water Level (Top) | TF-516 | CMT2 Long T/C Rod @ 40.59 in. (103.10 cm) Temperature |
| LDP-509 | CL3 to CMT1 Balance Line Uncompensated Water Level | TF-517 | CMT1 @ 75% Volume-Height minus 3.7 in. (9.40 cm) |
| LDP-510 | CL1 to CMT2 Balance Line Uncompensated Water Level | TF-518 | CMT2 Long T/C Rod @ 43.41 in. (110.26 cm) Temperature |
| PT-501 | CMT1 Pressure | TF-519 | CMT1 Long T/C Rod @ 46.23 in. (117.42 cm) Temperature |
| PT-502 | CMT-02 Pressure | TF-520 | CMT2 @ 75% Volume-Height minus 3.7 in. (9.40 cm) |
| HPS-509-1 | CMT-01 CL Balance Line Heat Transfer Coefficient | TF-521 | CMT1 @ 75% Volume-Height |
| HPS-509-2 | CMT-01 CL Balance Line Heater dT above fluid temperature | TF-522 | CMT2 Long T/C Rod @ 46.23 in. (117.42 cm) Temperature |
| HPS-509-3 | CMT-01 CL Balance Line Fluid temperature | TF-523 | CMT1 Long T/C Rod @ 49.05 in. (124.59 cm) Temperature |
| HPS-512-1 | CMT-02 CL Balance Line Heat Transfer Coefficient | TF-524 | CMT |
| HPS-512-2 | CMT-02 CL Balance Line Heater dT above fluid temperature | TF-525 | CMT1 @ 1/2 Upper-Head Height |
| HPS-512-3 | CMT-02 CL Balance Line Fluid temperature | TF-526 | CMT2 SPARGER 2\3 TEMP |

Table 3.12. Core Makeup Tank Instrument Names and Locations

| LDP, FMM, HPS, DP, and PT Cells | | Thermocouples | |
|---|---|---|---|
| Tag Name | Description | Tag Name | Description |
| TF-530 | CMT2 Long T/C Rod @ 51.87 in. (131.75 cm) Temperature | TF-527 | CMT1 Long T/C Rod @ 51.87 in. (131.75 cm) Temperature |
| TF-531 | CMT1 Balance Line @ CMT Inlet Temperature | TF-528 | CMT 23% Head Temp |
| TF-532 | CMT2 Long T/C Rod @ 56.61 in. (143.79 cm) Temperature | | |
| TF-533 | CMT1/CL Balance Line @ CL-3 Temperature | TF-542 | CMT2 @ 60% Volume-Height |
| TF-535 | CMT1 Injection Line Temperature | TF-543 | CMT1 @ 75% Volume-Height |
| TF-536 | CMT2/CL Balance Line @ CL-1 Temperature | TF-544 | CMT2 @ 75% Volume-Height |
| TF-537 | CMT1 @ 20% Volume-Height | TF-546 | CMT2 Balance Line @ CMT Inlet Temperature |
| TF-538 | CMT2 @ 20% Volume-Height | TF-547 | CMT1 Long T/C Rod @ 54.24 in. (137.77 cm) Temperature |
| TF-539 | CMT1 @ 50% Volume-Height | TF-548 | CMT2 Long T/C Rod @ 54.24 in. (137.77 cm) Temperature |
| TF-540 | CMT2 @ 50% Volume-Height | TF-549 | CMT1 Discharge Line Temperature |
| TF-541 | CMT1 @ 60% Volume-Height | TF-550 | CMT2 Discharge Line Temperature |
| | | TF-551 | CMT1 Short T/C Rod (225 degrees) 5.5 in. (13.97 cm) from top |

### 3.7.4 Passive Residual Heat Remover (PRHR) Heat Exchanger (HX)

The PRHR HX consists of a C-shaped heat exchanger, located inside the IRWST, and two connections to the primary loop. One inlet connection is between the HL2 ADS4 tee and the upper PRHR HX manifold on the IRWST. The outlet connection is between the lower PRHR HX manifold on the IRWST and the outlet plenum of SG2. The PRHR flow is actuated by an isolation valve (RCS-804) that opens on "S" signal, actuation of the ADS1 valve, or CMT injection valve opening, depending on the selected logic subroutine. The PRHR HX is connected to the upper and lower heat exchanger manifolds on the IRWST. It is made up of 88 individual tubes. See Figure 3.17 for an image of the PRHR HX. Table 3.13 contains a list of all instruments related to the PRHR.

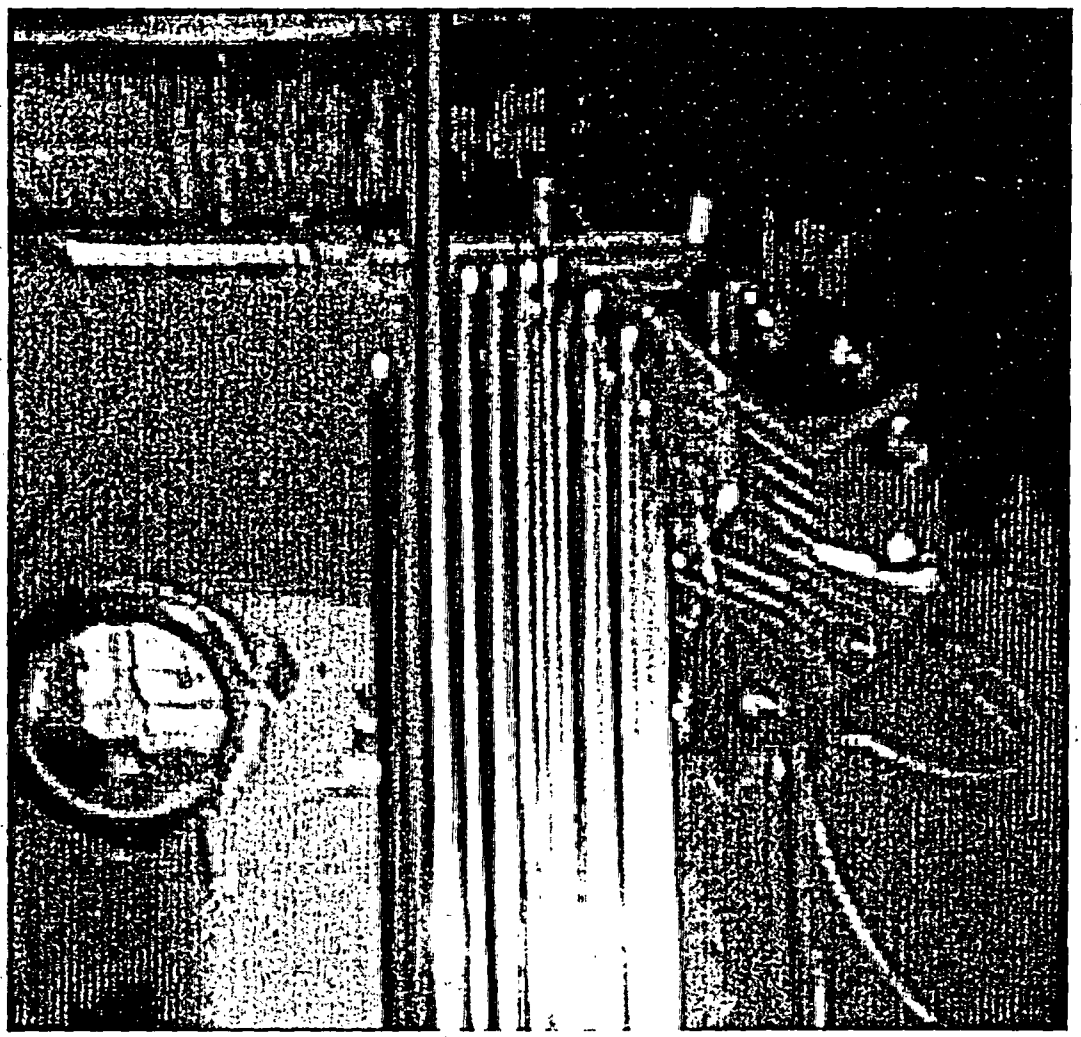

Figure 3.17. View of the PRHR HX Located Inside the IRWST

Table 3.13. PRHR Instrument Names and Locations

| LDP, FMM, and HPS | | Thermocouples | |
|---|---|---|---|
| **Tag Name** | **Description** | **Tag Name** | **Description** |
| FMM-802 | PRHR Inlet Flow | TF-803 | PRHR HX Inlet Temperature |
| FMM-804 | PRHR Outlet Flow | TF-804 | PRHR HX Outlet Temperature |
| LDP-801 | PRHR HX Inlet Head Uncompensated Water Level | TF-805 | PRHR HX Long Tube Outlet at Bend Temperature |
| LDP-802 | PRHR HX WR Uncompensated Water Level | TF-806 | PRHR HX Short Tube Outlet at Bend Temperature |
| HPS-801-1 | PRHR HX Inlet Heat Transfer Coefficient | TF-808 | PRHR HX Short Tube Outlet at Center Temperature |
| HPS-801-2 | PRHR HX Inlet Heater dT Above Fluid Temperature | TF-809 | PRHR HX Long Tube at Center Temperature |
| HPS-801-3 | PRHR HX Inlet Fluid Temperature | TF-810 | PRHR HX Short Tube Inlet at Bend Temperature |
| | | TF-811 | PRHR HX Long Tube Inlet at Bend Temperature |
| | | TF-812 | PRHR HX Outlet Head Temperature |
| | | TW-801 | PRHR HX Long Tube Outlet |
| | | TW-802 | PRHR HX Short Tube Outlet |
| | | TW-803 | PRHR HX Long Tube Lower Mid-piece |
| | | TW-804 | PRHR HX Short Tube Lower Mid-piece |
| | | TW-805 | PRHR HX Short Tube Upper Mid-piece |
| | | TW-806 | PRHR HX Long Tube Upper Mid-piece |
| | | TW-807 | PRHR HX Short Tube Inlet |
| | | TW-808 | PRHR HX Long Tube Inlet |

### 3.7.5 Accumulators (ACC)

The two ACC tanks are constructed of a long piece of pipe with a pipe cap and a thick plate. The plate is cut to fit in one end of the pipe, and a pipe cap type end is used to seal the other end. Table 3.14 lists the instruments associated with the accumulators.

Table 3.14. Accumulator Instrument Names and Locations

| LDP, FMM, DP, and PT Cells | | Thermocouples | |
|---|---|---|---|
| **Tag Name** | **Description** | **Tag Name** | **Description** |
| DP-401 | ACC1 Injection DP | TF-401 | ACC1 Outlet Temperature |
| DP-402 | ACC2 Injection DP | TF-402 | ACC2 Outlet Temperature |
| FMM-401 | ACC1 Injection Flow | TF-403 | ACC1 $N_2$ Top Temperature |
| FMM-402 | ACC2 Injection Flow | TF-404 | ACC2 $N_2$ Top Temperature |
| LDP-401 | ACC1 Uncompensated Water Level | TF-405 | ACC1 Injection Line Temperature |
| LDP-402 | ACC2 Uncompensated Water Level | TF-406 | ACC2 Injection Line Temperature |
| PT-401 | ACC1 Pressure | | |
| PT-402 | ACC2 Pressure | | |

Each ACC is connected to a DVI line, and the fluid flow initiates from an ACC to its respective DVI line by means of a check valve (RCS-423/424), which opens when plant pressure becomes less than the pressure in the ACC. See Figure 3.18 for an image of an ACC.

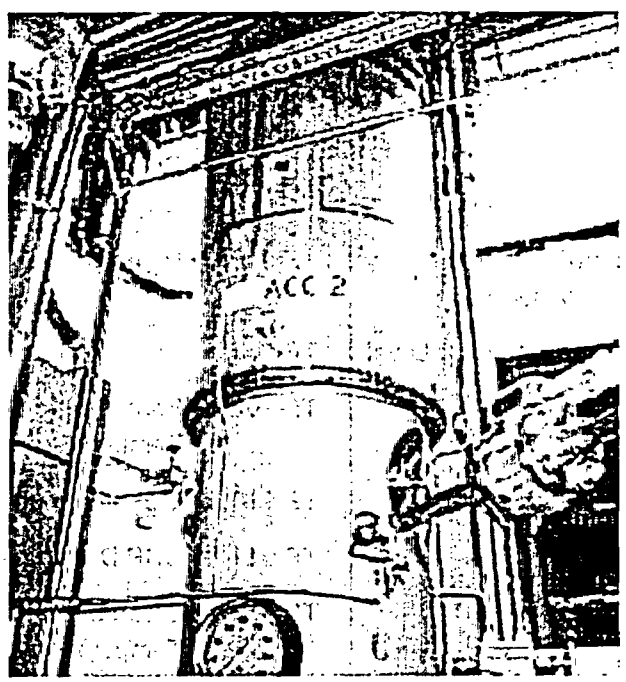


Figure 3.18. Photograph of One of the APEX Accumulators

### 3.7.6 Containment Sump

The primary containment sump tank is constructed of SS 304 plate, and the cylindrical section is capped with elliptical ends. The primary sump tank is connected to the ADS4 separators, the secondary sump, the break separator, DVI1 and 2, and the steam exhaust header. The sump collects all liquid flow from the break and ADS4 lines. Two containment sump recirculation lines are connected to the bottom of the primary sump and provide a recirculation path to the RPV via the DVI lines. Each line consists of an isolation valve with a parallel line with check valves. The isolation valves (CSS-909/910) open on decreasing IRWST level. A secondary sump is also provided to model containment sump volumes that are not available for long-term circulation. A curb overflow is simulated between the primary and secondary sumps by a weir plate. Table 3.15 lists the instruments associated with the primary and secondary sumps.

Table 3.15. Sump Instrument Names and Locations

| LDP, FMM, FVM, LCT, and PT Cells | | Thermocouples | |
|---|---|---|---|
| **Tag Name** | **Description** | **Tag Name** | **Description** |
| FMM-901 | Primary Sump-1 Recirculation Injection Flow | TF-901 | Primary Sump Inlet from Fill Line Temperature |
| FMM-902 | Primary Sump-2 Recirculation Injection Flow | TF-902 | Secondary Sump Bottom Temperature |
| FMM-905 | Break Separator Loop Seal Flow | TF-903 | Primary Sump Bottom Temperature |
| FVM-903 | Primary Sump Steam Exhaust Flow | TF-904 | Primary Sump/DVI2 Injection Line Temperature |
| LDP-901 | Primary Sump Uncompensated Water Level | TF-905 | Primary Sump @ Secondary Sump Crossover Level Temperature |
| LDP-902 | Secondary Sump Uncompensated Water Level | TF-906 | Primary Sump Exhaust Temperature |
| LDP-903 | CRT Uncompensated Water Level | TF-907 | Primary Sump @ Top Temperature |
| LDP-905 | Break Separator Uncompensated Water Level | TF-909 | Primary Sump/DVI1 Injection Line Temperature |
| PT-901 | Primary Sump Pressure | TF-910 | CRP Discharge to Primary Sump Temp |
| LCT-901 | Primary Sump Weight | TF-911 | CRP Discharge to IRWST Temperature |
| LCT-902 | Secondary Sump Weight | TF-912 | Break Separator Loop Seal Temperature |
| | | TF-913 | Break Separator Steam Outlet Temperature |
| | | TF-914 | CRT Outlet Temperature |

## 3.8 Instrumentation, Control, and Power Systems

This section describes the instrumentation, control, and power systems of the APEX test facility, as well as the data acquisition system, instrument devices, and associated control logic.

### 3.8.1 Instrumentation Description

The APEX test facility is equipped with approximately 600 instrument channels to capture the transient behavior of the safety systems. The APEX facility includes the following types of instrumentation channels:

- Thermocouples (TF/TR/TH/TW) are used to measure fluid, heater, and wall temperatures. Premium thermocouples with controlled purity thermocouple wire were incorporated.
- Magnetic flow meters (FMMs) are incorporated to measure single-phase liquid flows around the plant.
- Vortex shedding flow meters (FVMs) are used to measure single-phase vapor flow rates.
- Pressure transducers (PT) are used to measure the static pressures in various tanks and pipes within the facility.
- Differential pressure (LDP, DP) transducers are used to measure liquid levels in various tanks and pipes. The differential pressure cells are also used to measure pressure drops.
- Heated phase switches (HPSs) are used to determine the fluid phase at various points inside system piping. Each HPS measures fluid temperature, change in temperature ($\Delta T$) between the fluid and the heater, and a relative heat transfer coefficient.
- Load cell transducers (LCTs) are incorporated to measure the liquid mass inside the IRWST, primary sump, and secondary sump.
- Heater power (KW) to the core is measured with four power meters. The power applied to the PZR heaters is measured by an additional power meter.
- A level transducer (LT) capacitance probe is used to measure collapsed liquid level in the reactor vessel.

Instrumentation channels are subdivided into 10 different groups based on a particular location, using the numbering system described in Table 3.16.

Table 3.16. Instrument Tag Locations

| Channel Name | Location |
|---|---|
| xx-000s | Feed, Main Steam |
| xx-100s | Reactor Pressure Vessel |
| xx-200s | Primary Loop |
| xx-300s | SG |
| xx-400s | ACC |
| xx-500s | CMTs |
| xx-600s | PZR, ADS1–3 |
| xx-700s | IRWST |
| xx-800s | PRHR, CVS, RNS |
| xx-900s | Sump, ADS4-1, ADS4-2, and Break System |

### 3.8.2 Data Acquisition

The data acquisition system (DAS) writes the data into a single large database, as shown in Figure 3.19. Using a single database (rather than individual test files) offers the following advantages:

- improved management and maintenance
- enables retrieval to be independent of storage (i.e., the data are stored every second, but the database can be queried at another resolution, say every 5 seconds), which provides a very powerful and flexible retrieval capability
- easier comparisons between multiple tests

The DAS is manufactured by National Instruments (NI) and uses commercial off-the-shelf software. The signal type may be a 4–20 mA current signal, 1–5 VDC or 0–10 VDC voltage signal, or the millivolt signal originating from thermocouples. The instruments are connected to several terminal boards. Each terminal board can accept any combination of J-, K-, and T-type thermocouples and up to 32 channels of inputs with their own cold junction compensation. These terminal boards are also used for other types of signal inputs. Each terminal board is connected to one analog input module, which rests within a chassis that contains 12 modules. The DAS use three chassis to acquire the data. The signals from the chassis are then transferred to a computer that is equipped with a multifunction I/O board. Basically, the multifunction I/O boards switch their inputs between 622 channels at high speed to sample all input channels. The data for APEX are typically sampled at a rate of 1 Hertz per channel.

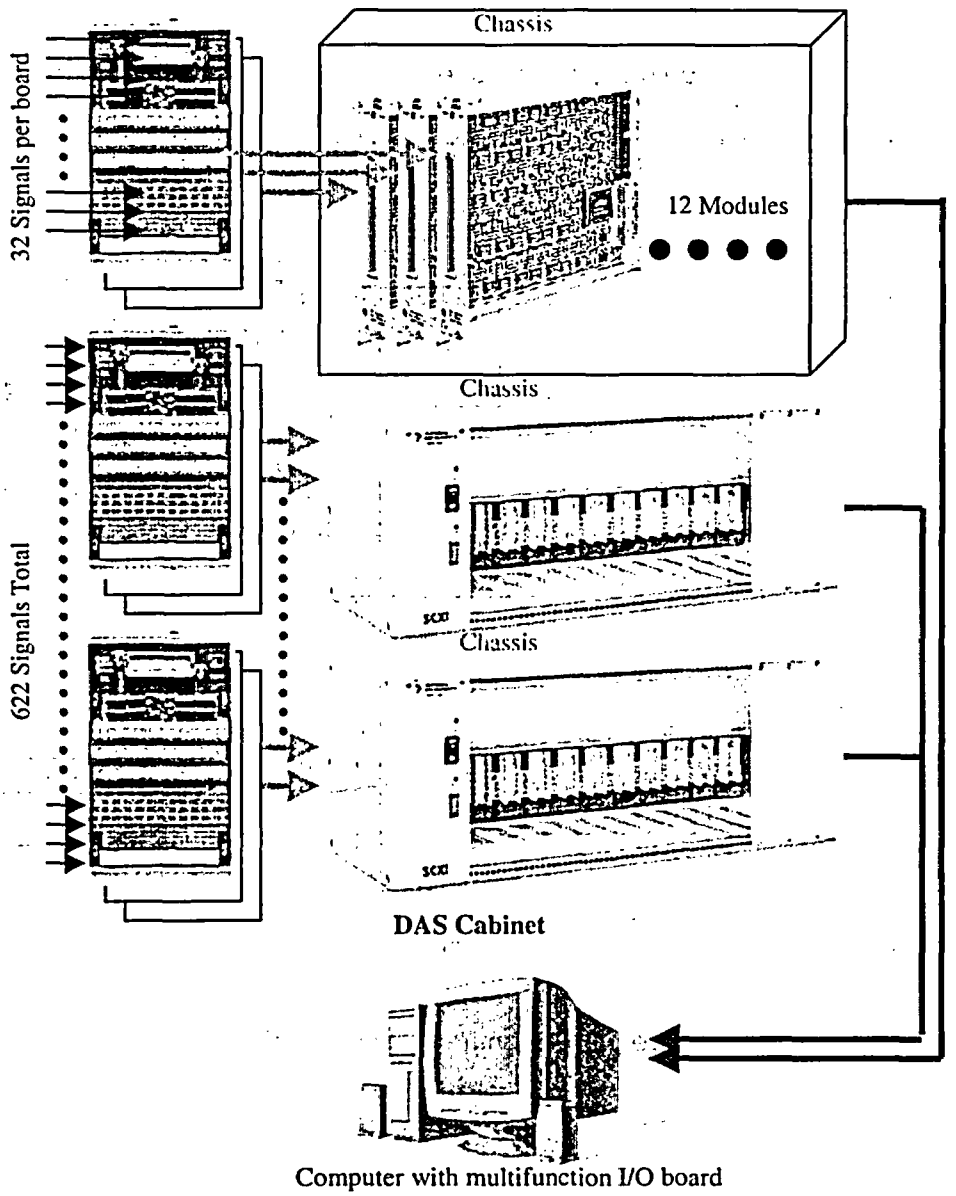


Figure 3.19. Data Acquisition System Hardware Overview

All of the data from input channels are acquired by NI-DAQ hardware/software and then converted into engineering units. The real-time data are sampled and stored in an NI Citadel database at one time per second per channel. Citadel is a proprietary database used for process data. OSU developed an export program to query the Citadel database and format the data file in ASCII text and NRC Data Bank binary file formats.

The NI DIAdem 8.1 trending software package is used to plot data for generating reports. DIAdem is capable of manipulating large data sets of more than a billion data points in up to 65,000 columns.

### 3.8.3 Control System and Control Logic

The APEX test facility control logic system includes various field process transmitters, operator switches, an OMRON programmable logic controller (PLC), a set of Fischer & Porter process controllers (PCs), and a supervisory host computer, as shown in Figure 3.20.

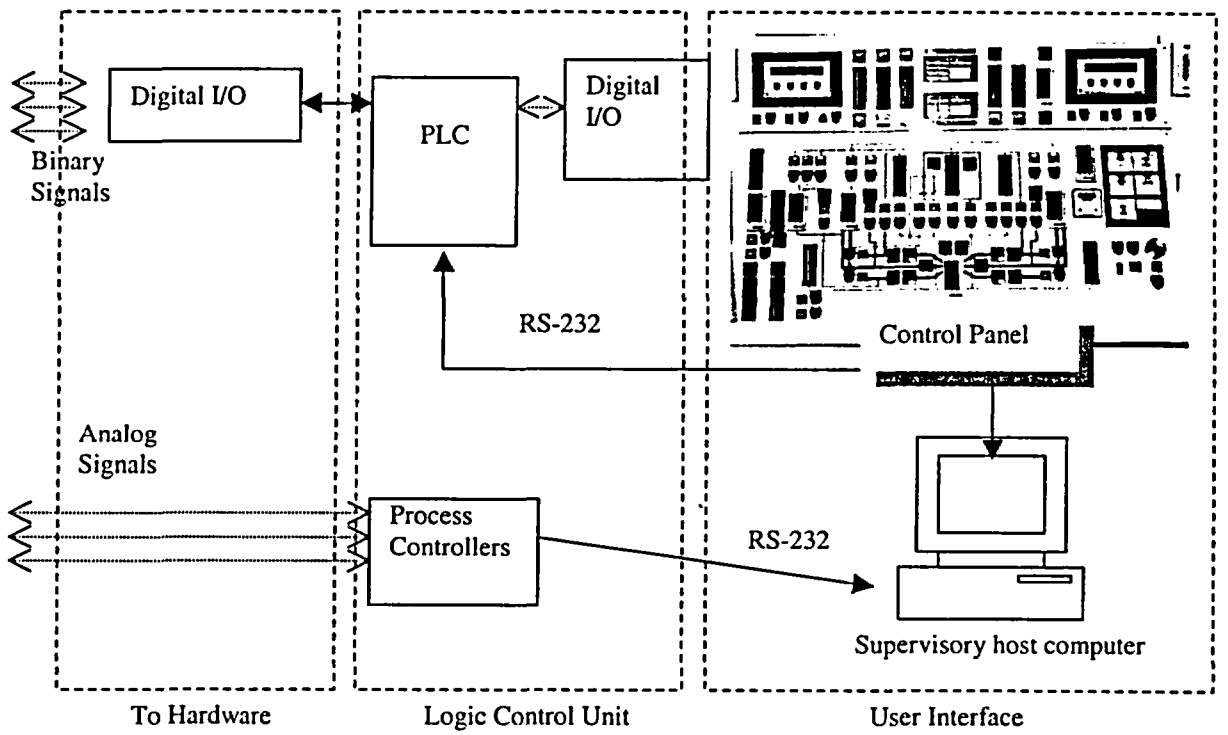


Figure 3.20. Control System Interface

The control system functions in three basic parts:

(1) The PLC performs all binary logic functions for safety, sequencing, and operational control.

(2) The PCs perform all dynamic (analog) process controls for smooth operation of variable control devices.

(3) The supervisory system provides a graphical computer interface between the operator and the facility.

The PLC consists of a central processor for program execution, a power supply, two local racks of digital I/O, and several remote I/O racks located throughout the facility. All inputs are sensed as 24-VDC signals. All outputs are driven by a 24-VDC supply to energize pneumatic valves, pump motor starters, control panel lights and alarms, and other components. Figure 3.21 is photograph of the APEX control panel.

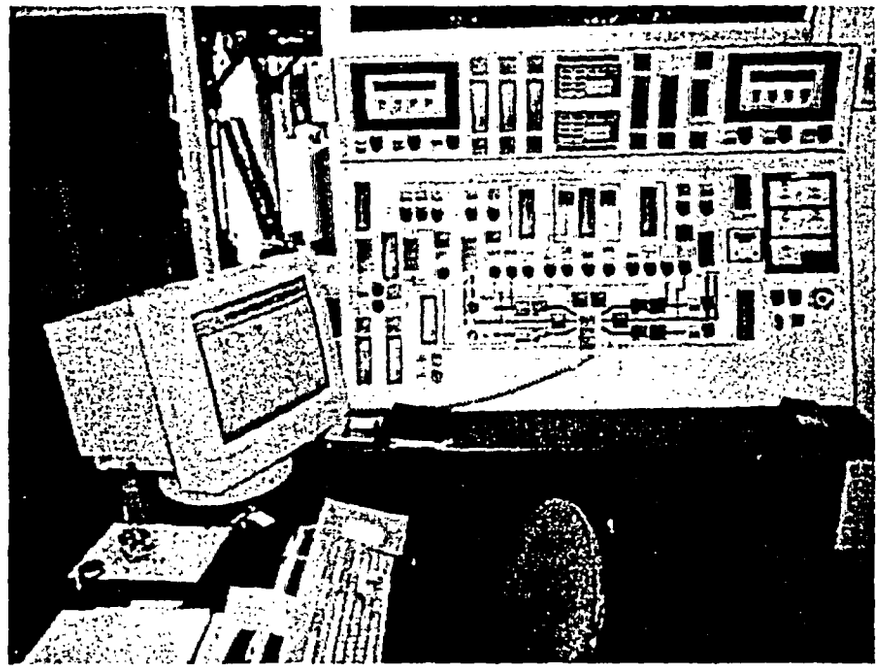

Figure 3.21. Photograph of the APEX Control Panel

The process control system consists of seven dedicated PCs with a total of 40 analog inputs and 20 analog outputs. Analog inputs are used to monitor the process, either directly or as calculated variables. They include tank level, system pressure, pump flow rate, and applied heater power. The controller performs a series of calculations to determine the likely state of the process and adjusts the analog output of the controlling device to maintain the process within defined parameters. The controlling devices include valves, power silicon control rectifiers (SCRs), and variable-speed pump controllers. The DAS and control computer are connected by a high-speed local area network.

The control system functions in three basic parts:

(1) The PLC performs all binary logic functions for safety, sequencing, and operational control.

(2) The PCs perform all dynamic (analog) process controls for smooth operation of variable control devices.

(3) The supervisory system provides a graphical computer interface between the operator and the facility.

The PLC consists of a central processor for program execution, a power supply, two local racks of digital I/O, and several remote I/O racks located throughout the facility. All inputs are sensed as 24-VDC signals. All outputs are driven by a 24-VDC supply to energize pneumatic valves, pump motor starters, control panel lights and alarms, and other components. Figure 3.21 is photograph of the APEX control panel.

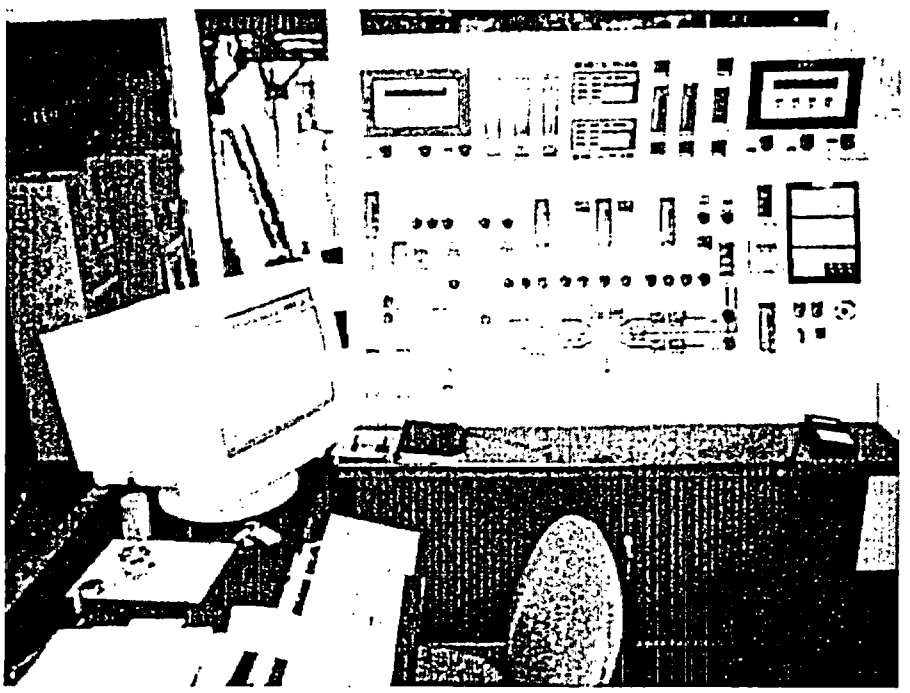

Figure 3.21. Photograph of the APEX Control Panel

The process control system consists of seven dedicated PCs with a total of 40 analog inputs and 20 analog outputs. Analog inputs are used to monitor the process, either directly or as calculated variables. They include tank level, system pressure, pump flow rate, and applied heater power. The controller performs a series of calculations to determine the likely state of the process and adjusts the analog output of the controlling device to maintain the process within defined parameters. The controlling devices include valves, power silicon control rectifiers (SCRs), and variable-speed pump controllers. The DAS and control computer are connected by a high-speed local area network.

There are six test logic routines implemented in APEX logic:

(1) Station Blackout Routine
(2) Small-Break Loss-of-Coolant Accident (LOCA) Routine
(3) Large-Break LOCA Routine
(4) Inadvertent ADS Initiation Routine
(5) Full-Pressure ADS Routine
(6) Natural Circulation Routine

### 3.8.4 Power System

The main purpose of the power system is to provide up to 1 megawatt of power to the reactor and PZR heater rods. Power comes from the local power grid at a voltage of 20,800 volts and is stepped down to a distribution voltage of 480 volts, three phase. From the 480-volt distribution power, one line (three-phase, max current ≈100A) is used for the pumps in the APEX facility (RCP1 to RCP4, MFP, CVSP, RNSP, CRP, and seal WTR fan). Another line (three-phase, max current ≈200A) provides the power for trace heaters. The three remaining lines are for the two Rx heater rod groups (three-phase, 500 kW max per line) and the PZR heater (three-phase, 20 kW max). Each of the heater power lines has the following components:

- 1 breaker to manually turn the power on/off
- 1 fuse for circuit protection
- 1 contactor to remotely turn the power on/off
- 1 phase angle-fired SCR to adjust the power level (SCR1 and SCR2 for Rx heater groups 1 and 2, SCR3 for the PZR heater)

During the test, the contactor controls the heater power (on/off), and the SCR signals are used to adjust the heater power level. The reactor heater rod SCRs, in conjunction with the heater controller, allow the APEX facility to simulate decay power by continually adjusting the reactor power level setpoint to follow the desired decay curve. See Figure 3.22 for a photograph of the SCR cabinet, and Figure 3.23 for a simplified sketch of the main power distribution system.

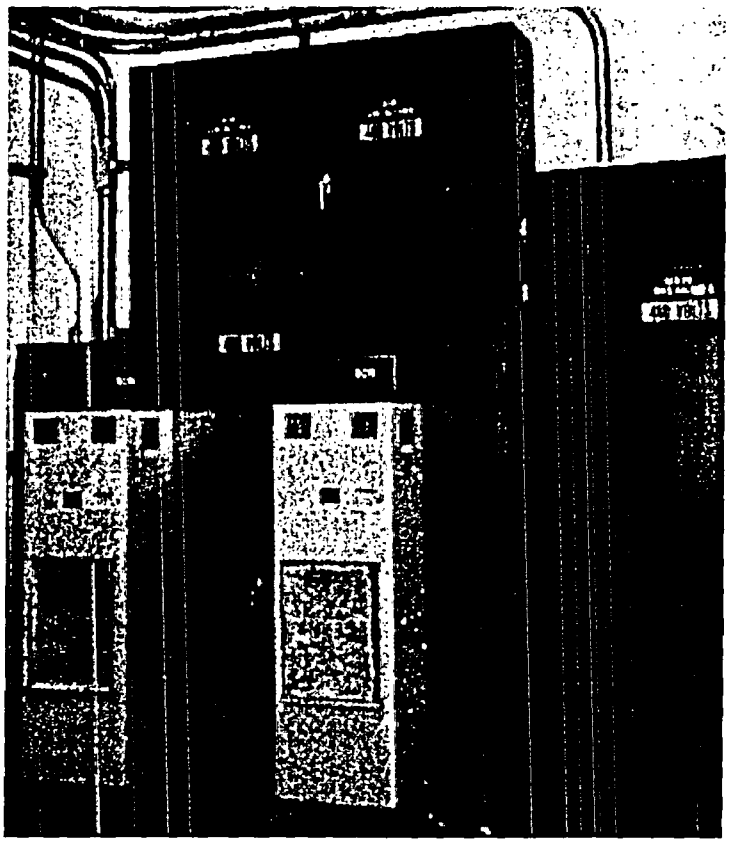

Figure 3.22. Photograph of the SCR Cabinet

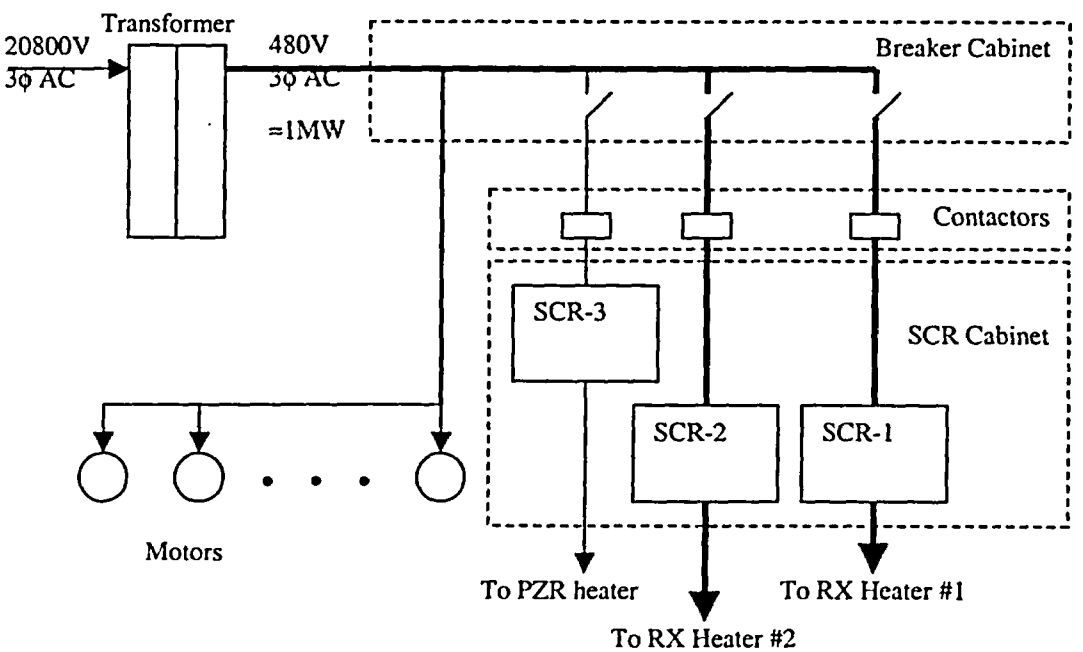


Figure 3.23. Main Power System Simple Layout

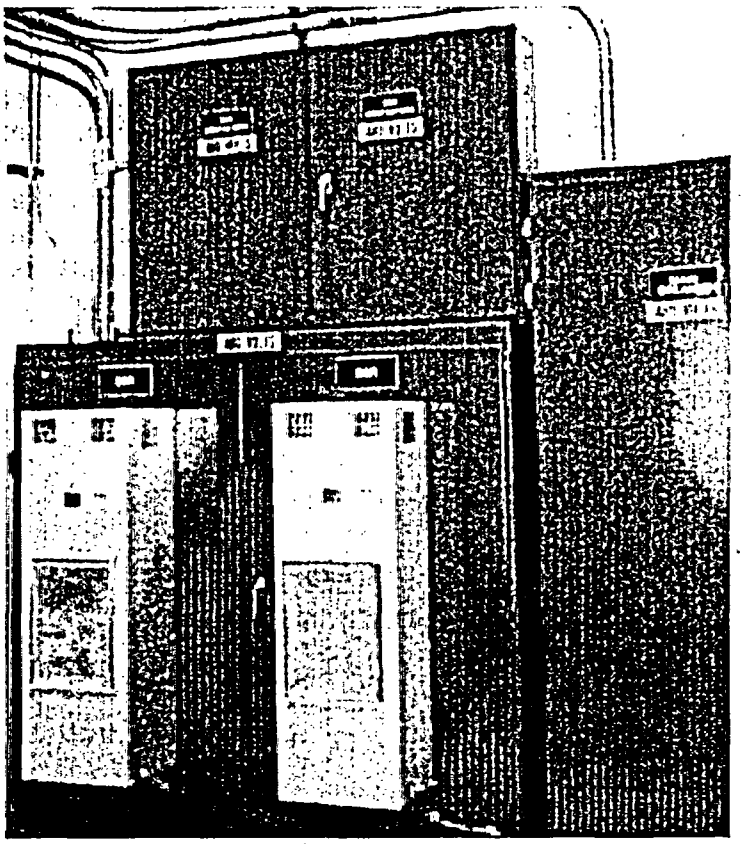

Figure 3.22. Photograph of the SCR Cabinet

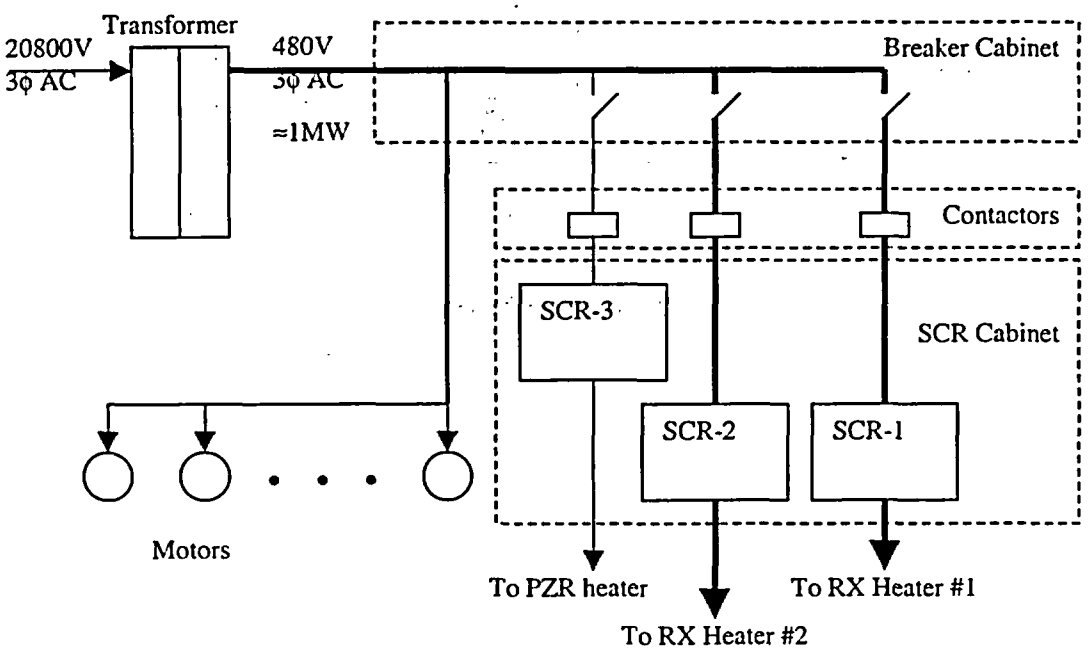


Figure 3.23. Main Power System Simple Layout

### 3.8.5 Break and ADS Measurement System (BAMS)

The BAMS, depicted in Figure 3.24, is used to measure two-phase volumetric flow rates from the break(s) and four stages of the ADS. All of the steam lines from the break separator, ADS4 separators, IRWST, and primary sump feed into the BAMS header and eventually vent via the exhaust header. All of the steam lines and moisture separators are heated with strip heaters to prevent condensation. Steam volumetric flow rate, pressure, and temperature are measured by vortex flow meters, pressure cells, and thermocouples respectively. Table 3.17 lists all instruments related to the ADS4-1/4-2 and break separator.

The BAMS system includes the following components:

- break separator
- two ADS4 separators
- ADS1–3 separator

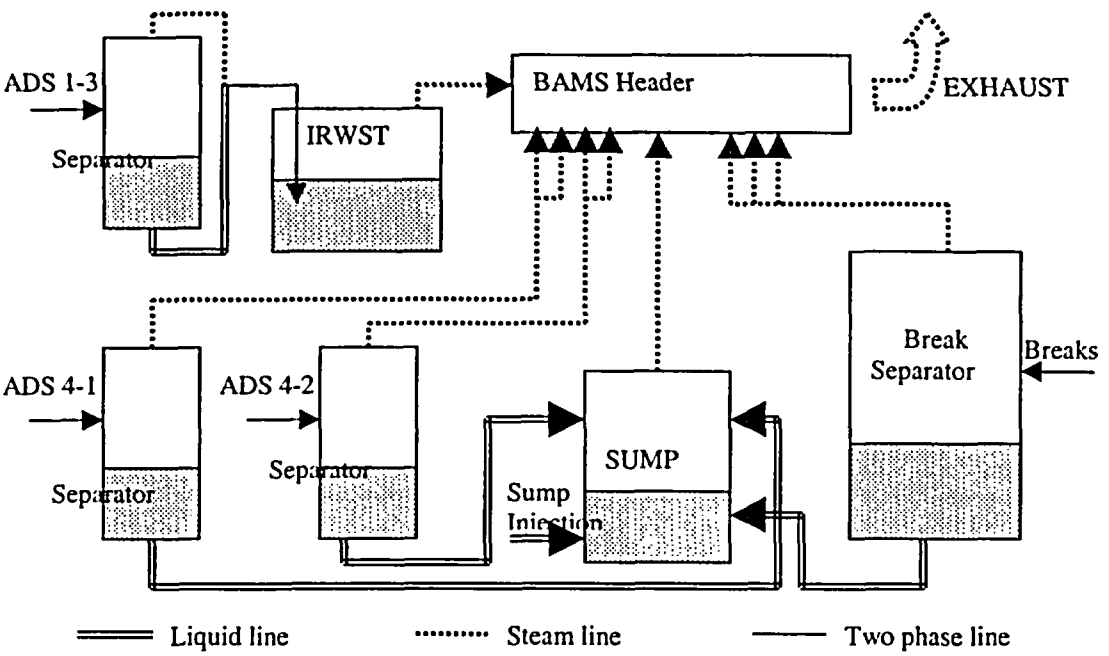


Figure 3.24. BAMS Layout

Table 3.17. ADS4-1/4-2, and Break Separator Instrument Names and Locations

| LDP, FVM, FMM, DP, and PT Cells | | Thermocouples | |
|---|---|---|---|
| Tag Name | Description | Tag Name | Description |
| DP-905 | Break Separator Entrance DP | TF-908 | Break Separator Inlet Temperature |
| FMM-905 | Break Separator Loop Seal Flow | TF-910 | CRP Discharge to Primary Sump Temperature |
| FVM-901 | BAMS HDR 6 in. Line Steam Flow | TF-911 | CRP Discharge to IRWST Temperature |
| FVM-902 | BAMS HDR 10 in. Line Steam Flow | TF-912 | Break Separator Loop Seal Temperature |
| FVM-904 | Break Separator 3 in. Line Steam Flow | TF-913 | Break Separator Steam Outlet Temperature |
| FVM-905 | Break Separator 6 in. Line Steam Flow | TF-914 | CRT Outlet Temperature |
| FVM-906 | Break Separator 8 in. Line Steam Flow | TF-915 | Break Separator 6 in. Steam Line Temperature |
| LDP-903 | CRT Uncompensated Water Level | TF-916 | BAMS Header 10 in. Steam Line Temperature |
| LDP-905 | Break Separator Uncompensated Water Level | TF-917 | BAMS Header Temperature |
| PT-902 | BAMS Header Pressure | TF-918 | Break Separator 8 in. Steam Line Temperature |
| PT-905 | Break Separator Pressure | TW-905 | Break Separator Wall Temperature |

The APEX test facility can model several different break locations:

- CL3 bottom break (TS-205 actuates)
- CL3 top break (TS-201 & T-205 both actuates)
- single-ended DVI break (TS-202 actuates, pressure equalization line open during warm-up, closed prior to break)
- single-ended CMT balance line break (TS-203 actuates, pressure equalization line open during warm-up, closed prior to break)
- HL2 bottom break (TS-204 actuates)
- CL4 bottom break (TS-206 actuates)
- double-ended CMT balance line break (TS-203 and TS-202 actuates)
- DEDVI break (TS-203 and TS-202 actuates)

The two-phase flow that exits the break is piped into the break separator. The primary purpose of the break separator is to separate the steam and liquid phase of two-phase flow for the convenience of measurement. Water/steam mixture enters through the middle and passes through a cyclone separator. The separated steam exits the top of the separator, while the liquid is collected and allowed to drain out of the bottom of the separator through a loop seal and into the primary sump. The wall of the separator is heated by a long strip heater to prevent steam condensation inside the separator.

The break separator steam outlet line is divided from a large pipe into three smaller parallel paths, which are recombined before the exhaust. The steam flow is routed through one of these three paths, depending on the expected flow rate. Each of these paths is controlled by an air-operated logic ball valve and measured by a vortex flow meter to control the separator liquid level within the desired range to contain the steam, while the liquid goes to the correct outlet. If the steam line size is too small for a given flow rate, the increased pressure will push the water out of the loop seal, and there will be a two-phase mixture in the liquid line (which cannot be measured). By contrast, if the selected steam line is too large, it is difficult to obtain an accurate measure of the steam flow rate because it is too small. The ADS4 separator steam line has a similar design, but uses only two paths. The primary and secondary sumps are used to simulate the containment.

The two ADS4 separators are similar in design to the break separator. The steam exiting the separators can be directed through one of two different sized pipes, depending on the expected flow rate. The reasoning behind the use of different size steam lines is the same as for the flow from the break separator. The liquid phase from each ADS4 separator is collected and directed through a loop seal and into the primary sump.

The ADS1–3 separator is a large cylinder. The exiting two-phase mixture flow from ADS1–3 valves is directed into the ADS1–3 separator through an inlet. The liquid flow exits the bottom of the separator, while the steam flow exits the separator via a different pipe located at the opposite side of the inlet. The steam volumetric flow rate is measured by a vortex flow meter (FVM-601). Liquid phase is directed out of the separator via a pipe at the bottom of the separator and measured by a magnetic flow meter. The steam and liquid phases are finally recombined and injected into the IRWST via a sparger.

In the prototype, the steam phase that exits the break condenses on the containment wall and drains back to the IRWST or sump. In the test facility, the steam phase is vented to the atmosphere. To compensate for the mass loss attributable to steam exhaust to the atmosphere, the containment condensate return system is available to inject fluid into the IRWST or sump at the same mass flow rate of the vented steam if desired. The condensate return system is fed by the feedwater storage tank (FST) into the condensate return tank (CRT) in which the water is preheated. The CRT contains heaters to preheat the water prior to injection into the IRWST or the primary sump. The outlet water temperature is measured by a thermocouple, and the measurement is feedback to the CRT heaters to maintain the proper outlet temperature. The liquid is pumped from the CRT by means of the condensate return pump (CRP) through either a recirculation line with the line resistance controlled by an orifice plate, or the IRWST or primary sump via motor-operated valves (CCS-928/927).

## 3.9 Balance of Plant

The APEX-AP1000 facility incorporated several of the AP1000 non-safety systems, including the CVS, RNS, SG, feedwater system, main steam system, and water purification system. These non-safety systems were designed and constructed to meet the necessary functional requirements for testing. The pipe routings and relative locations within the APEX facility are not necessarily prototypic of the AP1000 design.

### 3.9.1 Chemical and Volume Control System (CVS)

The CVS is used to maintain proper water chemistry in the primary coolant for a full-sized plant. The CVS pump is a Goulds 3-stage centrifugal pump. See Table 3.18 for a list of instruments related to the CVS. In the APEX facility, the CVS pump is used for the following five main purposes:

(1) maintenance of fluid during startup
(2) modeling AP1000 operation if desired
(3) normal supply of makeup water to the APEX facility
(4) hydrostatic testing
(5) backup pump for the main feedwater pump (MFP)

Table 3.18. CVS Instrument Names and Locations

| FMM, PT Cells, and Thermocouples | |
|---|---|
| **Tag Name** | **Description** |
| FMM-801 | CVS Discharge Flow |
| PT-801 | CVS Discharge Pressure |
| TF-801 | CVS Discharge Temperature |

### 3.9.2 Normal Residual Heat Removal System (RNS)

The RNS pump draws water from the IRWST or primary sump, injects it into the DVI line, and provides makeup water under low-pressure conditions. The RNS pump is used to fill the CMTs and ACCs before performing a test. See Table 3.19 for a list of instruments related to the RNS.

Table 3.19. RNS Instrument Names and Locations

| FMM and PT Cells | | Thermocouples | |
|---|---|---|---|
| **Tag Name** | **Description** | **Tag Name** | **Description** |
| FMM-803 | RNS to DVI2 Flow | TF-802 | RNSP Discharge Temperature |
| FMM-805 | RNS Discharge Flow | TF-813 | RNSP Discharge to DVI1 Temperature |
| PT-802 | RNS Discharge Pressure | TF-814 | RNSP Discharge to DVI2 Temperature |

Figure 3.25 depicts the performance curve for the RNS pump [CR4-100N (5.0 HP (3.73 kW))].

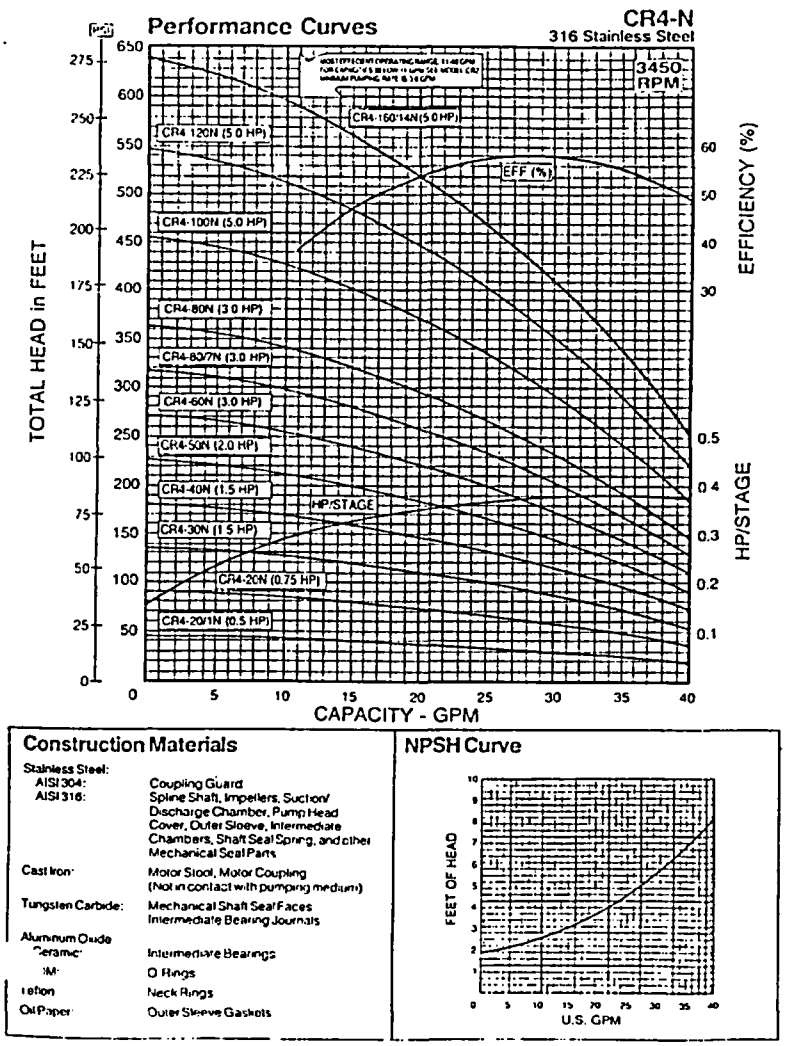


Figure 3.25. RNS Pump Performance Curves

### 3.9.3 Feedwater System

The purpose of the feedwater system is to provide water to the SG. The feedwater system consists of the demineralization system (DI), FST, and MFP, as shown in Figure 3.26. The FST stores water from the DI. Table 3.20 lists all instruments related to the FST, MFP, and SG steam vent.

For the main feed flow path, the MFP takes water from the FST and pumps it into both SGs. The MFP is a Goulds 3-stage centrifugal pump. The pump curve is at the end of this section. There is a magnetic flow meter (FMM-001 or FMM-002) and a motor-driven valve (MF-011 or MF-012) in each feed line (respectively) to monitor and control the feedwater flow.

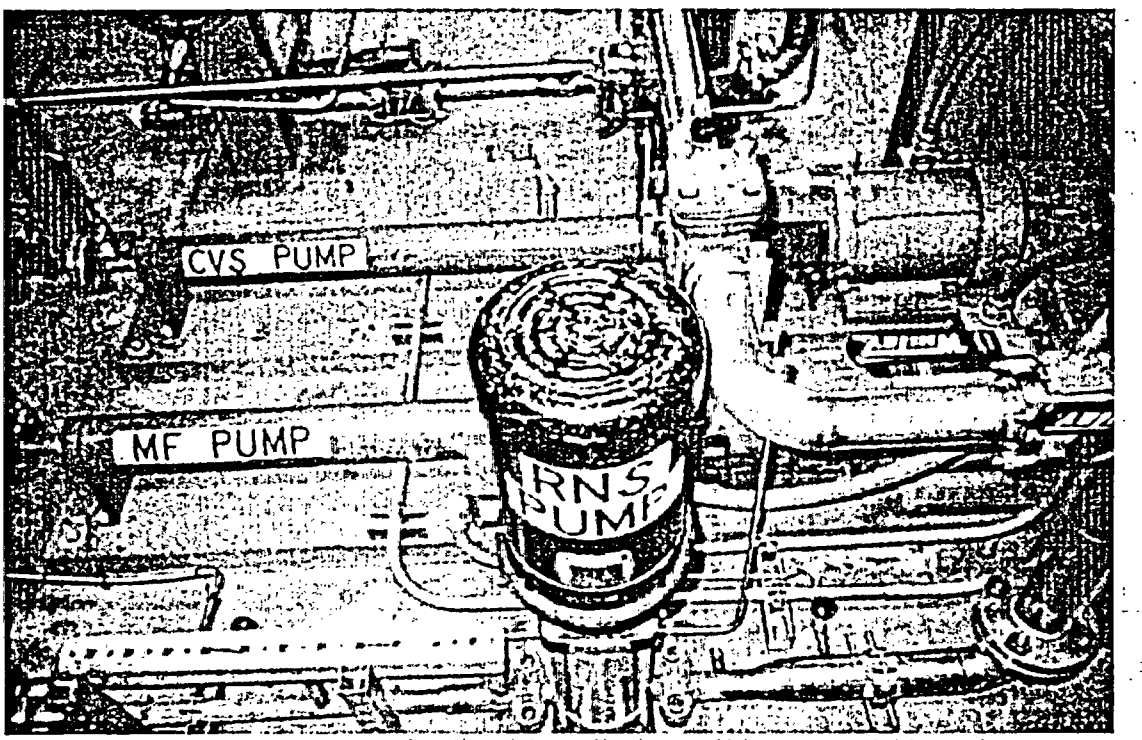


Figure 3.26. Image of RNS, CVS, and MF Pumps

When the steam exits the SG, there are two possible paths for it to follow:

(1) One path is controlled by a normally open air-operated ball valve (MS-001 for SG1 and MS-002 for SG2) and monitored by a vortex flow meter (FVM-001 for SG1 and FVM-002 for SG2).

(2) The other path is controlled by a normally closed air-operated ball valve (MS-009 for SG1 and MS-010 for SG2) and monitored by a vortex flow meter (FVM-009 for SG1 and FVM-010 for SG2).

Both of these lines will eventually exit the building through the steam exhaust. The difference between the two lines is that the first goes through the turbine simulation path with a motor-operated logic ball valve (MS-008) and monitored by a vortex flow meter (FVM-003), while the other is used for startup of the facility.

Table 3.20. FST, MFP, and SG Steam Vent Instrument Names and Locations

| LDP, FMM, FVM, and PT Cells | | Thermocouples | |
|---|---|---|---|
| **Tag Name** | **Description** | **Tag Name** | **Description** |
| FMM-001 | SG1 Feed Flow | TF-005 | Lab Ambient Temperature @ Ground Level |
| FMM-002 | CL2 Loop Flow | TF-006 | Lab Ambient Temperature @ 2nd Level |
| FVM-001 | SG1 Main Steam Flow | TF-007 | Lab Ambient Temperature @ 3rd Level |
| FVM-002 | SG2 Main Steam Flow | TF-009 | SG1 PORV Line Temperature |
| FVM-003 | Main Steam Combined Flow | TF-010 | SG2 PORV Line Temperature |
| FVM-009 | SG1 PORV Steam Flow | TF-301 | TF-301/SG1 (via Signal Conditioner) |
| FVM-010 | SG2 PORV Steam Flow | TF-310 | TF-310/SG2 (via Signal Conditioner) |
| LDP-001 | FST Level | TF-311 | SG1 Feed Header Temperature |
| PT-001 | MFP Discharge Pressure | TF-312 | SG2 Feed Header Temperature |
| PT-002 | MS Header Pressure | | |
| PT-003 | Lab Barometric Pressure | | |
| PT-009 | SG1 PORV Line Pressure | | |
| PT-010 | SG2 PORV Line Pressure | | |
| PT-301 | SG1 Pressure | | |
| PT-302 | SG2 Pressure | | |

### 3.9.4 Water Purification System

The water for the feedwater system comes from potable water. The DI purifies the incoming potable water for use in the secondary loop. The water first passes through two parallel resin traps (resin traps 1 and 2). It is then demineralized by four demineralization tanks, which are arranged into two parallel groups (demineralization banks 1 and 2). The water then passes through two additional resin traps (resin traps 3 and 4). The flow rate is then measured by a vortex flow meter (FVM-004), and an injection line then allows chemicals to be injected from a chemical addition tank. The chemicals that are added to the water include ammonium hydroxide ($NH_4OH$) and NALCO 1254. Ammonium hydroxide is used to reduce the pH in the system and to minimize corrosion of the components. NALCO 1254 is an additive that prevents buildup of sludge within the system. After all treatments, the feedwater is sent to the FST.

# 4. TEST MATRIX AND OVERVIEW

Eight NRC-sponsored beyond-DBA tests (listed in Table 4.1) were run at the APEX-AP1000 facility to confirm safety margins to support AP1000 design certification. Based on experience from previous AP600 design certification activities, these tests focused on DEDVI line breaks with various failures of the ADS.

Of the 8 beyond-DBA tests, three (NRC-AP1000-01, 03, and 05) considered DEDVI line breaks with failure of the ADS1, 2, and 3 valves, and ADS4 valves on the PZR and non-PZR sides of the plant. Two CL break tests (NRC-AP1000-04 and 06) were run to examine the sensitivity of ADS4 valve failure with respect to a smaller size breaks than a DEDVI line break. A Probabilstic Risk Assessment verification test (NRC-AP1000-10) and station blackout test (NRC-AP1000-11) were run to complete the confirmatory test matrix. Finally, a Mode 5 operation test (NRC-AP1000-02) was run with the ACCs and CMTs unavailable. Appendix C presents detailed time transient plots, sequence of events, and facility configurations for each test. These beyond-DBA tests were selected, based on previous experience with the AP600 design certification, as the scenarios which would potentially be the most challangeing to the AP1000 passive safety systems.

In addition, three upper plenum steady-state entrainment tests (NRC-AP1000-07, 08, and 09) were run to provide data for thermal-hydraulic code assessment, but those tests are not discussed in this report. Please note that all transient plots presented in this section are plotted against dimensionless time.

Table 4.1. APEX-AP1000 Confirmatory Test Matrix

| Test Number | Description | Date Completed |
|---|---|---|
| NRC-AP1000-01 | **DEDVI Line Break with Failure of ADS1, 2, and 3.**<br>Both ADS4 trains fully functional. | 6/5/03 |
| NRC-AP1000-02 | **Mode 5 Operation with Loss of RNS Cooling.**<br>No break. ADS1, 2, and 3 open. SG secondary side assumed drained. CMTs and ACCs unavailable or failed (one valve on PZR side available). | 9/30/04 |
| NRC-AP1000-03 | **DEDVI Line Break with Failure of 2 of 4 ADS4 Valves on PZR side.**<br>ADS1, 2, and 3 valves fully functional. | 6/11/03 |
| NRC-AP1000-04 | **CL #4, 1" Break with Failure of 1 of 4 ADS4 Valves on non-PZR side.**<br>ADS1, 2, and 3 valves fully functional. Containment sump degraded (CMT#1, ACC #1, sump recirculation line #1 and IRST line #1 unavailable). | 10/9/03 |
| NRC-AP1000-05 | **DEDVI Line Break with Failure of 2 of 4 ADS4 Valves on non-PZR side.**<br>ADS1, 2, and 3 valves fully functional. | 6/10/03 |
| NRC-AP1000-06 | **CL #4, 2" Break with Failure of 2 of 4 ADS4 Valves on non-PZR side and PRHR.**<br>ADS1, 2, and 3 valves fully functional. | 8/15/03 |
| NRC-AP1000-07* | **Upper Plenum Entrainment Test with Upper Internals Installed.**<br>Core inventory allowed to boil-off from top of hot legs to top of core. Three different power levels were run. | 8/24/04 |
| NRC-AP1000-08* | **Upper Plenum Entrainment Test with Modified Power Stepping.**<br>Repeat of NRC-AP1000-07 with additional power steps. | 9/7/04 |
| NRC-AP1000-09* | **Upper Plenum Entrainment Test with Upper Internals Removed.**<br>Core inventory allowed to boil-off from top of hot legs to top of core. Three different power levels were run. | 9/16/04 |
| NRC-AP1000-10 | **PRA Verification Test.**<br>Bottom of CL #4, 2" break with failure of 1 of 4 ADS4 valves on non-PZR side and failure of ADS1, 2, and 3 valves. | 4/29/04 |
| NRC-AP1000-11 | **Station Blackout.**<br>No break. Failure of 1 of 4 ADS4 valves on non-PZR side. | 7/29/04 |

*Not discussed in this report

## 4.1 Typical Sequence of Events for an APEX-AP1000 SBLOCA

This section presents the typical sequence of events for a small break (SB) LOCA scenario in the APEX-AP1000 test facility [Ref. 3]. The AP1000 safety logic (Appendix B) was closely modeled in the APEX test facility. Each SBLOCA test was initiated from steady-state operating conditions and started by opening a valve located on the primary loop piping. For SBLOCAs, the bottom of CL4 was typically chosen as the break location. Fluid flow from the break was directed to the break separator, where the vapor and liquid flows were measured separately. The vapor flow was then directed to the BAMS header, and the liquid flow to the primary sump. The SBLOCA scenario can be divided into five different phases, as shown in Figure 4.1 [Ref. 3]:

(1) High-Pressure Blowdown
(2) Natural Circulation
(3) ADS Blowdown
(4) IRWST Injection
(5) Sump Recirculation

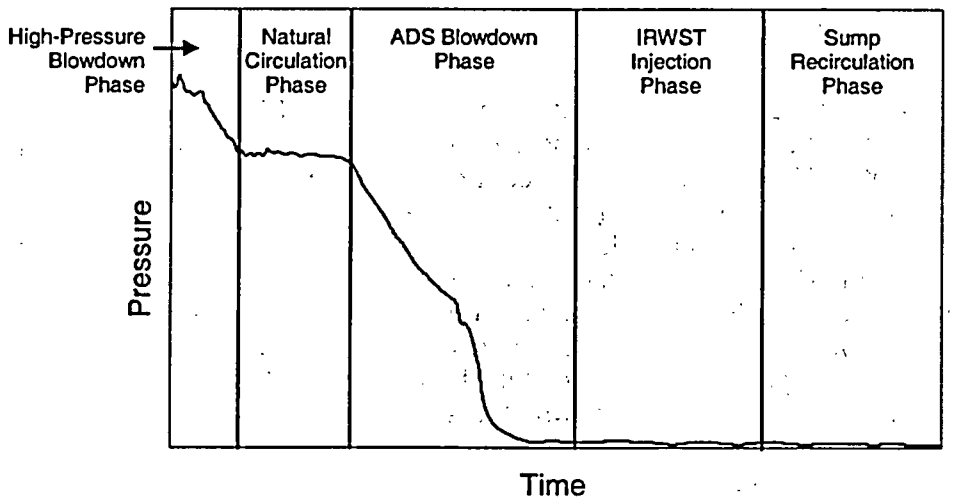


Figure 4.1 Pressure History for a Typical 2-inch Cold Leg Break in APEX [Ref. 3]

### 4.1.1 High-Pressure Blowdown Phase

The break in the primary loop caused a rapid initial blowdown of the system. Depending on the break size, this period was relatively short. As the PZR level decreased, it caused the issuance of an "S signal," which generated the following actions:

- PRHR isolation valves opened
- CMT isolation valves opened
- feedwater pump tripped
- steam generator steam flow isolated
- reactor coolant pumps tripped
- reactor power in decay mode to simulate a reactor scram

As the system blowdown continued, saturated conditions were reached in the HLs. The onset of saturated conditions in the HLs concluded the high-pressure blowdown phase.

### 4.1.2 Natural Circulation Phase

When the RCPs were tripped, the primary loop flow transitioned from forced to natural circulation. This natural circulation flow continued until voiding occurred in the primary side of the SG tubes. Operation of the PRHR and CMTs created additional paths for buoyancy-driven core heat removal. Water from the HL/ADS4 line connection rose to the PRHR inlet header and traveled through the PRHR HX. The cold water leaving the PRHR HX flowed to the CLs. In a similar manner, each CMT provided cooling to the core by recirculating its volume. Relatively hot water from the CLs rose into the CMT-PBL to the CMT's upper head. The hot water then displaced the cold water leaving the CMTs into the DVI injection line and finally into the RPV.

As the facility depressurized, steam collected or formed as a result of flashing in the CMT's upper head. This caused the CMT to drain and ceased the recirculation mode. In some cases, the CMTs partially refilled as a result of steam condensation. Eventually, the liquid level in the CMT reached the ADS1 actuation setpoint. The natural circulation phase of the transient concluded upon ADS1 actuation.

### 4.1.3 ADS Blowdown Phase

Both trains of the AP1000 ADS1–3 lines located on the top of the PZR were modeled in APEX. The flow nozzles used in the ADS lines were scaled to simulate choked flow, assuming pressure similitude subsequent to ADS3 actuation. The control logic opened ADS1, ADS2, and ADS3 in sequence. The ACCs typically began to inject sometime during ADS1–3 blowdown. The large flows caused by ACC injection typically delayed CMT draining. After ACC injection flow rates became low enough, the CMTs continued to drain. Eventually, the CMT liquid level dropped to the ADS4 actuation setpoint. APEX simulated both trains of the AP1000 ADS4 lines. After ADS4 actuation, the primary system depressurized to atmospheric conditions. This permitted the IRWST check valves to open in response to the hydrostatic head of the IRWST liquid. The onset of IRWST injection concluded the ADS blowdown phase.

### 4.1.4 IRWST Injection Phase

Upon IRWST injection, the liquid in the reactor core became subcooled. This condition persisted until the level in the IRWST was relatively low. At that time, the reduced IRWST injection flow rate was no longer sufficient to keep the core fluid subcooled. When saturated conditions were reached at the core exit, oscillations were observed in the IRWST injection flow, system pressure, RPV level, and ADS4 flow. These oscillations are an artifact of the APEX primary to secondary sump connect, were labeled "Return to Saturation Oscillations" (RSOs) in the APEX-AP600 confirmatory testing program, and became the subject of a separate parametric test. In the APEX-AP1000 and APEX-AP600 tests, these oscillations did not impact core cooling because the RPV liquid level always remained near the top of the HL. When the liquid level in the IRWST reached the sump recirculation setpoint, the sump recirculation valves opened. The oscillations were terminated at this time, and the IRWST injection phase concluded.

### 4.1.5 Sump Recirculation Phase

The sump recirculation phase marked the beginning of long-term cooling. Liquid from the primary sump flowed through the sump recirculation lines into the DVI lines and then into the RPV. The boiling in the core provided the density differences required to draw the water from the sump to the RPV. Steam generated in the core was vented through the ADS4 lines. Sump recirculation usually continued for 30 minutes until terminated by the operator, thus concluding the test. In some cases, the sump recirculation phase continued longer when a degraded sump was simulated.

## 4.2 Test NRC-AP1000-01

Test NRC-AP1000-01 simulated a DEDVI line break with a complete failure of ADS1, 2, and 3. This test was designed as a beyond-DBA scenario because of the multiple valve failures. All four ADS4 valves were available, and this test investigated the ability of the ADS4 system to accomplish system depressurization to allow for IRWST injection. The PRHR HX was inactive during this test.

The APEX-AP1000 facility models both trains of the AP1000 ADS1–3 lines located at the top of the PZR after a nozzle that models the scaled choked flow area of the AP1000. The ADS1–3 valve train typically discharges to the ADS1–3 separator, where the two-phase flow is separated and measured.

Figure 4.2 illustrates the facility configuration during this test and contains non-dimensional plots of RPV-wide collapsed liquid level, passive safety system injection flow rates (sides 1 and 2), and core heater rod temperatures. The DEDVI Line 1 break opened at zero seconds and created a rapid depressurization, which caused the CMTs to begin injection immediately. However, half of this makeup flow exited the DVI Line 1 break. As the facility depressurized, steam collected or formed as a result of flashing in the CMT's upper head. This caused the CMT to drain, terminating the natural recirculation phase of the transient. The ACCs typically begin injecting during ADS1–3 actuations, but since ADS1–3 were failed shut, ACC2 began injecting around time 1. When the liquid level in the CMTs was low enough, ADS4-1 opened and helped to depressurize the plant even further. After the ADS4 valves opened, CMT2 and ACC2 injection flow rates increased significantly. The reactor vessel collapsed liquid level remained approximately constant during ACC and CMT injection (between time 2.7 and 8) as the plant was depressurized using the ADS.

At around time 7, the plant reached atmospheric conditions. This permitted the IRWST check valves to open in response to the hydrostatic head of the IRWST liquid, thus ending the ADS blowdown phase of the transient. It should be noted that there was a noticeable overlap between when CMT2 injection flow ended and IRWST injection began, which provided adequate core cooling during this time period. As IRWST injection flow increased, the vessel collapsed liquid level began to rise around time 10. Later in the test (around time 14), CMT1 experienced short periods of refill as a result of condensation-induced pressure drops, which is an artifact of the one-quarter height scaling. For the remainder of the test, the HL water level remained high, and the core remained covered as a result of adequate injection flow from the IRWST. The test was ended before sump recirculation or long-term cooling was initiated. No heater rod high-temperature excursion was experienced, and the core remained adequately cooled during the entire test.

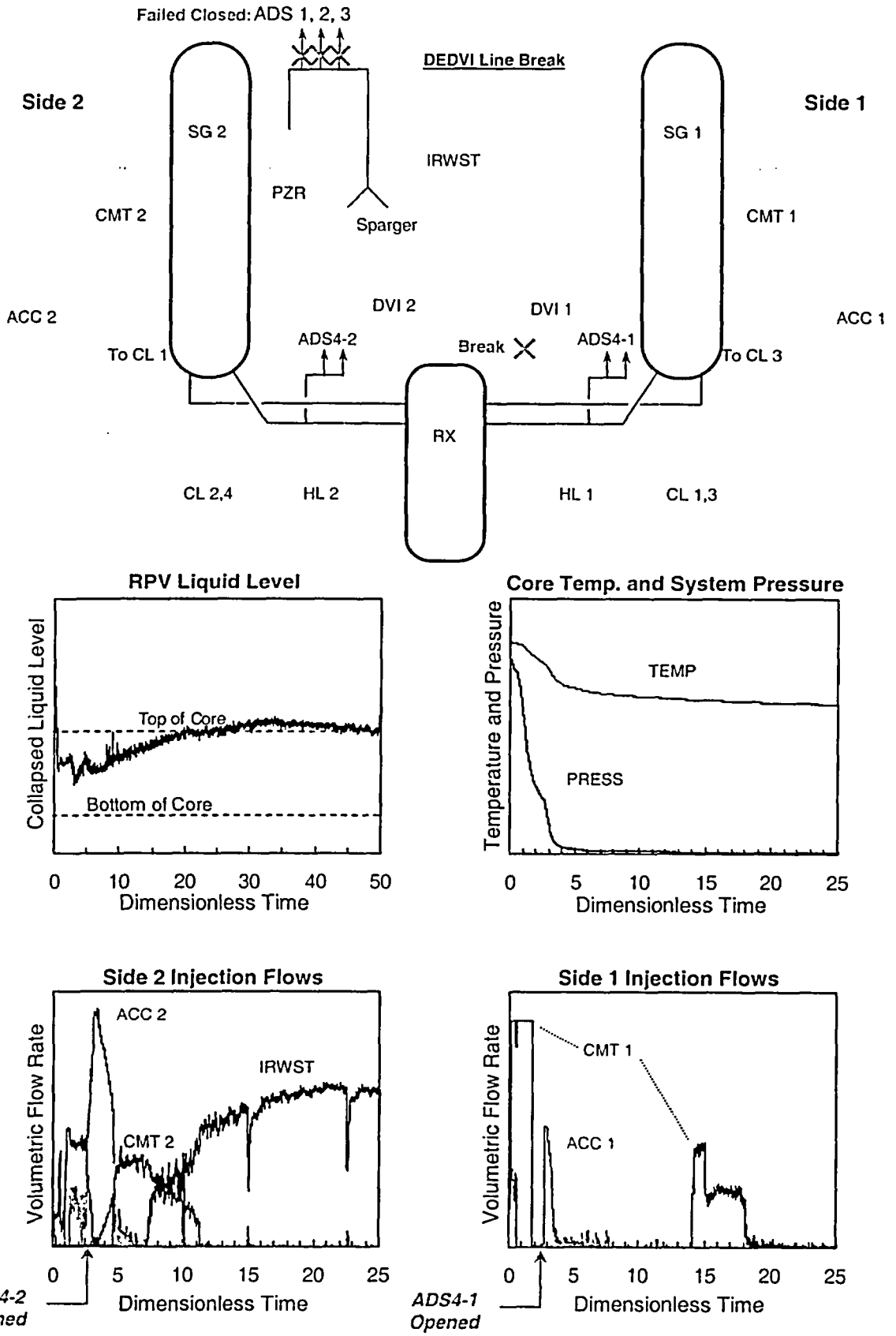


Figure 4.2 Test NRC-AP1000-01 Passive Safety System Performance.

## 4.3 Test NRC-AP1000-02

Test NRC-AP1000-02 investigated passive safety system performance during Mode 5 (cold shutdown) operation with a loss of the RNS. The objectives of this test were to determine system behavior during a loss of shutdown cooling. Specifically, if the RCS would pressurize sufficiently to prevent IRWST injection, and if counter-current flow limitation (CCFL) prevent the PZR from draining. There was no break in this test; ADS3 was opened at zero seconds (simulated two trains of ADS1, 2, and 3 in AP1000), the SG secondary side was assumed drained, the CMTs and ACCs were unavailable, and one ADS4 valve was failed closed. Power was increased to about 120 kW at the beginning of the test.

Figure 4.3 illustrates the facility configuration during this test, and contains non-dimensional plots of RPV-wide collapsed liquid level, IRWST injection flow rates, core heater rod temperatures, and PZR wide-range collapsed liquid level. The test was begun at zero seconds when the reactor power was at 120 kW to simulate a loss of RNS cooling. As water boiled off from the core and exited through the open ADS3 line, the RPV collapsed liquid level dropped to below the top of the core at around time 5. The ADS4-1 valve (non-PZR HL) failed to open on demand at around time 9.7 and decreased the RPV pressure to allow for IRWST injection. By time 10.2, the RPV collapsed liquid level rose above the top of the core and remained high until around time 20. The PZR completely drained just after IRWST injection began at around time 10. At about time 30, the sump recirculation valves were opened on low IRWST level, thus ending the IRWST injection phase, and the long-term cooling began. The core remained adequately cooled during the entire test.

## 4.4 Test NRC-AP1000-03

This test was a DEDVI line break with failure of two of the four ADS4 valves on the PZR side of the plant. The purpose of this test was to investigate the sensitivity of ADS4 valve failure on core coolability. Figure 4.4 shows the plant configuration for this test and plots of safety injection flow rates (sides 1 and 2), along with reactor vessel collapsed liquid level, and core temperature.

The break in DVI1 was opened at time zero, and the CMTs began injecting immediately as the primary system rapidly depressurized. As the CMTs emptied, the ADS1–3 valves began to actuate, beginning the ADS blowdown phase of the transient. Shortly after, ACC2 began injecting. The ADS4-1 valves opened just after time 1.7 to reduce the plant pressure to allow for IRWST injection, thus ending the ADS blowdown phase. IRWST injection began around time 14, while CMT2 injection ended around time 10. Between time 10 and 14, no makeup water was provided to the core.

As water was injected into the core from the IRWST, the core level increased. Eventually, the IRWST finished draining, and the plant successfully entered sump recirculation for long-term cooling around time 75. During the test, core temperature spiked a few times for very brief periods, but enough water was provided from the passive safety systems to keep the core adequately cooled throughout the entire test.

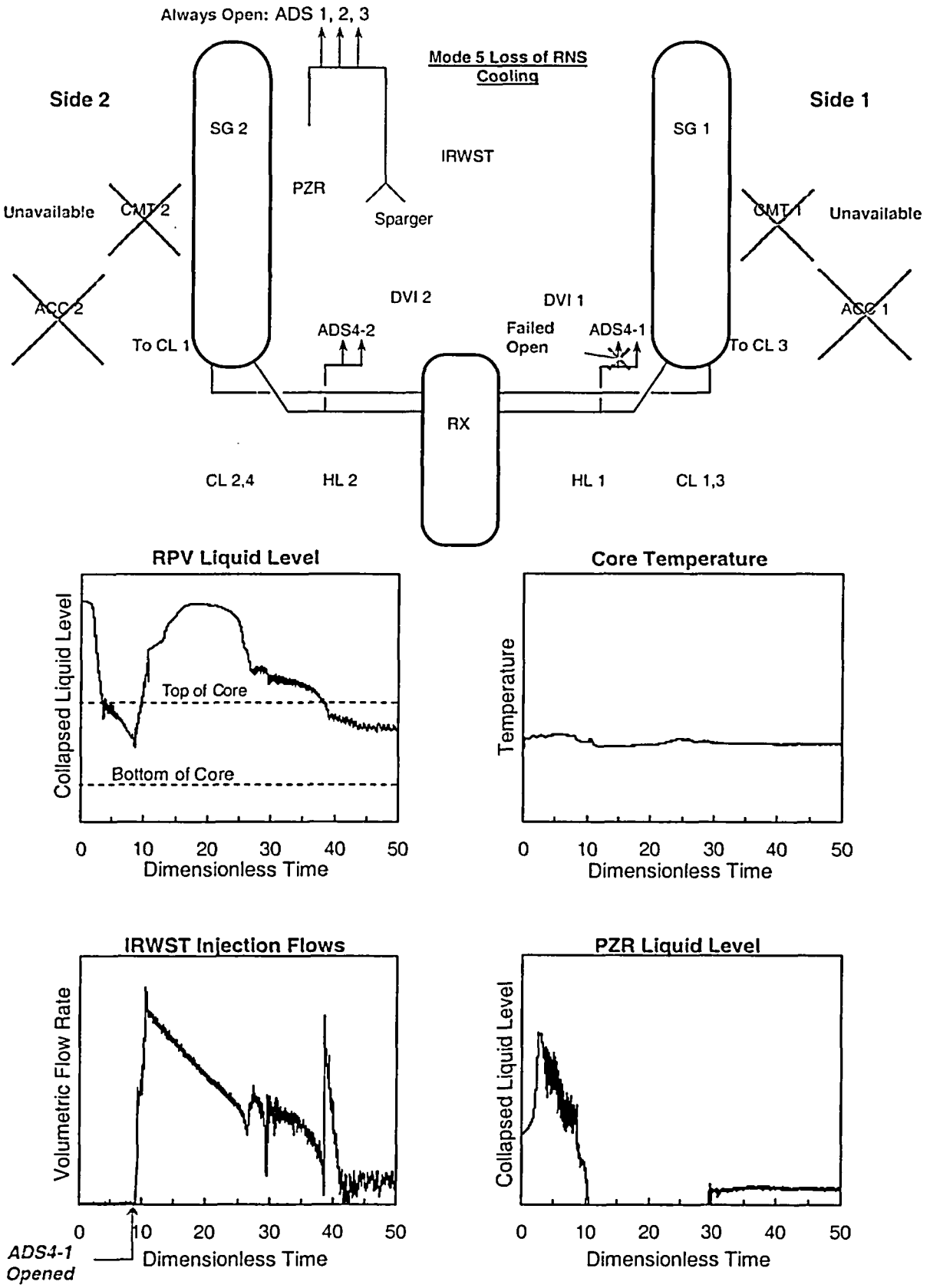


Figure 4.3 Test NRC-AP1000-02 Passive Safety System Performance.

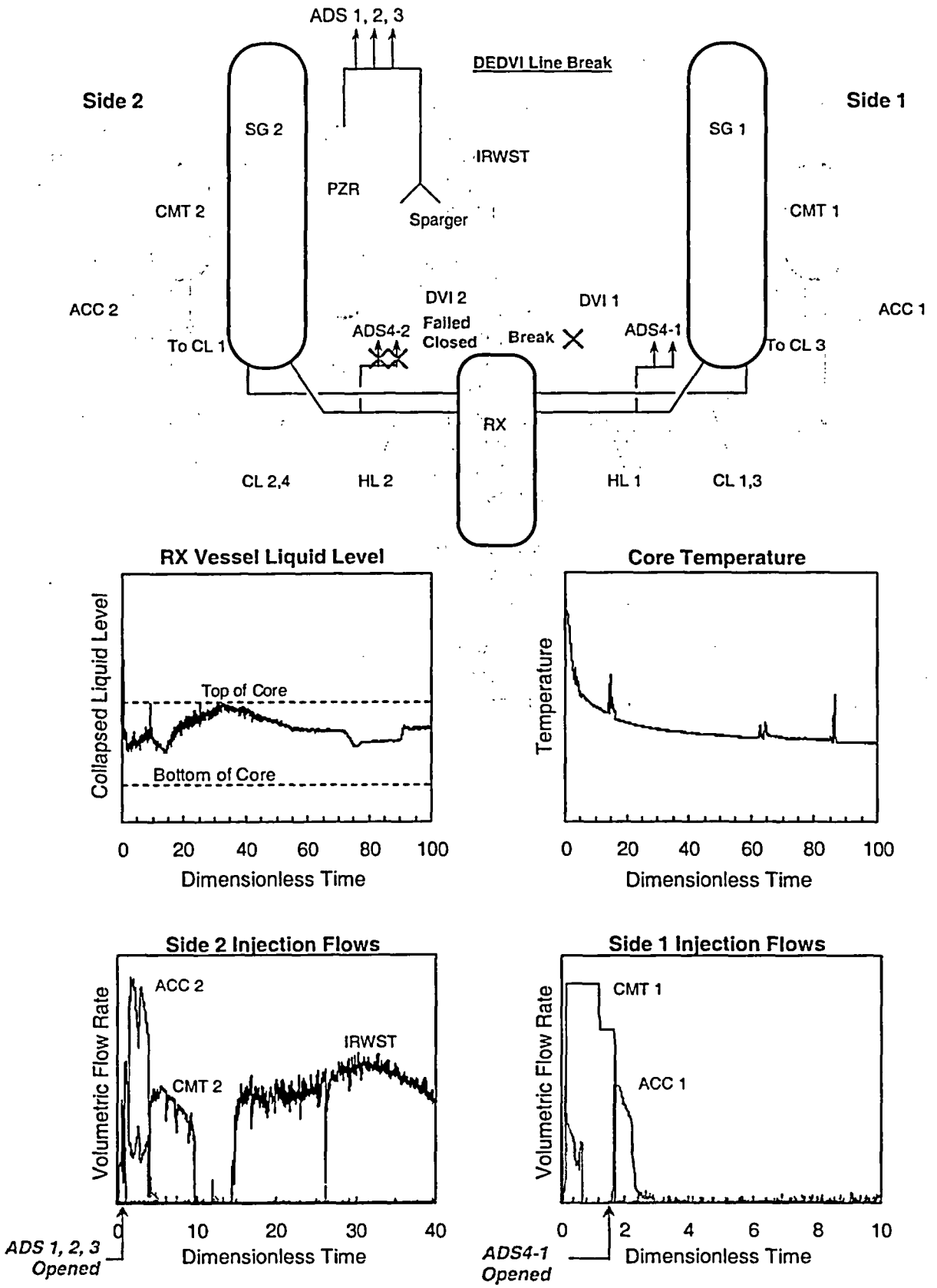


Figure 4.4 Test NRC-AP1000-03 Passive Safety System Performance.

## 4.5 Test NRC-AP1000-04

Test NRC-AP1000-04 was a beyond-DBA test simulating a 1-inch CL break with one ADS4 valve failed shut (50% line flow) on the non-PZR HL. In addition, CMT1, ACC1, sump recirculation line 1, and IRWST injection line 1 were unavailable. The intent of this test was to investigate the sensitivity of ADS4 valve failure on core coolability with loss of several safety injection paths, and to determine the impact of a simulated degraded sump on long-term cooling.

Figure 4.5 illustrates the facility configuration for this test, and contains plots of RPV-wide collapsed liquid level, passive safety injection flow rates (side 2), and core heater rod temperature and power. The break was initiated at zero seconds and CMT2 began injecting immediately as the natural circulation phase of the transient was entered. During the initial ADS blowdown phase, the reactor vessel collapsed water level dropped to the middle of the core. ACC2 began injecting around time 4 during ADS1–3 blowdown. The RPV collapsed liquid level continued to drop until IRWST injection began around time 7, thus ending the ADS blowdown phase of the transient. IRWST injection began before CMT2 was completely emptied, ensuring that makeup water was provided to the core at all times. At around time 20, the RPV liquid level began to decrease as IRWST injection flow rate decreased.

At about time 60, the primary sump valve was opened, which transitioned the plant from IRWST injection to long-term cooling. Primary sump overflow began, and water was recirculated from the sump to the IRWST, through the DVI2 line, and into the reactor vessel as the long-term cooling phase was entered. During sump recirculation, a drain at the bottom of the sump was opened to simulate a degraded sump. The presence of a degraded sump did not affect core coolability, and the core remained adequately cooled throughout the test. The core power was shown in Figure 4.5 to illustrate the standard decay power curve used in many APEX LOCA tests.

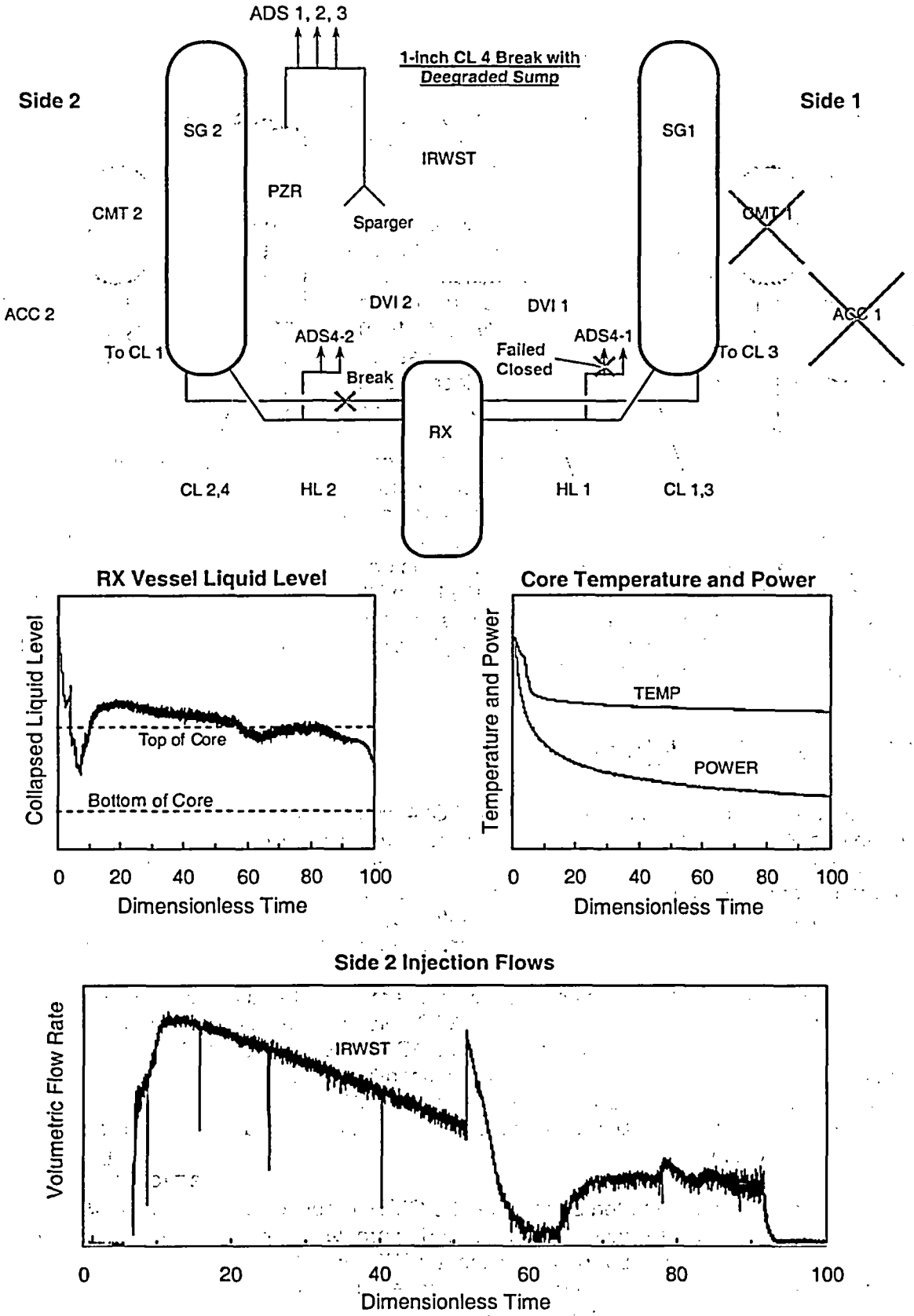


Figure 4.5 Test NRC-AP1000-04 Passive Safety System Performance.

## 4.6 Test NRC-AP1000-05

This test was a DEDVI line break with failure of two of the four ADS4 valves on the non-PZR side of the plant. This test was the counterpart to test NRC-AP1000-03, where two of the four ADS4 valves failed to open on the PZR side of the plant.

Figure 4.6 shows the plant configuration for this test and plots of injection flow rates (sides 1 and 2), along with reactor vessel level and core temperature. At time zero, the DVI Line 1 break was opened and the plant began to depressurize; the CMTs began injecting immediately. The plant went through the same natural circulation and ADS blowdown phases as in test NRC-AP1000-03. At around time 30 in test NRC-AP1000-05, the vessel inventory began to decrease because no injection flow was provided to the vessel. Water exiting the break and ADS4-2 line caused the vessel inventory to continue to decrease, even as the two-phase mixture level dropped below the bottom of the HL at around time 32.

Upper plenum entrainment into the HL and out the ADS4-2 line contined to deplete the rector vessel inventory from time 30 to 40, which lead to core uncovery before the IRWST injection could begin. At time 40, there was an increase in core tempertature and the heater rods were turned off to avoid damage. Consequently, failing closed the two ADS4 valves on the PZR side of the plant resulted in core heatup. The PZR was unable to drain during this test because of the presence of liquid entrainment out of ADS4-2 in HL2 or because of the presence of CCFL in the surge line from flow out the ADS1-3 valves. Section 5.2 of this report provides a comparison between tests NRC-AP1000-03 and 05, which explains why the core was uncovered in test NRC-AP1000-05 and not in test NRC-AP1000-03.

## 4.7 Test NRC-AP1000-06

This test was a 2-inch break off the bottom of CL4 with a failure of two of the four ADS4 valves on the non-PZR side of the plant. It was apparent from NRC-AP1000-05 that this type of ADS4 failure can lead to core uncovery, so the purpose of this test was to determine whether moving the break from DVI1 to CL4 resulted in similar core uncovery. Figure 4.7 shows the plant configuration for this test and plots passive safety system injection flow rate (side 2), along with reactor vessel level, core temperature, primary system pressure, and PZR collapsed liquid level.

As in previous tests, the break was opened at time zero. CMT1 and 2 began to inject immediately, but since the break was relatively small, the ADS setpoint (based on CMT low level) was not reached until around time 15 when the ADS1 and ADS2 valves actuated. After ADS1, 2, and 3 actuation, the total injection flow increased significantly until falling to zero by time 37, thus ending the ADS blowdown phase of the trainsient. The ADS blowdown phase in this test was significantly longer than the ADS blowdown phase in DVI line breaks, as would be expected from a smaller CL break.

IRWST injection had not started by the time the CMTs emptied. Without any additional safety injection, the reactor vessel water level continued to drop as a result of boiling in the core and upper plenum entrainment. Eventually, without IRWST injection, the core temperature rose as a result of boil-off of primary liquid, and a temperature excursion occurred at around time 50, similar to test NRC-AP1000-05. The heater rods were shut off to avoid damage, thus ending the test.

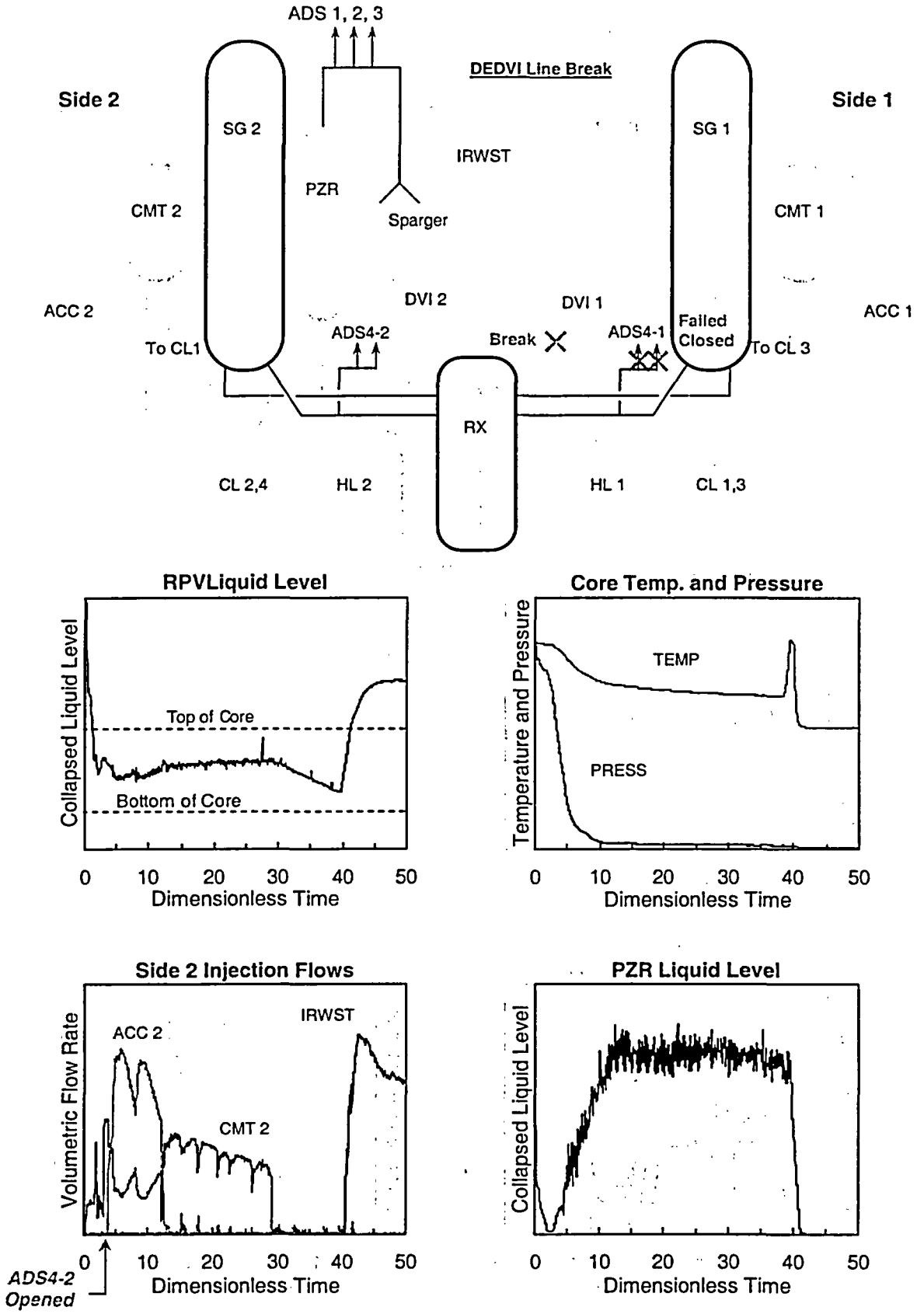


Figure 4.6 Test NRC-AP1000-05 Passive Safety System Performance.

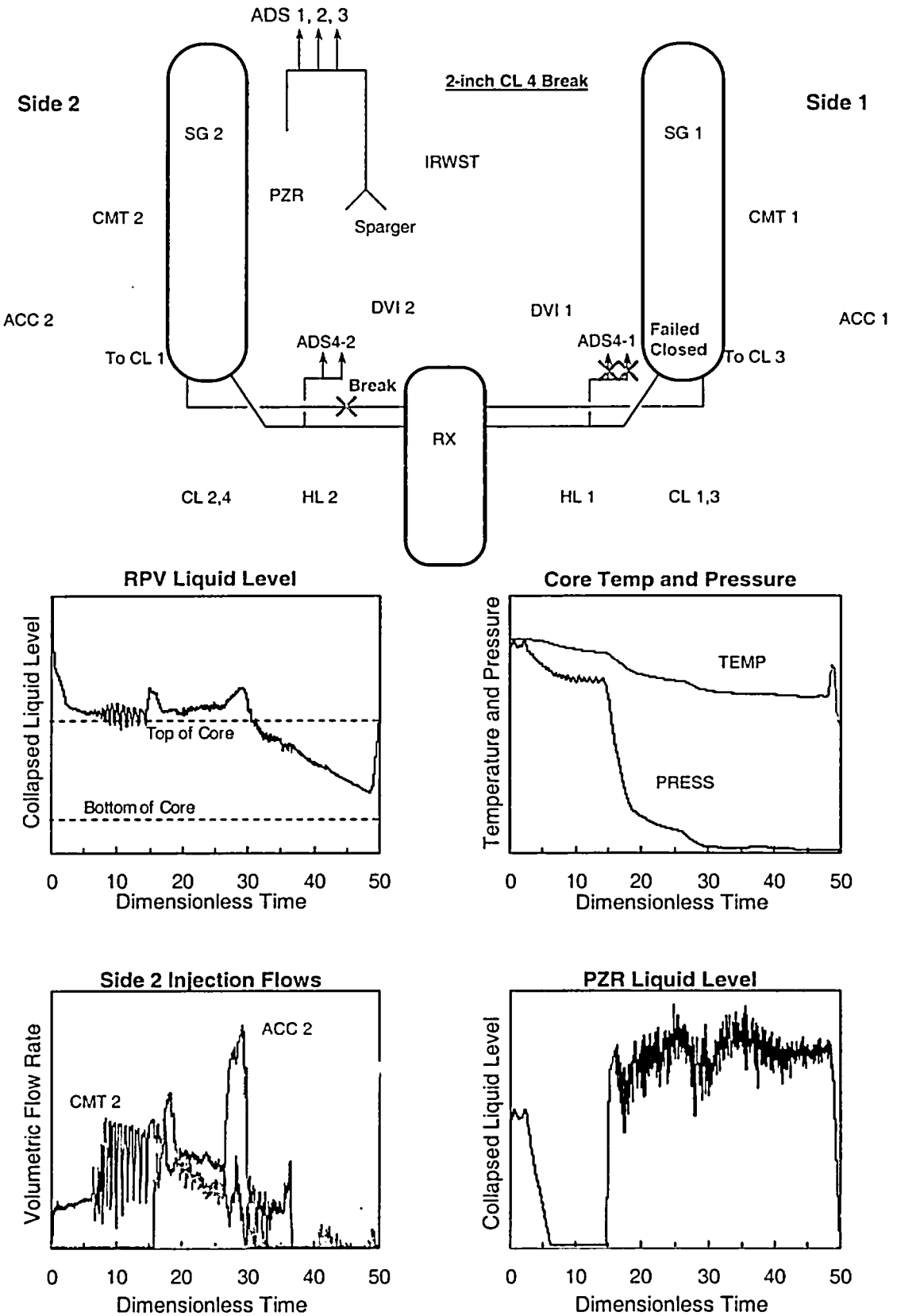


Figure 4.7 Test NRC-AP1000-06 Passive Safety System Performance.

## 4.8 Test NRC-AP1000-10

The objective of this test was to validate PRA assumptions with regard to multiple failures of the ADS. This test simulated a 2-inch cold leg break off the bottom of CL4. The test was initiated from normal operating temperature and pressure. For this test, ADS1–3 and one of the four ADS4 valves failed to open on the non-PZR side of the plant. The steam generator PORVs were allowed to cycle to help remove decay heat during the initial blowdown stage of the transient. The test was terminated after 30 minutes of steady-state long-term cooling.

Figure 4.8 shows the facility configuration for this test, along with figures showing the passive safety injection flow rate; RPV collapsed liquid level, and ADS4-1 and 2 flow qualities. For this test, the side 1 and side 2 injection timing and flow rates were very similar; hence, only side 2 is shown in Figure 4.8. The break was initiated at zero seconds, and the CMTs immediately began to drain. The ACCs began to inject shortly after ADS4 valve actuation at around time 3. This caused the plant to further depressurize and increased ACC injection flow rates considerably.

Between time 6 and 9, there was a noticeable oscillation of IRWST injection flow rate, core liquid level, and ADS4-2 line flow qualitiy. By time 9, the RPV pressure was very close to atmospheric and the HLs were almost completely flooded (not shown). This oscillatory behavior is consistent with separate effects experiments run in the Air-Water Test Loop for Advanced Thermal-hydraulic Studies (ATLATS) [Ref. 4], which investigated the intermittent nature of liquid entrainment from the HLs into a vertical ADS4 line. At around time 10, only liquid exited the ADS4 valves as water from the IRWST was injected at a high rate to the core.

The RPV liquid inventory reached a maximum around time 15, and then began to slowly decrease as the IRWST injection flow rate decreased. Oscillations were experienced again from time 26 to 35. These RSOs are consistent with previous AP600 tests, and are described in Section 4.1.4 of this report. The plant entered long-cooling at time 43, when the sump recirculation lines were opened, thus ending the IRWST injection phase of the transient. No high-temperature excursion was experienced and the core remained covered and adequately cooled throughout the test.

## 4.9 Test NRC-AP1000-11

This test simulated a station blackout with a failure of one of the four ADS4 valves on the non-PZR side of the plant. Previous tests (NRC-AP1000-05 and 06) showed that failure of ADS4 valves on the non-PZR side of the plant are the most challenging to the AP1000 passive safety systems.

The APEX-AP1000 control logic (Appendix B) was modified to simulate a station blackout (loss of all AC power). The core operated at a reduced power (600 kW) and with a modified decay power curve to preserve the integrated core energy. The SG PORVs were set to cycle between two relatively high pressures. When the SG water level decreased to a specified level as a result of PORV cycling, an "S" signal was sent to open the CMT injection valves and the PRHR HX outlet valve. The ADS was actuated at around time 68 based on the control logic.

Figure 4.9 shows the plant configuration for this test and plots of passive safety system injection flow rates (side 2), along with reactor vessel collapsed liquid level, PZR pressure and temperature, and core temperature. For the first several hours of the station blackout test, the PORVs cycled on and off. The "S" signal was generated around time 68, and the ADS1 valve actuated. The

plant immediately began to depressurize, and the ADS control logic depressurized the plant to allow passive safety system injection. The injection flow decreased very close to zero around time 70, but only for a short while until IRWST injection began. No temperature excursion was experienced, and the core remained covered and adequately cooled throughout the test, even with one of the four ADS4 valves failing to open on the non-PZR side.

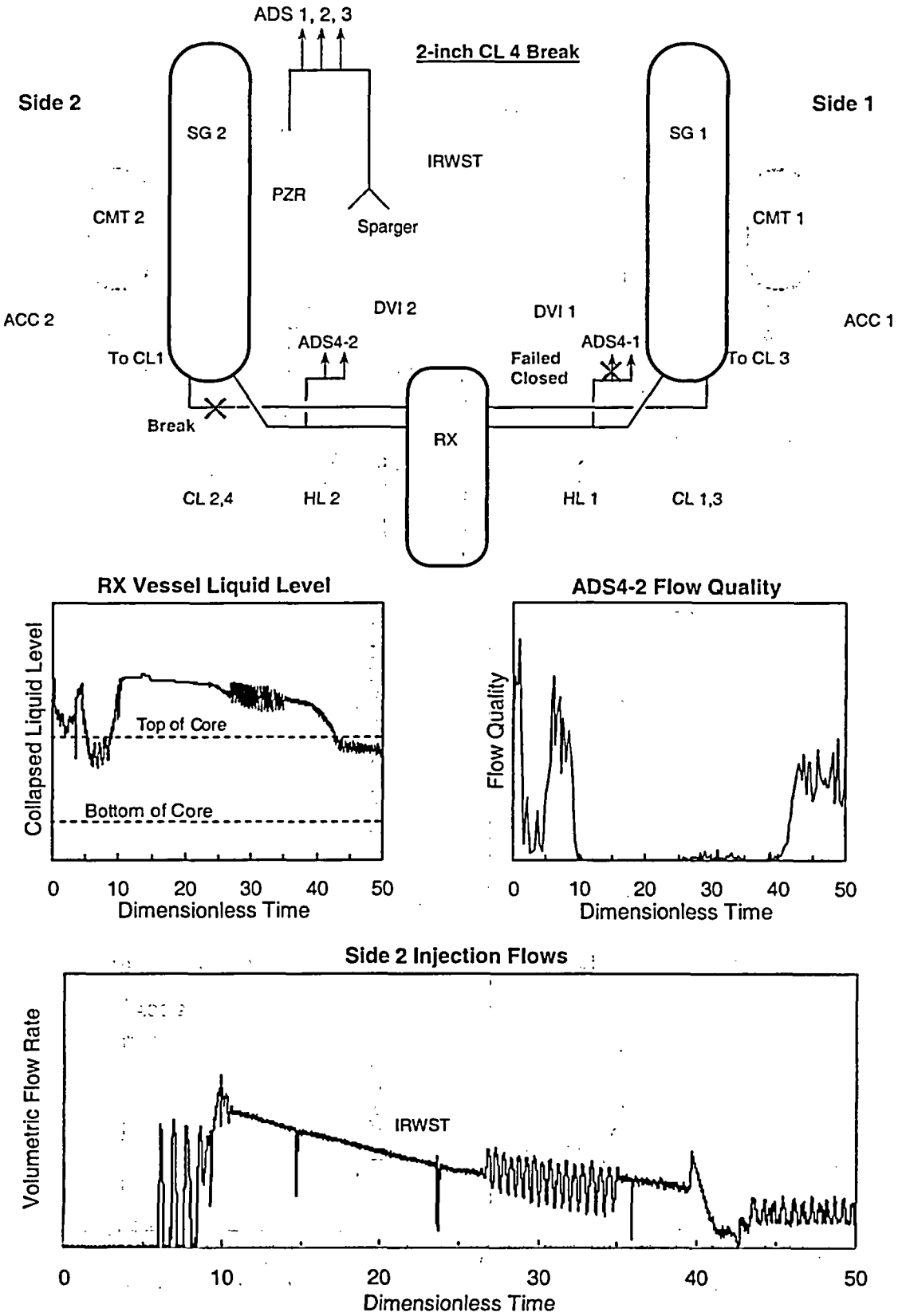


Figure 4.8 Test NRC-AP1000-10 Passive Safety System Performance.

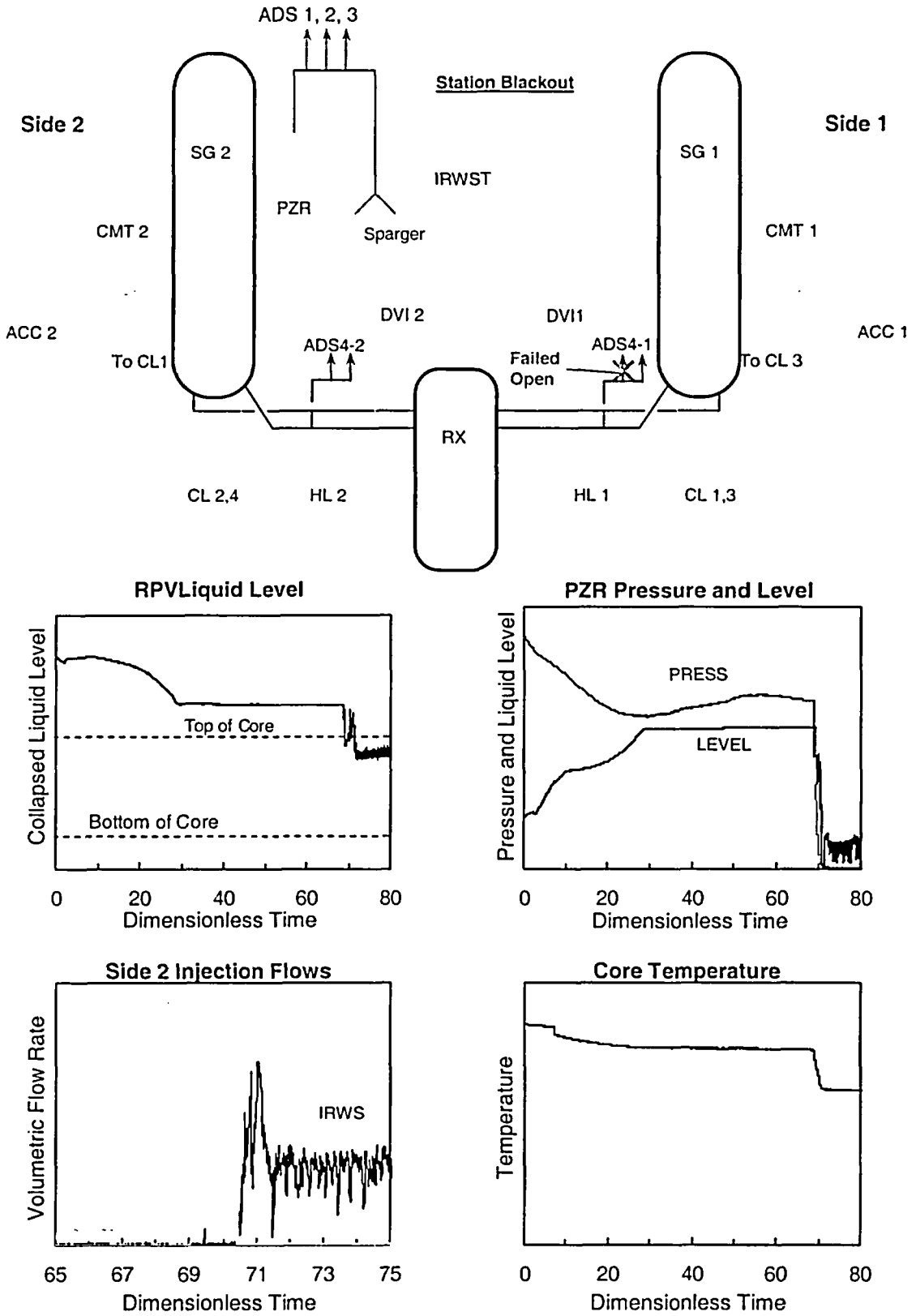


Figure 4.9 Test NRC-AP1000-11 Passive Safety System Performance.

# 5. COMPARISONS AND DISCUSSION

This section provides comparisons between design-basis test DBA-02 and beyond-DBA test NRC-AP1000-05, and between tests NRC-AP1000-03 and NRC-AP1000-05. The comparisons illustrate the fact that under select beyond-DBA scenarios, core uncovery was experienced in APEX-AP1000, while the similar design-basis test did not lead to core uncovery. In addition, comparison of beyond-DBA tests NRC-AP1000-03 and NRC-AP1000-05 helps to explain why the core uncovered when two of the four ADS4 valves were failed on the non-PZR side of the plant, compared to the same ADS4 failure on the PZR side of the plant.

## 5.1 Test DBA-02 versus Test NRC-AP1000-05

It is interesting to compare design-basis test DBA-02 [Ref. 5] to beyond-DBA test NRC-AP1000-05. Both tests simulated a DEDVI line break with ADS4 valve failure on the non-PZR side of the plant. The only difference between the two tests was that in DBA-02, only one of the four ADS4 valves were failed closed, while in NRC-AP1000-05, two of the four ADS4 valves were failed closed. Figure 5.1 shows a comparison of reactor vessel collapsed level for DBA-02 and NRC-AP1000-05. As previously shown in Figure 4.6, the core uncovered in NRC-AP1000-05 as a result of the increased rate at which water was entrained out of the upper plenum, into the HL, and out ADS4-2. In DBA-02, IRWST injection was significantly delayed as shown in Figure 5.2. In NRC-AP1000-05, the reactor vessel liquid level dropped fast enough and IRWST injection never began, since the heater rods were shut off around time 32 to avoid damage to the facility. It is also important to note that there existed a significant amount of time in DBA-02 (between time 23 and 28) when the reactor vessel did not receive any injection flow as shown in Figure 5.2. During this period, core cooling was maintained by boil-off of the existing vessel inventory.

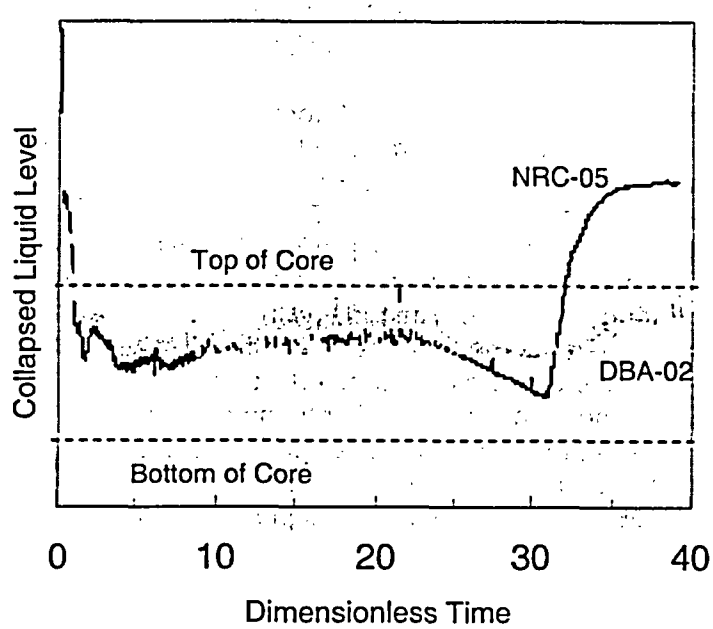


Figure 5.1 Reactor Vessel Liquid Level (DBA-02 and NRC-AP1000-05).

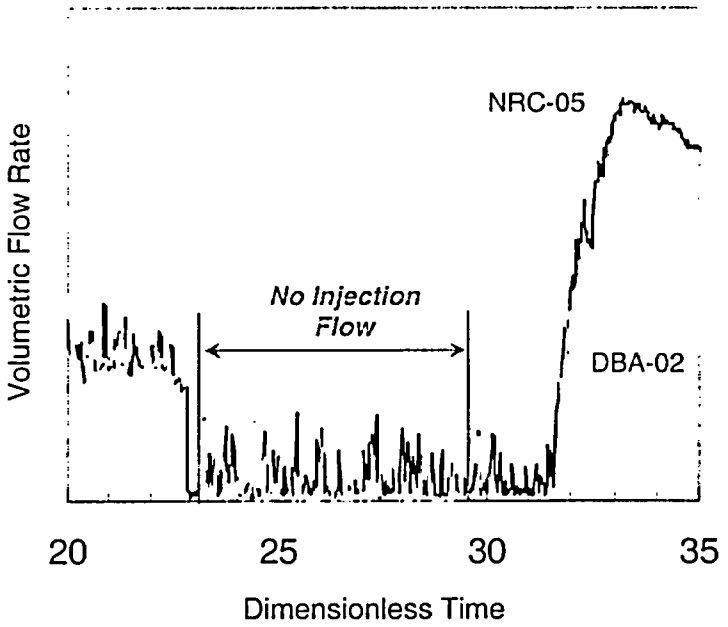


Figure 5.2 IRWST Injection Flow Rates (DBA-02 and NRC-AP1000-05).

Figure 5.3 compares the PZR water level for both tests. At around time 10, the PZR was able to drain as the plant depressurized in DBA-02, providing additional makeup water to the core, but in NRC-AP1000-05, the PZR wasn't able to drain until the heater rods were turned off at around time 30. The PZR was unable to drain in NRC-AP1000-05 because of liquid entrainment in HL2 flowing out the ADS4-2 line. This phenomenon is discussed in more detail in Section 5.2.

Examination of the ADS4-2 flow quality (Figure 5.4) for both tests shows significant liquid carryover from the reactor vessel and entrainment from the HL out the ADS4-2 line. Even after the two-phase mixture dropped below the bottom of the HL in NRC-AP1000-05 (time 25 in Figure 5.1) the ADS4-2 quality was still relatively low (~0.6). The primary mechanism through which water left the reactor vessel at low vessel liquid levels (liquid level below the bottom of the HLs) was upper plenum entrainment. Droplets from the two-phase reactor vessel mixture level were entrained by the steam, passed through the upper internals (with some droplets de-entraining), and entered the hot leg. From there, some droplets struck the HL pipe walls and created an annular flow of liquid out the ADS4 line or were de-entrained into the HL liquid level and entrained out the vertical ADS4 line by a mechanism of liquid entrainment in horizontal pipes with vertical-up branches [Ref. 4]. In DBA-02, there was still one operational ADS4 valve on the non-PZR side of the plant, providing another outlet for the steam. In NRC-AP1000-05, all of the steam exited the ADS4-2 line and the DEDVI break. Hence, a higher flow quality was observed in NRC-AP1000-05 than in DBA-02.

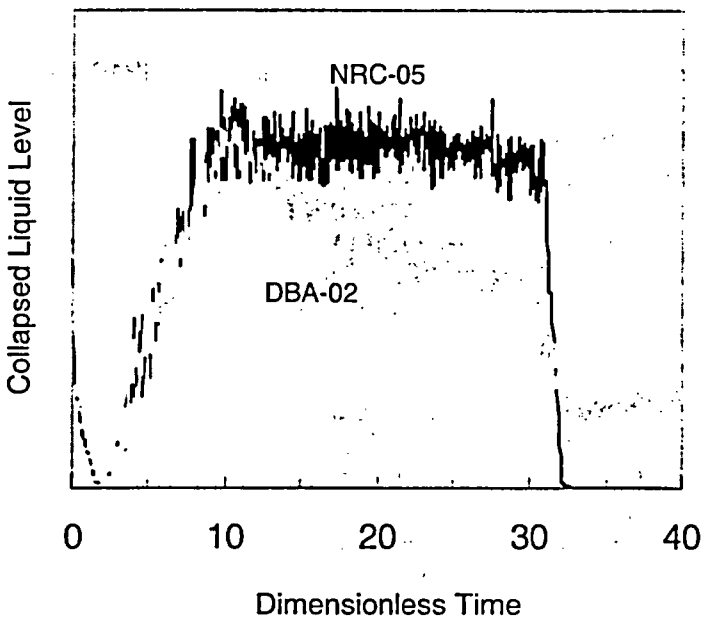


Figure 5.3 PZR Liquid Levels (DBA-02 and NRC-AP1000-05).

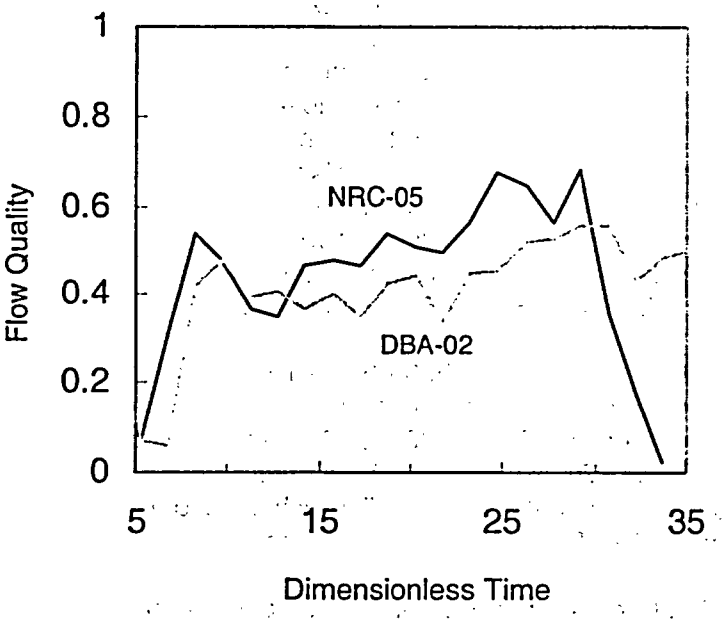


Figure 5.4 ADS4-2 Flow Qualities (DBA-02 and NRC-AP1000-05).

## 5.2 Test NRC-AP1000-03 versus NRC-AP1000-05

As previously shown, core uncovery was experienced in NRC-AP1000-05, but not in NRC-AP1000-03. The only difference between these two DVI line break tests was the location of the ADS4 valve failures. In NRC-AP1000-03 (no core uncovery), two of the four ADS4 valves were failed closed on the PZR side of the plant, while in NRC-AP1000-05 (core uncovery), two of the four ADS4 valves were failed closed on the non-PZR side of the plant. As the plant went through the ADS blowdown phase of the transient, water was entrained through the ADS4-2 line in NRC-AP1000-05 and the ADS4-1 line in NRC-AP1000-03. Both tests had the exact same timing (i.e., control logic), except that the heater rods were turned off in NRC-AP1000-05 at around time 25 to avoid damage to the facility.

The pressure transient was almost exactly the same for both tests, as shown in Figure 5.5. There was a slight difference between tests NRC-AP1000-03 and NRC-AP1000-05 in system pressure at around time 10. For both tests, there was no injection flow to the core between time 17 and 25, as shown in Figure 5.6. During this time of no injection flow, the quality out of the open ADS4 valves for both tests was relatively low, ~0.6 for test NRC-AP1000-05 and ~0.4 for test NRC-AP1000-03, as shown in Figure 5.7.

As shown in Figure 5.8, the RPV collapsed liquid level began to decrease in both tests at around the same time (time 18). However, the RPV liquid level decreased faster in test NRC-AP1000-05 than in test NRC-AP1000-03. At around time 21, the two-phase mixture level in the vessel for both tests dropped below the bottom of the HL, as shown in Figure 5.9. Figure 5.10 shows an oscillation in the HL2 liquid level in both tests at about the same time the RPV two-phase mixture level dropped below the bottom of the HL. Examination of the HL1 liquid level (Figure 5.11) does not reveal any noticeable oscillations between time 21 and 25. In test NRC-AP1000-05, the liquid in HL2 was entrained out the ADS4-2 line, while no liquid was entrained out the ADS4-2 line in test NRC-AP1000-03, since it was failed closed in that test. Hence, the source of the initial oscillations in HL2 was not attributable to the presence of HL entrainment. Examination of the PZR surge line liquid level (Figure 5.12) reveals that the PZR began to slowly drain in surges during the HL2 oscillations. Therefore, the oscillations in hot leg level were attributable to the PZR draining. In addition, in test NRC-AP1000-03, the oscillations in HL2 slowly diminished over time, while they were maintained in test NRC-AP1000-05 by the presence of liquid entrainment out of ADS4-2. Figure 5.13 shows the PZR liquid level for both tests.

In summary, compared to test NRC-AP1000-03, the RPV liquid level dropped faster in test NRC-AP1000-05 because of the presence of the PZR, which enhanced liquid entrained out the open ADS4 line in test NRC-AP1000-05. As shown in Figure 5.14, IRWST injection was significantly delayed in NRC-AP1000-03, but never began in NRC-AP1000-05. (Test NRC-AP1000-05 was terminated at time 25, which caused IRWST injection to begin.) Lack of injection water from the IRWST caused the core to uncover in test NRC-AP1000-05.

In similar full-scale AP600 tests run in ROSA [Ref. 3], core uncovery was not experienced. This is because the APEX facility has a reduced IRWST head, since it was scaled to one-quarter height. Hence, the delay in IRWST injection is a known conservatism in the APEX test facility.

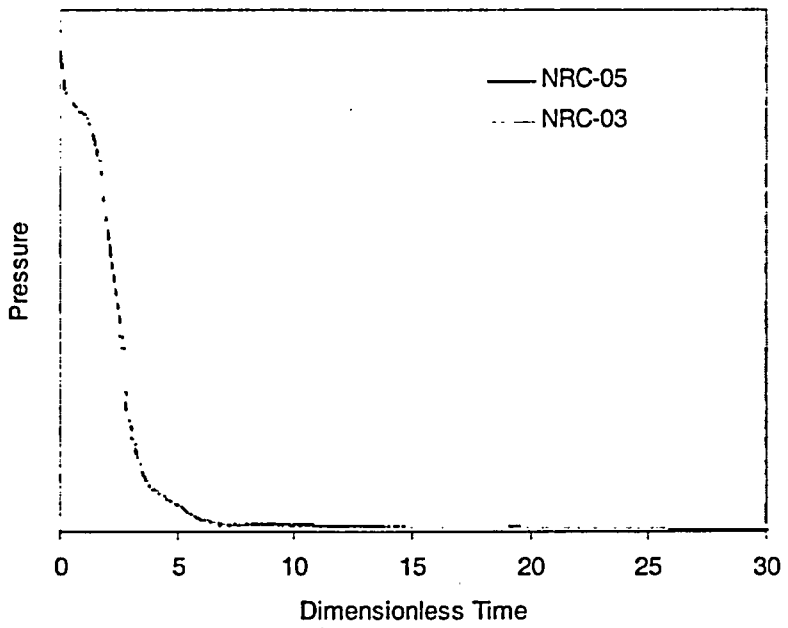


Figure 5.5 System Pressures (NRC-AP1000-03 and 05)

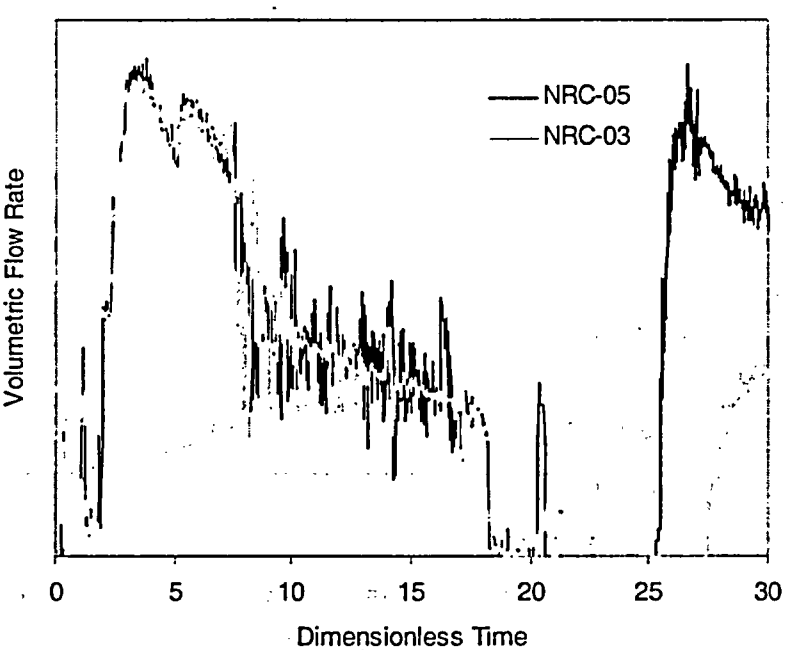


Figure 5.6 Safety Injection Flow Rates (NRC-AP1000-03 and 05)

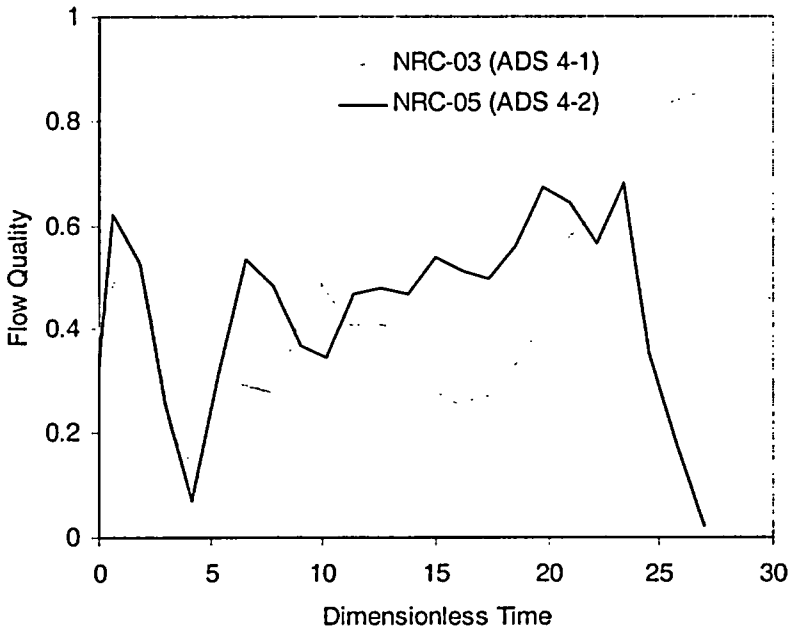


Figure 5.7 ADS4 Flow Qualities (NRC-AP1000-03 and 05)

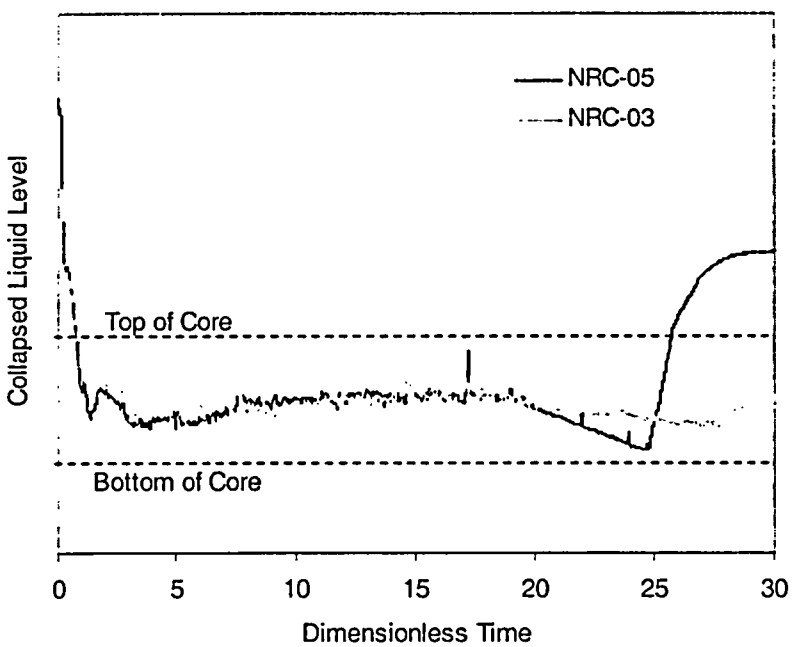


Figure 5.8 RPV Collapsed Liquid Levels (NRC-AP1000-03 and 05)

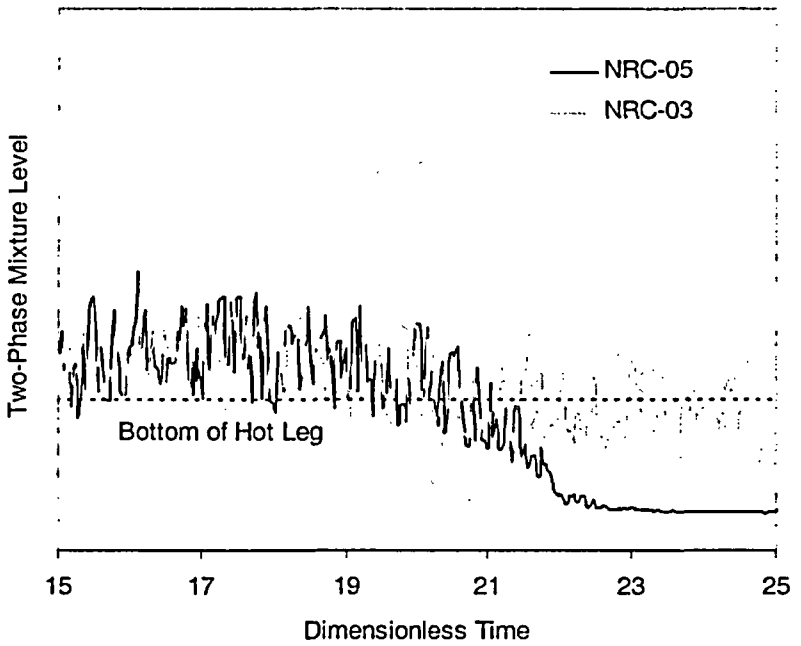


Figure 5.9 RPV Two-Phase Mixture Levels (NRC-AP1000-03 and 05)

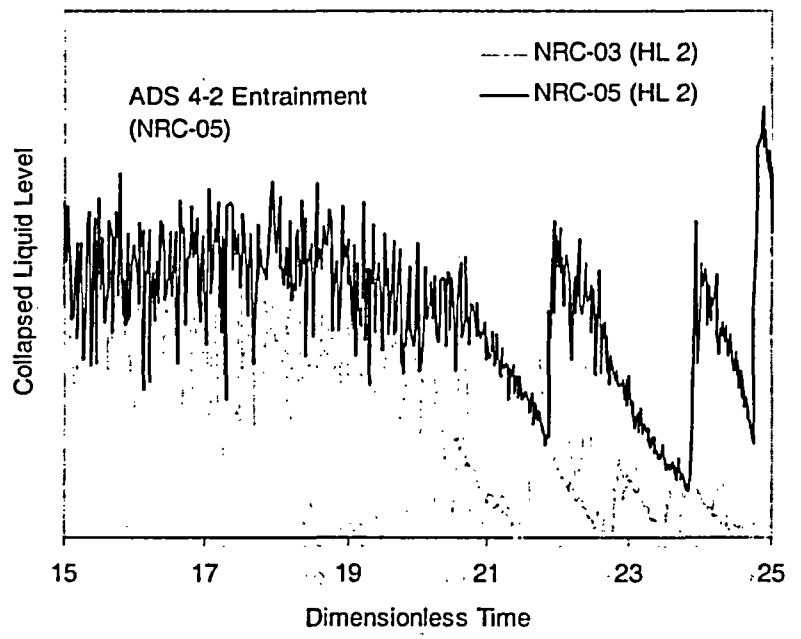


Figure 5.10 HL2 Collapsed Liquid Levels (NRC-AP1000-03 and 05)

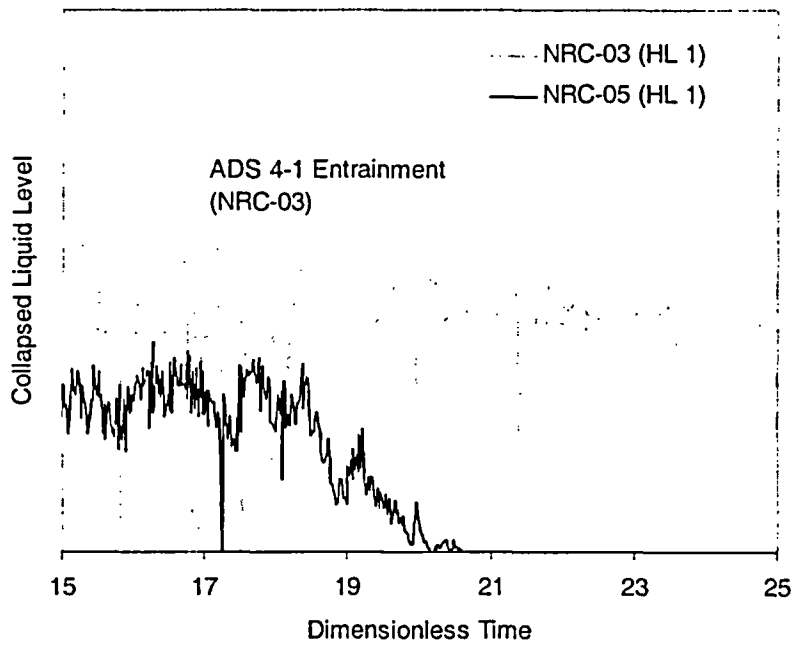


Figure 5.11 HL1 Collapsed Liquid Levels (NRC-AP1000-03 and 05)

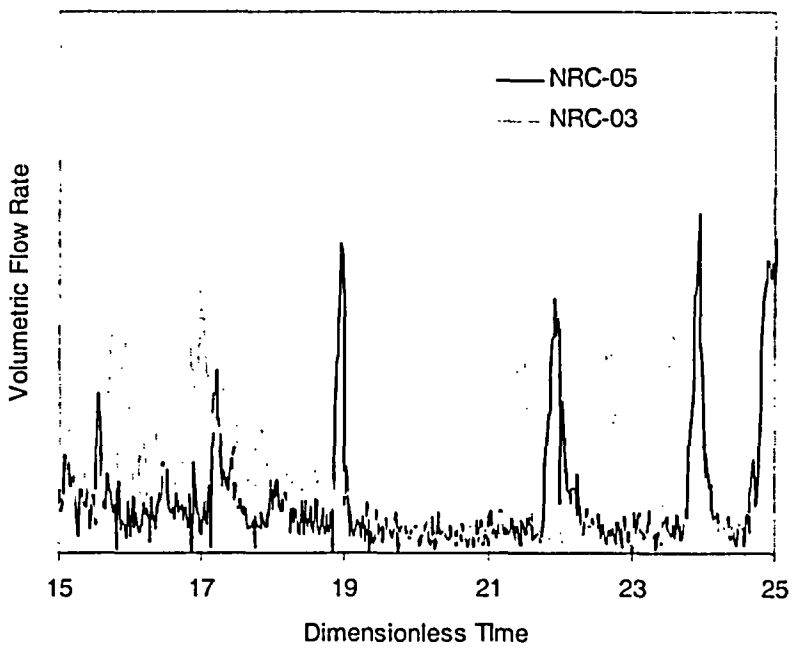


Figure 5.12 PZR Surge Line Liquid Levels (NRC-AP1000-03 and 05)

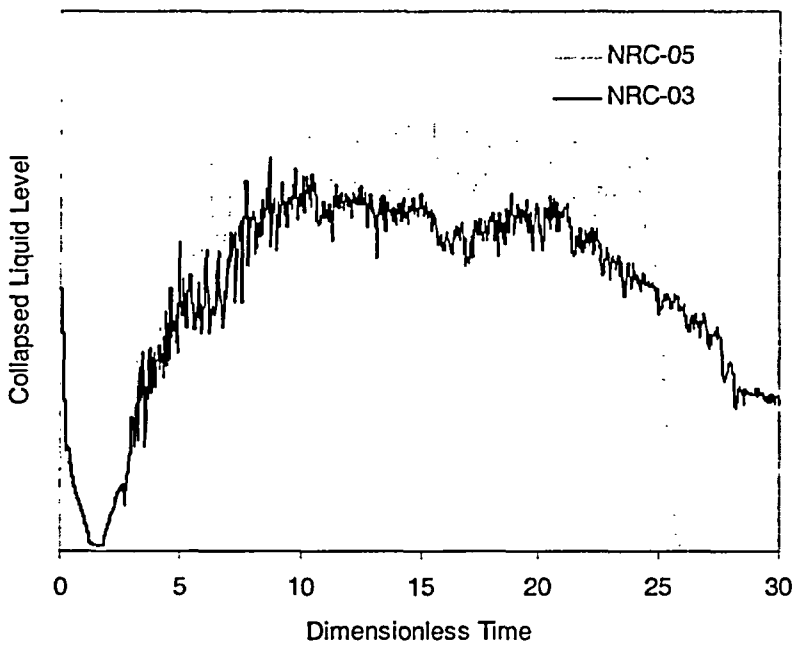


Figure 5.13 PZR Collapsed Liquid Levels (NRC-AP1000-03 and 05)

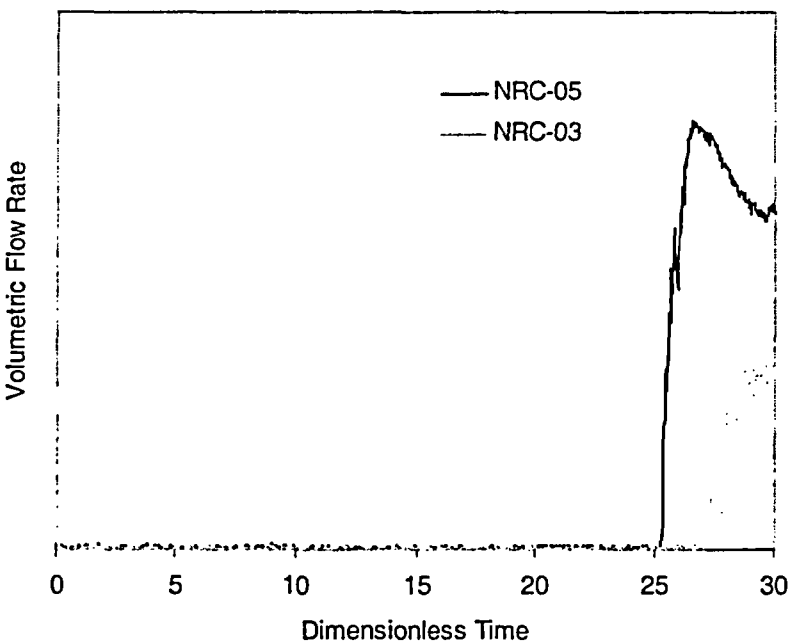


Figure 5.14 IRWST Injection Flow Rates (NRC-AP1000-03 and 05)

# 6. SUMMARY AND CONCLUSIONS

The APEX facility is a unique thermal-hydraulic integral system test facility used to assess the performance of passive safety systems in the Westinghouse AP600 and AP1000 designs. To address performance specific to the AP1000 design, the APEX facility underwent significant modifications in 2002 in order to more accurately represent the AP1000 reactor. Those facility modifications included an increase in the maximum core power; new PZR and surge lines; larger CMTs; larger-diameter ADS4 system piping; and decreased line resistances for the CMTs, ADS4, and PRHR HX. A comprehensive scaling analysis, performed by Reyes and presented in Appendix A, guided the facility modifications to ensure that AP1000 conditions were preserved in the APEX experiments.

The accident scenarios investigated in the APEX-AP1000 facility included 1- and 2-inch CL breaks, DEDVI line breaks, Mode 5 operation with loss of RNS cooling, and station blackout. Based on experience from analyzing previous AP600 tests, one of the main purposes of the APEX-AP1000 test program was to investigate the sensitivity of ADS failure on core coolability.

Based on the experiments run in APEX, the following conclusions can be made:

(1) The APEX-AP1000 tests confirm significant liquid entrainment and carryover of water to the ADS4 system during and after ADS4 valve actuation.

(2) Test results from NRC-AP1000-03, 05, and DBA-02 show that failure of ADS4 valves on the non-PZR side of the plant results in a greater delay in IRWST injection than failure of ADS4 valves on the PZR side of the plant.

(3) Failure of two out of four ADS4 valves on the non-PZR side of the plant results in core uncovery (based on the two-phase mixture level) during simulated DEDVI line and cold leg breaks.

(4) Review of the APEX-AP1000 test results conclusively show that the core remains cooled and heatup was not experienced for most of the beyond-DBA tests.

# 7. REFERENCES


1. [ ] a,b,c

2. Bessette, D., and di Marzo, M., "Transition from Depressurization to Long-Term Cooling in AP600 Scaled Integral Test Facilities," *Nuclear Engineering and Design*, Vol. 188, pp. 331–344, Elsevier, 1999.

3. Reyes, J.N., et al., "Final Report of NRC AP600 Research Conducted at Oregon State University," NUREG/CR-6641, U.S. Nuclear Regulatory Commission, Washington, DC, 1999.

4. Welter, K.B., et al., "Experimental Investigation and Theoretical Modeling of Liquid Entrainment in a Horizontal Tee with a Vertical Branch," *International Journal of Multiphase Flow*, Vol. 30, No. 12, pp. 1451–1484, December 2004.

5. [ ] a,b,c

6. [ ] a,b,c

7. U.S. Nuclear Regulatory Commission, "APEX Testing in Support of AP1000," Memorandum from Jack Rosenthal (RES) to Jared Wermiel (NRR), Washington, DC, 2004.

8. [ ] a,b,c

9. Zuber, N., "A Hierarchical, Two-Tiered Scaling Analysis: An Integrated Structure and Scaling Methodology for Severe Accident Technical Issue Resolution," Appendix D to NUREG/CR-5809, U.S. Nuclear Regulatory Commission, Washington, DC, November 1991.

10. [ ] a,b,c

11. American Nuclear Society, "American National Standard for Decay Heat Power in Light-Water Reactors," ANSI/ANS-5.1.24, La Grange, IL, 1979.

12. Lay, J.F., *Statistical Mechanics and Thermodynamics of Matter*, Harper and Row Publishers, New York, pp. 453–456, 1990.

13. Moody, F.J., *Introduction to Unsteady Thermofluid Mechanics*, A Wiley-Interscience Publication, New York, p. 60, 1990.

14. Henry, F.E., and Fauske, H.K., "The Two-Phase Critical Flow of One-Component Mixtures in Nozzles, Orifices, and Short Tubes," *Journal of Heat Transfer, ASMAE Transactions*, Vol. 93, No. 2, pp. 179–187, 1971.

15. Pimentel, D., "Two-Phase Fluid Break Flow Measurements and Scaling in the Advanced Plant Experiment (APEX)," Master's Thesis, Oregon State University, May 1999.

16. Kataoka, I., and Ishii, M., "Mechanistic Modeling and Correlations for Pool-Entrainment Phenomenon," NUREG/CR-3304, U.S. Nuclear Regulatory Commission, Washington, DC, April 1983.

17. Dallman, J.C. and Kirchner, W.L., "De-Entrainment Phenomena on Vertical Tubes in Droplet Cross Flow," NUREG/CR-1421, U.S. Nuclear Regulatory Commission, April 1980.

18. Chen, C.Y., "Filtration of Aerosols by Fibrous Media," *Chem.* Rev. 55, p. 595, 1955.

19. [ ] a,b,c

20. [ ] a,b,c

21. [ ] a,b,c

22. Bluman, G.W., and Cole, J.D., "Similarity Methods for Differential Equations," *Applied Mathematical Sciences 13*, Springer-Verlag, New York, 1974.

# APPENDIX A.

...

# APPENDIX A. SCALING ANALYSIS

The following scaling analysis was performed by Reyes and was used to guide the APEX-AP1000 test facility modifications. The basis for the majority of this work is the original AP600 Scaling Analysis, WCAP-14270, which was performed to support the design of the existing Advanced Plant Experiment (APEX) facility at Oregon State University (OSU) [Ref. 1]. The analyses presented herein provide the scaling criteria that need to be implemented to model the AP1000 design changes in the APEX test facility. This analysis, in conjunction with the AP1000 design information, has been used to identify and guide the design modifications needed to make the APEX facility suitable for AP1000 testing.

## A.1 Introduction

As part of the AP600 design certification, the APEX test facility was constructed at OSU. The APEX facility is a low-pressure, one-quarter height, integral systems test facility that can model the long-term core cooling phenomena associated with an advanced passive plant using passive safety systems. Extensive scaling studies were performed so that the AP600 thermal-hydraulic phenomena of interest would be accurately modeled in the APEX facility. The APEX facility operates at one-half time scale and at a reduced pressure and temperature scale. Using the scaled parameters, a test in the APEX facility occurs twice as fast as a transient in the actual design. A total of 28 integral system tests were successfully performed for Westinghouse and the U.S. Department of Energy in support of the AP600 design certification. In addition, a total of 47 confirmatory tests were successfully performed for the NRC.

### A.1.1 Comparison of the AP600 and AP1000 Design Parameters

The most significant difference between AP600 and AP100 is the increased core power. The reactor vessel volume remains unchanged. The SG tube surface area, PZR volume, and RCP flow have all increased to accommodate the increased core power. Table A.2 compares the changes to the passive safety system design. In particular, the volume of the CMTs and the IRWST has been increased; the flow capacity for the IRWST, ADS4, and PRHR has been increased by reducing the resistance in each line; and the PRHR surface area has also increased. The Westinghouse Plant Parameters document [Ref. 8] provides the details of the AP1000 design. Table A.1 compares the key design parameters of the AP1000 design with those of the AP600 reactor.

Table A.1 Important NSSS Design Changes [Ref. 8]

| Parameter | AP600 | AP1000 |
|---|---|---|
| Reactor Core Power, MWt | 1933 | 3400 |
| Hot Leg Temperature, °F | 600 | 610 |
| Number of Fuel Assemblies | 145 | 157 |
| Active Fuel Length, ft | 12 | 14 |
| Average Linear Power, kW/ft | 4.10 | 5.707 |
| Average Heat Flux, Btu/(hr-ft$^2$) | 142,869 | 198,933 |
| Steam Generator Heat Transfer Area per unit, ft$^2$ | 75,180 | 123,538 |
| Reactor Coolant Pump Flow, gpm | 51,000 | 78,750 |
| Pressurizer Volume, ft$^3$ | 1,600 | 2,100 |

Table A.2 Changes to Passive Safety System Design Features

| Component | AP600 | AP1000 | Comment |
|---|---|---|---|
| IRWST | | | |
| Volume, $ft^3$ | 70,798 | 75,300 | The IRWST level has been increased in the AP1000 by using more accurate level instruments. This permits a high operating level. |
| Water Level, ft | 28.0 | 28.79 | |
| Line Resistance, % | 100% | 32% | |
| Design Flow Rate, % | 100% | 184% | |
| CORE MAKEUP TANKS | | | |
| Number | 2 | 2 | The CMT volume and flow rate have been increased to provide additional safety injection flow. CMT elevations are maintained at the AP600 level. The duration of CMT injection is maintained similar to AP600. |
| Volume, $ft^3$ | 2000 | 2512 | |
| Line Resistance, % | 100% | 64% | |
| Design Flow Rate, % | 100% | 124% | |
| ACCUMULATORS | | | |
| Number | 2 | 2 | The accumulators are the same as AP600. Accumulator sizing is based on LBLOCA performance and is determined largely on reactor vessels volume. |
| Volume, $ft^3$ | 2000 | 2000 | |
| Pressure, psig | 700 | 700 | |
| AUTOMATIC DEPRESSURIZATION STAGES 1-3 | | | |
| Location | Top PZR | Top PZR | The first three stages of ADS are the same as AP600. Their sizing basis is to reduce pressure to permit adequate injection from the accumulators and to permit transition to $4^{th}$ stage ADS. |
| Configuration | 6 paths | 6 paths | |
| Vent Area, % | 100% | 100% | |
| AUTOMATIC DEPRESSURIZATION STAGE 4 | | | |
| Location | Hot Leg | Hot Leg | The ADS$4^{th}$ stage vent area is increased more than the ratio of the core power. The $4^{th}$ stage ADS venting is the most important design feature to allow for stable IRWST/sump injection during long-term core cooling. |
| Configuration | 4 paths | 4 paths | |
| Line size | 10-inch | 10-inch | |
| Nominal Vent Area, % | 100% | 176% | |
| Line Resistance | 100% | 28% | |
| Capacity | 100% | 189% | |

Table A.2 Changes to Passive Safety System Design Features

| Component | AP600 | AP1000 | Comment |
|---|---|---|---|
| PASSIVE RHR HEAT EXCHANGER | | | |
| Type | C-Tube | C-Tube | The AP1000 PRHR HX retains the AP600 configuration. The heat transfer surface area is increased by extending the length of the heat exchanger. The inlet and outlet piping has been increased resulting in higher flow rates. |
| Surface Area, % | 100% | 122% | |
| Design Flow Rate, % | 100% | 174% | |
| Design Heat Trans., % | 100% | 172% | |
| CONTAINMENT | | | |
| Diameter, ft | 130 | 130 | The AP1000 containment volume and design pressure are increased to accommodate higher mass and energy releases. |
| Overall Height, ft | 189.83 | 215.33 | |
| Design Pressure, psig | 45 | 59 | |
| Net Free Volume, $ft^3$ | $173 \times 10^6$ | $2.07 \times 10^6$ | |
| PASSIVE CONTAINMENT COOLING SYSTEM | | | |
| Water Storage Tank Volume (Top of Overflow), gallons | 580,000 | 580,000 | The PCS water storage tank was increased to accommodate higher flow rates. The PCS flow rates have been increased based on the increased in core power. |

### A.1.2 Modifications to the APEX Test Facility

Based on a review of the design changes listed in Tables A.1 and A.2, and their detailed description in the AP1000 Plant Parameters document [Ref. 8], the set of modifications listed in Table A.3 were made to APEX to best simulate AP1000 thermal-hydraulic behavior.

Table A.3 Proposed Modifications to the APEX Test Facility

| Component | Modification to APEX |
|---|---|
| Reactor Power | Increase core power by 67%. (Maximum of 1 MW) |
| Pressurizer | Increase PZR volume.<br>Reduce PZR surge line diameter. |
| Steam Generator Heat Transfer Area | No change required for testing. |
| Reactor Coolant Pump Flow | No change required for testing. |
| Core Makeup Tanks | Increase CMT volumes by 25%.<br>Reduce line resistance to 64% of original value. |
| Accumulators | No changes to original design. |
| IRWST | Increase IRWST liquid level. |
| Automatic Depressurization Stages 1-3 | No changes to original design. |
| Automatic Depressurization Stage 4 | Increase ADS4 flow area by 76%.<br>Reduce line resistance to 28% of original value. |
| Passive Residual Heat Removal (PRHR) Heat Exchanger (HX) | Increase PRHR flow capacity by 74% by reducing line resistance. No change in surface area/tube number required for testing. |
| Containment Sump Flood-Up Elevation | Change flood-up elevation in primary sump tank. |
| Passive Containment Cooling System | Not part of APEX testing program. |

### A.1.3 Rationale for APEX Modifications

This section presents the rationale for the proposed modifications. An increase in the reactor core power is needed to preserve the proper power-to-volume scaling ratio. This is a key feature of the original scaling analysis and is essential to simulating decay heat behavior, loop natural circulation and primary system depressurization rates. The APEX power increase is limited to 1 MW without having to replace the power distribution system. This power represents ~2.8% decay power for the AP1000 on a scaled basis. An increase in PZR volume is essential because it is a major source of liquid to the core during primary system blowdowns. The NRC identified a need for the reduction in PZR surge line diameter at the conclusion of the AP600 research program [Ref. 2]. This modification is needed to ensure properly scaled PZR draining behavior during primary system blowdowns, and properly scaled surge line pressure drop behavior during ADS1-3 operation.

Increases to the APEX SG tube volume and heat transfer area were not deemed necessary for several reasons. First, their tube volume is small compared to the remainder of the primary system. Second, they are oversized for the decay power operations involved in testing. That is, they have much more surface area than needed to remove core heat. One impact of not increasing the SG surface area is an increase in the core fluid temperature rise, but this is well

within the design constraints of the existing facility. The increased number of tubes, however, significantly reduces the primary loop pressure drop because of the increased number of parallel flow paths in the SG. As a result, the APEX facility is not able to match the scaled primary loop natural circulation flow rates that arise early in SBLOCA transients. However, all of the passive safety system and sump recirculation natural circulation flows can be properly scaled.

An increase in RCP flow capacity was not necessary because the pumps are tripped at the start of each transient. Their primary contribution during testing is their resistance, which will be preserved.

The CMT volumes will be increased because they are an essential part of the passive safety system response. ADS actuation is dependent on the CMT liquid volume. The CMT line resistance shall also be reduced to simulate the scaled CMT draining rates. CMT volume and flow rate are critical to the transition from ADS4 blowdown to IRWST injection. Full-pressure ADS4 blowdown transition tests are being considered.

The IRWST injection flow rate has a significant impact on core cooling. Therefore, the IRWST lines will be modified to increase their flow capacity to match the AP1000 design on a scaled basis. The onset of IRWST injection is dependent on the liquid level height in the tank. The APEX IRWST minimum liquid volume will be preserved to match the design change. However, the scaled liquid height and IRWST liquid volume cannot be exactly preserved simultaneously. The containment sump flood-up curb height will be adjusted accordingly.

The fourth-stage valves of the automatic depressurization system (ADS4) ensure that the primary system pressure will be reduced below the IRWST liquid level head so that injection can begin. The increased flow area is needed to properly simulate the AP1000 ADS4 operation. In addition, the resistance of each ADS4 line will be decreased accordingly to properly match the pressure drop behavior under non-choked flow conditions.

Increases to the PRHR heat exchanger tube volume and surface area were not deemed necessary for the experiment. As with the SG, the PRHR tube volume is small compared to the primary loop volume. Furthermore, it is oversized for the decay power operations involved in testing. That is, they have much more surface area than needed to remove core heat. The impact of not increasing the PRHR will be an increase in the core fluid temperature rise. This is well within the design constraints of the existing facility. Properly scaled natural circulation flow rates are ensured by adjusting the PRHR loop resistance.

The ADS1-3 valves and the accumulators remain the same as the original AP600 design. Therefore, these components will not be modified for the AP1000 testing program.

### A.1.4 Applicability of the AP600 Scaling Analysis

The original scaling analysis performed in support of the design of the APEX test facility for AP600 certification is documented in WCAP-14270. The comprehensive report represents the first successful application of the hierarchical two-tiered scaling (H2TS) methodology for the design and construction of an experimental test facility. Westinghouse issued the report in January 1995 [Ref. 1]. The objective of the scaling study was to obtain the physical dimensions of a test facility that would simulate the flow and heat transfer behavior of importance to the AP600 passive safety system operation. The report includes all of the scaling criteria that were needed to define the geometry and operating conditions of the reduced-scale APEX test facility.

Figure A.1 shows the general scaling methodology used to design the APEX test facility for the AP600 test program. First, the general objective of the test program was stated. The general objective was to assess the passive safety system operation for loss-of-coolant-accidents (LOCAs). A small-break loss-of-coolant accident (SBLOCA) phenomena identification and ranking table (PIRT) was then developed to identify the important thermal-hydraulic phenomena that should be preserved in the test facility. The next step was to perform a scaling analysis for each of the AP600 operational modes during the LOCA. The four key modes of operation identified were natural circulation, system depressurization, venting/draining/injection, and recirculation. The analyses resulted in a set of dimensionless groups and similarity criteria that had to be preserved in the test facility. These similarity criteria were derived from the governing equations of mass, momentum, and energy conservation for the system, subsystems, and components for each of the four operating modes. The similarity criteria were used to obtain the scaling ratios needed to design the test facility geometry and operating conditions.

As shown in Figure A.1, the scaling ratios were developed for a specific set of experiment objectives, which produce a specific set of system responses (i.e., operation modes and thermal-hydraulic phenomena) within a specific plant geometry. A review of the scaling ratios reveals that they are also directly applicable to the design of the APEX-AP1000 test facility for the following reasons.

First, the experiment objectives of the APEX-AP1000 test program are a subset of the AP600 experiment objectives. Therefore, the same operation modes and thermal-hydraulic phenomena will be produced.

Westinghouse recently issued an AP1000 PIRT and Scaling Assessment, which reviews the original scaling analysis effort and assesses the applicability of the original AP600 test program to the AP1000 design [Ref. 6]. Westinghouse concluded that the AP1000 PIRT was the same as the AP600 PIRT, with the exception of the potential higher importance of HL entrainment during the post-ADS4 actuation phases of the SBLOCA. Therefore, entrainment scaling of the post-ADS4 actuation phase was of particular interest to the present study.

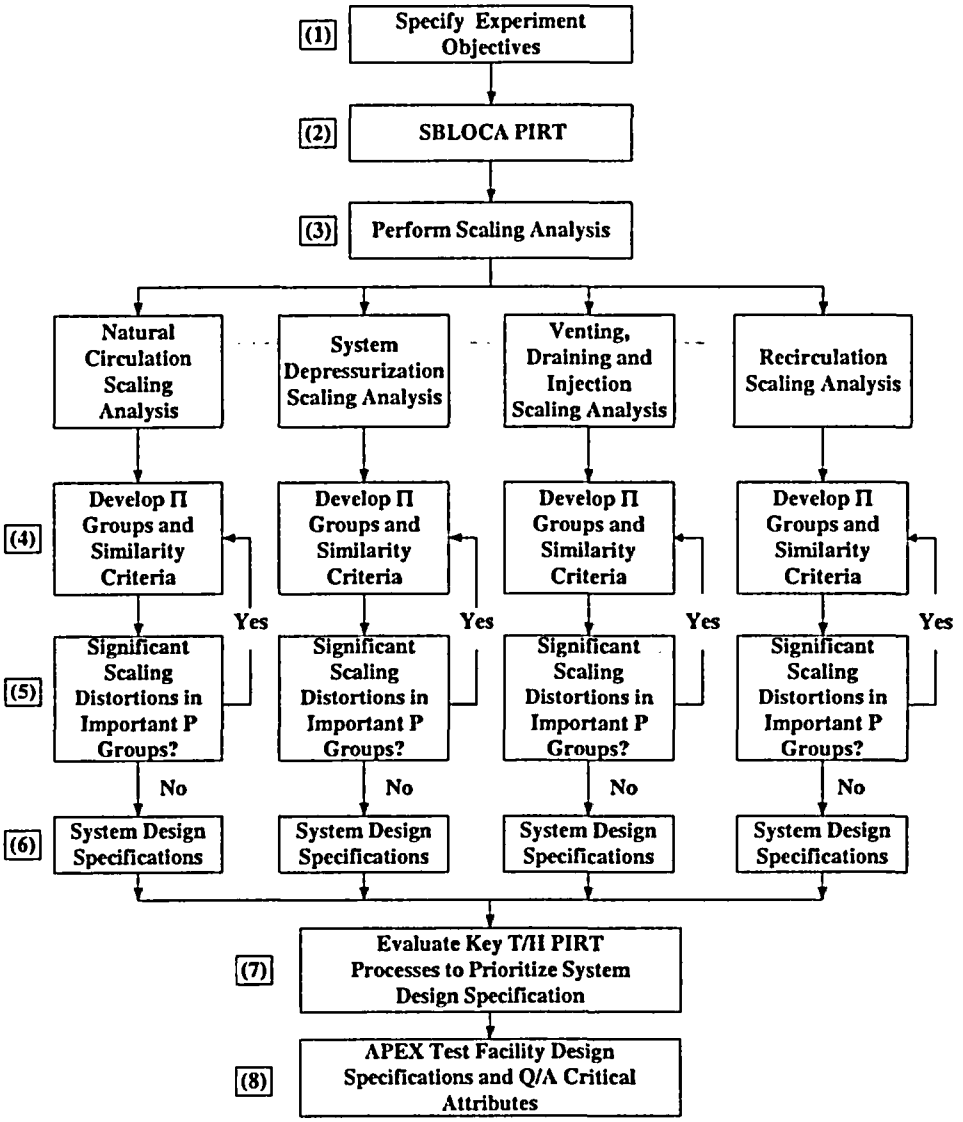


Figure A.1 General Scaling Methodology for the APEX Test Facility [Ref. 1]

Second, the AP1000 design is geometrically similar to the AP600 design. This means that there is a one-to-one correspondence of primary loop components, arranged in the same sequence, and all of the important AP1000 geometric scales, (i.e., cross-sectional flow areas, volumes, lengths) can be related to the AP600 design by constant scaling factors.

In conclusion, the general scaling methodology remains the same. Therefore, the scaling ratios obtained in the original scaling analysis, with a few exceptions, can be directly applied to the design of an APEX-AP1000 test facility. The following section describes the scope of the scaling assessment for the APEX-AP1000 test facility.

### A.1.5 Scope of the Current Scaling Assessment

The following analyses have been included in the OSU APEX-AP1000 Scaling Report to guide the design of the APEX test facility modifications presented in Table A.3:

- Core Decay Power Scaling Analysis
- IRWST, CMT, and PZR Liquid Volume and Height Scaling Analysis
- IRWST, CMT, PRHR, and Sump Recirculation Line Scaling
- Pressurizer Surge Line Scaling Analysis
- RCS Depressurization Scaling Analysis
- ADS4 Blowdown Scaling Analysis
- Upper Plenum Pool Entrainment Scaling Analysis

The core decay power analysis was needed to develop the revised decay power algorithm for the tests. The original power scaling ratios were used in the decay power scaling analysis. The IRWST, CMT, and PZR volume scaling analyses were straightforward and implemented the original volume scaling ratios. Similarly, the original line resistance scaling ratios were used to scale the IRWST, CMT, PRHR, and sump recirculation line pressure drops. The PZR surge line scaling analysis represents a change to the original scaling analysis. That is, it is intended to provide a better representation of the PZR draining process. The PZR surge line scaling analysis resulted in a new diameter scaling ratio for the PZR surge line. The ADS4 blowdown scaling analysis represents an improved depressurization scaling analysis technique based on the energy equation. Of particular interest to this study, is the transition from ADS4 blowdown to IRWST injection. The upper plenum pool entrainment scaling analysis is intended to provide a better simulation of the upper plenum entrainment and de-entrainment processes. This analysis also includes an upper core plate flow area scaling analysis to better simulate counter-current flooding in the upper core plate.

## A.2 Hierarchical Two-Tiered Scaling (H2TS) Methodology

The H2TS methodology was used to develop the similarity criteria necessary to scale the APEX-AP1000 systems and processes of importance to an SBLOCA transient. The H2TS methodology was developed by the NRC and is fully described in Appendix D to NUREG/CR-5809 [Ref. 9]. This is the same methodology that was used to develop the similarity criteria for the original APEX facility.

Figure A.2 is taken from NUREG/CR-5809. It presents the four basic elements of the H2TS analysis methodology. The first element consists of subdividing the plant into a hierarchy of systems. Each system was subdivided into interacting subsystems, which were further subdivided into interacting modules, which were further subdivided into interacting constituents (materials), which were further subdivided into interacting phases (liquid, vapor, or solid). Each phase could be characterized by one or more geometrical configurations, and each geometrical configuration could be described by three field equations (mass, energy, and momentum conservation equations). Each field equation could be characterized by several processes.

After identifying and subdividing the system of interest, the next step was to identify the scaling level at which the similarity criteria should be developed. This was determined by examining the phenomena being considered. For example, if the phenomenon being considered involved mass, momentum, or energy transport between materials such as water and solid particles, the scaling analysis was performed at the constituent level. If the phenomenon of interest involved mass, momentum, or energy transport between vapor and liquid, the scaling analysis was performed at the phase level. Therefore, identifying the scaling level depended on the phenomenon being addressed.

Thermal-hydraulic phenomena involving integral RCS interactions, such as primary system depressurization or loop natural circulation, were examined at the "system" level. Thermal-hydraulic phenomena, such as SG heat transfer, were examined at the "subsystem" level. Specific interactions between the steam-liquid mixture and the stainless steel structure were examined at the "constituent" level.

Chapter 3 presents the scaling analyses that were performed for the different APEX-AP1000 test facility modifications. It identifies the thermal-hydraulic phenomena of interest, the system level (i.e., control volume) at which the analysis was performed, the geometrical configuration, the applicable balance equations and the processes important to the thermal-hydraulic phenomena of interest.

The H2TS methodology required performing a "top-down" (system) scaling analysis, which examined the synergistic effects on the system caused by complex interactions between the constituents which are deemed important by the PIRT. Its purpose was to use the conservation equations at a given scaling level to obtain characteristic time ratios and similarity criteria. It also identified the important processes to be addressed in the bottom-up scaling analysis.

The H2TS methodology also required performing a "bottom-up" (process) scaling analysis, which developed similarity criteria for specific processes, such as flow pattern transitions and flow-dependent heat transfer. The focus of the bottom-up scaling analysis was to develop similarity criteria to scale individual processes of importance to system behavior as identified by the PIRT.

### A.2.1 Time Ratios

The basic objective of the H2TS methodology was to develop sets of characteristic time ratios for the transfer processes of interest. This was done by writing the control volume balance equations for each constituent "k" as follows:

$$\frac{d V_k \psi_k}{dt} = \Delta[Q_k \psi_k] \pm \Sigma (j_{kn} A_{kn}) + S_k \tag{A.1}$$

where

$$\Delta[Q_k \psi_k] = [Q_k \psi_k]_{in} - [Q_k \psi_k]_{out} \tag{A.2}$$

In equation (A.1) the $\psi_k$ term represents the conserved property; $\psi_k = \rho$, $\rho u$ or $\rho \varepsilon$ (mass, momentum, or energy per unit volume); $V_k$ is the control volume; $Q_k$ is the volumetric flow rate; $j_{kn}$ is the flux of property $\psi_k$ transferred from constituent "k" to "n" across the transfer area $A_{kn}$. Hence, $\Delta[Q_k \psi_k]$ represents the usual mass, momentum, or energy convection terms, and $\Sigma j_{kn} A_{kn}$ represents transport process terms such as condensation, and $S_k$ represents the distributed sources, such as decay power or body forces acting internal to the control volume. Equation (A.1) can be put in dimensionless form by specifying the following dimensionless groups in terms of the constant initial and boundary conditions:

$$V_k^+ = \frac{V_k}{V_{k,0}}, \psi_k^+ = \frac{\psi_k}{\psi_{k,0}}, Q_k^+ = \frac{Q_k}{Q_{k,0}}, j_{kn}^+ = \frac{j_{kn}}{j_{kn,0}}, A_{kn}^+ = \frac{A_{kn}}{A_{kn,0}}, S_k^+ = \frac{S_k}{S_{k,0}} \tag{A.3}$$

Substituting these groups into equation (A.1) yields:

$$V_{k,0} \psi_{k,0} \frac{d V_k^+ \psi_k^+}{dt} = Q_{k,0} \psi_{k,0} \Delta[Q_k^+ \psi_k^+] \pm \Sigma \left( j_{kn,0} A_{kn,0} \right) j_{kn}^+ A_{kn}^+ + S_{k,0} S_k^+ \tag{A.4}$$

Dividing both sides of this equation by $Q_{k,0}\, \psi_{k,0}$ yields:

$$\tau_k \frac{d V_k^+ \psi_k^+}{dt} = \Delta[Q_k^+ \psi_k^+] \pm \Sigma \Pi_{kn} j_{kn}^+ A_{kn}^+ + \Pi_{sk} S_k^+ \tag{A.5}$$

where the *residence time* of constituent "k" is

$$\tau_k = \frac{V_{k,0}}{Q_{k,0}} \tag{A.6}$$

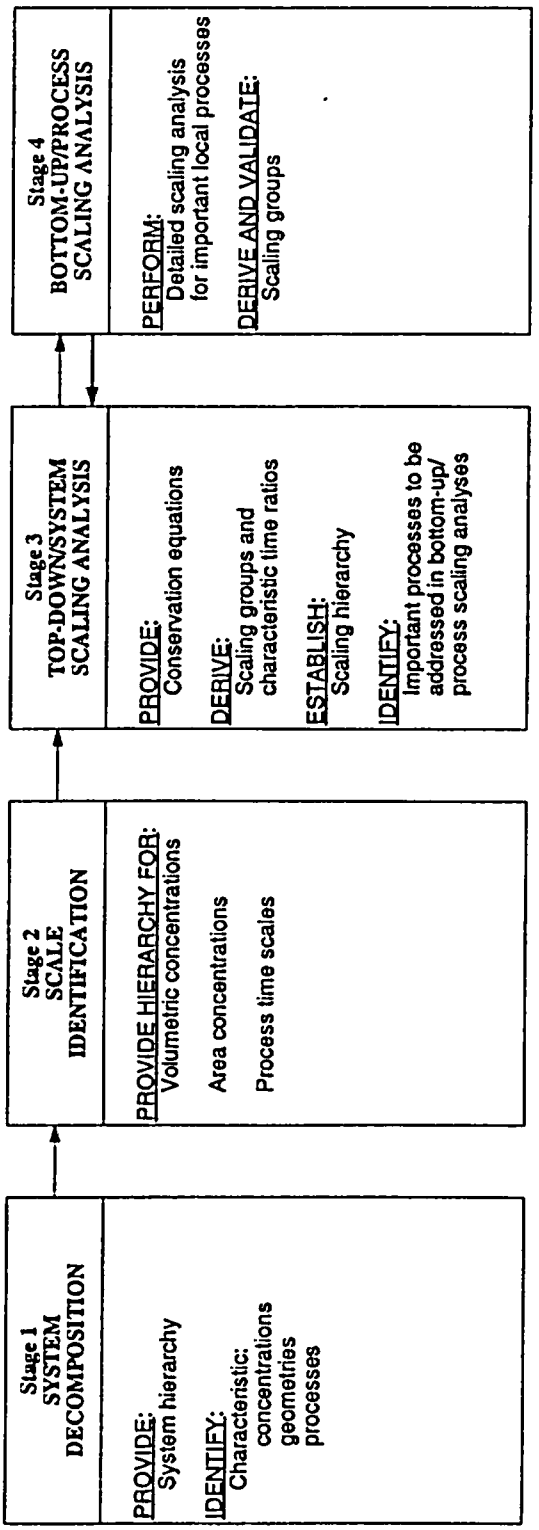


Figure A.2 Flow Diagram for the Hierarchical, Two-Tiered Scaling Analysis [Ref. 9]

and the *characteristic time ratio* for a transfer process between constituents "k" and "n" is given by:

$$\Pi_{kn} = \frac{j_{kn,0} A_{kn,0}}{Q_{k,0} \Psi_{k,0}} \tag{A.7}$$

The characteristic time ratio for the distributed source term within the control volume is given by:

$$\Pi_{sk} = \frac{S_{k,0}}{Q_{k,0} \Psi_{k,0}} \tag{A.8}$$

Because each transfer process has a characteristic time ratio, it is possible to rank the importance of each process by comparing the time ratios. If a specific transfer process is to have the same effect in the prototype and the model, the characteristic time ratios must be preserved.

### A.2.2 Process Ranking Using Characteristic Time Ratios

Let us define $M[(P_{i,j}), (P_{i+1,j}),...(P_{Ni,Nj})]$ as the set of time ratios that characterize all of the individual processes that occur during the evolution of a transient. The subscripts $i, j, N_i, N_j$ identify the specific process, the hierarchical level, the total number of specific processes, and the total number of hierarchical levels, respectively.

Because of differences in geometrical scale and fluid properties, it is impossible to exactly duplicate the "time ratio set" for the full-scale prototype, $M_p$, in a reduced-scale model. That is, exact similitude for all processes cannot be preserved; therefore:

$$M_p \neq M_m \tag{A.9}$$

The subscript, *p*, refers to the full-scale prototype and the subscript, *m*, refers to the reduced-scale model.

It is possible to design a reduced-scale test facility that preserves the similitude of a subset of time ratios $T[\Pi_{i,j}]$, that characterize the processes of greatest importance to the transient. This optimizes the model design to investigate the important processes, while distorting the less-important processes.

To determine which processes govern the overall evolution of a transient, numerical estimates of the characteristic time ratios for the prototype and the model must be obtained for each hierarchical level of interest. Physically, each characteristic time ratio, $\Pi_i$, is composed of a specific frequency, $\omega_i$, which is an attribute of the specific process, and the residence time constant, $\tau_{cv}$, for the control volume. That is:

$$\Pi_i = \omega_i \tau_{cv} \tag{A.10}$$

The specific frequency defines the mass, momentum, or energy transfer rate for a particular process. The residence time defines the total time available for the transfer process to occur within the control volume. A numerical value of:

$$\Pi_i < 1 \tag{A.11}$$

means that only a small amount of the conserved property would be transferred in the limited time available for the specific process to evolve. As a result, the specific process would not be important to the overall transient. A numerical value of:

$$\Pi_i \geq 1 \tag{A.12}$$

means that the specific process evolves at a high enough rate to permit significant amounts of the conserved property to be transferred during the time period, $\tau_{cv}$. Such processes would be important to the overall transient behavior.

### A.2.3 Scaling Criteria Development

The scaling analysis results in a set of characteristic time ratios (dimensionless Π groups) and similarity criteria for each mode of operation. Because it is impossible to identically satisfy all of the similarity criteria simultaneously, the set only includes those criteria that must be satisfied in order to scale the most important phenomena identified by the PIRT.

Scaling criteria.were developed by requiring that the characteristic time ratios for a subset of specific processes in the prototype (usually those of greatest importance) are matched in the model at each hierarchical level. That is,

$$T\{\Pi_i\}_m = T\{\Pi_i\}_p \tag{A.13}$$

These criteria were satisfied by adjusting the physical geometry, fluid properties, and operating conditions of the model, thereby optimizing the model design for the specific process of interest.

### A.2.4 Evaluation of Scale Distortion

The scaling criteria were evaluated to determine if the scale model geometry, boundary conditions, or operating conditions would introduce significant scaling distortions. Distortions were also evaluated relative to other modes of operation.

The effect of a distortion in the model for a specific process can be quantified as follows:

$$DF = \frac{[\Pi_i]_p - [\Pi_i]_m}{[\Pi_i]_p} \tag{A.14}$$

The distortion factor, DF, physically represents the fractional difference in the amount of conserved property transferred through the evolution of a specific process in the prototype to the amount of conserved property transferred through the same process in the model during their respective residence times. A distortion factor of zero would indicate that the model ideally simulates the specific process. A distortion factor of +0.05 would indicate that the specific process in the model transfers 5 percent less of the conserved property (on a scaled basis) than the same process in the prototype. The distortion factor can also be written as:

$$DF = 1 - [\omega_i]_R [\tau_{cv}]_R \tag{A.15}$$

or

$$DF = 1 - [\Pi_i]_R \qquad \text{(A.16)}$$

The degree to which a specific transfer process could impact a particular transient can be determined by comparing the *maximum* characteristic time ratio for each of the transfer processes that arise during the transient.

Upon satisfying the important scaling criteria, the component geometries and operating conditions were specified for the APEX-AP1000 test facility.

## A.3 Scaling Analysis for the APEX-AP1000 Modifications

This chapter presents the scaling analyses performed to obtain the component geometries and system operating conditions for the APEX-AP1000 test facility. Tables A.4 and A.5 present the scaling ratios that were derived in WCAP-14270 and used for the design of the APEX-AP1000 test facility modifications.

Table A.4 APEX-AP1000 Primary Loop Scaling Ratios from WCAP-14270 [Ref. 1]

| Parameter | Desired Scaling Ratio |
|---|---|
| CORE | a,b,c |
| Length Ratio | |
| Flow Area Ratio | |
| Fluid Velocity Ratio | |
| Power Ratio | |
| Fluid Residence Time Ratio | |
| Mass Flow Ratio | |
| Volume Ratio | |
| Power/Volume Ratio | |
| HOT AND COLD LEGS | |
| Length Ratio | |
| Diameter Ratio | |
| Flow Area Ratio | |
| Volume Ratio | |
| Fluid Velocity Ratio | |
| Fluid Residence Time Ratio | |
| Mass Flow Ratio | |
| PRESSURIZER | |
| Volume Ratio | |
| Liquid Height Ratio | |

Table A.5 APEX-AP1000 Passive Safety System Scaling Ratios from WCAP-14270

| Parameter | Desired Scaling Ratio |
|---|---|
| CORE MAKEUP TANK | a,b,c |
| Length Ratio | |
| Flow Area Ratio | |
| Draining Mass Flow Rate Ratio | |
| Volume Ratio | |
| ACCUMULATOR | |
| Volume Ratio | |
| Mass Flow Ratio | |
| IRWST | |
| Length Ratio | |
| Flow Area Ratio | |
| Draining Mass Flow Rate Ratio | |
| Volume Ratio | |
| LOWER CONTAINMENT SUMPS | |
| Length Ratio | |
| Flow Area Ratio | |
| Draining Mass Flow Rate Ratio | |
| Volume Ratio | |

The horizontal HL and CL scaling ratios were established based on preserving flow regime transitions in the legs.

The 1:2 time scaling requirement has been imposed on all of the system components and operations. The scaling ratios presented in Tables A.4 and A.5 have been applied in the following sections to obtain the revised APEX component geometries as needed to match the new AP1000 design.

### A.3.1 Core Decay Power and Flow Area Scaling Analysis

One of the key changes to the AP1000 is the increase in core thermal power from 1,933 MW thermal to 3,400 MW thermal. Three modifications were made to the APEX test facility as a result of the power change:

- A higher power core was installed.
- The core flow area was adjusted.
- The decay power algorithm was modified.

#### *A.3.1.1 Maximum Core Power*

Based on the power scaling ratio given in Table A.4, the new core power needed in APEX to match a 3% decay power in the AP1000 was:

(A.17)

This resulted in a desired power in APEX of 1.06 MW thermal. A new 48 rod bundle core with a [ ]$^{a,b,c}$ thermal power was installed. This represents a [ ]$^{a,b,c}$ decay power.

#### *A.3.1.2 Core Flow Area*

Based on the core flow area ratio given in Table A.4, the new core flow area needed in APEX to properly match the scaled core flow area in AP1000 was:

(A.18)

The AP1000 effective core flow area is [ ]$^{a,b,c}$. Using the scaling ratio in equation (A.18), the desired APEX-AP1000 core flow area is [ ]$^{a,b,c}$ or [ ]$^{a,b,c}$. Using 48 heaters, each having a [ ]$^{a,b,c}$ diameter, results in an actual core flow area of [ ]$^{a,b,c}$.

#### *A.3.1.3 Decay Power Algorithm*

Establishing the initial conditions for ADS4 operation and long-term cooling requires that the total energy input into the system, to the point of reaching the transition pressure be properly scaled. The integrated core power ratio is written as follows:

$$E_{core,R} = \frac{\int_o^{t_m} q_{core,m}\, dt_m}{\int_o^{t_p} q_{core,p}\, dt_p} \qquad \text{(A.19)}$$

where $t_m$ is the time it takes in APEX-AP1000 to reach the ADS4 opening pressure, and $t_p$ is the time it takes in AP1000 to reach the ADS4 opening pressure. Since the ideal core power scaling ratio given in Table A.4 is [ ]$^{a,b,c}$ and the ideal time scaling ratio is 1:2, the integrated core power ratio should be [ ]$^{a,b,c}$.

The 1979 Decay Heat Standard for Light-Water Reactors was used to model the decay power curve for the AP1000 [Ref. 11]. Figure A.3 shows the decay power algorithm for the APEX-AP1000 test facility. The power algorithm is designed to match the ideally scaled AP1000 decay power after ~160 seconds. Similarly, as shown in Figure A.4, the total integrated decay power matches after 160 seconds.

a,b,c

Figure A.3 Comparison of the APEX-AP1000 Decay Power Algorithm and the Ideally Scaled AP1000 Decay Power Curve

a,b,c

Figure A.4 Comparison of the APEX-AP1000 Integrated Decay Power to the Ideally Scaled AP1000 Decay Power

### A.3.2 IRWST, CMT, Sump, and Pressurizer Geometric Scaling Analysis

Table A.6 presents the results of applying the scaling ratios of Table A.5 to the AP1000 IRWST, CMT, sump, and PZR.

Table A.6 Results of IRWST, CMT, Sump, and Pressurizer Geometry Scaling

| Parameter | Scaling Ratio | AP1000* | APEX Ideal | APEX Actual | Units | AP1000* | APEX Ideal | APEX Actual | Units |
|---|---|---|---|---|---|---|---|---|---|
| IRWST Liq. Volume (min.) | | | | | | | | | |
| IRWST Liq. Level (min.) | | | | | | | | | |
| IRWST Liq. Surface Area | | | | | | | | | |
| IRWST Level Setpoint for Sump Recirculation | | | | | | | | | |
| IRWST Liq. Head on DVI | | | | | | | | | |
| CMT Volume | | | | | | | | | |
| CMT Internal Diameter | | | | | | | | | |
| CMT Internal Height | | | | | | | | | |
| CMT Volume for ADS-1 Actuation | | | | | | | | | |
| CMT Volume for ADS4 Actuation | | | | | | | | | |
| Sump Liq. Volume Below DVI Elevation | | | | | | | | | |
| Difference Between DVI and Sump Flood-up Elevations** | | | | | | | | | |
| Sum Liq. Surface Area | | | | | | | | | |
| Pressurizer Volume | | | | | | | | | |
| Pressurizer Liq. Volume | | | | | | | | | |
| Pressurizer Inside Diameter | | | | | | | | | |

a,b,c

* AP1000 Plant Parameters Document [Ref. 8]

** Assumes break occurs in loop compartment

### A.3.3 ADS4, IRWST, CMT, PRHR, and Sump Recirculation Line Scaling

A detailed analysis of the pressure drops in the passive safety system balance and injection lines was provided in Section A.7 of WCAP-14270 [Ref. 1]. The pressure drop for a section of pipe having a constant diameter is given by the following equation:

$$\Delta P = \frac{1}{2}\left(\frac{fl}{D} + K\right)\rho v^2 \qquad \text{(A.20)}$$

where $f$ is the Darcy friction factor, $l/D$ is the piping length to diameter ratio, $K$ is the form loss coefficient due to fittings and bends, and $v$ is the fluid velocity in the section of pipe. For single-phase, non-choked, fluid flow with fluid property similitude, the ratio of the model to the prototype can be written as:

$$\Delta P_R = F_{T,R}\, v_R^2 \qquad \text{(A.21)}$$

In this equation, $F_{T,R}$ is the ratio of the total friction and form loss coefficients. To preserve the line pressure drops, it is required that the pressure drop ratio, $\Delta P_R$, be 0.25 and that the velocity ratio, $v_R$, be 0.5. Substituting these scaling ratios into the equation above yields the following requirement:

$$F_{T,R} = 1 \qquad \text{(A.22)}$$

For the piping under consideration, the form loss coefficients, $K$, dominate. That is, the presence of valves, elbows, and other fittings make the value of $K$ much larger than the value of $fl/D$. In light of this fact, the line resistance can be adjusted using a flow orifice.

The AP1000 line resistance data, $R$ (ft/gpm$^2$), is expressed in terms of head loss over the square of volumetric flow rate. That is, the line resistance is expressed in terms of measured quantities as follows:

$$R = \frac{g_c \Delta P}{g \rho Q^2} \qquad \text{(A.23)}$$

The resistance is related to the friction and form loss factors as follows:

$$R = \frac{1}{2}\left(\frac{fl}{D} + K\right)\frac{1}{a^2} \qquad \text{(A.24)}$$

where $a$ is the flow area of the pipe. Therefore, the units of line resistance are often expressed as 1/ft$^4$. The flow area scaling ratio is given as 1:48. Therefore, the line resistance scaling ratio for single-phase fluid under non-choked flow conditions is given as:

$$R_R = 48^2 = 2304 \qquad \text{(A.25)}$$

Table A.7 lists the range of line resistance values required for the IRWST and sump recirculation lines in the APEX-AP1000 test facility. Table A.8 presents similar values for the CMT and PRHR lines.

The ADS4/HL nozzle diameter and resistance was scaled as with previous lines. However, the two ADS4 branch lines that comprise a single ADS4 train on a HL require a different scaling approach because the intent is to model two ADS4 branch lines with a single line in the APEX-AP1000 test facility. That is, the flow area of one APEX ADS4 branch line must equal the scaled flow area of two AP1000 branch lines:

$$a_{APEX} = \frac{2a_{AP1000}}{48} \tag{A.26}$$

In terms of a diameter scaling ratio, the ratio of a single ADS4 branch line diameter in APEX to a single ADS4 branch line in the AP1000 is:

$$D_{ADS,R} = \frac{1}{\sqrt{24}} \tag{A.27}$$

Table A.9 presents the ADS4 line diameters and resistance assuming that two AP1000 ADS4 branch lines are modeled with a single branch line in APEX.

Table A.7 IRWST and Sump Recirculation Line Resistance Values (ft/gpm$^2$) [Ref. 8]

| | AP1000 | | | | IDEAL APEX | | | |
|---|---|---|---|---|---|---|---|---|
| **Path/Line** | **I.D. (in)** | **Min** | **Nom** | **Max** | **I.D. (in)** | **Min** | **Nom** | **Max** |
| IRWST TO SUMP TEE | | | | | | | | |
| Line A | | | | | | | | |
| Line B | | | | | | | | |
| SUMP TEE TO MOV ISOLATION VALVE | | | | | | | | |
| Line A | | | | | | | | |
| Line B | | | | | | | | |
| MOV ISOLATION VALVE TO CHECK SQUIB VALVE | | | | | | | | |
| Line A | | | | | | | | |
| Line B | | | | | | | | |
| CHECK/SQUIB VALVES PARALLEL PATHS | | | | | | | | |
| Line A | | | | | | | | |
| Line B | | | | | | | | |
| CHECK/SQUIB VALVES TO DVI INJECTION LINE TEE | | | | | | | | |
| Line A | | | | | | | | |
| Line B | | | | | | | | |
| IRWST INJECTION LINE TO DVI NOZZLE | | | | | | | | |
| Line A | | | | | | | | |
| Line B | | | | | | | | |
| SUMP RECIRC. PATH TO IRWST INJECTION LINE TEE | | | | | | | | |
| Line A | | | | | | | | |
| Line B | | | | | | | | |
| IRWST DRAIN TO CONTAINMENT | | | | | | | | |
| Line A | | | | | | | | |
| Line B | | | | | | | | |

a,b,c

Table A.8 CMT and PRHR Line Resistance Line Values (ft/gpm$^2$) [Ref. 8]

| | AP1000 | | | | IDEAL APEX | | | |
|---|---|---|---|---|---|---|---|---|
| **Component** | **I.D. (in)** | **Min** | **Nom** | **Max** | **I.D. (in)** | **Min** | **Nom** | **Max** |
| CORE MAKEUP TANK | | | | | | | | |
| CL Balance Line | | | | | | | | |
| CMT to ACC Tee | | | | | | | | |
| ACC to DVI | | | | | | | | |
| PRHR | | | | | | | | |
| RCS HL to ADS4 Reducer | | | | | | | | |
| ADS4 Reducer to PRHR Reducer | | | | | | | | |
| PRHR Reducer to PRHR HX Inlet | | | | | | | | |
| PRHR HX Inlet | | | | | | | | |
| PRHR HX Tube | | | | | | | | |
| PRHR HX Outlet | | | | | | | | |
| PRHR HX Outlet to SG | | | | | | | | |

a,b,c

Table A.9 ADS-4 Line Resistance Values(ft/gpm$^2$) [Ref. 8]

| ADS4 | AP1000 | | | | IDEAL APEX | | | |
|---|---|---|---|---|---|---|---|---|
| | **I.D. (in)** | **Min** | **Nom** | **Max** | **I.D. (in)** | **Min** | **Nom** | **Max** |
| ADS4/HL Nozzle | | | | | | | | |
| ADS4 Branch Line | | | | | | | | |
| ADS4-1 (50%) | | | | | | | | |
| ADS4-1 100%) | | | | | | | | |
| ADS4-2 (50%) | | | | | | | | |
| ADS4-2 (100%) | | | | | | | | |

a,b,c

## A.4 Pressurizer Surge Line Scaling

This section represents a change to the original PZR surge line scaling analysis presented in WCAP-14270, which focused on preserving the two-phase flow regime transitions. However, a recent NRC analysis performed by Bessette and Di Marzo suggests that preserving the PZR draining behavior is more important to the outcome of SBLOCA transients [Ref. 2]. Based on a thorough review of the NRC analysis, the PZR surge line was modified to properly simulate the AP1000 PZR draining behavior.

Bessette and Di Marzo expressed the governing momentum balance equation for the PZR surge line filling and draining process, in dimensionless form, as follows:

$$\dot{Z}\left|\dot{Z}\right| + AZ = B \tag{A.28}$$

where:

$$A = \frac{\frac{C}{\rho g} + 1}{\frac{\Phi_{LO}^2}{2}\left(\frac{S_{PZR}}{S_{SL}}\right)^2\left(f\frac{L}{D} + K\right)} \tag{A.29}$$

$$B = \frac{\frac{C}{\rho g} - \frac{P_{PZR}}{\rho g H_{PZR}} - (1-\alpha)\frac{H_{SL}}{H_{PZR}}}{\frac{\Phi_{LO}^2}{2}\left(\frac{S_{PZR}}{S_{SL}}\right)^2\left(f\frac{L}{D} + K\right)} \tag{A.30}$$

and

$$C = \rho g \frac{S_{PZR}}{S_{SL}} \tag{A.31}$$

Integrating equation (A.28) yields the PZR surge line filling and draining period:

$$\tau_{SL} = 2\left(\frac{H_{PZR}}{g}\right)^{1/2}\left[\left(\frac{B^{1/2}}{A}\right)_{\alpha=0} + \left(\frac{B^{1/.2}}{A}\right)_{\alpha=0.8}\right] \tag{A.32}$$

For the APEX-AP1000, a 1:2 scale time period is required. Preserving a one-half time scale PZR surge line filling and draining period requires that:

$$(H_{PZR})_R^{1/2} = \frac{1}{2} \tag{A.33}$$

and that:

$$\left(\frac{B^{1/2}}{A}\right)_R = 1 \tag{A.34}$$

The APEX-AP1000 PZR liquid height, $H_{PZR}$, is [ ]$^{a,b,c}$. Therefore, the scaling criterion given by equation (A.33) is met.

Table A.10 presents the results obtained for equation (A.34). The value is close to unity. It has been assumed that the ratio of the Martinelli-Nelson two-phase flow multiplier, $\Phi_{LR}$, is unity.

In addition to preserving the surge line drain and fill rates, it is desired that the pressure drop ratio in the surge line be [ ]$^{a,b,c}$. That is:

(A.35)

This requires:

(A.36)

As shown in Table A.10, for the line size selected, the friction factor ratio is [ ]$^{a,b,c}$ and the velocity ratio in the surge line is [ ]$^{a,b,c}$. This yields the desired DP ratio of [ ]$^{a,b,c}$.

Table A.10 Results of Pressurizer Surge Line Scaling Analysis

| Parameter | AP1000 | APEX |
|---|---|---|
| Roughness (in) | | |
| ID (in) | | |
| Relative Roughness | | |
| Reynolds Number | | |
| Friction Factor | | |
| Calculated Pressure Drop Ratio | | |
| Friction Factor Ratio | | |
| (fL/d) Ratio | | |
| Pressurizer ID (in) | | |
| $H_{PZR(ft)}$ | | |
| Head at 1 atm (ft) | | |
| HsL (ft) | | |
| $A_R$ (Bessette & di Marzo) | | |
| $B_R$ (Bessette & di Marzo) | | |
| $(B_R)^{1/2}/A$ | | |

a,b,c

## A.5 Reactor Coolant System Depressurization Scaling Analysis

This section presents a revised depressurization scaling analysis for the APEX-AP1000 test facility. It represents a more comprehensive analysis than that presented in the original WCAP-14270. Figure A.5 presents the scaling analysis flow diagram for primary system depressurization. First, the governing set of equations for the depressurization of a two-phase fluid system was developed. This resulted in obtaining a depressurization rate equation. Next, a top-down system level scaling analysis was performed for the RCS, assuming multiple vent and injection paths. This included the development of scaling criteria for sizing the break and ADS flow areas. Last, a bottom-up analysis was performed to describe the scaling of local transport processes, such as the critical flow through the breaks and ADS valves.

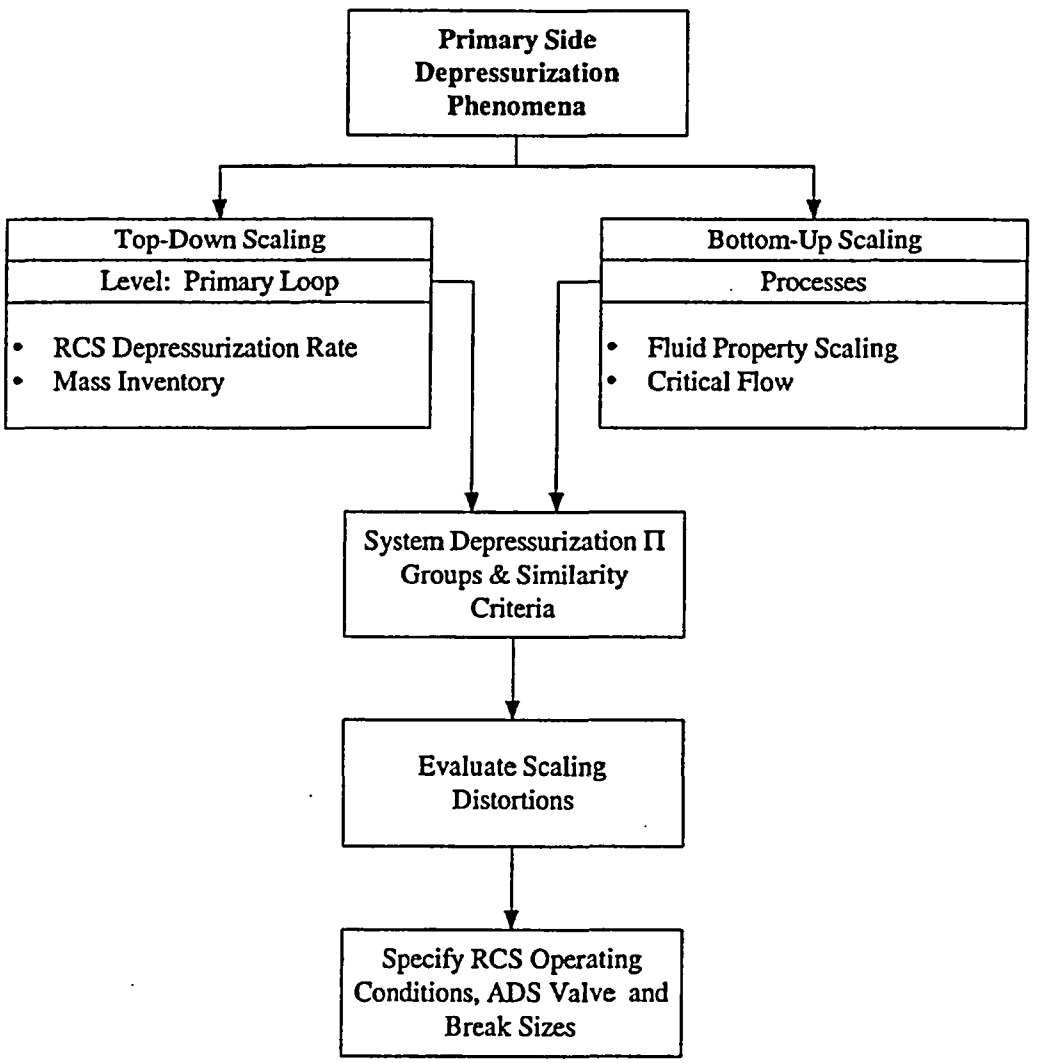


Figure A.5 Flow Chart of the Primary Side Depressurization Scaling Analysis

### A.5.1 Reference Pressure for LOCA Transients

A variety of primary loop blowdown tests will be performed in APEX. The integral system tests will be performed under pressure-scaled conditions to observe all of the passive safety system functions. A series of *full-pressure* tests shall also be performed to examine the transition from ADS4 operation to IRWST injection.

Figure A.6 presents typical trends for the RCS and SG pressures during a SBLOCA transient in the APEX facility. The opening of a break is immediately followed by a period of subcooled blowdown, during which the primary system depressurizes to a pressure equivalent to the SG PORV setpoint. Hence, the primary and secondary system pressures will meet at the onset of saturation conditions in the primary as shown in the figure. The AP600 scaling analysis was the first research to recognize that the onset of primary loop saturation offered a common reference point for the purpose of scaling. This fact, coupled with the concept that the depressurization of systems under phase equilibria conditions exhibits self-similarity, offered the possibility of performing pressure-scaled testing.

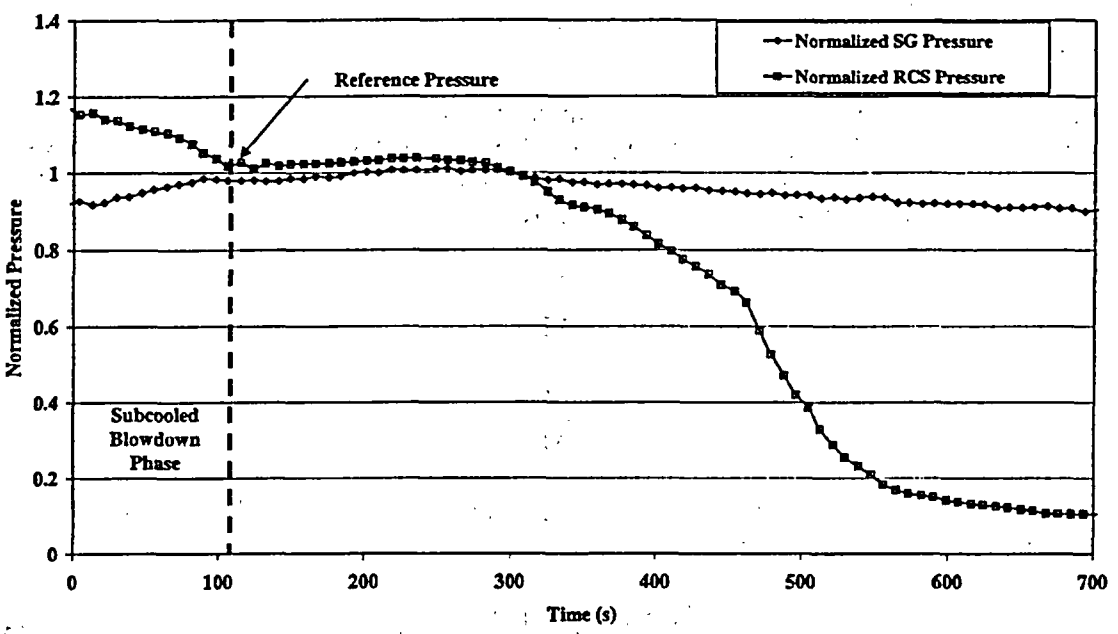


Figure A.6 Primary and Secondary Side Pressures During a Typical 2-Inch Break LOCA in APEX

For the AP1000, the reference pressure for the onset of saturation conditions in the primary loop coincides with the SG PORV pressure setpoint of 1,200 psia. For the APEX-AP1000, this value will be set at 345 psia. The goal of the pressure-scaled testing is to provide the full range of passive safety system behavior for a given transient in the proper event sequence. This data can be used to benchmark the thermal-hydraulic safety analysis codes. However, by scaling the break and ADS1-3 flow areas relative to the saturation reference pressure, the timing of the subcooled blowdown portion of the transient will not proceed at one-half time scale. For rapid blowdowns, such as the DEDVI line break, this effect is negligible. This was demonstrated by the excellent comparisons obtained between the APEX and the full-pressure ROSA AP600 DEDVI tests.

The AP600 test program revealed that the transition from ADS4 operation to the start of IRWST injection was important to core cooling. Therefore, this test program will include a series of full-pressure ADS4 blowdown tests to carefully examine the ADS4 transition under prototypic fluid pressures and temperatures.

### A.5.2 Governing Equations for RCS Two-Phase Fluid Depressurization

The mass conservation equation for an RCS control volume undergoing a depressurization event is given by:

$$\frac{dM}{dt} = \Sigma \dot{m}_{in} - \Sigma \dot{m}_{out} \qquad \text{(A.37)}$$

where M is the fluid mass within the RCS and $\dot{m}$ represents the mass flow rate entering or leaving the RCS. The energy conservation equation for the RCS fluid is expressed as follows:

$$\frac{dU}{dt} = \Sigma(\dot{m}h)_{in} - \Sigma(\dot{m}h)_{out} + q_{SG} + q_{core} + q_{loss} - P\frac{dV}{dt} \qquad \text{(A.38)}$$

where $U$ is the bulk internal energy of the fluid within the RCS; $h$ is the enthalpy of the fluid entering or leaving the RCS; $q_{SG}$, $q_{core}$ and $q_{loss}$ are the SG energy transfer rate, core power, and heat loss, respectively; $P$ is the RCS pressure; and $V$ is the RCS volume. The specific internal energy and specific volume are defined, respectively, as follows:

$$e = \frac{U}{M} \qquad \text{(A.39)}$$

$$v = \frac{V}{M} \qquad \text{(A.40)}$$

The total change in specific internal energy is written in terms of partial differentials with respect to pressure and specific volume, as follows:

$$de = \left(\frac{\partial e}{\partial P}\right)_v dP + \left(\frac{\partial e}{\partial v}\right)_p dv \qquad \text{(A.41)}$$

Substituting equation (A.39) into (A.38) yields:

$$\frac{dMe}{dt} = \Sigma(\dot{m}h)_{in} - \Sigma(\dot{m}h)_{out} + q_{SG} + q_{core} + q_{loss} - P\frac{dV}{dt} \qquad \text{(A.42)}$$

Expanding the term on the left-hand side of equation (A.42), substituting equation (A.37), and rearranging yields:

$$M\frac{de}{dt} = (\Sigma \dot{m}_{in})(h_{in} - e) - (\Sigma \dot{m}_{out})(h_{out} - e) + q_{SG} + q_{core} + q_{loss} - P\frac{dV}{dt} \qquad \text{(A.43)}$$

In equation (A.43), it has been assumed that $h_{in}$ is the same for all the injection locations, and $h_{out}$ is the same for all the vent paths. Substituting equation (A.41) into (A.43), and rearranging yields:

$$M\left(\frac{\partial e}{\partial P}\right)_v \frac{dP}{dt} = (\Sigma \dot{m}_{in})(h_{in} - e) - (\Sigma \dot{m}_{out})(h_{out} - e) + q_{SG} + q_{core} + q_{loss} - P\frac{dV}{dt} - M\left(\frac{\partial e}{\partial v}\right)_p \frac{dv}{dt} \quad \text{(A.44)}$$

Using equation (A.40) and the mass conservation equation, the last term on the right-hand side of equation (A.44) is written as:

$$M\left(\frac{\partial e}{\partial v}\right)_p \frac{dv}{dt} = \left(\frac{\partial e}{dv}\right)_p \frac{dV}{dt} - v\left(\frac{\partial e}{\partial v}\right)_p (\Sigma \dot{m}_{in} - \Sigma \dot{m}_{out}) \quad \text{(A.45)}$$

Substituting back into equation (A.44) yields:

$$M\left(\frac{\partial e}{\partial P}\right)_v \frac{dP}{dt} = (\Sigma \dot{m}_{in})\left[h_{in} - e + v\left(\frac{\partial e}{\partial v}\right)_p\right] - (\Sigma \dot{m}_{out})\left[h_{out} - e + v\left(\frac{\partial e}{\partial v}\right)_p\right] + q_{SG} + q_{core} + q_{loss} - \left[P + \left(\frac{\partial e}{\partial v}\right)_p\right]\frac{dV}{dt} \quad \text{(A.46)}$$

which is the "depressurization rate equation." For the RCS control volume, which has rigid boundaries, equation (A.46) becomes:

$$M\left(\frac{\partial e}{\partial P}\right)_v \frac{dP}{dt} = (\Sigma \dot{m}_{in})\left[h_{in} - e + v\left(\frac{\partial e}{\partial v}\right)_p\right] - (\Sigma \dot{m}_{out})\left[h_{out} - e + v\left(\frac{\partial e}{\partial v}\right)_p\right] + q_{SG} + q_{core} + q_{loss} \quad \text{(A.47)}$$

The net energy transfer rate is given as:

$$q_{net} = q_{SG} + q_{core} + q_{loss} \quad \text{(A.48)}$$

Equation (A.47) is the governing equation for depressurization behavior in the RCS.

### A.5.3 Top-Down Reactor Coolant System Depressurization Scaling Analysis

The mass conservation equation, equation (A.37), is expressed in dimensionless form by dividing each term by its respective initial condition and further dividing by the mass flow rate of the fluid leaving the break. This results in the following dimensionless mass balance equation:

$$\tau_{RCS} \frac{dM^+}{dt} = \Pi_m \Sigma \dot{m}^+_{DVI} - \Sigma \dot{m}^+_{Brk} \tag{A.49}$$

where the superscript "+" indicates normalization with respect to initial conditions. The residence time constant, ($\tau_{rcs}$), for the depressurization transient is given by:

$$\tau_{rcs} = \frac{M_o}{\Sigma \dot{m}_{Brk,o}} \tag{A.50}$$

and the characteristic time ratio is given by:

$$\Pi_m = \frac{\Sigma \dot{m}_{INJ,o}}{\Sigma \dot{m}_{Brk,o}} \tag{A.51}$$

$\Pi_m$ is the system mass flow rate ratio. For a constant injection flow rate, $\Pi_m$ represents the total liquid mass injected into the RCS during the residence time ($\tau_{rcs}$).

Equation (A.47) can be expressed in dimensionless form by dividing each term by its respective initial condition. The normalized terms are as follows:

$$M = M_o M^+ \tag{A.52}$$

$$P = P_o P^+ \tag{A.54}$$

$$q_{net} = q_{net,o} q^+_{net} \tag{A.53}$$

$$\Sigma \dot{m}_{DVI} = \Sigma \dot{m}_{DVI,o} \Sigma \dot{m}^+_{DVI} \tag{A.55}$$

$$\Sigma \dot{m}_{Brk} = \Sigma \dot{m}_{Brk,o} \Sigma \dot{m}^+_{Brk} \tag{A.56}$$

$$\left[h_{DVI} - e + v\left(\frac{\partial e}{\partial v}\right)_p\right] = \left[h_{DVI} - e + v\left(\frac{\partial e}{\partial v}\right)_p\right]_o \left[h_{DVI} - e + v\left(\frac{\partial e}{\partial v}\right)_p\right]^+ \tag{A.57}$$

$$\left[h_{Brk} - e + v\left(\frac{\partial e}{\partial v}\right)_p\right] = \left[h_{Brk} - e + v\left(\frac{\partial e}{\partial v}\right)_p\right]_o \left[h_{Brk} - e + v\left(\frac{\partial e}{\partial v}\right)_p\right]^+ \tag{A.58}$$

Substituting these equations into (A.47) and dividing through by $\dot{m}_{Brk,o}\left[h_{Brk} - e + v\left(\frac{\partial e}{\partial v}\right)_p\right]_o$ yields the dimensionless depressurization rate equation:

$$M^+\left(\frac{\partial e}{\partial P}\right)_v^+ \tau_{RCS}\frac{\partial P^+}{\partial t} = \frac{\Pi_h}{\Pi_\varepsilon}\Sigma\dot{m}_{DVI}^+\left[h_{DVI} - e + v\left(\frac{\partial e}{\partial v}\right)_p\right]^+ - \frac{\Sigma\dot{m}_{Brk}^+}{\Pi_\varepsilon}\left[h_{Brk} - e + v\left(\frac{\partial e}{\partial v}\right)_p\right]^+ + \frac{\Pi_\Gamma}{\Pi_\varepsilon}q_{net}^+ \quad \text{(A.59)}$$

where the characteristic time ratios are given by:

$$\Pi_h = \frac{\Sigma\dot{m}_{DVI,o}\left[h_{DVI} - e + v\left(\frac{\partial e}{\partial v}\right)_p\right]_o}{\Sigma mdot_{Brk,o}\left[h_{Brk} - e + v\left(\frac{\partial e}{\partial v}\right)_p\right]_o} \quad \text{(A.60)}$$

$$\Pi_\Gamma = \frac{q_{net,o}}{\Sigma\dot{m}_{Brk,o}\left[h_{Brk} - e + v\left(\frac{\partial e}{\partial v}\right)_p\right]_o} \quad \text{(A.61)}$$

$$\Pi_\varepsilon = \varepsilon_o = \frac{p_o\left(\frac{\partial e}{\partial P}\right)_{v,o}}{\left[h_{Brk} - e + v\left(\frac{\partial e}{\partial v}\right)_p\right]_o} \quad \text{(A.62)}$$

$\Pi_h$ is the energy flow rate ratio. It represents the ratio of the total energy change due to fluid injection to the energy change caused by the break flow. $\Pi_\Gamma$ is the power ratio. It represents the ratio of the net heat into the system to the rate of fluid energy transport through the break. $\Pi_\varepsilon$ is the fluid mixture dilation property group.

Equation (A.62) reveals that the fluid dilation property group couples the system intensive energy change to the intensive energy at the break. For high pressure systems venting to ambient, the fluid properties at the break are determined at critical flow conditions.

Evaluating the RCS time constant, $\tau_{rcs}$, and the dimensionless groups $\Pi_m$, $\Pi_h$, $\Pi_r$, requires knowledge of the pressure-scaled fluid properties and the critical mass flux. These parameters are evaluated in the bottom-up scaling analysis that follows.

### *A.5.3.1 Similarity of Pressure Trajectories in Dimensionless Phase Space*

One of the goals of the test program is to operate the APEX facility such that the pressure trends that evolve in APEX for a given scenario would be the same for a similar scenario in AP1000 when the results are plotted in dimensionless phase space. That is, plotting scenario pressure histories as $P/P_o$ versus $t/\tau_{RCS}$, or $P/P_o$ versus $M/M_o$, would yield overlaying curves for the two facilities. This condition can be achieved by satisfying the following requirements:

The scenarios are initiated from the same initial condition in dimensionless phase space. In this case $P^+$ at $t^+=0$, is 1. The rate of change, (i.e., slope), is preserved in dimensionless phase space. This imposes the following scaling criterion:

$$\left(\frac{dP^+}{dt^+}\right)_R = 1 \tag{A.63}$$

Satisfying the requirement given by equation (A.63) means preserving the dimensionless $\Pi$ groups on the right-hand side of equation (A.59). If the two requirements listed above are satisfied, the following is true:

$$\left(\frac{P}{P_o}\right)_{APEX} = \left(\frac{P}{P_o}\right)_{AP1000} \tag{A.64}$$

This means that the dimensionless pressure at any point along the scenario trajectory will be the same in APEX and AP1000.

Figure A.7 shows how the saturation pressures in APEX would relate to the saturation pressures in AP1000. In this figure, $P_o$ for AP1000 is 8.27 MPa (1200 psia), while $P_o$ for APEX is 2.36 MPa (342 psia). These pressures correspond to the turbine bypass pressure relief setpoints on the secondary side.

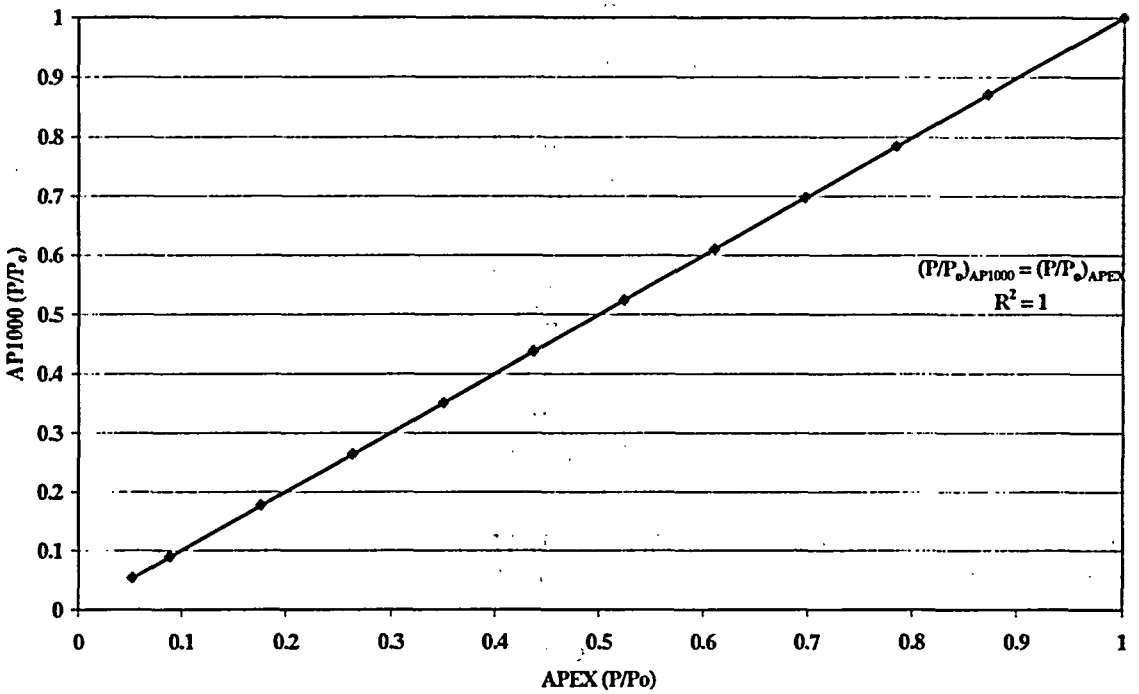


Figure A.7 Scaling Relationship Between AP1000 and APEX Saturation Pressure

### A.5.4 Bottom-Up Scaling Depressurization Scaling Analysis

The objective of the bottom-up scaling analysis was to obtain the closure relations needed to evaluate the scaling ratios developed through the top-down analysis. These closure relations are dependent on fluid properties. Therefore, the first step in the bottom-up analysis was to develop the method to relate fluid properties in AP1000 to those at reduced pressure in APEX.

#### *A.5.4.1 Self-Similarity of Fluid Properties in Phase Equilibria ($P_{sat}$ Scaling)*

The equation of state for many of the important thermodynamic properties, $\psi(P)$, of the saturated fluid can be described by a simple power function as follows:

$$\psi = \psi_o \left(\frac{P}{P_o}\right)^{\xi} \tag{A.65}$$

where $\psi_o$ can be evaluated at an arbitrary reference pressure, $P_o$, within the range of applicability of equation (A.65) and $\xi$ is an empirically determined constant. For saturated water, having a pressure between atmospheric and approximately 15 MPa (2175 psia), the following thermodynamic properties are well-correlated by equation (A.65) as demonstrated in Figures A.8 through A.11.

$$\frac{Pv_{fg}}{h_{fg}} = \left(\frac{Pv_{fg}}{h_{fg}}\right)_o \left(\frac{P}{P_o}\right)^{0.11} \tag{A.66}$$

$$s_f = s_{f,o}\left(\frac{P}{P_o}\right)^{0.20} \tag{A.67}$$

$$v_g = v_{g,o}\left(\frac{P}{P_o}\right)^{-1.02} \tag{A.68}$$

$$v_{fg} = v_{fg,o}\left(\frac{P}{P_o}\right)^{-1.06} \tag{A.69}$$

The form of equation (A.65) has the special property of being "invariant" with respect to a two-parameter transformation in scale. That is, rescaling the variables such that:

$$\psi = C_1\psi^* \tag{A.70}$$

$$\psi_o = C_1\psi_o^* \tag{A.71}$$

$$P = C_2P^* \tag{A.72}$$

$$P_o = C_2P_o^* \tag{A.73}$$

where $C_1$ and $C_2$ are constants, and substituting these rescaled variables into equation (A.65) yields:

$$\psi^* = \psi_o^*\left(\frac{P^*}{P_o^*}\right)^{\xi} \tag{A.74}$$

The form of the equation of state remains unchanged. This type of transformation is known as a "stretching" or "similarity" transformation. The special feature of invariance with scale implies that the points and slopes of any curves in the $(\psi,P)$ phase space can be related to corresponding points and slopes in the $(\psi^*, P^*)$ phase space [Ref. 12]. This type of scale invariance is known as "self-similarity." Self-similarity can be defined as a repetition of detail at descending scales. If the dimensionless pressure ratios are preserved in the scale model, self-similarity dictates that the dimensionless fluid properties ($\psi/\psi_o$) will also be preserved.

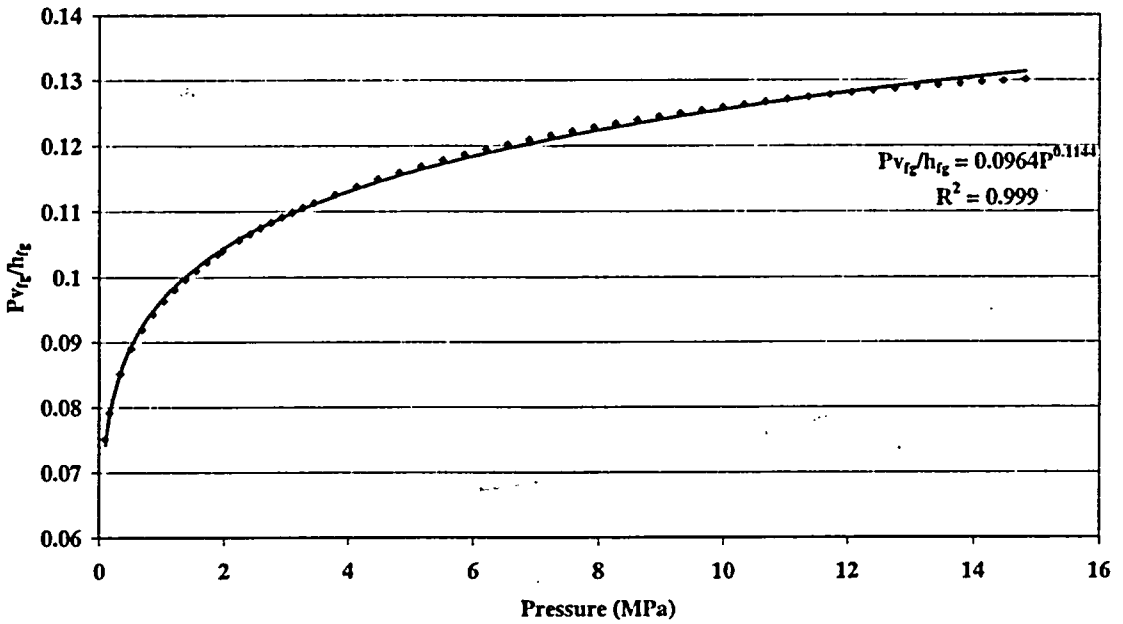


Figure A.8 Power Law for $Pv_{fg}/h_{fg}$ as a Function of Pressure

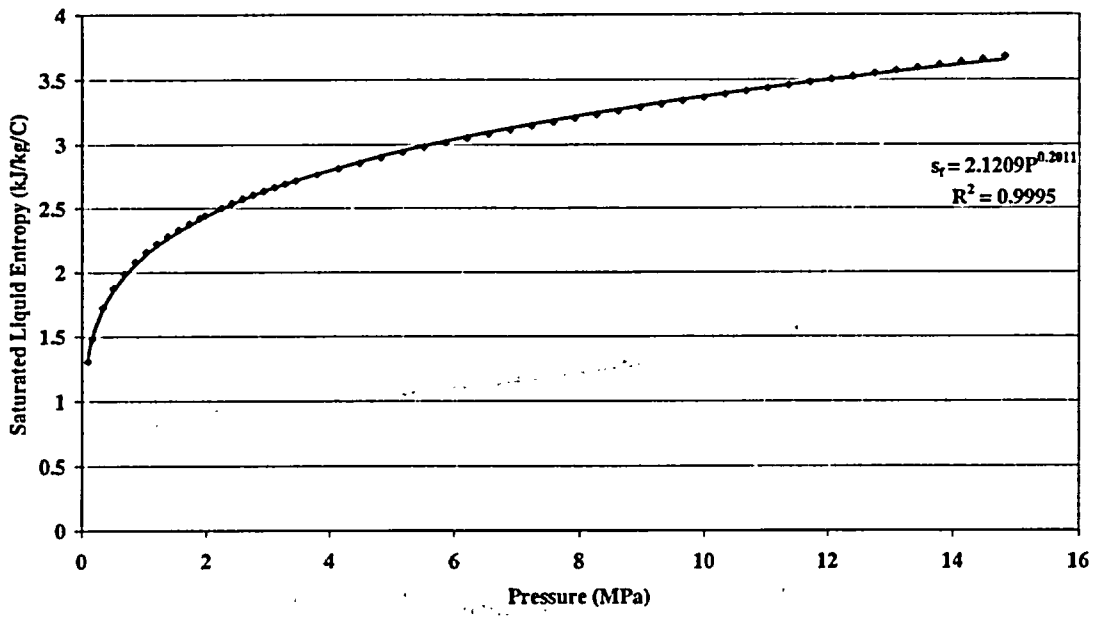


Figure A.9 Power Law for $s_f$ as a Function of Pressure

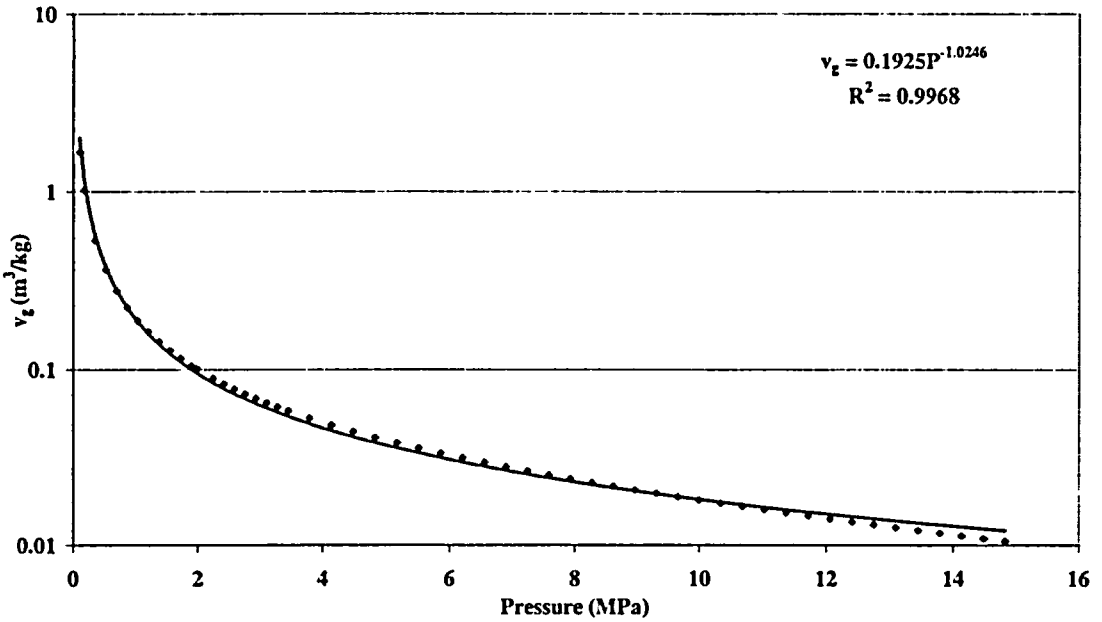


Figure A.10 Power Law for $v_g$ as a Function of Pressure

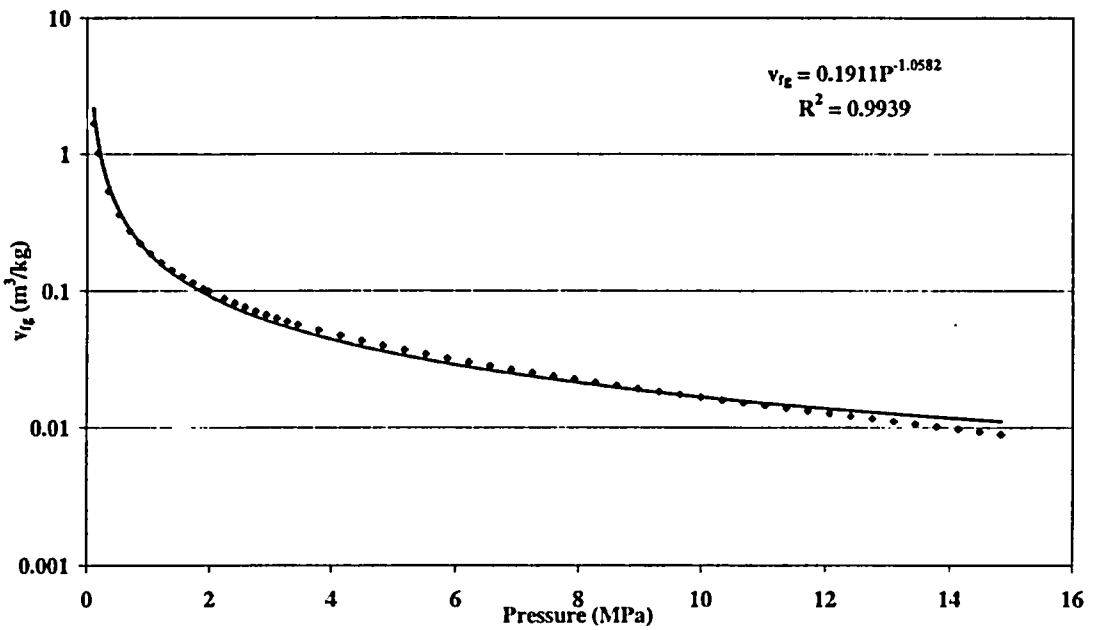


Figure A.11 Power Law for $v_{fg}$ as a Function of Pressure

### *A.5.4.2 Equations of State for Saturated Pressure and Temperature ($T_{sat}$ Scaling)*

The Clausius-Clapeyron equation is the classical differential equation that defines the slope *dP/dT*, for a phase equilibrium curve. It is derived assuming that the Gibb's free energies for the two-phases being considered are equal [Ref. 12]. Using the saturated definition for the Gibb's free energy and relating the change in entropy to the latent heat of vaporization and the saturation temperature yields the well-known Clausius-Clapeyron equation:

$$\frac{dP}{dT} = \frac{h_{fg}}{v_{fg} T} \tag{A.75}$$

An analytical expression for an equation of state relating saturation pressure to saturation temperature can be obtained as follows. Substituting equation (A.66) into (A.75), where $\xi$ is 0.11 for water, and rearranging yields:

$$\left(\frac{P}{P_o}\right)^{\xi-1} dP = \left(\frac{h_{fg}}{v_{fg}}\right)_o \frac{1}{T} dT \tag{A.76}$$

Integrating from $P_o$ to $P_{sat}$ and from $T_o$ to $T_{sat}$ yields the desired relationship between $P_{sat}$ and $T_{sat}$.

$$P_{sat}(T_{sat}) = P_o \left[1 + \xi \left(\frac{h_{fg}}{P v_{fg}}\right)_o \mathrm{Ln}\left(\frac{T_{sat}}{T_o}\right)^{1/\xi}\right] \tag{A.77}$$

Figure A.12 shows that equation (A.77) is quite accurate for the range of conditions examined.

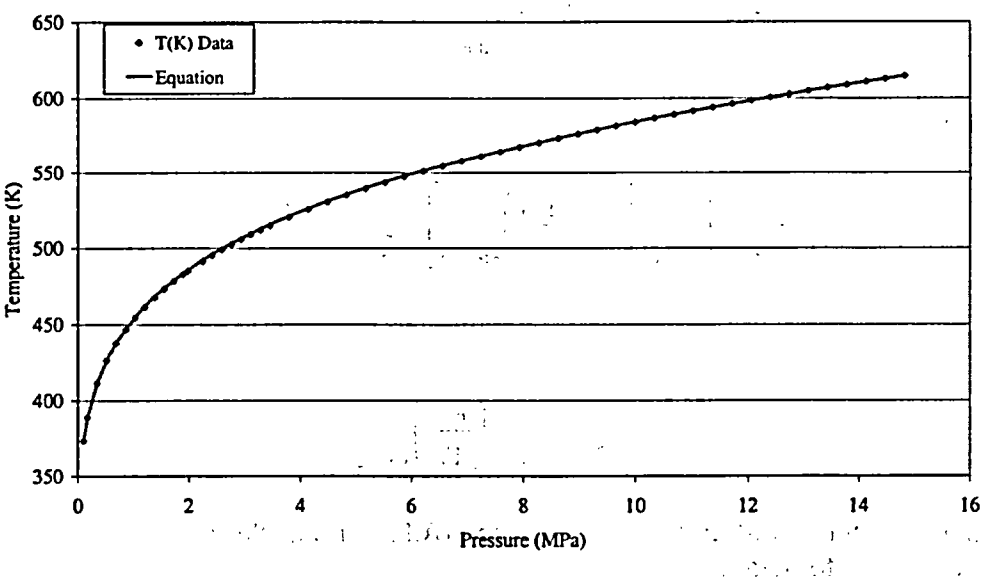


Figure A.12 Comparison of Equation (A.77) to Steam Tables

Equation (A.77) can be rearranged to obtain saturation temperature in terms of saturation pressure. The result is:

$$T_{sat}\ (P_{sat}) = T_o\ \exp\left\{-\frac{1}{\xi}\left(\frac{Pv_{fg}}{h_{fg}}\right)_o\left[1-\left(\frac{P_{sat}}{P_o}\right)^{\xi}\right]\right\} \tag{A.78}$$

This equation can be accurately approximated using the following identity:

$$\exp\ (\beta) \approx 1 + \beta \tag{A.79}$$

for $\beta << 1$ which is applicable to the current situation. Thus equation (A.78) is approximated by:

$$T_{sat} = T_o\left\{1 - \frac{1}{\xi}\left(\frac{Pv_{fg}}{h_{fg}}\right)_o\left[1 - \left(\frac{P_{sat}}{P_o}\right)^{\xi}\right]\right\} \tag{A.80}$$

Rearranging equation (A.80) yields:

$$\left(\frac{h_{fg}}{Pv_{fg}}\right)_o\left[1 - \left(\frac{T_{sat}}{T_o}\right)\right] = \frac{1}{\xi}\left[1 - \left(\frac{P_{sat}}{P_o}\right)^{\xi}\right] \tag{A.81}$$

This equation is valid for both APEX and AP1000 for the range of saturated conditions being examined. Writing this equation for APEX yields:

$$\left(\frac{h_{fgo}}{P_o v_{fgo}}\right)_{APEX}\left[1 - \left(\frac{T_{sat}}{T_o}\right)_{APEX}\right] = \frac{1}{\xi}\left[1 - \left(\frac{P_{sat}}{P_o}\right)^{\xi}_{APEX}\right] \tag{A.82}$$

and for AP1000:

$$\left(\frac{h_{fgo}}{P_o v_{fgo}}\right)_{AP1000}\left[1 - \left(\frac{T_{sat}}{T_o}\right)_{AP1000}\right] = \frac{1}{\xi}\left[1 - \left(\frac{P_{sat}}{P_o}\right)^{\xi}_{AP1000}\right] \tag{A.83}$$

Recalling that:

$$\left(\frac{P_{sat}}{P_o}\right)_{APEX} = \left(\frac{P_{sat}}{P_o}\right)_{AP1000} \tag{A.84}$$

it is recognized that the right-hand side of equation (A.82) and (A.83) are identical. Therefore, they can be set equal to obtain:

$$\left(\frac{h_{fgo}}{P_o v_{fgo}}\right)_{APEX}\left[1 - \left(\frac{T_{sat}}{T_o}\right)_{APEX}\right] = \left(\frac{h_{fgo}}{P_o v_{fgo}}\right)_{AP1000}\left[1 - \left(\frac{T_{sat}}{T_o}\right)_{AP1000}\right] \tag{A.85}$$

Rearranging this equation yields the desired saturation temperature scaling relation:

$$\left(\frac{T_{sat}}{T_o}\right)_{AP1000} = \left(\frac{h_{fgo}}{P_o v_{fgo}}\right)_R \left(\frac{T_{sat}}{T_o}\right)_{APEX} - \left[\left(\frac{h_{fgo}}{P_o v_{fgo}}\right)_R - 1\right] \tag{A.86}$$

Equation (A.86) is linear as shown in Figure A.13 for the APEX and AP1000 reference temperatures (i.e., the saturation temperatures for the corresponding APEX and AP1000 reference pressures). Figure A.13 compares the approximate solution given by equation (A.86) to the exact result obtained using the steam tables.

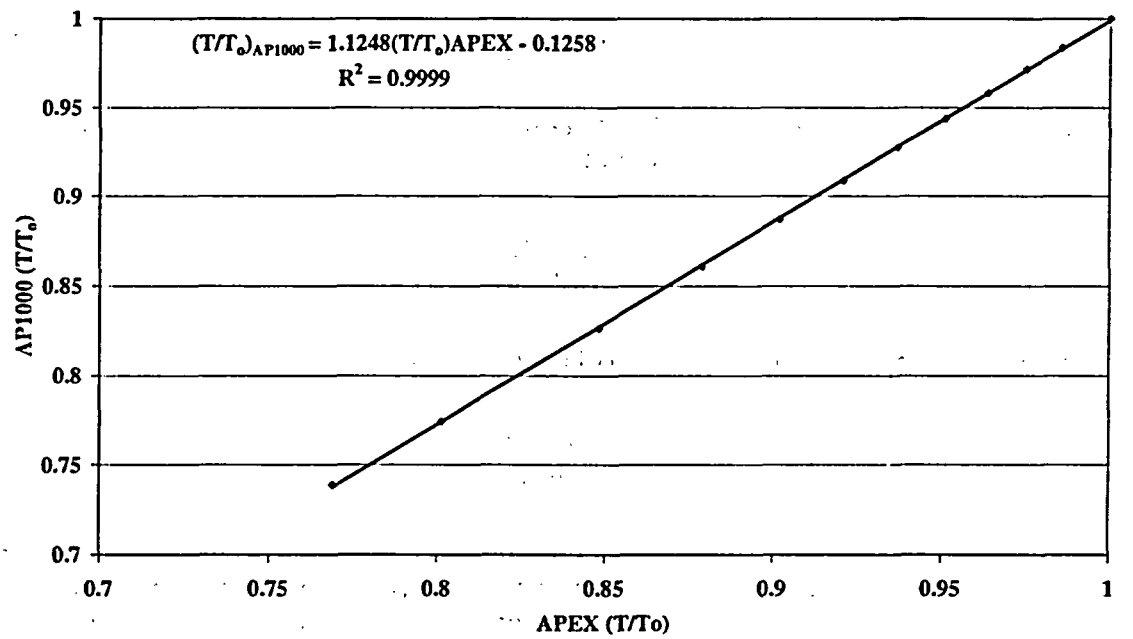


Figure A.13 Scaling Relationship Between AP1000 and APEX Saturation Temperature

### *A.5.4.3 Dilation Property Group for Saturated Liquid-Vapor Blowdowns*

This section demonstrates how the dilation property group, $\Pi_t$, given by equation (A.62), is evaluated for different fluid conditions. For a two-phase fluid mixture in phase equilibrium, the following thermodynamic relations are applicable for the mixture specific internal energy and the mixture specific volume, respectively:

$$e = e_f + x e_{fg} \tag{A.87}$$

$$v = v_f + x v_{fg} \tag{A.88}$$

Eliminating the fluid mixture equilibrium quality, $x$, between equations (A.87) and (A.88) yields the following expression for specific internal energy:

$$e = e_f + \frac{v - v_f}{v_{fg}} e_{fg} \tag{A.89}$$

The partial derivative of this equation with respect to specific volume, at constant pressure, yields:

$$\left(\frac{\partial e}{\partial v}\right)_P = \frac{e_{fg}}{v_{fg}} \tag{A.90}$$

Lastly, the latent heat of vaporization is given by:

$$h_{fg} = P v_{fg} + e_{fg} \tag{A.91}$$

Substituting equations (A.87) through (A.91) into equation (A.62) yields the following expression for the saturated mixture dilation property group:

$$\Pi_\varepsilon = \frac{1}{\left[v_f + x_{Brk}\, v_{fg}\right]} \left(\frac{P v_{fg}}{h_{fg}}\right) \left(\frac{\partial e}{\partial P}\right)_v \tag{A.92}$$

where the equilibrium vapor quality at the break is given by $x_{Brk}$:

$$x_{Brk} = \frac{h_{Brk} - h_f}{h_{fg}} \tag{A.93}$$

Let us examine the pressure dependencies of the terms that comprise the fluid mixture dilation property group given by equation (A.92). The property group ($Pv_{fg}/h_{fg}$) has already been evaluated as shown in Figure A.8 and found to be described by equation (A.66), a power law that exhibits self-similarity for a wide range of saturation pressures.

The last term on the right-hand side of equation (A.92), $(\partial e/\partial P)_v$, is a partial derivative that requires examining the change in the fluid mixture internal energy with respect to pressure *while holding the mixture specific volume, v, constant.* It should not be confused with the total specific internal energy change with respect to pressure. An adequate model for this term can be obtained by developing an expression for the mixture internal energy as a function of pressure while at constant specific volume and taking the derivative with respect to pressure. Therefore, the term $(\partial e/\partial P)_v$ shall be evaluated assuming that the system expands along a trajectory which maintains the specific volume of the mixture at a constant value, $v_o$, which is the initial specific volume of the saturated mixture. That is,

$$e = e_f + e_{fg}\left(\frac{v_o - v_f}{v_{fg}}\right) \tag{A.94}$$

For the depressurization transients of interest to this analysis, the saturated mixture blowdown begins with the system nearly filled with saturated liquid with the exception of a small vapor volume located in the pressure vessel head. Since the density of the liquid phase is much greater than that of the vapor phase, the initial system vapor quality is very low and hence the

initial fluid mixture specific volume is essentially the same as the saturated liquid phase specific volume. Thus the value of $v_o$, implemented in equation (A.94) is closely approximated by $v_{fo}$. Figure A.14 shows how the mixture internal energy varies with pressure assuming a constant specific volume, $v_o = v_{fo}$, during the depressurization process. The plot has been made dimensionless to collapse the trends for a variety of initial pressures.

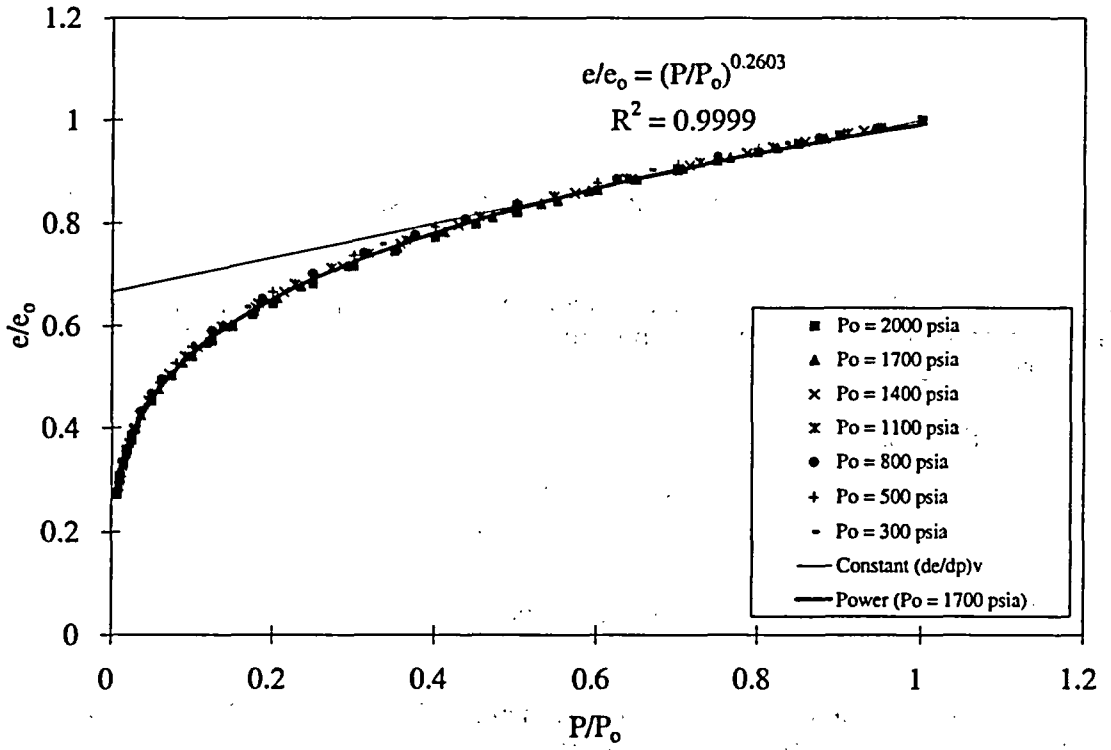


Figure A.14 Plot of Dimensionless Mixture Specific Energy as a Function of Dimensionless Pressure

Note that for pressure ratios greater than ~0.5, the trend is linear, indicating that the slope, $(\partial e/\partial P)_v$, is a constant in this region. As shown in the figure, the following power law ($R^2$ = 0.9999) accurately describes the mixture-specific internal energy ratio for a wide range of normalized pressures.

$$\left(\frac{e}{e_o}\right)_{v_{fo}} = \left(\frac{P}{P_o}\right)^{0.2603} \tag{A.95}$$

Taking the derivative of this equation with respect to pressure yields the expression for the desired partial derivative:

$$\left(\frac{\partial e}{\partial P}\right)_{v_{fo}} = 0.2603\frac{e_{fo}}{P}\left(\frac{P}{P_o}\right)^{0.2603} \tag{A.96}$$

It should be noted that the numerical constants arising in equations (A.95) and (A.96) are particular to the case where the initial fluid mixture-specific volume and specific energy are given by $v_{fo}$ and $e_{fo}$, respectively. Different constants are obtained at different initial vapor qualities for the saturated mixture.

Substituting equations (A.66) and (A.96) into (A.92) yields the following equation for the dilation property group.

$$\Pi_\varepsilon = \frac{0.2603}{\left[v_f + x_{Brk}\, v_{fg}\right]} \left(\frac{e_f\, v_{fg}}{h_{fg}}\right)_o \left(\frac{P}{P_o}\right)^{-0.6257} \tag{A.97}$$

Equation (A.97) can be readily evaluated for two bounding cases, saturated liquid breaks and saturated vapor breaks.

The fluid conditions for breaks located at low points in the RCS can be approximated assuming saturated liquid at the break. For these conditions, $x_{Brk}$ would be approximately zero, and equation (A.97) would become:

Saturated Liquid Breaks:

$$\Pi_{\varepsilon_f} = 0.2603 \left(\frac{e_f\, v_{fg}}{v_f\, h_{fg}}\right)_o \left(\frac{P}{P_o}\right)^{-0.6257} \tag{A.98}$$

Here it has also been assumed that $v_f$ does not change significantly over the range of pressure of interest.

The fluid conditions for breaks located at high points in the RCS (e.g., ADS1-3) can be approximated assuming saturated vapor at the break. For these conditions, $x_{Brk}$ would equal one and equation (A.97) would become:
saturated vapor breaks:

$$\Pi_{\varepsilon_g} = 0.2603 \left(\frac{e_f}{h_{fg}}\right)_o \left(\frac{P}{P_o}\right)^{0.4443} \tag{A.99}$$

To obtain this equation, use has been made of equation (A.68), the power law for the vapor-specific volume. Equations (A.97) and (A.99) are written in terms of scaling ratios, as follows:

$$\left(\Pi_{\varepsilon_f}\right)_R = \left(\frac{e_f\, v_{fg}}{v_f\, h_{fg}}\right)_{o,R} \tag{A.100}$$

and

$$\left(\Pi_{\varepsilon_g}\right)_R = \left(\frac{e_f}{h_{fg}}\right)_{o,R} \tag{A.101}$$

where equation (A.64) has been implemented to eliminate the pressure ratios.

### *A.5.4.4 Critical Flow Models*

For the blowdown cases of interest to this study, all of the break flows are assumed to be choked. This section presents two critical flow models (a saturated vapor model and a saturated liquid model) used to estimate the break mass flow rate:

In general, the break mass flow rate is expressed as:

$$\dot{m}_{Brk} = C_D G_c A_{Brk} \tag{A.102}$$

where $C_D$ is the discharge coefficient, $G_c$ is the critical mass flux and $A_{Brk}$ is the break flow area.

#### A.5.4.4.1 Saturated Steam

This initial critical mass flow rate for saturated steam, approximated as a perfect gas, is given by Moody [Ref. 13]:

$$\dot{m}_{Brk,o} = C_D\ A_{Brk} \left(\frac{2}{\gamma + 1}\right)^{\frac{\gamma+1}{2(\gamma-1)}} \left[\gamma \rho_{go} P_o\right]^{1/2} \tag{A.103}$$

where $C_D$ is the discharge coefficient, $A_{Brk}$ is the break flow area and $\gamma$ is the ratio of specific heats, which is approximately 1.33 for steam.

The transient, pressure-dependent, critical mass flow rate for the steam would be:

$$\dot{m}_{Brk} = \dot{m}_{Brk,o} \left(\frac{P}{P_o}\right)^{\frac{1+\gamma}{2\gamma}} \tag{A.104}$$

Once again, we find a power law, self-similar in pressure.

#### A.5.4.4.2 Saturated Liquid

The models typically implemented for the case of saturated liquid choke flow are the homogeneous equilibrium model or the Henry-Fauske model [Ref. 14]. An earlier study of APEX data indicated that the Henry-Fauske model at saturated liquid conditions best fit the APEX data [Ref. 15].

The Henry-Fauske critical flow model for saturated liquid is given by the following set of equations:

$$G_c = \left[ \left\{ (v_g)_{Brk} - v_f \right\} \frac{x_{Brk}}{(0.14)(s_{fg})_{Brk}} \left(\frac{d s_f}{dP}\right)_{Brk} \right]^{-1/2} \tag{A.105}$$

and

$$\frac{P_{Brk}}{P} = 1 - \frac{v_f\ G_c^2}{2P} \tag{A.106}$$

In these equations, the parameters with the subscript "Brk" are evaluated at the break plane. All other parameters are evaluated at the system conditions. Thus, $P_{Brk}$ is commonly known as the throat pressure, while P is the stagnation pressure. A typical value of equilibrium quality for the saturated liquid breaks observed in APEX was $x_{Brk}$ equal to 0.03.

The saturated liquid entropy derivative on the right-hand side of equation (A.105) was obtained by taking the derivative of equation (A.67) with respect to pressure. This yielded the following expression for $(ds_f/dP)$:

$$\frac{ds_f}{dP} = 0.2 \frac{s_{f,o}}{P} \left( \frac{P}{P_o} \right)^{0.2} \tag{A.107}$$

Equations (A.105) and (A.106) were solved iteratively to obtain the critical flow rates for saturated liquid breaks in APEX and AP1000. Figure A.15 presents the result of this analysis. Furthermore, it indicates that the critical flow model also obeys a power law that is self-similar in pressure. That is:

$$G_c \approx G_{co} \left( \frac{P}{P_o} \right)^{0.7063} \tag{A.108}$$

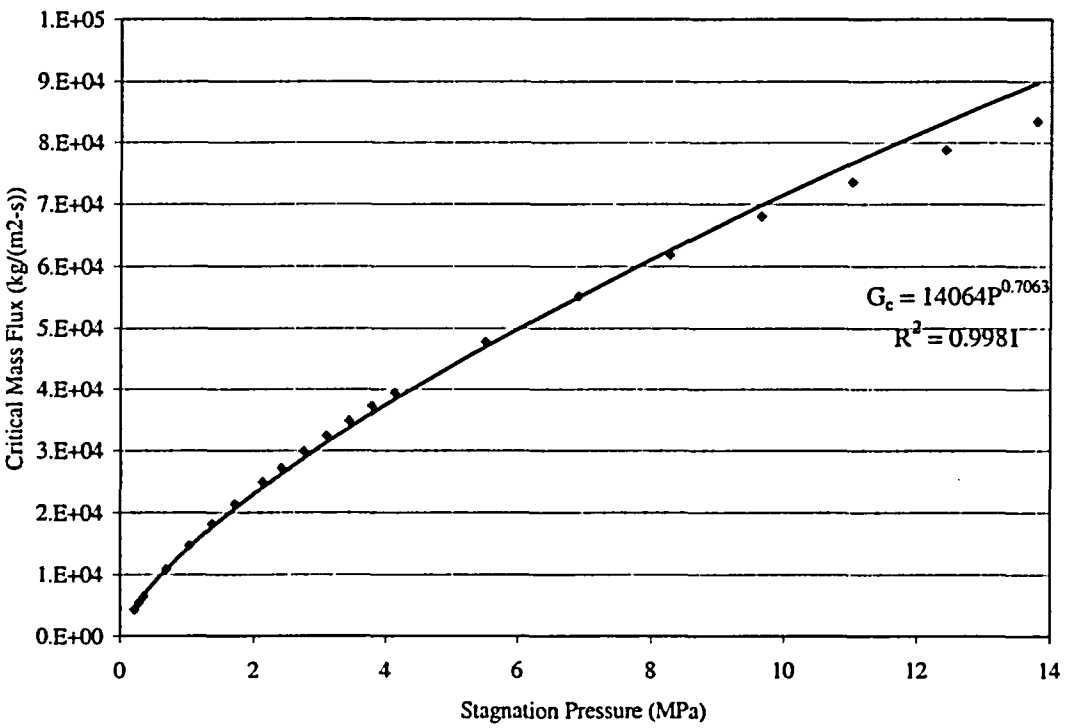


Figure A.15 Critical Mass Flux for Saturated Liquid Breaks as Predicted by the Henry Fauske Model ($x_{Brk}$ = 0.03)

Using equation (A.102), the mass flow rate for saturated liquid breaks can be expressed as:

$$\dot{m}_{Brk} \approx \dot{m}_{Brk,o}\left(\frac{P}{P_o}\right)^{0.7063} \tag{A.109}$$

Equations (A.104) and (A.109) served as the closure relations for the top-down scaling dimensionless groups, $\Pi_m$, $\Pi_h$, $\Pi_r$, and the time constant $\tau_{RCS}$.

### A.5.5 RCS depressurization and Inventory Scaling Criteria

It is desired that APEX-AP1000 depressurization rate and the rate at which the RCS mass inventory changes be preserved in dimensionless phase space, ($P^+$,$M^+$). That is, the following similarity criteria shall be imposed:

$$\left(\tau_{RCS}\frac{dM^+}{dt}\right)_R = 1 \tag{A.110}$$

$$\left(\tau_{RCS}\frac{dP^+}{dt}\right)_R = 1 \tag{A.111}$$

where:

$$\tau_{RCS,R} = \left[\frac{M_{RCS}}{\dot{m}_{Brk}}\right]_{o,R} \tag{A.112}$$

and the one-half time scale requirement has been set.

If these criteria are preserved and the same initial conditions, $(P^+, M^+)_o$ are imposed in APEX-AP1000,

$$(\tau_{RCS})_R = \frac{1}{2} \tag{A.113}$$

the same process trajectory will result when plotted in dimensionless phase space. Applying these conditions to the dimensionless balance equations given by equations (A.49) and (A.59) means that the following scaling criteria must be on the order of unity.

$$\Pi_{m,R} = \left(\frac{\dot{m}_{INJ,o}}{\dot{m}_{Brk,o}}\right)_R \tag{A.114}$$

$$\left(\frac{\Pi_h}{\Pi_e}\right)_R = \left[\frac{\Sigma \dot{m}_{DVI,o}\left[h_{DVI} - e + v\left(\frac{\partial e}{\partial v}\right)_P\right]_o}{\dot{m}_{Brk,o}\,P_o\left(\frac{\partial e}{\partial P}\right)_{v,o}}\right]_R \tag{A.115}$$

$$\left(\frac{\Pi_\Gamma}{\Pi_\varepsilon}\right)_R = \left[\frac{q_{net,o}}{\dot{m}_{Brk,o}\, P_o \left(\frac{\partial e}{\partial P}\right)_{v,o}}\right]_R \tag{A.116}$$

$$(\Pi_\varepsilon)_R = \left[\frac{P_o \left(\frac{\partial e}{\partial P}\right)_{v,o}}{\left[h_{Brk} - e + v\left(\frac{\partial e}{\partial v}\right)_p\right]_o}\right]_R \tag{117}$$

The SBLOCA cases considered in the analysis are the case of saturated vapor at the ADS1-3 location and saturated liquid at the break and ADS4 locations.

*A.5.5.1 Saturated Vapor Break Flow Areas*

For saturated vapor breaks, the following would be applicable:

$$h_{Brk} = h_g \tag{A.118}$$

Thus, implementing equations (A.89) through (A.91) yields:

$$\left[h_{Brk} - e + v\left(\frac{\partial e}{\partial v}\right)_p\right]_o = \frac{v_g\, h_{fg}}{v_{fg}} \tag{A.119}$$

Similarly:

$$\left[h_{DVI} - e + v\left(\frac{\partial e}{\partial v}\right)_p\right]_o = \left[\frac{h_{fg}\, v_f}{v_{fg}} - \Delta h_{sub}\right]_o \tag{A.120}$$

The injected liquid subcooling is defined as $h_f - h_{DVI}$. Using these fluid property relations, it is now possible to evaluate equations (A.113) through (A.117). Substituting the critical flow equation for saturated vapor, equation (A.103), and the RCS time constant ratio given by equation (A.110) into (A.111) yields.

$$\left[\frac{M_{RCS}}{A_{Brk}\left[\rho_{go} P_o\right]^{0.5}}\right]_R = \frac{1}{2} \tag{A.121}$$

The $M_{RCS}$ ratio shall be set such that:

$$M_{RCS,R} = \frac{1}{192} \tag{A.122}$$

Substituting this condition into equation (A.120) and solving for the break area ratio yields:

$$(A_{Brk})_R = \frac{1}{96}\left(\frac{1}{[\rho_{go} P_o]^{1/2}}\right)_R \tag{A.123}$$

*A.5.5.2 Saturated Liquid Break Flow Areas*

For saturated liquid breaks, the following would be applicable:

$$h_{Brk} = h_f \tag{A.124}$$

Thus, implementing equations (A.89) through (A.91) results in:

$$\left[h_{Brk} - e + v\left(\frac{\partial e}{\partial v}\right)_p\right]_o = \frac{v_f\ h_{fg}}{v_{fg}} \tag{A.125}$$

Substituting the critical flow equation for saturated liquid, equation (A.109), and the RCS time constant ratio given by equation (A.110), into (A.111) yields:

$$\left[\frac{M_{RCS}}{C_D A_{Brk} P_o^{0.7063}}\right]_R = \frac{1}{2} \tag{A.126}$$

Assuming similar discharge coefficients, substituting equation (A.122) and rearranging, yields the break flow area ratio:

$$(A_{Brk})_R = \frac{1}{96}\left(\frac{1}{P_o^{0.7063}}\right)_R \tag{A.127}$$

Equations (A.123) and (A.127) become identical for the case of fluid property similitude. That is:

$$(A_{Brk})_R = \frac{1}{96} \tag{A.128}$$

*A.5.5.3 ADS Valve Flow Area Scaling Ratios*

Operation of the ADS is initiated when the CMT liquid level drops below a prescribed setpoint. This typically occurs subsequent to PZR draining. Therefore, most of the flow is single-phase steam. As a result, the ADS1 and ADS2 valves will be scaled in accordance with equation (A.123). That is:

$$(A_{ADS1,2})_R = \frac{1}{96}\left(\frac{1}{[\rho_{go} P_o]^{1/2}}\right)_R \tag{A.129}$$

The opening of the ADS3 valve shall be used to transition to fluid property similitude conditions. This procedure was first implemented in the NRC's AP600 test program to allow actuation of the ADS4 valves at higher operating pressures. The flow area for the APEX ADS3 valve was designed such that:

$$(A_{ADS\text{-}3})_{APEX} = \frac{1}{96}\Sigma(A_{ADS1,2,3})_{AP}1000 \qquad (A.130)$$

The procedure was such that ADS1 and ADS2 would open sequentially as specified by the safety logic. Then ADS1 and ADS2 would be closed and APEX ADS3, representing the sum of flow areas for all three stages, would be opened. Thus the ADS1-3 train would be configured for fluid property similitude and long-term cooling.

The ADS4 valve flow area was sized based on fluid property similitude, as follows:

$$(A_{ADS4})_R = \frac{1}{96} \qquad (A.131)$$

### *A.5.5.4 DVI Mass Flow Rate Scaling Ratio*

All of the injection flow rates will be scaled as follows for the one-half time scale. This is done by preserving the line resistance and relative elevation in the IRWST, CMT, and ACCs. Thus:

$$(\dot{m}_{DVI,o})_R = \frac{1}{96} \qquad (A.132)$$

### *A.5.5.5 Net Power Scaling Ratio*

Substituting equation (A.96) into (A.116) and setting the result equal to one yields the net power scaling ratio. Use has been made of the fact that $(P/P_o)_R$ is unity. The core decay power scaling has already been set in Section A.3 to be 1:96.

$$(q_{net,o})_R = [\dot{m}_{Brk}\, e_{fo}]_R \qquad (A.133)$$

## A.5.6 Initial Conditions and Flow Areas

Table A.11 presents the initial conditions for the APEX test facility for a LOCA transient. These parameters will be modified for other transients such as the station blackout.

Table A.11 APEX-AP1000 LOCA Initial Conditions

| Parameters | AP1000 | APEX | Units |
|---|---|---|---|
| Decay Power (2.8%) | | | |
| RCS Pressure | | | |
| SG Operating Pressure | | | |
| CL Temperature | | | |
| SG Operating Pressure | | | |
| SG PORV Setpoint (Reference Pressure) | | | |
| SG Shell Side Liquid Level | | | |
| SG Shell Side Liquid Mass | | | |
| SG Shell Side Vapor Mass | | | |
| PZR Liquid Volume | | | |
| ACC Gas Pressure | | | |

a,b,c

Table A.12 presents the flow areas required for the ADS valves as used for LOCA transients, Table A.13 presents the ADS1 and 2 flow areas for the special case of a transient initiated by the inadvertent opening of the ADS1 valve, Table A.14 presents the scaled break sizes, and Table A.15 presents the numerical values for the RCS time constant and P ratios.

Table A.12 Summary of APEX-AP1000 ADS1-4 Valve Flow Areas for LOCA

| Component | Scaling Ratio | AP1000 | APEX | Units | AP1000 | APEX | Units |
|---|---|---|---|---|---|---|---|
| ADS1-2 FLOW AREAS FOR LOCA (SATURATED STEAM) | | | | | | | a,b,c |
| ADS1 Single Valve Effective Flow Area (min) | | | | | | | |
| ADS1 Single Valve Effective Throat I.D. | | | | | | | |
| ADS1 Two Valves Effective Flow Area (combined) | | | | | | | |
| ADS1 Two Valves Effective Throat I.D. (combined) | | | | | | | |
| ADS2 Single Valve Effective Flow Area (min) | | | | | | | |
| ADS2 Single Valve Effective Throat I.D. | | | | | | | |
| ADS2 Two Valves Effective Flow Area (combined) | | | | | | | |
| ADS2 Two Valves Effective Throat I.D. combined | | | | | | | |
| ADS1-3 FLOW AREAS COMBINED (FLUID PROPERTY SIMILITUDE) | | | | | | | |
| ADS1,2,3 Single Train Effective Flow Area (min) | | | | | | | |
| ADS1,2,3 Single Train Effective Throat I.D. | | | | | | | |
| ADS1,2,3 Two Trains Effective Flow Area (combined) | | | | | | | |
| ADS1,2,3 Two Trains Effective Throat I.D. (combined) | | | | | | | |
| ADS4 FLOW AREAS PER HOT LEG (FLUID PROPERTY SIMILITUDE) | | | | | | | |
| ADS4 Single Train (50% Effective Flow Area) | | | | | | | |
| ADS4 Single Train Effective Throat I.D. | | | | | | | |
| ADS4 Two Trains (100% Effective Flow Area) | | | | | | | |
| ADS4 Two Trains Effective Throat I.D. (combined) | | | | | | | |

Table A.13 Summary of APEX-AP1000 ADS1-2 Valve Flow Areas for Inadvertent Opening of ADS

| Component | Scaling Ratio | AP1000 | APEX | Units | AP1000 | APEX | Units |
|---|---|---|---|---|---|---|---|
| ADS1-2 FLOW AREAS FOR INADVERTENT ADS OPEN IN TRANSIENT (SATURATED LIQUID) | | | | | | | A,b,c |
| ADS1 Single Valve Effective Flow Area (mini) | | | | | | | |
| ADS1 Single Valve Effective Throat I.D. | | | | | | | |
| ADS1 Two Valves Effective Flow Area (combined) | | | | | | | |
| ADS1 Two Valves Effective Throat I.D. (combined) | | | | | | | |
| ADS2 Sin le Valve Effective Flow Area (min) | | | | | | | |
| ADS2 Single Valve Effective Throat I.D. | | | | | | | |
| ADS2 Two Valves Effective Flow Area (combined) | | | | | | | |
| ADS2 Two Valves Effective Throat I.D. (combined) | | | | | | | |

Table A.14 APEX-AP1000 Break and Steam Generator PORV Sizes. LOCA FLOW AREAS
(Pressure Scaled Two Phase Fluid)

| Component | Scaling Ratio | AP1000 | APEX | Units |
|---|---|---|---|---|
| 2-INCH COLD LEG BREAK | | | | |
| Flow area | | | | |
| Diameter | | | | |
| DOUBLE-ENDED DVI LINE BREAK | | | | |
| DVI Nozzle Flow Area | | | | |
| Diameter | | | | |
| STEAM GENERATOR PORV FLOW AREA (SINGLE-PHASE STEAM) | | | | |
| *PORV Equivalent Flow Area | | | | |
| PORV Equivalent Throat Diameter | | | | |

a,b,c

*Based on 1.02 x $10^6$ lbm/hr at 1200 psia for AP1000

Table A.15 Time Constants and Π Groups for APEX Pressure Scaled LOCAs

| Π Group | Saturated Vapor Breaks | Saturated Liquid Breaks |
|---|---|---|
| (t/τRCS),R | | |
| Πm,R | | |
| $\left(\frac{\Pi_h}{\Pi_\varepsilon}\right)_R$ | | |
| $\left(\frac{\Pi_\Gamma}{\Pi_\varepsilon}\right)_R$ | | |
| $(\Pi_\varepsilon)_R$ | | |

a,b,c

## A.5.7 Summary and Conclusions

This section presents the results of the SBLOCA scaling analysis. The goal was to scale the APEX initial conditions and break flow areas such that the RCS depressurization rate and corresponding cooldown rate would be preserved in dimensionless phase space. The two types of break conditions considered were (1) all-saturated vapor at the break, such as the stuck-open ADS1-3, and (2) an all-saturated liquid break, which was the assumed condition for the HL break.

The scaling analysis provided the RCS initial conditions and the break flow areas. All of the Π groups, as shown in Table A.14, were found to have values on the order of 1, with the exception of the fluid property group under pressure-scaled conditions.

An examination of the Π groups ratios indicates that for saturated vapor breaks (i.e., stuck-open ADS1-3) the depressurization and cooldown rate will be reasonably simulated in APEX. Some distortion may occur in simulating the HL break because conditions at the break will likely be two-phase rather than saturated liquid as assumed in the analysis. The validity of this assumption will depend on whether the injection flows keep the break conditions near the saturated liquid state.

For the conditions of fluid property similitude, all of the Π group ratios listed in Table A.14 will be one. Thus, the full-pressure tests that will be performed in APEX to assess the transition from ADS4 operation to IRWST injection are expected to yield depressurization behavior that is similar to the AP1000. The next chapter presents the scaling analysis for the full-pressure ADS4 blowdown phenomena.

## A.6 Scaling Analysis of the Full-Pressure ADS4 Blowdown to IRWST Injection Transition Period

The APEX-AP1000 test facility was modified to conduct full-pressure studies of the thermal-hydraulic phenomena that arise during the transition from ADS4 blowdown to the onset of IRWST injection. This transition period was previously studied under full-pressure conditions in the SPES and ROSA-AP600 test facilities. This period was deemed to be very important by analysts because there is a limited amount of liquid available for core cooling while the system depressurizes to the IRWST injection setpoint. Operating the APEX facility under reduced-pressure conditions during this phase of a transient results in distorting the conditions at which the IRWST begins to drain.

In the AP1000, IRWST injection would initiate when the primary system pressure drops below ~0.198 MPa (28.7 psia), based on the minimum initial IRWST liquid level. At this pressure, the flow at the ADS4 valves would be still be choked (i.e., essentially single-phase vapor flow) and independent of the ADS4 line resistance. However, for the one-quarter height IRWST in APEX, the onset of flow would not begin until the primary system pressure dropped below ~0.125 MPa (18.2 psia). At this pressure, the ADS4 flow would be unchoked and, therefore, the ADS4 flow rate would be dependent on ADS4 line resistance.

In an effort to eliminate the ADS4 flow distortions in APEX during this transition period, a series of full-pressure ADS4 blowdown tests were performed. This requireed configuring APEX to provide pressure control for ADS4 blowdowns initiating from steady-state conditions, pressuring the IRWST to simulate full-height conditions and adjusting the IRWST line resistance to achieve properly scaled injection flow rates under full-height IRWST conditions. This section presents the scaling analysis performed to design the ADS4 blowdown to IRWST injection transition tests.

### A.6.1 Description of the ADS4 Blowdown to IRWST Injection Thermal-hydraulic Phenomena

Figure A.16 presents an overview of the thermal-hydraulic phenomena that arise during a typical ADS4 blowdown. This figure characterizes the phenomena in terms of RPV mixture level (or liquid mass) versus the system pressure. The ADS4 valves open when the liquid volume in either of the two CMTs drops below 20% of its initial volume. At $P_{ADS4}$, the pressure at which the ADS4 valves open, two-phase fluid choke flow will exist at the ADS4 valves. All of the liquid located above the top of the HLs, (i.e., the entrance to the ADS4 line), will eventually be swept out of the ADS4 valves. The amount of liquid located above the HLs is dependent on the amount of level swell in the core. When the fluid mixture level drops below the top of the HLs, the flow out of the ADS4 valves can be best described as a high-quality vapor choke flow. Liquid boil-off in the core, liquid flashing to vapor, and liquid carryover from the upper plenum will act to reduce the liquid inventory in the RPV. Because there are no other sources of liquid during this phase of the transient, primary system pressure must drop below the IRWST liquid level head pressure, $P_{IRWST}$, before the RPV mixture level reaches the top of the core. When the primary system pressure drops below $P_{IRWST}$, less some small check valve cracking pressure, IRWST liquid flow will act to reflood the RPV.

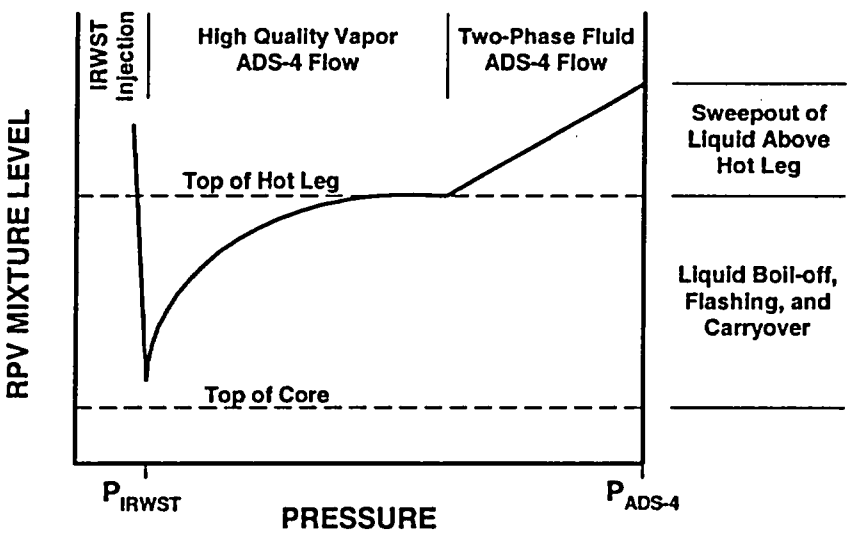


Figure A.16 Description of the Transition from ADS4 Blowdown to the Onset of IRWST Injection

Figure A.17 shows how the thermal-hydraulic phenomena described in this section have been addressed in the top-down and bottom-up scaling analyses. First a top-down scaling analysis was performed to obtain a single governing equation in terms of $dP^+/dM^+$. Next, a bottom-up scaling analysis was performed to describe the local thermal-hydraulic processes, including critical flow, core fluid boil-off, and core mixture level swell.

### A.6.2 Top-Down RCS Depressurization and Mass Inventory Scaling Analysis (Pressure Similitude)

The mass balance equation and depressurization rate equation developed in Section A.5 are directly applicable to this analysis. However, the initial conditions and processes to be examined are specific to the transition period from ADS4 blowdown to IRWST injection under full-pressure conditions. The objective of this analysis is to develop the criteria for preserving the AP1000 depressurization and mass inventory behavior for the transition period as described in dimensionless phase space ($M^+$, $P^+$).

The following mass balance equation was developed for the RCS in Section A.5.2.

$$\frac{dM}{dt} = \sum \dot{m}_{in} - \sum \dot{m}_{out} \qquad \text{(A.134)}$$

During the ADS4/IRWST transition period, there will be no sources of liquid injection; therefore, the first term on the right-hand side of equation (A.134) can be deleted. Furthermore, the only vent paths to be considered in this analysis shall be the ADS4 valves.

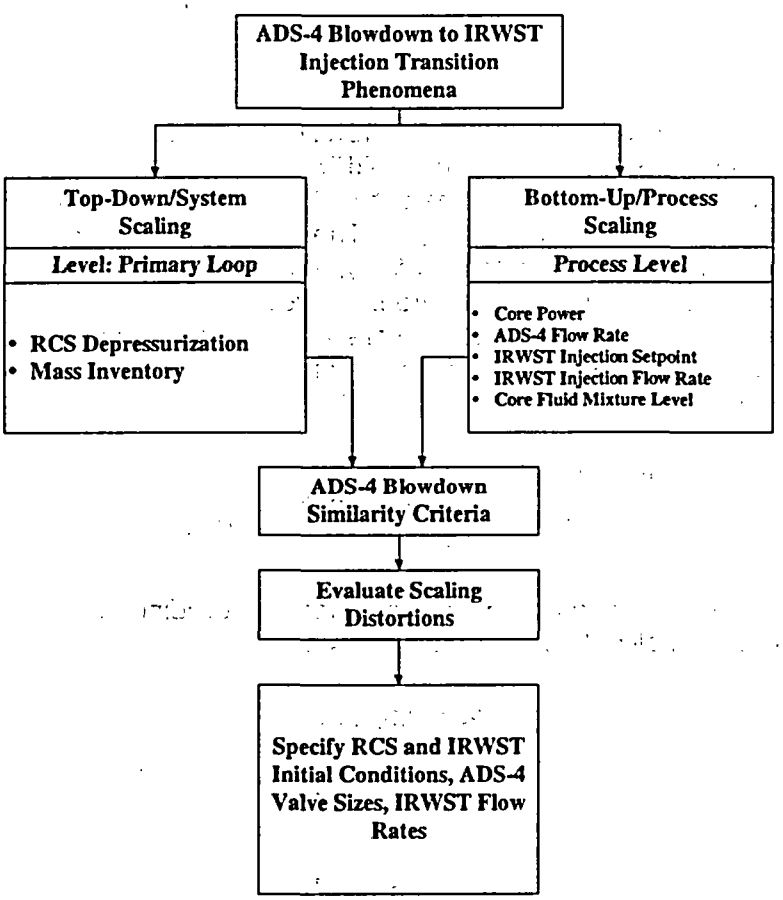


Figure A.17 Scaling Analysis Flow Chart for the Full Pressure ADS4 Blowdown Experiments

Applying these assumptions results in the following equation:

$$\frac{dM}{dt} = - \dot{m}_{ADS4} \tag{A.135}$$

The following depressurization rate equation was also developed for the RCS in Section A.5.2.

$$M\left(\frac{\partial e}{\partial P}\right)_v \frac{dP}{dt} = (\Sigma \dot{m}_{in})\left[h_{in} - e + v\left(\frac{\partial e}{\partial v}\right)_p\right] - (\Sigma \dot{m}_{out})\left[h_{out} - e + v\left(\frac{\partial e}{\partial v}\right)_p\right] + q_{SG} + q_{core} + q_{loss} \tag{A.136}$$

During the ADS4/IRWST transition period, the SGs will be isolated. Therefore, the $q_{SG}$ term can be deleted. The heat loss will be negligible compared to the core decay heat. Therefore, the $q_{loss}$ term can also be neglected. Applying these assumptions and those for the mass balance equation yields:

$$M\left(\frac{\partial e}{\partial P}\right)_v \frac{dP}{dt} = - \dot{m}_{ADS4}\left[h_{ADS4} - e + v\left(\frac{\partial e}{\partial v}\right)_p\right] + q_{core} \tag{A.137}$$

It is noted that the key behavior of interest to the transition period can be described in terms of system pressure versus RCS mass inventory (or RPV mixture level) as shown in Figure A.20. The process could also be described in terms of two time scales. The first is the time required for the RCS to depressurize from $P_{ADS4}$ to $P_{IRWST}$. The second is the time required to deplete the RCS mass inventory from its initial condition, $M_{RCS,o}$, to its final mass inventory state which may or may not be sufficient to keep the core covered. However, rather than working with time scales, a departure from previous analyses, the present analysis was simplified by developing a single governing equation in terms of RCS mass and pressure. This was done by dividing equation (A.137) by the mass balance equation (A.135). The result is:

$$M\left(\frac{\partial e}{\partial P}\right)_v \frac{dP}{dM} = \left[h_{ADS4} - e + v\left(\frac{\partial e}{\partial v}\right)_p\right] - \frac{q_{core}}{\dot{m}_{ADS4}} \tag{A.138}$$

This equation can be expressed in non-dimensional form by dividing each term by its respective initial conditions. The normalized terms are as follows:

$$M = M_{RCS,o} M^+ \tag{A.139}$$

$$P = P_{RCS,o} P^+ \tag{A.140}$$

$$q_{core} = q_{core,o} q^+_{core} \tag{A.141}$$

$$\dot{m}_{ADS4} = \dot{m}_{ADS4,o} \dot{m}^+_{ADS4} \tag{A.142}$$

$$\left(\frac{\partial e}{\partial P}\right)_v = \left(\frac{\partial e}{\partial P}\right)_{v,o}\left(\frac{\partial e}{\partial P}\right)_v^+ \tag{A.143}$$

$$\left[h_{ADS4} - e + v\left(\frac{\partial e}{\partial v}\right)_P\right] = \left[h_{ADS4} - e + v\left(\frac{\partial e}{\partial v}\right)_P\right]_o\left[h_{ADS4} - e + v\left(\frac{\partial e}{\partial v}\right)_P\right]^+ \tag{A.144}$$

Substituting these dimensionless initial conditions into (A.138) and dividing through by $P_o\left(\frac{\partial e}{\partial P}\right)_{v,o}$ yields the non-dimensional governing equation:

$$\left(\frac{\partial e}{\partial P}\right)_v^+ \frac{dP^+}{dM^+} = \frac{1}{\Pi_\varepsilon}\left[h_{ADS4} - e + v\left(\frac{\partial e}{\partial v}\right)_P\right]_o - \frac{\Pi_\Gamma}{\Pi_\varepsilon}\left(\frac{q_{core}}{\dot{m}_{ADS4}}\right)_o \tag{A.145}$$

where the dimensionless property group $\Pi_\varepsilon$ is given as in the previous chapter as:

$$\Pi_\varepsilon = \frac{P_o\left(\frac{\partial e}{\partial P}\right)_{v,o}}{\left[h_{ADS4} - e + v\left(\frac{\partial e}{\partial v}\right)_P\right]_o} \tag{A.146}$$

and the power-to-energy flow rate ratio is:

$$\Pi_\Gamma = \frac{q_{core,o}}{\dot{m}_{ADS4,o}\left[h_{ADS4} - e + v\left(\frac{\partial e}{\partial v}\right)_P\right]_o} \tag{A.147}$$

Hence, to simulate the transition behavior in APEX-AP1000, the dimensionless groups defined in equations (A.146) and (A.147) must be preserved. For the full-pressure conditions proposed for the ADS4 blowdown test series, fluid property similitude reduces the ratio of these groups to:

$$\Pi_{\varepsilon,R} = 1 \tag{A.148}$$

and

$$\Pi_{\Gamma,R} = \left(\frac{q_{core,o}}{\dot{m}_{ADS4,o}}\right)_R \tag{A.149}$$

The property group, $\Pi_\varepsilon$ in AP1000 and APEX-AP1000 are identical and, therefore, the similarity criterion is automatically satisfied.

### A.6.3 Bottom-Up Scaling Analysis

This section describes the scaling analyses performed for the ADS4 blowdown/IRWST transition phenomena. The core power and ADS4 choked flow rate behavior have already been assessed in Section A.5. The core power has been scaled as [ ]$^{a,b,c}$. Similarly, when fluid property similitude exists, the choked flow conditions at the ADS4 valves are preserved, and the mass flow rate is scaled at [ ]$^{a,b,c}$ because the ADS4 flow areas have been scaled by [ ]$^{a,b,c}$. Thus, equation (A.149) becomes:

$$\Pi_{\Gamma,R} = 1 \tag{A.150}$$

which indicates that this dimensionless group will also be preserved in APEX-AP1000.

#### *A.6.3.1 Flashing and Liquid Boil-off Rate*

The flashing phenomena is automatically preserved by establishing the initial pressure and subcooling conditions in APEX as those in the AP1000 for the ADS4 blowdown phase. The liquid mass boil-off rate in the core, under steady-state conditions is described as follows:

$$\dot{m}_{Boil\text{-}off} = \frac{q_{core}}{h_{fg} + h_{subcooled}} \tag{A.151}$$

For fluid property similitude, the ratio of this equation (i.e., APEX to AP1000) becomes:

$$\dot{m}_{Boil\text{-}off,R} = q_{core,R} = \frac{1}{96} \tag{A.152}$$

which is the required value to preserve the one-half time scale requirement. However, it is noted that the volume of the APEX downcomer is large on a scaled basis. Of particular interest to the full-pressure ADS4 blowdown tests is the downcomer volume between the bottom of the CL and the top of the heated fuel elevation. This region represents a source of liquid that resides in the downcomer at an elevation above the top of the heated fuel. For APEX, this region has a length of [ ]$^{a,b,c}$ and a corresponding volume of [ ]$^{a,b,c}$. For AP1000, this region has a length of [ ]$^{a,b,c}$ and a volume of [ ]$^{a,b,c}$. The length scale ratio is 1:4, as desired. However, the volume scale ratio is 1:100, which is approximately 2 times the desired value of 1:192.

At a system pressure of [ ]$^{a,b,c}$, the amount of saturated liquid mass that could be contained in this region for AP1000 would be [ ]$^{a,b,c}$. For the similar region in APEX, this corresponds to [ ]$^{a,b,c}$.

During the transition period of the ADS4 blowdown, the primary source of water will be the 20% liquid volume remaining in the CMT. For the fluid conditions stated earlier, this corresponds to a volume of [ ]$^{a,b,c}$ in AP1000 and [ ]$^{a,b,c}$ in APEX-AP1000. It is desired that a 1:2 boil-off time scale be simulated. Therefore, the following scaling criterion must be preserved:

$$\tau_{Boil\text{-}off,R} = \left( \frac{\rho_f (V_{CMT} + V_{DC})(h_{fg} + h_{subcooled})}{q_{core}} \right)_R = 0.5 \quad \text{(A.153)}$$

For the case of fluid property similitude and a fixed core power ratio, this criterion becomes:

$$(V_{CMT} + V_{DC})_R = \frac{1}{192} \quad \text{(A.154)}$$

Because the downcomer volume in APEX is oversized, this criterion can be satisfied by initiating the ADS4 blowdown in APEX with a reduced liquid inventory in the CMT starting the ADS4 blowdown with a 12.5% volume rather than a 20% volume would satisfy this requirement.

### *A.6.3.2 IRWST Full-Height Liquid Head and Injection Flow Rate*

Simulating the full-pressure ADS4 blowdown transition in APEX will require a full-height liquid head in the IRWST. This will be achieved by pressurizing the APEX IRWST to a pressure of [ ]$^{a,b,c}$ to simulate full-height AP1000 conditions. Similarly, the IRWST line resistance shall be increased such that the initial IRWST mass flow rate at the simulated full-height conditions is [ ]$^{a,b,c}$. Flow tests shall be performed to fine-tune the IRWST line resistance.

### *A.6.3.3 Core Fluid Mixture Level Swell*

The initial liquid mass distribution in the RCS will determine the conditions at which the HL uncovers. As shown in Figure A.20, when the HL uncovers, the ADS4 flow transitions from two-phase choked flow to essentially single-phase vapor choked flow. This choked flow transition is important because the RCS depressurization rate will depend on the type of choked flow conditions at the ADS4 valves.

Properly modeling the initial RCS liquid mass distribution requires preserving the core fluid mixture level swell. The equation for level swell is given by:

$$H_{mix} = \frac{H_{collapsed}}{1 - <\alpha_c>} \quad \text{(A.155)}$$

where $H_{mix}$ is the fluid mixture level, $H_{collapsed}$, is the collapsed liquid level and $<\alpha_c>$ is the average core void fraction. To preserve the level swell in the core, the following similarity criterion must be preserved:

$$\left( \frac{H_{collapsed}}{H_{mix}} \right)_R = (1 - <\alpha_c>)_R \quad \text{(A.156)}$$

which implies that the average core void fraction ratio must also be preserved. That is:

$$(<\alpha_c>)_R = 1 \quad \text{(A.157)}$$

The void fraction as a function of position in the core was obtained using the drift-flux relationship [Ref. 15]:

$$\alpha(z)=\frac{j_g(z)}{C_o\, j(z) + V_{gj}} \tag{A.158}$$

At stagnant loop conditions, $j_f$ is zero, so equation (A.158) becomes:

$$\alpha(z)=\left[C_o + \frac{V_{gj}}{j_g(z)}\right]^{-1} \tag{A.159}$$

The volumetric vapor flux, $j_g$, was found using the following relation:

$$j_g(z)=\frac{1}{\rho_g\, a_c\, h_{fg}} \int_{L_{NB}}^{z} q'(z)dz \tag{A.160}$$

where $L_{NB}$ is the non-boiling height. The core averaged void fraction, $<\alpha_c>$, was obtained by integration as follows:

$$\langle\alpha_\varepsilon\rangle=\frac{1}{L_c}\int_{L_{NB}}^{L_c} \alpha(z)dz \tag{A.161}$$

APEX-AP1000 will implement a constant axial power profile. Therefore, equation (A.158) is given by:

$$j_g(z)=\frac{q_{core}\,(z - L_{NB})}{\rho_g\, a_c\, h_{fg}\, L_c} \tag{A.162}$$

Substituting equations (A.157) and (A.160) into (A.159) yields the core averaged void fraction for constant axial power:

$$\langle\alpha_\varepsilon\rangle=\frac{1}{C_o}\left[1-\frac{L_2}{C_o\,\Pi_z(L_c-L_{NB})}\mathrm{Ln}\left(1+\frac{C_o\,\Pi_z(L_c-L_{NB})}{L_c}\right)\right] \tag{A.163}$$

where $\Pi_{zuber}$ is the Zuber number, rearranged as:

$$\Pi_{zuber}=\frac{q_{core}}{\rho_g\, v_{gj}\, a_c\, h_{fg}} \tag{A.164}$$

The AP1000 is assumed to have a chopped cosine shape axial power profile defined as follows.

$$q(z)=\int_{-L_c/2}^{z} q'_c\cos\left(\frac{\Pi z}{L_c}\right)dz \qquad (A.165)$$

Integrating equation (A.163) yields:

$$q(z)=q'_c\frac{L_c}{\pi}\left[1+\sin\left(\frac{\pi z}{L_c}\right)\right] \qquad (A.166)$$

Substituting equation (A.164) into equations (A.158) yields:

$$j_g(z)=\frac{q'_c L_c}{\pi\rho_g a_c h_{fg}}\left[1+\sin\left(\frac{\pi z}{L_c}\right)\right] \qquad (A.167)$$

Equation (A.165) was substituted into (A.159) and numerically integrated to obtain the core averaged void fraction for the AP1000. The churn-turbulent drift-flux correlation was used to assess equation (A.157) for both APEX and AP1000. That is:

$$v_{gj}=1.53\left[\frac{\sigma g\Delta\rho}{\rho_{liter}^2}\right]^{1/4} \qquad (A.168)$$

Table A.16 presents the data used to calculate the core average void fraction for the case of an ADS4 blowdown from [ ]$^{a,b,c}$ and a decay heat of [ ]$^{a,b,c}$. The core averaged void fraction was found to be [ ]$^{a,b,c}$ for APEX and 60% for AP1000.

Figure A.18 compares the axial void fraction profiles in AP1000 and APEX-AP1000 for an average subchannel for this ADS4 blowdown case. The difference in void fraction profiles arises because the power profiles have different shapes. The core exit void fractions were calculated to be [ ]$^{a,b,c}$ and [ ]$^{a,b,c}$ for AP1000 and APEX respectively.

Table A.16 Comparison of APEX and AP1000 Core Averaged Void Fractions

| Parameter | AP1000 | APEX-AP1000 | Units |
|---|---|---|---|
| Core Flow Area ($a_c$) | | | |
| Core Heated Length | | | |
| Power (2.1% Decay) | | | |
| Average Linear Power at Decay Heat | | | |
| Pressure | | | |
| $\rho_g$ | | | |
| $P_l$ | | | |
| $\sigma$ | | | |
| $H_g$ | | | |
| $H_L$ | | | |
| $C_o$ | | | |
| $v_{gj}$ | | | |
| $<\alpha_c>$ | | | |

a,b,c

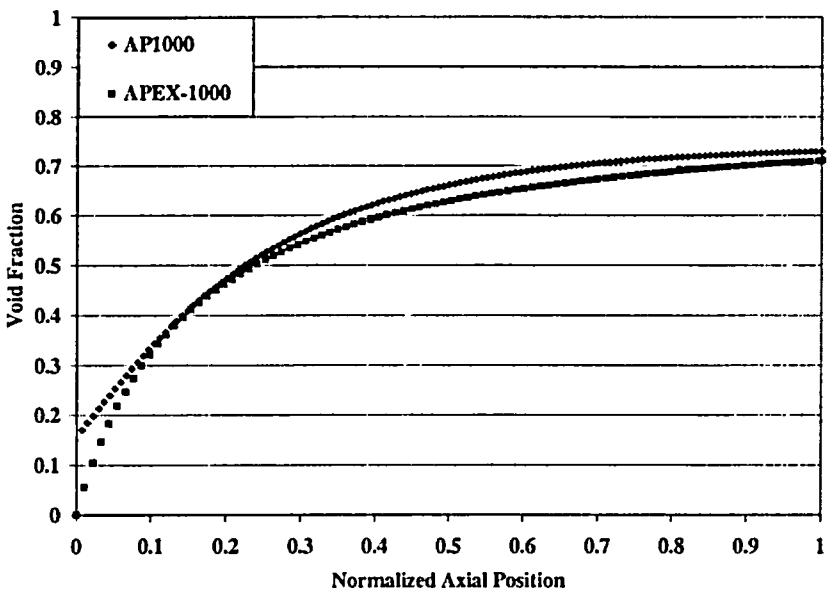


Figure A.18 Comparison of AP1000 and APEX Axial Void Fraction Profiles for an Average Subchannel

### *A.6.3.4 Initial Conditions for the Full-Pressure ADS4 Blowdown Tests*

The following table presents the initial conditions for a full-pressure ADS4 test in APEX-AP1000. The test shall be initiated from steady-state conditions. The decay power and system pressure were selected based on the results of Chapter 15 of the AP1000 Safety Analysis Report. The highest decay power observed while actuating ADS4 was ~2.0% for the DEDVI case. The typical pressure at which ADS4 actuates is [ ]$^{a,b,c}$.

Table A.17 Proposed Initial Conditions for a Full Pressure ADS4 Blowdown Test In APEX-AP1000

| Parameter | AP1000 | APEX-AP1000 | Units |
|---|---|---|---|
| RCS Pressure | | | |
| 2% Core Decay Power | | | |
| Initial CMT Volume | | | |
| ADS4 Flow Areas – 100% | | | |
| ADS4 Flow Areas – 50% | | | |
| IRWST Nominal Liquid Level | | | |
| IRWST Head Pressure | | | |

a,b,c

## A.7 Upper Plenum Entrainment Scaling

Top-down component-level and bottom-up process-level scaling analyses have been performed to establish the upper plenum geometry and flow conditions that should be modeled in the APEX-AP1000 integral system test facility. Figure A.19 describes the scaling analysis process.

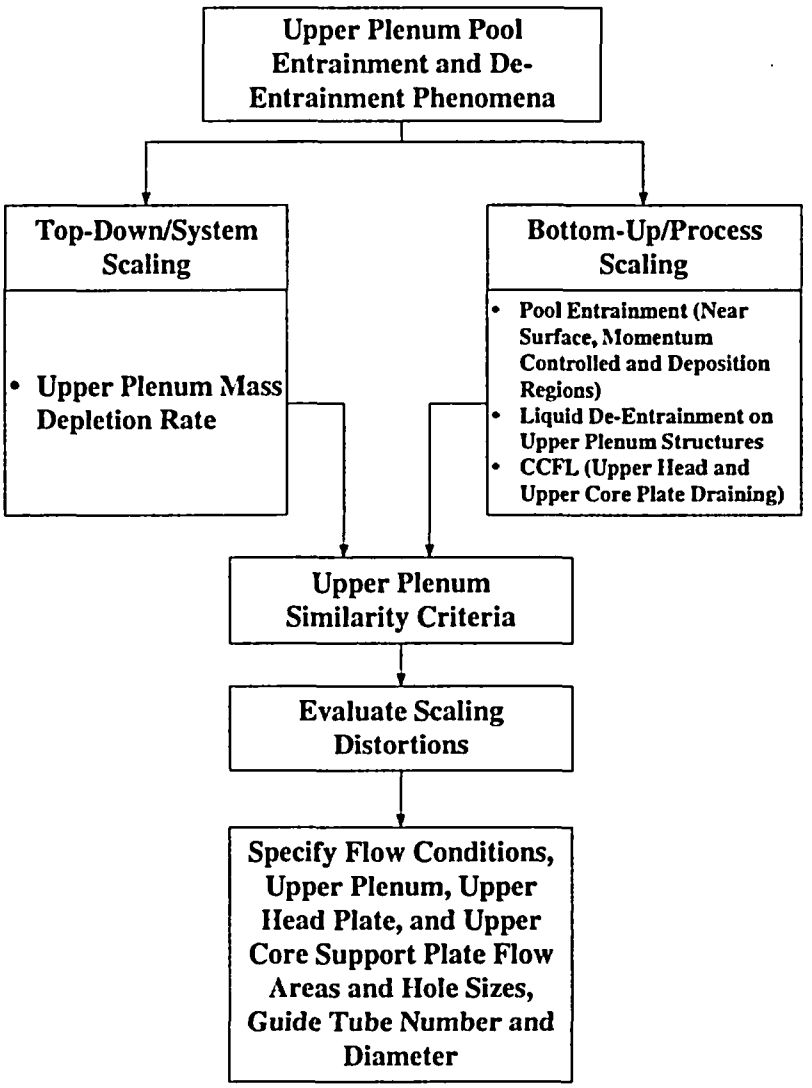


Figure A.19 Upper Plenum Scaling Analysis Flow Chart

The main objective of the analysis was to obtain the scaling ratios that would preserve, on a scaled basis, the rate at which the liquid level in the upper plenum decreases during pool boiling. The top-down scaling analysis resulted in a non-dimensional mass balance equation for the upper plenum control volume. The bottom-up scaling analysis provided the closure relationships for the top-down analysis. In particular, pool boiling entrainment was examined for the near-surface, momentum-dominated and deposition regions of the upper plenum.

### A.7.1 Top-Down Scaling Analysis

The control volume shown in Figure A.20 was defined for the upper plenum for the purpose of writing the mass balance equation.

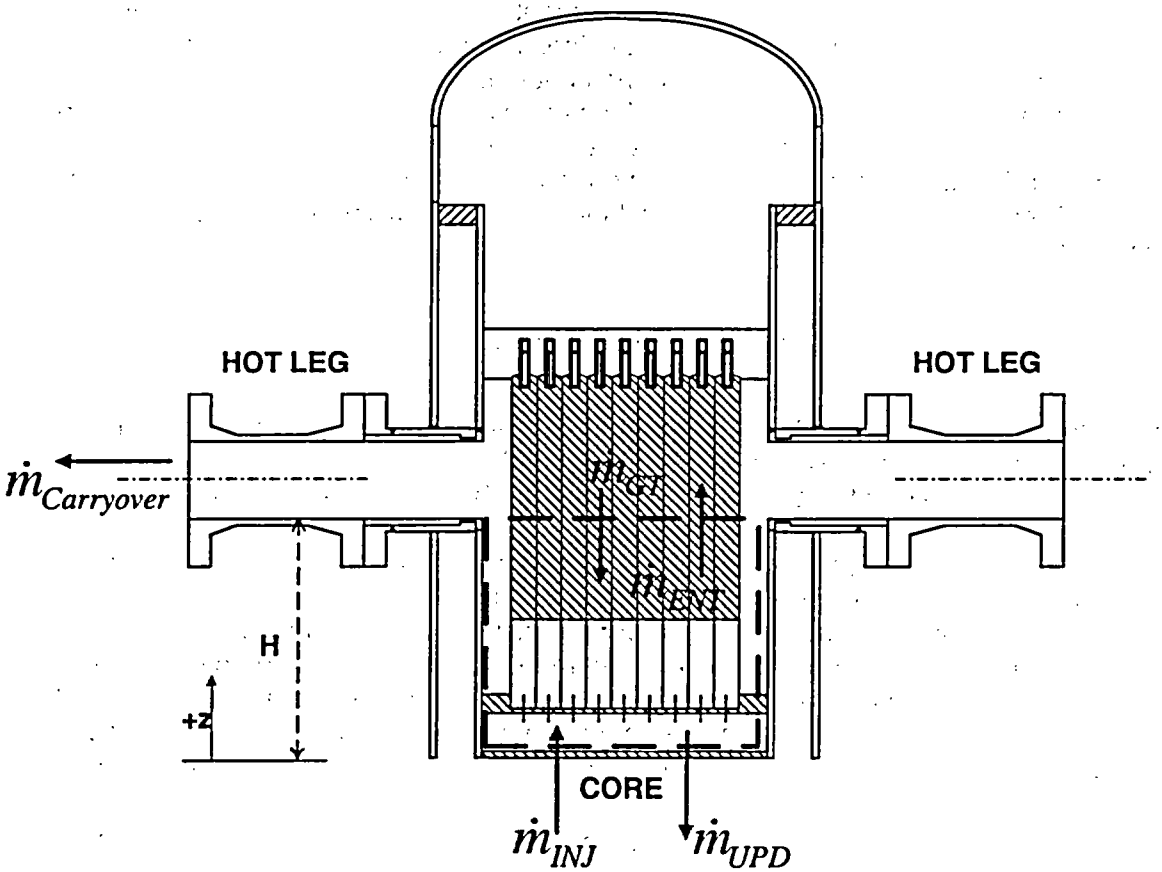


Figure A.20 Upper Plenum Control Volume Located Below the Hot Legs

The *liquid* mass conservation equation for the upper plenum is written as follows:

$$\frac{dM_{UP}}{dt} = \dot{m}_{IN} - \dot{m}_{OUT} \tag{A.169}$$

The upper plenum flow cross-sectional area, $a_{UP}$, is constant inside the control volume and the liquid is assumed to be incompressible; therefore, liquid density $r_L$ is uniform and constant. The vertical upward direction is defined as the z-coordinate. Thus, removing the constants from the derivative on the left-hand side of equation (A.169) yields:

$$a_{UP}\rho_L\frac{dz}{dt} = \dot{m}_{IN} - \dot{m}_{OUT} \tag{A.170}$$

One source of liquid to the control volume is liquid mass flow from the core region due to safety injection. During the later part of ADS4 operation, IRWST injection would be supplying liquid to

the core. A second source of liquid to the upper plenum is de-entrainment on the vertical guide tubes. A third source of liquid mass into the control volume is draining from the upper head through the upper support plate.

The primary path of liquid mass loss from the upper plenum is through the HL. When the liquid level is below the bottom of the HL, pool entrainment results, causing liquid droplets to be carried with the steam out the HL to the ADS4 line. Another source of mass loss is attributable to draining from the upper plenum through the upper core plate back into the core. Loss of upper plenum liquid mass as a result of flashing or boiling as a result of stored energy release from upper plenum structures are not considered applicable during this phase of the transient. Equations for the liquid mass loss and injection terms are presented in the bottom-up scaling analysis. Expanding equation (A.170) to include the individual liquid mass source and sink terms yields:

$$a_{UP}\rho_L\frac{dz}{dt} = \dot{m}_{INJ} + \dot{m}_{GT} - \dot{m}_{ENT} - \dot{m}_{UPD} \tag{A.171}$$

The first term on the right-hand side represents the sum of the DVI injection flows that tend to fill the upper plenum via the downcomer (i.e., CMT, ACC, IRWST, and sump flows). It is the mass flow rate of liquid entering the control volume through the core. The second term on the right-hand side represents the guide tube de-entrainment rate. It is the mass flow rate of liquid that is de-entrained by the upper plenum structure and that eventually drains as a liquid film into the control volume. The third term on the right-hand side is the liquid entrainment rate. It is the mass flow rate of liquid produced by the vapor interaction with the liquid (i.e., near surface, momentum-controlled or deposition pool entrainment). This liquid is carried out of the control volume, where a portion is de-entrained by the guide tubes and the remainder is carried out to the HL. The last term on the right-hand side represents mass flow rate of liquid that drains out of the control volume by gravity through the upper core plate back into the core region.

### *A.7.1.1 Dimensionless Liquid Mass Balance*

Equation (A.171) can be made dimensionless using the following initial and boundary conditions:

$$z^+_{INJ} = \frac{z}{H} \tag{A.172}$$

where *H* is the vertical length between the top of the core and the bottom of the HL. The dimensionless injection mass flow rate is given as:

$$\dot{m}^+_{INJ} = \frac{\dot{m}_{INJ}}{\dot{m}_{INJ,O}} \tag{A.173}$$

The dimensionless guide tube de-entrainment rate is given as:

$$\dot{m}^+_{GT} = \frac{\dot{m}_{GT}}{\dot{m}_{GT,O}} \tag{A.174}$$

The dimensionless liquid entrainment rate is given as:

$$\dot{m}^{+}_{ENT} = \frac{\dot{m}_{ENT}}{\dot{m}_{ENT,O}} \tag{A.175}$$

The dimensionless upper plenum draining rate is given as:

$$\dot{m}^{+}_{UPD} = \frac{\dot{m}_{UPD}}{\dot{m}_{UPD,O}} \tag{A.176}$$

Substituting these ratios into equation (A.171) and dividing both sides of the equation by the initial entrainment mass flow rate yields the dimensionless mass balance equation for the upper plenum liquid.

$$\tau_{ENT}\frac{dz^{+}}{dt} = \Pi_{INJ}\dot{m}^{+}_{INJ} + \Pi_{GT}\dot{m}^{+}_{GT} - \dot{m}^{+}_{ENT} - \Pi_{UPD}\dot{m}^{+}_{UPD} \tag{A.177}$$

In this equation, the liquid entrainment reference time scale has been defined as:

$$\tau_{ENT} = \frac{a_{UP}\rho_{L}H}{\dot{m}_{ENT,O}} \tag{A.178}$$

Thus the dimensionless time coordinate for upper plenum emptying due to liquid entrainment is given by:

$$t^{+} = \frac{t}{\tau_{ENT}} \tag{A.179}$$

All of the remaining filling and draining processes are therefore, expressed in terms of the liquid entrainment process. That is, the dimensionless P groups of equation (A.177) are written as:

$$\Pi_{INJ} = \frac{\dot{m}_{INJ,O}}{\dot{m}_{ENT,O}} \tag{A.180}$$

$$\Pi_{GT} = \frac{\dot{m}_{GT,O}}{\dot{m}_{ENT,O}} \tag{A.181}$$

$$\Pi_{UPD} = \frac{\dot{m}_{UPD,O}}{\dot{m}_{ENT,O}} \tag{A.182}$$

Equations (A.178) through (A.182) will be evaluated in the bottom-up scaling analysis.

### *A.7.1.2 Preserving the Upper Plenum Draining Rate During Integral System Testing*

The desired outcome of this scaling analysis is to establish the geometry and flow conditions in APEX that would preserve the upper plenum draining rate when plotted in dimensionless phase space. That is, plotting the upper plenum liquid level history in terms of the dimensionless

spatial coordinate, $z^+$, and the dimensionless time coordinate, $t^+$, would yield overlaying curves for the model and the prototype. This condition can be achieved by satisfying the following requirements.

The scenarios are initiated from the same initial condition in dimensionless phase space. In this case, $z^+$ at $t^+ = 0$ is 1.

The rate of change (i.e., slope) is preserved in dimensionless phase space. This imposes the following scaling criterion:

$$\left(\frac{dz^+}{dt^+}\right)_R = 1 \tag{A.183}$$

Note that $(z^+)_R$ and $(t^+)_R$ are unity. Satisfying the requirement given by equation (A.183) can only be accomplished by preserving the ratios of the individual P groups on the right-hand side of equation (A.177). The APEX facility transient response was originally designed to operate at one-half time scale ($t_R = 0.5$) which means that the reference time scale ratio, $\tau_R$, must also be one-half to keep $(t^+)_R$ at unity. Because the APEX facility height is fixed at one-quarter scale, and the flow area is roughly fixed at [ ]$^{a,b,c}$, certain physical limitations have already been established. Nonetheless, minor modifications to the upper plenum structures are possible. To preserve the one-half scale timing of integral system transient behavior, it is desired that:

$$\left(\frac{dz}{dt}\right)_R = \frac{1}{2} \tag{A.184}$$

Substituting equations (A.172) and (A.179) into (A.184) yields:

$$\left(\frac{H}{\tau_{ENT}}\right)_R \left(\frac{dz^+}{dt^+}\right)_R = \frac{1}{2} \tag{A.185}$$

Imposing the requirement given by equation (A.183) yields:

$$\left(\frac{H}{\tau_{ENT}}\right)_R = \frac{1}{2} \tag{A.186}$$

This is a direct result of the one-half time scale requirement. Substituting equation (A.178), assuming fluid property similitude, and rearranging yields the following simple scaling criterion for the upper plenum:

$$\left(\frac{\dot{m}_{ENT,O}}{a_{UP}}\right)_R = \frac{1}{2} \tag{A.187}$$

For the case where liquid entrainment is the dominant mechanism (i.e., the largest mass transfer term on the right-hand side of the balance equation), equation (A.187) coupled with a correlation for liquid entrainment represents the governing scaling criterion. The next section presents the bottom-up scaling analysis and includes liquid entrainment equations that can be used to provide closure to equation (A.187).

### A.7.2 Bottom-up Scaling Analysis

This section examines the following upper plenum filling and draining mechanisms:

- pool entrainment
- guide tube de-entrainment
- the effects of counter-current flow limitations (CCFL) on upper plenum draining

The phenomenon of interest to this study is upper plenum pool entrainment. The following section presents a review of the phenomenon and the existing predictive models.

#### *A.7.2.1 Pool Entrainment*

The basic equations of pool entrainment will be derived to provide a theoretical context for their application to the scaling analysis. Here, the discussion will consist of a brief derivation of Ishii's pool entrainment equations. Following this derivation, certain questions regarding the application of these equations in scaling the AP1000 experiments will be addressed. In particular, it will be necessary to examine the vertical extent of various entrainment regions, the flow regime in the pool, the question of flooding, the phenomena of re-entrainment from a falling film, and the issue of enhanced deposition as a result of the lateral motion of the flow. In Ishii's pool entrainment model, the entrainment is defined as the ratio of the droplet to vapor mass flux, and represented phenomenologically by the following equation [Ref. 16]:

$$E_{fg}\ (h, j_g) = \frac{\rho_f j_f}{\rho_g j_g} = \frac{\dot{\varepsilon}(j_g)}{\rho_g j_g} \int_0^{D_{max}} f_D(D, j_g) \int_{v_h}^{\infty} g(v_i, D, j_g)\, dv_i\, dD \qquad \text{(A.188)}$$

Here ε-dot is the mass flux of droplets at the liquid surface which is a function of the vapor superficial velocity, $j_g$. As the droplets generated at the surface vary in size from zero to some maximum diameter, a distribution function for the droplet diameters is employed. This function, $f_D$, gives the fraction of droplets within any given range, $dD$, and is itself a function of $j_g$. Obviously, since all the droplets must fall within the range, $0 \le D \le D_{max}$:

$$\int_0^{D_{max}} f_D(D, j_g)\, dD = 1 \qquad \text{(A.189)}$$

Furthermore, the droplets so generated will have an initial velocity, $v_i$, which depends upon both the superficial velocity, $j_g$, and the droplet diameter, $D$. Hence, a distribution function, $g$, is needed for the initial velocity, such that:

$$\int_0^{\infty} g(v_i, D, j_g)\, dv_i = 1 \qquad \text{(A.190)}$$

As written, equation (A.189) depends upon the maximum droplet diameter to define an upper limit of integration. By using the pool entrainment data to determine various experimental constants, Ishii found the best agreement for:

$$D^*_{max} = 7.24\, j_g^{*-1} \qquad \text{(A.191)}$$

In this equation, the asterisk denotes a dimensionless variable, such that:

$$D^* = \frac{D}{\sqrt{\frac{\sigma}{g\Delta\rho}}} \tag{A.192}$$

and

$$j_g^* = \frac{j_g}{\left[\frac{\sigma g \Delta\rho}{\rho_g^2}\right]^{1/4}} \tag{A.193}$$

With regard to the second integral in equation (A.188), the lower limit, $v_h$, is the minimum initial velocity required for a droplet of diameter, $D$, to reach height, h. With regard to its dependence on the droplet diameter, $v_h = 0$, for droplets in the range $0 \le D \le D_c$, where the critical diameter, $D_c$, is the diameter of the largest droplet which can be suspended by vapor drag. Thus, the droplets within this range can reach height h by virtue of drag alone and hence need no initial velocity. On the other hand, droplets in the range $D_c < D \le D_{max}$ are too large to be suspended by vapor drag and hence fall back into the pool after losing their initial momentum. Consequently, these droplets must possess a minimal initial velocity, $v_h$, to reach the height in question. With regard to these calculations, the critical droplet diameter, $D_c$, is first obtained by balancing the weight of the droplet with the vapor drag:

$$g\Delta\rho\pi\frac{D_c^3}{6} = \pi\frac{D_c^2}{4}C_D\frac{1}{2}\rho_g j_g^2 \tag{A.194}$$

where

$$C_D = \frac{10.76}{Re^{1/2}} \tag{A.195}$$

Solving equation (A.194) for the critical diameter subject to the drag relation given by equation (A.195) yields:

$$D_c^* = 4\, j_g^* (N_{\mu_g})^{1/3} \tag{A.196}$$

where the viscosity number is given by:

$$N_{\mu_g} = \frac{\mu_g}{(\rho_g \sigma\sqrt{\sigma/g\Delta\rho})^{1/2}} \tag{A.197}$$

As mentioned above, $v_h = 0$ for diameters within the range $0 \le D \le D_c$. For diameters within the range $D_c < D \le D_{max}$, $v_h$ is determined by neglecting drag compared to gravity and calculating the velocity needed to reach height $h$.

$$v_h = \sqrt{2gh\frac{\Delta\rho}{\rho_f}}; \text{for } D_c < D \le D_{max} \tag{A.198}$$

Thus, in terms of dimensionless parameters:

$$v_h^* = 0 \text{ ; for } 0 \le D^* < D_c^* \tag{A.199}$$

and

$$v_h^* = \sqrt{2h^*}\left[\frac{\rho_g}{\rho_f}\right]^{1/2} \text{ ; for } D_c^* < D^* \le D_{max}^* \tag{A.200}$$

Having discussed the basic equation and the limits of integration, it remains to determine expressions for the surface mass flux, $\varepsilon$ dot, the diameter distribution function, $f_D$, and the velocity distribution function, $g$. To this end, observe first of all that near the water surface, $v_h$ goes to zero for all droplet diameters in accordance with equations (A.199) and (A.200). Hence, by virtue of equations (A.188), (A.189), and (A.190):

$$E_{fg}\ (0, j_g) = \frac{\dot{\varepsilon}(j_g)}{\rho_g j_g} \int_0^{D_{max}^*} f_D(D, j_g) \int_0^{\infty} g(v_i, D, j_g)\, dv_i\, dD = \frac{\dot{\varepsilon}(j_g)}{\rho_g j_g} \tag{A.201}$$

Using the limited data available for near surface entrainment, Ishii determined that [Ref. 16]:

$$E_{fg}\ (0, j_g) = \frac{\dot{\varepsilon}(j_g)}{\rho_g j_g} = 4.84 \times 10^{-3}\left[\frac{\rho_g}{\Delta\rho}\right]^{-1.0} \tag{A.202}$$

Thus:

$$\dot{\varepsilon}(j_g) = 4.84 \times 10^{-3} \rho_g j_g \left[\frac{\rho_g}{\Delta\rho}\right]^{-1.0} \tag{A.203}$$

To determine the distribution function, $f_D$, observe that after the droplets in the supercritical range have fallen back into the pool, one is left with droplets in the subcritical range. Since these droplets are sufficiently small to be suspended by vapor drag, they do not fall back into the pool. Consequently, the entrainment above a certain height remains constant except for the phenomenon of deposition on solid surfaces. Moreover, since these droplets are in the range $0 \le D \le D_c$, $v_h = 0$ by virtue of equation (A.199), and equation (A.188) can be integrated for a subrange of droplet sizes subject to equation (A.190) to yield:

$$\frac{\dot{\varepsilon}(j_g)}{\rho_g j_g} \int_0^{D} f_D(D, j_g) \int_0^{\infty} g(v_i, D, j_g)\, dv_i\, dD = \frac{\dot{\varepsilon}(j_g)}{\rho_g j_g} \int_0^{D} f_D(D, j_g)\, dD \tag{A.204}$$

Now, on the basis of experimental data, it has been determined that:

$$\frac{\dot{\varepsilon}(j_g)}{\rho_g j_g} \int_0^{D} f_D(D, j_g)\, dD = C(D^*)^{1.5}(j_g^*)^{1.5} \tag{A.205}$$

By differentiating this equation with respect to $D$, one obtains:

$$\frac{\dot{\varepsilon}(j_g)}{\rho_g j_g} f_D(D, j_g) = \frac{1.5C}{\sqrt{\sigma/g\Delta\rho}} (D^*)^{0.5} (j_g^*)^{1.5} \tag{A.206}$$

By comparing to the experimental data and utilizing equation (A.203), Ishii obtained:

$$f_D(D, j_g) = \frac{0.077}{\sqrt{\sigma/g\Delta\rho}} (D^*)^{0.5} (j_g^*)^{1.5} \tag{A.207}$$

To obtain the velocity distribution function, Ishii first made a rough model based on the breakup of liquid ligaments to determine the initial velocity of a droplet of diameter $D$ in a vapor stream of superficial velocity $j_g$. Such a breakup mechanism is consistent only with churn flow in the pool and, therefore, is inapplicable for pools in the bubbly or annular flow regimes. Accordingly, Ishii's entire model is limited to situations where there is churn flow in the pool because the initial velocity distribution derived from this assumption impacts all the subsequent correlations. With respect to this initial velocity, Ishii set up a rough equation based on the above mechanism and utilized experimental data to obtain [Ref. 16]:

$$v_i^* = 75.17\, j_g^{*1/4}\, N_{\mu_g}^{1/4}\, D^{*-1/4} \left[\frac{\rho_g}{\rho_f}\right]^{1/2} D_H^{*0.21} \left[\frac{\rho_g}{\Delta\rho}\right]^{0.115} \tag{A.208}$$

Moreover, since no information was available on the distribution of initial velocities, Ishii assumed that a single initial velocity characterizes a droplet of a given size, $D$, such that the distribution reduces to a delta function:

$$g(v_i, D, j_g) = \delta\left( v_i^* - 75.17\, j_g^{*1/4}\, N_{\mu_g}^{1/4}\, D^{*-1/4} \left[\frac{\rho_g}{\rho_f}\right]^{1/2} D_H^{*0.21} \left[\frac{\rho_g}{\Delta\rho}\right]^{0.115} \right) \tag{A.209}$$

Having determined expressions for all parameters in equation (A.188), the entrainment as a function of height can now be determined. To this end, observe from equation (A.208) that the initial velocity of a given droplet decreases with increasing size. Nonetheless, since there is a maximum droplet size, even the heaviest droplets will possess a minimal initial velocity and, therefore, will rise a definite height before falling back into the pool. Thus, there will be no fall out before a minimum height is attained, so there will be a near-surface region where the entrainment is constant. Above this height, entrainment will decrease as first the heavier and then the lighter droplets within the supercritical range fall back into the pool. This second region is, therefore, called the momentum-controlled region because the entrainment at any given height is dependent upon the droplets having sufficient initial momentum to reach the height in question. Finally, after all the supercritical droplets have fallen out of the flow, the entrainment will consist only of those droplets small enough to be suspended by the vapor drag. Thus, above a certain height the droplets stop falling back into the pool and are taken out of the flow entirely as a result of deposition on solid surfaces. For this reason, the third region is referred to as the deposition-controlled region.

The extent of the near-surface region can be determined by setting the initial velocity of the largest droplets equal to the initial velocity, $v_h$, needed to attain a particular height, h, and then solving for this height. The velocity of the largest droplets can be obtained by substituting the maximum diameter from equation (A.50) into equation (A.208). As usual, $v_h$ is given by equation (A.200):

$$\sqrt{2h^*}\left[\frac{\rho_g}{\rho_f}\right]^{1/2} = 75.17\, j_g^{*1/4}\, N_{\mu_g}^{1/4}\left[7.24\, j_g^{*-1}\right]^{-1/4}\left[\frac{\rho_g}{\rho_f}\right]^{1/2} D_H^{*0.21}\left[\frac{\rho_g}{\Delta\rho}\right]^{0.115} \qquad \text{(A.210)}$$

From this relation the near surface region can be shown to extend from:

$$0 \le h^* \le 1.038\times10^3\, j_g^*\, N_{\mu_g}^{1/2}\, D_H^{*0.42}\left[\frac{\rho_g}{\Delta\rho}\right]^{0.23} \qquad \text{(A.211)}$$

where the upper limit on $h^*$ is obtained by solving equation (A.210). Within this region, $v_h$ is effectively zero since $v_h < v_i$ for all droplet sizes. Thus, using equations (A.188) and (A.202), the entrainment becomes:

$$E_{fg}\,(h, j_g) = \frac{\dot{\varepsilon}(j_g)}{\rho_g j_g}\int_0^{D_{max}} f_D(D, j_g)\int_{v_h}^{\infty} g(v_i, D, j_g)\,dv_i\,dD = \frac{\dot{\varepsilon}(j_g)}{\rho_g j_g} = 4.84\times10^{-3}\left[\frac{\rho_g}{\Delta\rho}\right]^{-1.0} \qquad \text{(A.212)}$$

Above the near-surface region is the momentum-controlled region where the heavier droplets within the supercritical range progressively fall back into the pool. The lower limit for this region is given by the right-hand side of equation (A.211). The upper limit is determined by the point at which all the supercritical droplets have fallen out of the stream so that only subcritical droplets remain. To determine this limit, it is first necessary to substitute equation (A.196) into equation (A.208) to get the initial velocity of a critically sized droplet and then to set the resulting expression equal to the initial velocity, $v_h$, given by equation (A.200). When these steps are performed, the following expression is obtained:

$$\sqrt{2h^*}\left[\frac{\rho_g}{\rho_f}\right]^{1/2} = 75.17\, j_g^{*1/4}\, N_{\mu_g}^{1/4}\left[4\, j_g^*(N_{\mu_g})^{1/3}\right]^{-1/4}\left[\frac{\rho_g}{\rho_f}\right]^{1/2} D_H^{*0.21}\left[\frac{\rho_g}{\Delta\rho}\right]^{0.115} \qquad \text{(A.213)}$$

On the basis of this relation and equation (A.196), the momentum-controlled region can be shown to extend from:

$$1.038\times10^3\, j_g^*\, N_{\mu_g}^{1/2}\, D_H^{*0.42}\left[\frac{\rho_g}{\Delta\rho}\right]^{0.23} \le h^* \le 1.413\times10^3\, N_{\mu_g}^{1/3}\, D_H^{*0.42}\left[\frac{\rho_g}{\Delta\rho}\right]^{0.23} \qquad \text{(A.214)}$$

To determine the entrainment as a function of height within these limits, it is first necessary to determine the diameter of the largest supercritical droplet having the initial velocity needed to reach the point in question. Denoting this diameter $D_h$, substituting the variable $D_h$ into equation (A.208), and setting the result equal to equation (A.200), yields the following expression:

$$\sqrt{2h^*}\left[\frac{\rho_g}{\rho_f}\right]^{1/2} = 75.17\, j_g^{*1/4}\, N_{\mu_g}^{1/4}\, [D_h^*]^{-1/4}\left[\frac{\rho_g}{\rho_f}\right]^{1/2} D_H^{*0.21}\left[\frac{\rho_g}{\Delta\rho}\right]^{0.115} \tag{A.215}$$

In this expression, $D_h$ should not be confused with the hydraulic diameter $D_H$. If equation (A.215) is solved for $D_h$, one obtains:

$$D_h^* = \frac{(75.17)^4}{2^2}\frac{j_g^*}{h^{*2}}\, N_{\mu_g}\, D_H^{*0.84}\left[\frac{\rho_g}{\Delta\rho}\right]^{0.46} \tag{A.216}$$

Now, since all droplets within the range $D_h < D \le D_{max}$ lack sufficient initial momentum to reach height $h$, only diameters within the range $0 \le D \le D_h$ remain within the flow. Moreover, since all droplets remaining within the flow have initial velocities greater than or equal to $v_h$, $v_h$ is effectively zero for these droplets. Hence, the entrainment at height h is given by:

$$E_{fg}\ (h, j_g) = \frac{\dot{\varepsilon}(j_g)}{\rho_g j_g}\int_0^{D_h} f_D(D, j_g)\int_{v_h}^{\infty} g(v_i, D, j_g)\, dv_i\, dD = \frac{\dot{\varepsilon}(j_g)}{\rho_g j_g}\int_0^{D_h} f_D(D, j_g)\, dD \tag{A.217}$$

Utilizing equations (A.202) and (A.207), and switching to dimensionless coordinates yields:

$$E_{fg}\ (h, j_g) = 4.84 \times 10^{-3}\left[\frac{\rho_g}{\Delta\rho}\right]^{-1.0}\int_0^{D_h^*} 0.077 (D^*)^{0.5} (j_g^*)^{1.5}\, dD^* \tag{A.218}$$

Finally, integrating this equation subject to the expression for $D_h$ given by equation (A.216) yields the entrainment as a function of height in the momentum-controlled region:

$$E_{fg}\ (h, j_g) = 5.417 \times 10^6\, \frac{j_g^{*3}}{h^{*3}}\, N_{\mu_g}^{1.5}\, D_H^{*1.25}\left[\frac{\rho_g}{\Delta\rho}\right]^{-0.31} \tag{A.219}$$

Above the momentum-controlled region lies the deposition-controlled region, which only droplets within the subcritical diameter range can reach. Since these droplets can be suspended entirely by vapor drag, $v_h = 0$ for these droplets in accordance with equation (A.191). Hence, the entrainment is given by:

$$E_{fg}\ (h, j_g) = \frac{\dot{\varepsilon}(j_g)}{\rho_g j_g}\int_0^{D_c} f_D(D, j_g)\int_{v_h}^{\infty} g(v_i, D, j_g)\, dv_i\, dD = \frac{\dot{\varepsilon}(j_g)}{\rho_g j_g}\int_0^{D_c} f_D(D, j_g)\, dD \tag{A.220}$$

where $D_c$ is the diameter of a critically sized droplet. Utilizing equations (A.202) and (A.207), and switching to dimensionless coordinates yields:

$$E_{fg}\ (h, j_g) = 4.84 \times 10^{-3}\left[\frac{\rho_g}{\Delta\rho}\right]^{-1.0}\int_0^{D_c^*} 0.077 (D^*)^{0.5} (j_g^*)^{1.5}\, dD^* \tag{A.221}$$

Integrating this equation subject to the expression for $D_c$ given by equation (A.196) gives the entrainment in the deposition-controlled region:

$$E_{fg}\ (h, j_g) = 1.988 \times 10^{-3}\ j_g^{*3}\ N_{\mu_g}^{1/2} \left[\frac{\rho_g}{\Delta\rho}\right]^{-1.0} \tag{A.222}$$

As written, equation (A.222) predicts that entrainment remains constant with height. However, because of deposition on solid surfaces, the entrainment will decrease. Ishii makes the case that the deposition rate should be proportional to the entrainment itself, so that the entrainment decreases exponentially with height. On the basis of experimental data, Ishii determines an exponential attenuation term and adjusts the leading constant to yield:

$$E_{fg}\ (h, j_g) = 7.13 \times 10^{-4}\ j_g^{*3}\ N_{\mu_g}^{1/2} \left[\frac{\rho_g}{\Delta\rho}\right]^{-1.0} \exp\ (-0.205\ (h/D_H)) \tag{A.223}$$

Then, to ensure a smooth transition at the boundary and hence consistency among his equations, Ishii sets equation (A.223) for the deposition-controlled region equal to equation (A.219) for the momentum-controlled region to obtain the following equation for the transition height [Ref. 16]:

$$h^*\ \exp\ (-0.068\ (h^*/D_H^*)) = 1.97 \times 10^3\ \ N_{\mu_g}^{1/3}\ D_H^{*0.42} \left[\frac{\rho_g}{\Delta\rho}\right]^{0.23} \tag{A.224}$$

When the deposition term is small, the equation can be approximated as:

$$h^* = 1.97 \times 10^3\ \ N_{\mu_g}^{1/3}\ D_H^{*0.42} \left[\frac{\rho_g}{\Delta\rho}\right]^{0.23} \tag{A.225}$$

The entrainment correlations, $E_{fg}$, listed above can be expressed in terms of mass flow rate using the following definition:

$$E_{fg} = \frac{\rho_f\ j_f}{\rho_g\ j_g} \tag{A.226}$$

and the liquid mass continuity equation:

$$\dot{m}_{ENT} = \rho_f\ j_f\ a_{up} \tag{A.227}$$

Substituting equation (A.226) into (A.227) yields:

$$\dot{m}_{ENT} = \rho_g\ j_g\ E_{fg}\ a_{up} \tag{A.228}$$

This places the entrainment equations in the form needed to evaluate the dimensionless groups obtained in the top-down scaling analysis.

In summary, based on Ishii's pool entrainment model, the following entrainment relations are predicted [Ref. 16]:

Near-Surface Region:

$$0 \le h^* \le 1.038 \times 10^3 \; j_g^* \; N_{\mu_g}^{1/2} \; D_H^{*0.42} \left[\frac{\rho_g}{\Delta\rho}\right]^{0.23} \tag{A.229}$$

$$E_{fg}\,(h, j_g) = 4.84 \times 10^{-3} \left[\frac{\rho_g}{\Delta\rho}\right]^{-1.0} \tag{A.230}$$

$$\dot{m}_{ENT} = 4.84 \times 10^{-3} \Delta\rho \, j_g \, a_{up} \tag{A.231}$$

Momentum-Controlled Region:

$$1.038 \times 10^3 \; j_g^* \; N_{\mu_g}^{1/2} \; D_H^{*0.42} \left[\frac{\rho_g}{\Delta\rho}\right]^{0.23} \le h^* \le 1.97 \times 10^3 \; N_{\mu_g}^{1/3} \; D_H^{*0.42} \left[\frac{\rho_g}{\Delta\rho}\right]^{0.23} \tag{A.232}$$

$$E_{fg}\,(h, j_g) = 5.603 \times 10^6 \; \frac{j_g^{*3}}{h^{*3}} \; N_{\mu_g}^{1.5} \; D_H^{*1.25} \left[\frac{\rho_g}{\Delta\rho}\right]^{-0.31} \tag{A.233}$$

$$\dot{m}_{ENT} = 5.603 \times 10^6 \; \rho_g \, a_{UP} \frac{j_g^{*4}}{h^{*3}} \left[\frac{\sigma g \Delta\rho}{\rho_g^2}\right]^{.25} N_{\mu_g}^{1.5} \; D_H^{*1.25} \left[\frac{\rho_g}{\Delta\rho}\right]^{-0.31} \tag{A.234}$$

Deposition-Controlled Region:

$$1.97 \times 10^3 \; N_{\mu_g}^{1/3} \; D_H^{*0.42} \left[\frac{\rho_g}{\Delta\rho}\right]^{0.23} \le h^* \tag{A.235}$$

$$E_{fg}\,(h, j_g) = 7.13 \times 10^{-4} \; j_g^{*3} \; N_{\mu_g}^{1/2} \left[\frac{\rho_g}{\Delta\rho}\right]^{-1.0} \exp\,(-0.205\,(h/D_H)) \tag{A.236}$$

$$\dot{m}_{ENT} = 7.13 \times 10^{-4} \; \rho_g \, a_{UP} \, j_g^{*4} \left[\frac{\sigma g \Delta\rho}{\rho_g^2}\right]^{.25} N_{\mu_g}^{1/2} \left[\frac{\rho_g}{\Delta\rho}\right]^{-1.0} \exp\,(-0.205\,(h/D_H)) \tag{A.237}$$

As previously mentioned, these equations are built upon a particular entrainment mechanism under the assumed conditions of churn flow in the pool. Thus, the validity of these equations hinges upon the satisfaction of this initial assumption.

### *A.7.2.2 Upper Plenum Liquid Entrainment Rate Scaling Criteria*

The upper plenum geometry and flow conditions can be determined by substituting the entrainment correlations into the scaling criterion given by equation (A.187).

Near-Surface Region:

Substituting equation (A.231) into (A.187) and assuming fluid property similitude, yields the following relation:

$$j_{g,R} = \frac{1}{2} \tag{A.238}$$

This ratio is established by controlling the core power and fixing the upper plenum flow area. Performing a simple steady-state energy balance for the core yields:

$$\rho_g j_g a_{UP} (h_{fg} - \Delta h_{SC}) = \dot{q} \tag{A.239}$$

where $Dh_{SC}$ is the core subcooling, and $q$ is the core power. Rearranging and substituting into equation (A.238) yields:

$$\left(\frac{\dot{q}}{a_{UP}}\right)_R = \frac{1}{2} \tag{A.240}$$

Currently, the APEX upper plenum flow area, $a_{UP}$, ratio is approximately equal to [ ]$^{a,b,c}$. Thus, the core power scaling ratio becomes:

$$\dot{q}_R = \frac{1}{96} \tag{A.241}$$

The requirements for liquid entrainment in the near-surface region can be easily met.

Momentum-Controlled Region:

Substituting equation (A.234) into equation (A.187) and assuming fluid property similitude yields:

$$\left(\frac{j_g^4 D_H^{1.25}}{h^3}\right)_R = \frac{1}{2} \tag{A.242}$$

Fixing $j_{g,R}$ to 1:2 and $h_R$ to 1:4 yields the following scaling ratio for the hydraulic diameter of the upper plenum:

$$D_{H,R} = \left(\frac{1}{8}\right)^{0.8} = 0.1895 \tag{A.243}$$

This new scaling criterion shall be applied in the upper plenum design section.

Deposition-Controlled Region:

Substituting equation (A.237) into equation (A.187) and assuming fluid property similitude yields:

$$\left[ j_g^4 \exp\left( -.205 \frac{h}{D_H} \right) \right]_R = \frac{1}{2} \tag{A.244}$$

The form of this criterion requires that it be assessed numerically for the model and the prototype.

### *A.7.2.3 Scaling Criterion for Lateral De-Entrainment*

A study of droplet de-entrainment on vertical tubes in droplet cross-flow was performed by Dallman and Kirchner at Los Alamos Scientific Laboratory in 1980 [Ref. 17]. The study included both analytical and experimental research. Droplets of a known size were sprayed perpendicular to vertical conduits situated in a draft induced wind tunnel. The two geometries examined were square channels (76.2 mm square) and cylindrical tubes (25.4 mm, 63.5 mm, and 101.6 mm diameters). The air velocities were varied from 0 m/s to 14 m/s and the liquid droplet velocities were varied from 10 m/s to 15 m/s. It was found that the de-entrainment efficiency for a single tube was only weakly dependent on the tube diameter, air velocity, droplet mean velocity, total liquid flow rates for air velocities below 14 m/s, and droplet mass flux rates greater than 2 kg/(m$^2$-s). In fact, the de-entrainment rate was nearly a constant value of 0.19 for cylinders and 0.27 for square tubes for this range. That is:

$$\eta_l = 0.19 \text{ (For Cylinders)} \tag{A.245}$$

and

$$\eta_l = 0.27 \text{ (For a 76.2 mm Square Tube)} \tag{A.246}$$

The authors cited the work of Chen [Ref. 18] as providing a method of extrapolating the single tube data to an array of tubes. Namely, the de-entrainment efficiency for horizontal droplet flow through "k" rows of identical vertical tubes with a constant diameter to pitch ratio is:

$$\eta_k = A[1 - C(1 - \eta_l(1 + 4.5(D/P)^2)^k] \tag{A.247}$$

where $C$ is a geometric factor dependent on pitch to diameter ratios. The constant $A$ is unity for a staggered array with no line of sight through the array. Equation (A.247) indicates that preserving the upper plenum guide tube de-entrainment efficiency requires preserving the guide tube diameter to pitch ratio and the number of guide tube rows. Therefore, the first criterion can be written as:

$$(D/P)_R = 1 \tag{A.248}$$

For the diameter-to-pitch ratios in this study, very high entrainment efficiencies (i.e., greater than 90%) are achieved with just three staggered rows of guide tubes. Therefore, the number of guide tube rows beyond three does not contribute much to the de-entrainment process. Furthermore, an examination of the AP1000 upper plenum structure geometry reveals the following [Refs. 16, 17, and 18]:

(1) The upper core plate includes a significant number of holes at its periphery. De-entrainment of liquid from the peripheral holes will occur on the core barrel walls, because there are no guide tubes to impede the flow.

(2) There are several [ ]$^{a,b,c}$ diameter flow holes located adjacent to each HL. No de-entrainment will occur at those sites. Thus, the entrainment efficiency at those sites is zero. Modeling of those flow holes in the APEX test facility will be important.

(3) Liquid from the central internal flow holes will be de-entrained at a relatively high de-entrainment efficiency (i.e., on the guide tubes). Thus, the flow through the peripheral flow holes will dominate the behavior.

(4) The flow path of least resistance for the fluid is radially outward toward the periphery of the upper internals.

The upper plenum can be effectively divided into two zones: a peripheral zone that exhibits no de-entrainment and an internal guide tube zone with a relatively high de-entrainment efficiency. Rather than preserving the row numbers, the scaling approach shall be to preserve the flow area averaged de-entrainment efficiency for the internal guide tube zone. That is, the following scaling criterion will be applied:

$$\eta_{eff,R} = 1 \tag{A.249}$$

Effective De-Entrainment Efficiency

For purpose of this analysis, the AP1000 guide tube bundle has been divided into five flow zones, from I = 4 at the center of the upper plenum to i = 0 at the periphery of the upper plenum. The total liquid mass flow rate entering the flow zones through the upper core plate and traveling to the periphery of the guide tube bundle is given by:

$$\dot{m}_{Periphery} = \Sigma \dot{m}_i (1 - \eta_k)_i \tag{A.250}$$

where k represents the number of guide tube rows between a flow zone and the guide tube bundle periphery. For the AP1000, the upper plenum flow zones have been selected such that k = i. Dividing by the total liquid mass flow rate through the upper core plate yields the fraction of entrained liquid reaching the periphery. One minus this value yields the equation for the desired effective de-entrainment efficiency. That is:

$$\eta_{eff} = 1 - \frac{\Sigma \dot{m}_i (1 - \eta_k)_i}{\dot{m}_{UCP}} \tag{A.251}$$

Substituting equation (A.247) into (A.251) yields:

$$\eta_{eff} = 1 - \Sigma\left(\frac{\dot{m}_i}{\dot{m}_{UCP}}\right)[1 - A(1 - C\Phi^k)]_i \qquad \text{(A.252)}$$

where:

$$\Phi = 1 - \eta_1[1 + 4.5(D/P)^2] \qquad \text{(A.253)}$$

Furthermore, for the case of a constant inlet mass flux, $\rho v$, equation (A.253) becomes a flow area averaged de-entrainment efficiency:

$$\eta_{eff} = 1 - \Sigma\left(\frac{a_i}{a_{UCP}}\right)[1 - A(1 - C\Phi^k)]_i \qquad \text{(A.254)}$$

For the case of *A* and *C* equal to 1, and i = k, this equation reduces to:

$$\eta_{eff} = 1 - \Sigma\left(\frac{a_i}{a_{UCP}}\right)\Phi^i \qquad \text{(A.255)}$$

Equations (A.247) and (A.249) shall be used to help scale the lateral de-entrainment phenomenon.

### *A.7.2.4 Scaling Criterion for the Upper Core Plate*

The two key phenomena to be preserved by scaling the upper core plate flow holes are:

- Upper plenum flow distribution
- Counter-current flooding limitation (CCFL) at the core upper support plate holes.

Flow through the upper core plate at the guide tube bundle periphery will dominate the entrainment behavior in the upper plenum. In particular, the flow area directly adjacent to the HLs has unimpeded access to the HLs. Thus, preserving the flow distribution in the upper core plate will be essential to proper simulation of the entrainment behavior in the upper plenum. The following scaling criterion will be implemented:

$$\left(\frac{a_{Periphery}}{a_{UCP}}\right)_R = 1 \qquad \text{(A.256)}$$

Similarly, the upper core plate flow area at the entrance to the HLs shall also be preserved as follows:

$$\left(\frac{a_{HL}}{a_{UCP}}\right)_R = 1 \qquad \text{(A.257)}$$

Preserving the counter-current flooding behavior in the upper core plate requires that the Kutateladze number flooding limit, defined in terms of $j_g^*$ in this analysis, be preserved in APEX. That is:

$$\frac{j_g}{\left[\frac{\sigma g \Delta\rho}{\rho_g^2}\right]^{1/4}} = 4 \qquad \text{(A.258)}$$

For the condition of fluid property similitude, properly matching the Kutateladze number requires that $j_g$ in APEX match that in AP1000. That is:

$$(j_{g,UCP})_R = 1 \qquad \text{(A.259)}$$

Thus, the flow area of the APEX upper core plate must be scaled as 1:96, as follows:

$$(a_{UCP})_R = \frac{1}{96} \qquad \text{(A.260)}$$

Furthermore, the minimum upper core plate hole diameter must be greater than ~2.0 inches, so that the onset of the flooding behavior is not dependent on the hole diameter.

### *A.7.2.5 Scaling Criterion for the Upper Support Plate*

The upper support plate separates the upper plenum from the reactor vessel head. The plate provides support for the control rod guide tubes and includes 12 [ ]$^{a,b,c}$ diameter holes that permit the upper head to drain into the upper plenum. During the pool entrainment process, it is expected that the upper head will be empty of liquid. Nonetheless, it has been included to document the scaling basis for this component.

Because the flow area represented by the drain holes is quite small, the flooding behavior and flow distribution cannot both be simultaneously preserved. Since the upper head is essentially a dead-ended volume (there is a small bypass flow path from the upper head to the upper downcomer), flooding behavior will not be as important as the flow distribution. That is, CCFL is not expected to occur in the plate. The dominant phenomenon will be the pressurized draining of the upper head as a result of the flashing of liquid during a depressurization event. As a result, the drain hole number and distribution will be preserved and the flow area will be scaled as follows:

$$(a_{USP})_R = \frac{1}{48} \qquad \text{(A.261)}$$

*A.7.2.6 Design of APEX Upper Plenum Guide Tube Bundle, Upper Core Plate, and Upper Support Plate*

Based on the top-down and bottom-up scaling analyses presented in the previous sections, the following scaling approach was adopted for the upper plenum guide tubes, upper core plate, and upper support plate:

- Preserve the upper plenum hydraulic diameter ratio using equation (A.243).
- Preserve the local upper plenum subchannel hydraulic diameter ratio using equation (A.243).
- Preserve the total upper plenum flow area based on [ ]$^{a,b,c}$ flow area scaling.
- Preserve the guide tube diameter to pitch ratio using equation (A.248).
- Preserve the effective de-entrainment efficiency for the guide tube bundle using equation (A.249).
- Preserve the upper core plate flow area distribution using equations (A.256) and (A.257).
- Preserve the vapor volumetric flux, $j_g$, in the upper core plate holes using equation (A.260).
- Preserve the upper support plate flow distribution and flow area using equation (A.261).

With regard to the scaling basis for the upper plenum guide tube bundle, the momentum-controlled entrainment scaling criterion given by equation (A.243) has been selected to guide the modification to the APEX upper internals. The basis for this selection is as follows. The near surface entrainment rates can be properly simulated in APEX solely by maintaining $j_{gR}$ at a constant value of 0.5. In that sense, no modification to the facility would be needed. However, the momentum-controlled entrainment rates can only be matched by preserving both the $j_{gR}$ and the hydraulic diameter ratios. It will be shown that the deposition-controlled region is both unimportant and not achievable in the one-quarter length scale APEX facility.

Figure A.21 depicts the upper core plate geometry. There are a total of 13 flow holes. The six holes on the periphery are 1.91 inch in diameter and represent approximately 37% of the total upper core plate flow area, compared to 38% in the AP1000. The flow holes at the entrance of each HL represent 6.2% of the total flow area as in the AP1000.


Figure A.21 APEX Upper Core Plate Geometry

Figure A.22 illustrates the APEX upper core plate guide tube pitch and diameter. Figure A.23 presents the APEX upper support plate flow hole location. Table A.18 presents the revised upper plenum geometry design based on matching the scaling criteria given above.

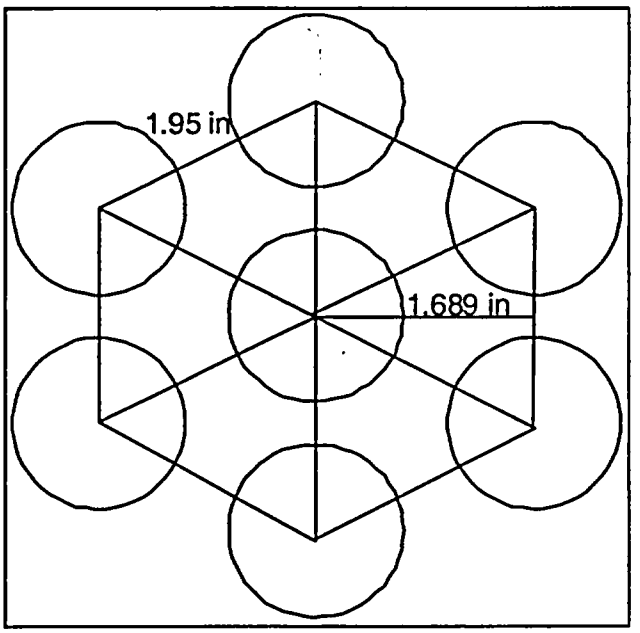


Figure A.22 APEX Upper Plenum Guide Tube Pitch and Diameter

a,b,c

Figure A.23 APEX Upper Support Plate Flow Hole Locations

Table 18 Comparison of the APEX and AP1000 Upper Plenum Geometries

| Component | AP1000 | APEX | Units |
|---|---|---|---|
| UPPER PLENUM | | | a,b,c |
| Core Barrel Inside Diameter | | | |
| Length* | | | |
| Flow Area with Internals | | | |
| Total Wetted Perimeter | | | |
| Total Hydraulic Diameter | | | |
| SUPPORT COLUMNS | | | |
| Number | | | |
| Diameter | | | |
| GUIDE TUBES | | | |
| Number | | | |
| Pitch | | | |
| Equivalent Diameter | | | |
| Pitch-to-Diameter Ratio | | | |
| Subchannel Flow Area | | | |
| Subchannel Wetted Perimeter | | | |
| Subchannel Hydraulic Diameter | | | |
| UPPER CORE PLATE | | | |
| Number of Large Thru Holes | | | |
| Total Thru Hole Flow Area | | | |
| Number of Guide Tube Flow Holes | | | |
| Total Guide Tube Flow Area | | | |
| Number of Support Column Flow Holes | | | |
| Total Support Column Flow Area | | | |
| Total Upper Core Plate Flow Area | | | |
| Peripheral Flow Area | | | |
| Ratio of Peripheral Flow Area to Total Area | | | |
| HL Entrance Flow Area | | | |
| Ratio of HL Entrance Flow Area to Total Area | | | |
| UPPER SUPPORT PLATE | | | |
| Number of Holes | | | |
| Hole Diameter | | | |
| Total Flow Area | | | |

*Bottom of HL to Top of Active Fuel

### A.7.2.7 *Assessment of Pool Entrainment Limiting Conditions*

This section examines the limiting conditions for the APEX entrainment tests. A core power of 1 MW in APEX represents a 2.8% decay power in the AP1000. The greatest vapor generation rates would be achieved at saturation conditions at 1 atmosphere. These conditions would produce an upper plenum vapor volumetric flux, $j_g$, of 11.2 m/s and 5.7 m/s in AP1000 and APEX, respectively. Applying these conditions to the entrainment transition and rate correlations presented in the previous section results in Figure A.24.

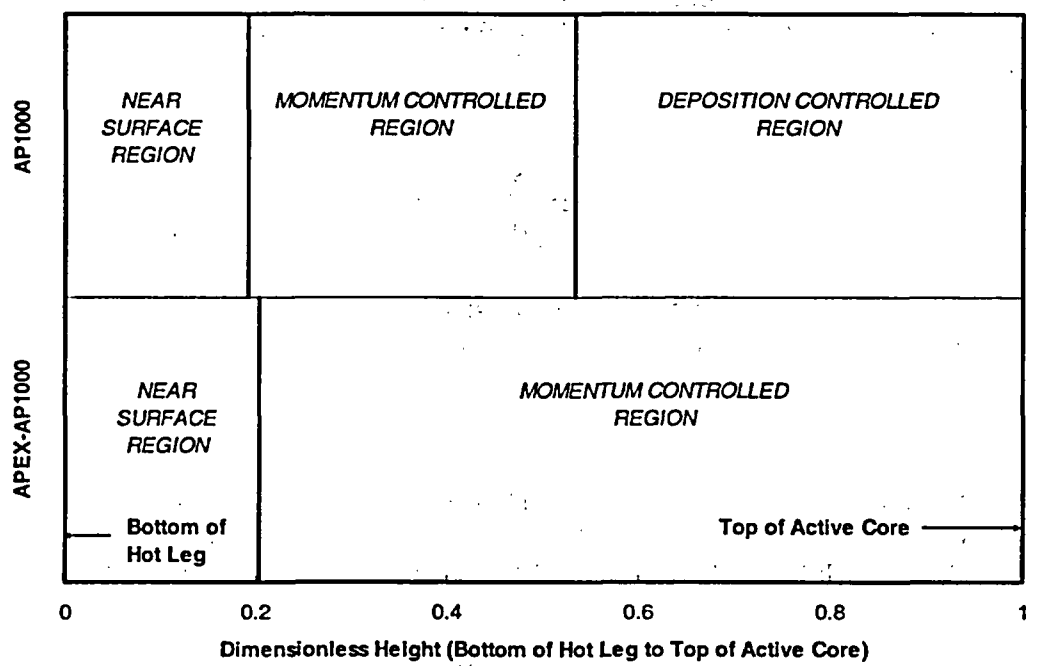


Figure A.24 Assessment of AP1000 and APEX Upper Plenum Pool Entrainment Regimes for a 2.8% Core Decay Power at Atmospheric Pressure

This figure shows how the different pool entrainment regions would exist in the upper plenums for the prescribed set of conditions. As the level drops below the HL, both the AP1000 and APEX upper plenums would exhibit entrainment characteristic of the near surface region. The entrainment rates that would be observed in APEX in this region are well-scaled, as is the transition to the momentum-controlled region. ***It is very important to note that the entrainment rates in the near surface region are a factor of 150 times greater than the entrainment rates generated in the momentum-controlled region.***

The figure shows that well-scaled entrainment behavior in APEX is expected to a depth of about 18.9 cm (0.55 in terms of dimensionless height in Figure A.24) below the HL. Below this depth, APEX is in the momentum-controlled region, whereas AP1000 would be in the deposition-controlled region at the equivalent scaled depth. ***It is also important to note that the entrainment rates in the momentum-controlled region are a factor of 4–6 times greater than the entrainment rates generated in the deposition-controlled region.***

With regard to the test facility scaling, the entrainment rate is well-scaled for depths to approximately the middle of the upper plenum. Below this depth, the APEX entrainment rates will range from 4 to 16 times greater, on a scaled basis, than what would be expected in the AP1000. Thus, the APEX facility will conservatively simulate the entrainment behavior when the level is below the midpoint of the upper plenum.

In general, relative to the near-surface region and momentum-controlled region entrainment rates, the deposition-controlled region entrainment rates are quite small.

On the basis of the conditions prescribed earlier, some preliminary calculations can be made to narrow down the flow conditions in the problem. First, since it is imperative that churn flow exists in the pool, it is necessary to determine if the flow is between the limits of bubbly and annular flow. For bubbly flow, Ishii gives the limit as [Ref. 17]:

$$j_g^* = 0.325\left[\frac{\rho_g}{\rho_f}\right]^{1/2} = 0.008 \qquad \text{(A.262)}$$

where the previous density values have been substituted into Ishii's formula to give the numerical result. For annular flow, the criterion is given by [Ref. 17]:

$$j_g^* = 3.1 \qquad \text{(A.263)}$$

For these conditions, the value of $j_g^*$ was found to be 1.75 for AP1000, and 0.89 for APEX. Thus, the $j_g^*$ values fall between these limits for both the model and the prototype. Thus, churn flow exists in the pool for both systems over the full range of operating conditions, making Ishii's equations applicable to the analysis.

The next issue to be resolved is whether the flooding criterion is exceeded. After all, if the flooding criterion is exceeded, all of the liquid will be quickly expelled from the pool as a rising film, making the entrainment of droplets irrelevant. As is well known, the flooding criterion depends upon the diameter of the channel. For diameters in the range $3 \le D_H^* \le 20$, Ishii restates the Wallis criterion in the following form [Ref. 14]:

$$\frac{j_g^*}{\sqrt{D_H^*}} = 0.5 \qquad \text{(A.264)}$$

Furthermore, for diameters within the range $D_H^* \ge 30$, Ishii gives the Kutateladze criterion as [Ref. 17]:

$$j_g^* = 4 \qquad \text{(A.265)}$$

The dimensionless hydraulic diameters, $D_H^*$, for AP1000 and APEX were for these conditions were found to be 135 and 29, respectively. Using equation (A.248) for APEX and AP1000 or equation (A.247) for APEX, the criterion indicates that flooding in the upper plenum will not occur for the 2.8% power conditions described.

The next question to be addressed is whether the deposition on the wall is sufficiently large that one must consider re-entrainment from a falling film back into the vapor. In addressing this question, observe that only a fraction of the droplets are taken out of the flow by deposition. Furthermore, only a fraction of this fraction is re-entrained from the film back into the flowing vapor. Consequently, since only a fraction of the liquid removed by deposition is re-entrained back into the flow, it would seem that conservative results could be obtained by ignoring deposition in the first place. The only objection to this conservatism would be if deposition removes large droplets from the flow which are replaced by smaller droplets as a result of re-entrainment. Since this effect could shift the droplet distribution to subcritical diameters that are more easily carried by the vapor, the entrainment might be increased at large heights. However, a second and quite convincing argument is as follows. Since the data used by Ishii were based on flow in tubes, the phenomena of deposition and re-entrainment was necessarily present in the experiments themselves and, therefore, already included in the correlations. Given this fact, the equations may be used straightforwardly without having to account for this added effect.

### A.7.3 Evaluation of Scale Distortion

Properly simulating the upper plenum pool entrainment process requires that the following ratios be on the order of unity:

$$t_R^* = \left( \frac{\dot{m}_{ENT,O}\, t}{a_{UP}\, \rho_L\, H} \right)_R \tag{A.266}$$

$$\Pi_{INJ,R} = \left( \frac{\dot{m}_{INJ,O}}{\dot{m}_{ENT,O}} \right)_R \tag{A.267}$$

$$\Pi_{GT,R} = \left( \frac{\dot{m}_{GT,O}}{\dot{m}_{ENT,O}} \right)_R \tag{A.268}$$

$$\Pi_{UPD,R} = \left( \frac{\dot{m}_{UPD,O}}{\dot{m}_{ENT,O}} \right)_R \tag{A.269}$$

The numerical values for each of the non-dimensional ratios are presented in Table A.17 for the near-surface entrainment and momentum-controlled entrainment regions. The data obtained from the assessment of limiting conditions presented in the previous section were used in the evaluation. The desired timescale ratio, $t_R$, of 0.5 was used to assess equation (A.266). All of the injection flow rates have been scaled to 1:96. Furthermore, equation (A.269) can be interpreted as the ratio of effective de-entrainment efficiencies. That is:

$$\Pi_{GT,R} = \eta_{eff,R} \tag{A.270}$$

The facility has been scaled to match the onset of upper plenum draining behavior when CCFL conditions are present at the upper core plate flow holes.

The ratio of the gravity-driven draining rates for the APEX and AP1000 upper plenums is given by:

$$\left(\dot{m}_{UPD,O}\right)_R = \left| a_{UCP} \left(H_{UP} - h\right)^{1/2} \right|_R \tag{A.271}$$

Table A.19 indicates that the APEX-AP1000 upper plenum geometry and long-term cooling operating conditions match the pool entrainment scaling criterion very well with the exception of $P_{UPD,R}$.

Table A.19 Ratio of Π Groups for Near Surface and Momentum Controlled Upper Plenum Entrainment

| Non-Dimensional Ratio | Near Surface | Momentum Controlled |
|---|---|---|
| $(t^+)_R$ | | |
| $\Pi_{inj,R}$ | | |
| $\Pi_{GT,R}$ | | |
| $\Pi_{UPD,R}$ | | |
| $(j_g^+)_R$ | | |

a,b,c

### *A.7.3.1 Impact of Reduced Flow Area in the Upper Core Plate*

The greatest source of distortion will be the upper plenum draining rate with a Π ratio of 0.5. This distortion arises because matching the flooding behavior at the upper core plate required reducing the upper core plate flow area such that the Kutateladze number was identically preserved. This delayed draining effect is conservative relative to core cooling. In addition, the vapor jetting behavior at the upper core plate produces a local vapor volumetric flux $j_g$ equivalent to what would be observed in the AP1000. Preserving a 1:1 vapor velocity in a 1:4 length upper plenum will produce conservative results. It is expected that the proposed set of upper internals will overestimate the amount of entrained liquid on a scaled basis. This is a conservative feature of the experiment.

## A.8 Summary and Conclusions

This document presents the scaling analysis performed to guide the OSU APEX-AP1000 test facility modifications. The purpose of the test program is to provide high-quality benchmark data for the reactor safety analysis codes. Previous testing in APEX has demonstrated that all of the thermal-hydraulic phenomena observed in the large-scale AP600 facilities such as ROSA-AP600 or SPES were also observed in APEX, thereby providing a broad data base for code assessment. However, the most faithful representation of the AP600 phenomena was for the very long-term cooling phase, which occurs at low system pressure. The APEX-AP1000 test program will be modified to include full-pressure ADS4 blowdown tests to investigate the transition period that leads to the onset of IRWST injection. This scaling analysis provides the basis for the following plant modifications:

| Component | Modification to APEX |
|---|---|
| Reactor Power | Increase core power by 67%. (Maximum of 1MW). |
| PZR | Increase PZR volume.<br>Reduce PZR Surge Line Diameter. |
| CMTs | Increase CMT volumes by 25%.<br>Reduce line resistance to 64% of original value. |
| IRWST | Increase IRWST liquid level. |
| ADS4 | Increase ADS4 flow area by 76%.<br>Reduce line resistance to 28% of original value. |
| PRHR HX | Increase PRHR flow capacity by 74% by reducing line resistance. No change in surface area/tube number required for testing. |
| Containment Sump Flood-Up Elevation | Change flood-up elevation in primary sump tank. |

The following paragraphs briefly summarize the results of the study.

(1) The original AP600 Scaling Analysis, WCAP-14270, which was performed in support of the design of the existing Advanced Plant Experiment (APEX) facility at OSU was found to be applicable to the APEX-AP1000 design for two reasons. First, the thermal-hydraulic phenomena to be studied fell within the scope of the original AP600 test program, with the exception of upper plenum behavior. Second, the AP1000 is geometrically similar to the AP600. As a result, all of the tank volumes, flow areas, and line resistance scaling ratios found in WCAP-14270 were used in the present study.

(2) An NRC PZR surge line study by Di Marzo and Bessette was used to guide the modifications to the APEX-AP1000 PZR surge line. The reduced line diameter is expected to produce a better simulation of the PZR draining behavior.

(3) The RCS depressurization scaling analysis represents a more comprehensive approach than that implemented in the original AP600 study. Nonetheless, the similarity criteria derived in this report resulted in scaling ratios that were identical to those in the original

study. It was found that the characteristic time ratios for AP1000 would be well-matched in APEX-AP1000. The greatest distortion (a factor of 2) was the result of pressure-scaled fluid properties.

(4) A scaling analysis has been performed to design the APEX-AP1000 to simulate the important phenomena that occur during the transition from ADS4 blowdown to the onset of IRWST injection. The key phenomena have been identified and described, and the scaling analysis indicates that full-pressure ADS4 blowdown tests can be performed using the modified APEX-AP1000 test facility. Chapter 15 of the Westinghouse AP1000 Safety Analysis Report indicates that ADS4 actuation typically occurs near 100 psia. The maximum decay power, ~2.0%, at the time of ADS4 valve opening was calculated for the DEDVI break. These initial conditions will be examined as part of the testing. The AP1000 core axial void fraction profile and core averaged void fraction were shown to be preserved in APEX-AP1000.

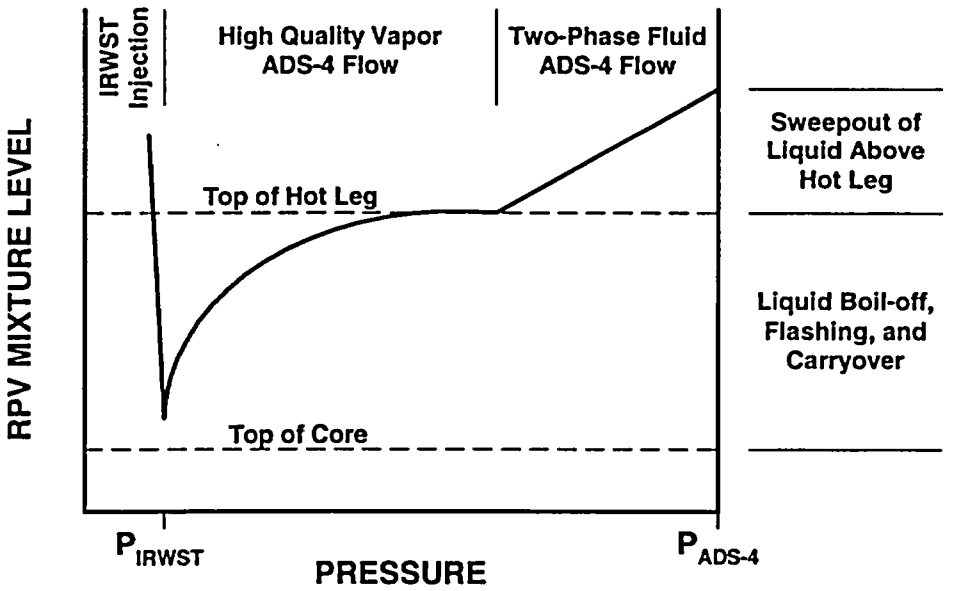


(5) A detailed pool entrainment scaling analysis has been performed to design the upper plenum components in APEX-AP1000. The analysis indicates that well-scaled entrainment behavior in APEX is expected to a depth of about 18.9 (0.55 in terms of dimensionless height) cm below the HL. Below this depth, APEX is in the momentum-controlled region, whereas AP1000 would be in the deposition-controlled region at the equivalent scaled depth. It was found that the entrainment rates in the near-surface region are a factor of 150 times greater than those generated in the momentum-controlled region, which are a factor of 4-6 times greater than those generated in the deposition-controlled region. Thus, the APEX facility will conservatively simulate the entrainment behavior when the level is below the midpoint of the upper plenum. In addition, the vapor volumetric flow rate ratio, ($j_{g,R}$) , at the upper core plate holes has been set to unity to preserve the Kutateladze number. This adds an additional conservatism to the pool entrainment process because the local vapor jets at

the upper core plate holes will extend into the upper plenum, thereby increasing liquid entrainment.

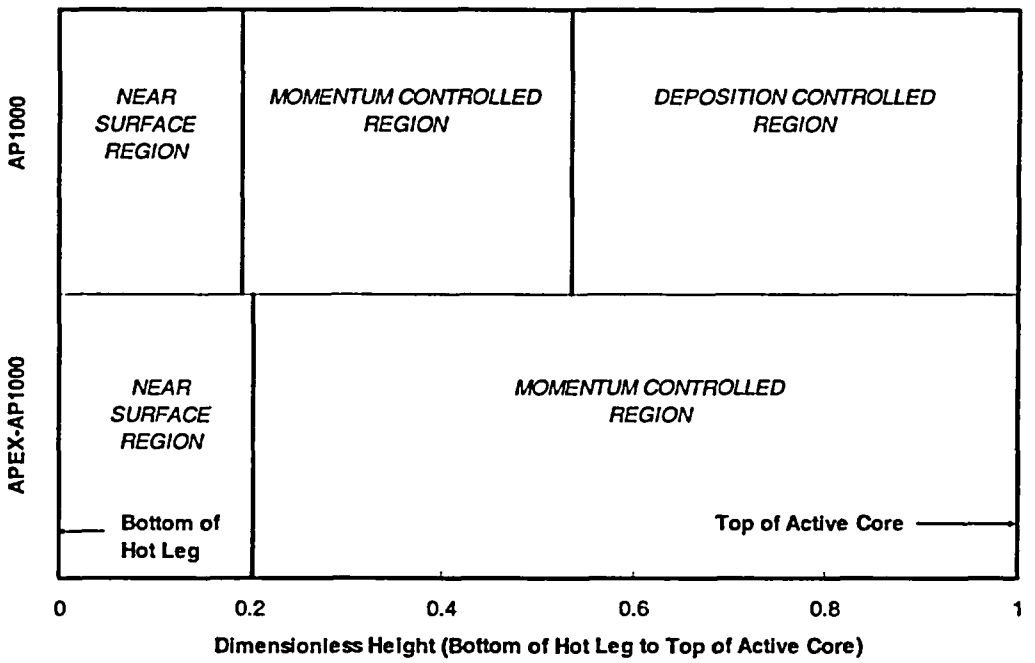

# APPENDIX B.

...

# APPENDIX B. APEX COMPONENT DIMENSIONS, CONTROL LOGIC, AND SETPOINTS

## B.1 Component Dimensions

Tables B.1 through B.11 contain detailed component dimensions (and, in some cases, thermocouple locations) for the reactor pressure vessel (RPV), pressurizer (PZR), steam generators (SGs), in-containment refueling water storage tank (IRWST), core makeup tanks (CMTs), accumulators (ACCs), primary and secondary sumps, and safety system line dimensions and resistances. Figure B.1 is a map of the thermocouples in the RPV downcomer.

Table B.1 Reactor Pressure Vessel Components

| Component | No. | Dimensions | Reference |
|---|---|---|---|

a,b,c

Table B.1 Reactor Pressure Vessel Components

| Component | Dimension | Reference |
|---|---|---|
| a,b,c | | |

a,b,c

Figure B. 1 Thermocouple Map of Downcomer

Table B.2 Thermocouple Legend for Figure B.1

a,b,c

| Thermocouple Map Number | Tag Number | Radial Position | Thermocouple Map Number | Tag Number | Radial Position |
|---|---|---|---|---|---|

Table B.2 Thermocouple Legend for Figure B.1

a,b,c

| Thermocouple Map Number | Tag Number | Radial Position | Thermocouple Map Number | Tag Number | Radial Position |
|---|---|---|---|---|---|
| | | | | | |

Table B.3 Pressurizer Components

a,b,c

| Component | No. | Dimensions | Reference |
|---|---|---|---|
| | | | |

Table B.4 Steam Generators (Each) Components

| Component | No. | Dimensions | Reference |
|---|---|---|---|

a,b,c

Table B.5 IRWST Components

a,b,c

| Component | No. | Dimensions | Reference |
|---|---|---|---|
| | | | |

Table B.6 Core Makeup Tank Components

a,b,c

| Component | No. | Dimensions | Reference |
|---|---|---|---|
| | | | |

Table B.7 Accumulator Components

a,b,c

| Component | No. | Dimensions | Reference |
|---|---|---|---|
| | | | |

Table B.8 Primary Sump Components

a,b,c

| Component | No. | Dimensions | Reference |
|---|---|---|---|
| | | | |

Table B.9 Secondary Sump Components

| Component | No. | Dimensions | Reference |
|---|---|---|---|

a,b,c

Table B.10 Summary of Safety System Line Dimensions

a,b,c

| Name | Material | Data and Dimensions | Location and Connections (Valves and Equipment) |
|---|---|---|---|

## B.2 Control Logic and Controller Setpoints

Tables B.12 through B.23 contain detailed control logic and setpoints for station blackouts; SBLOCAs; LBLOCAs; inadvertent ADS initiation; full-pressure ADS initiation; automatic actuation of PRHR and CMT on "S" signal; automatic actuation of ADS1-4 on CMT level or timers; automatic control of SG pressure, liquid water level, feedwater flow, and main steam flow; automatic control of PZR pressure and level; programmed reactor decay power and control of core exit temperatures; and programmed CVS and RNS pump flow rates.

Table B.12 Station Blackout Routine Logic

a,b,c

| Step | Condition |
|---|---|
| | |

Table B.13 Small-Break LOCA Routine Logic

| Step | Condition |
| --- | --- |

a,b,c

Table B.14 Large-Break LOCA Routine Logic (Much the same as Small-Break LOCA routine logic except the test initialization)

| Step | Condition |
|---|---|
| | |

a,b,c

Table B.15 Inadvertent ADS Initiation Routine Logic

| Step | Condition |
|---|---|
| | |

a,b,c

Table B.16 Full-Pressure ADS Routine Logic

| Step | Condition |
|---|---|
| | |

a,b,c

**Natural Circulation Routine**

This routine permits operation of the reactor controller in manual or automatic mode, with or without RCPs and with no "S" signal or automatic trip functions. This routine allows flexibility to custom-tailor a test without requiring extensive re-programming.

The setpoint in Table B.17 show each bi-stable device and its associated set/reset points. Most of these values can be readily modified by the operator and, in some cases, vary among the different logic routines. The table contains the tag name of the device, the specific point (e.g., HH for High High), the set/reset points applicable to the logic routine, and the logic diagram sheet number(s) showing the device.

Table B.17 APEX Controller Set Point Values for Natural Circulation Routine

| Routine | Trip | Reset | Action(s) |
|---|---|---|---|

a,b,c

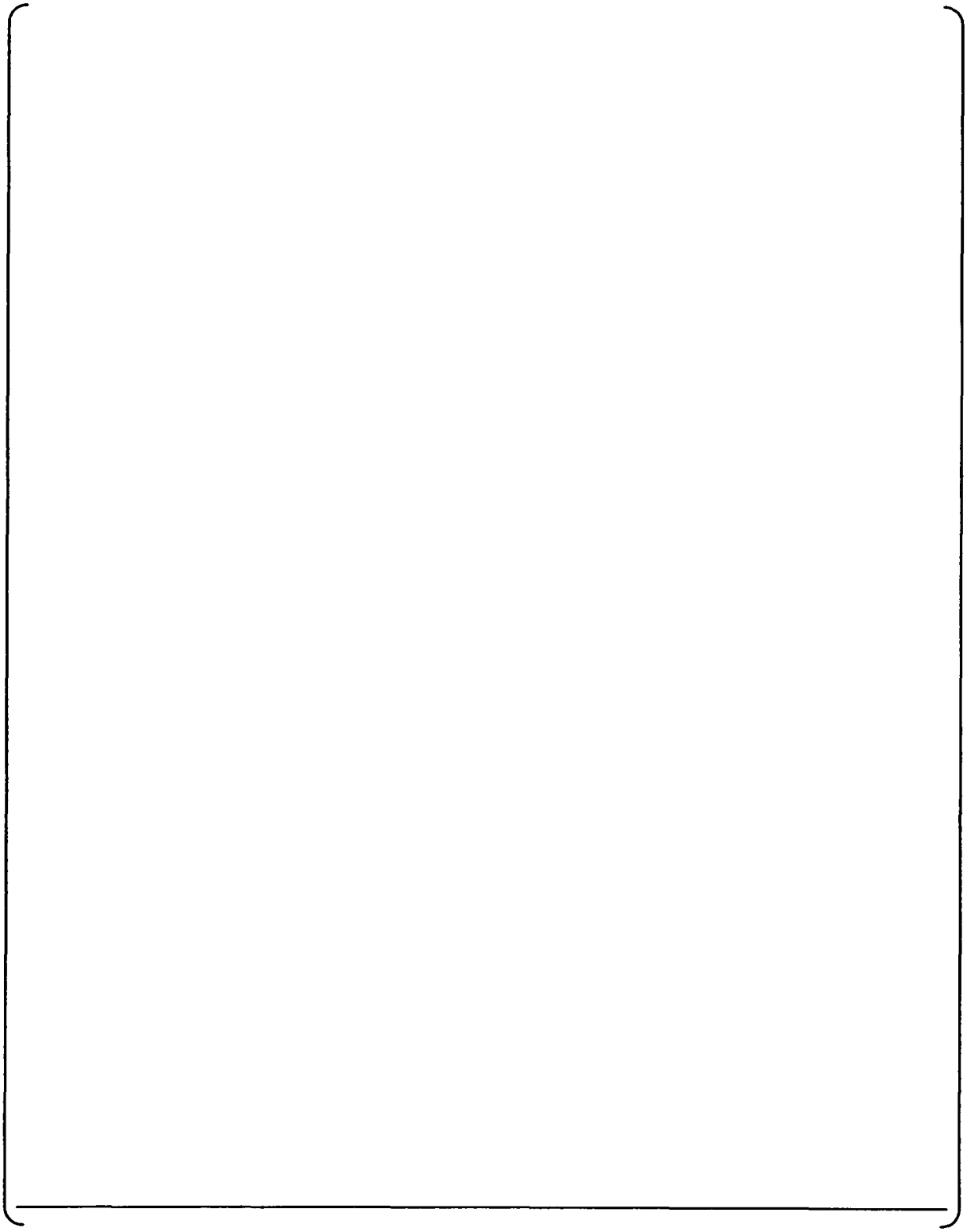

Table B.17 APEX Controller Set Point Values for Natural Circulation Routine

| Routine | Trip | Reset | Action(s) |
|---|---|---|---|

a,b,c

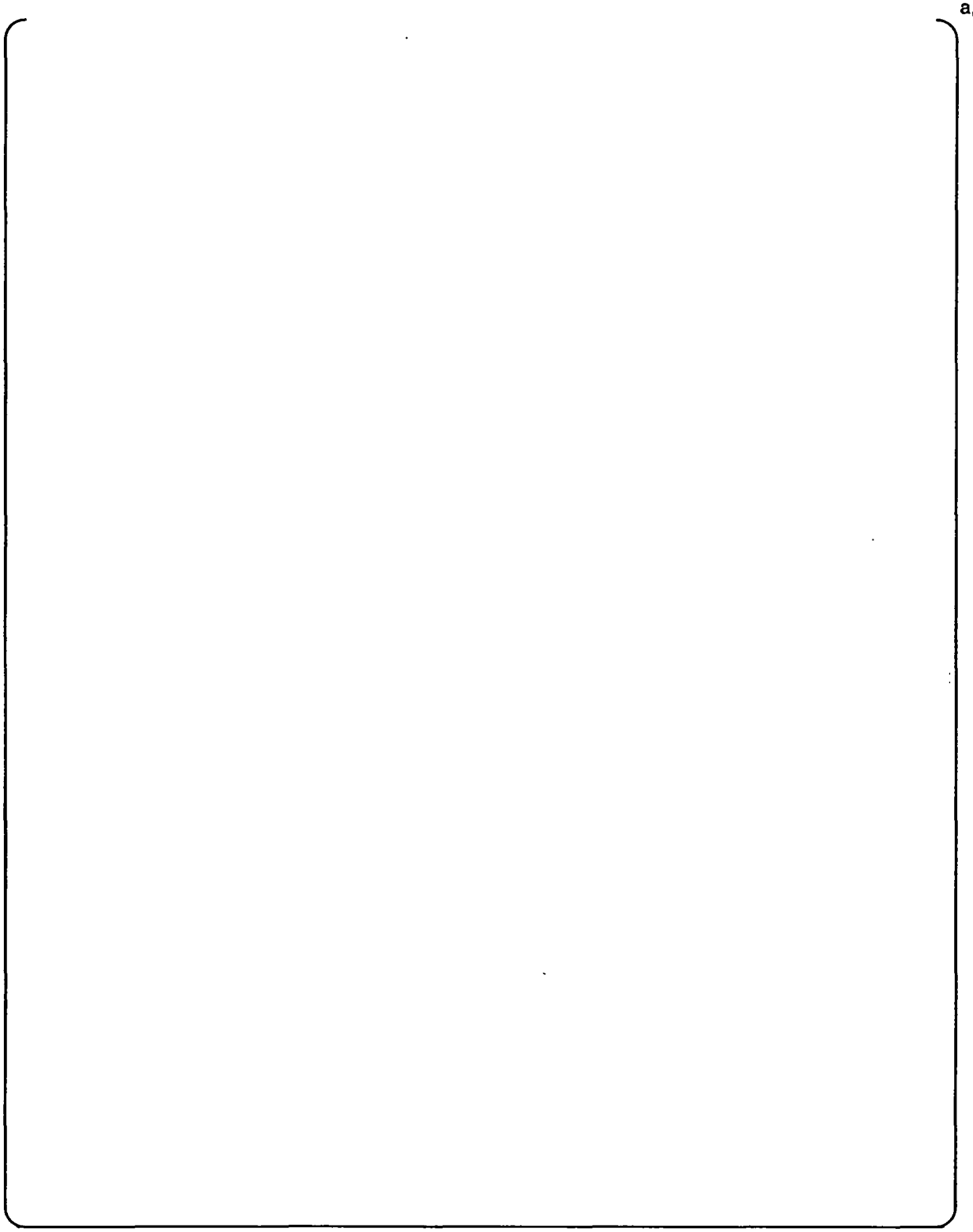

Table B.17 APEX Controller Set Point Values for Natural Circulation Routine

| Routine | Trip | Reset | Action(s) |
|---|---|---|---|

a,b,c

Table B.17 APEX Controller Set Point Values for Natural Circulation Routine

| Routine | Trip | Reset | Action(s) |
|---|---|---|---|
| | | | |

a,b,c

Table B.18 Automatic Actuation of PRHR and CMT on "S" signal

| Conditions (And) | Actions |
| --- | --- |
| | |

a,b,c

Table B.19 Automatic Actuation of ADS 1-4 on CMT Level or Timers

| Conditions | Actions |
| --- | --- |
| | |

a,b,c

Table B.20 Automatic Control of SG Pressure, Liquid Water Level, Feedwater Flow, and Main Steam Flow

| Input Signal | Output signal to |
|---|---|
| | |

a,b,c

Table B.21 Automatic Control of PZR Pressure and Level

| Input Signal | Output signal to |
|---|---|
| | |

a,b,c

Table B.22 Programmed Reactor Decay Power and Control of Core Exit Temps

| Input Signal | Output signal to |
|---|---|
| | |

a,b,c

Table B.23 Programmed CVS and RNS Pump Flow Rates

| Input Signal | Output signal to |
|---|---|
| | |

a,b,c

# APPENDIX C.

...

# APPENDIX C. TEST TRANSIENT PLOTS AND SEQUENCE OF EVENTS

This appendix contains transient plots, facility configuration, and sequence of events for tests NRC-AP1000-01, 02, 03, 04, 05, 06, 10, and 11. Facility information can be found in Chapter 3 and Appendix B of this report. The main purpose of the APEX-AP1000 confirmatory testing was to examine the performance of passive safety systems.

## C.1 NRC-AP1000-01

The purpose of this test was to determine the impact on passive safety system behavior that resulted from a DEDVI break with a major failure of ADS system. It was similar in intent to Test NRC-26, which was run for AP600 design certification, in the sense that in NRC-26, a major failure of the ADS system was simulated. However, Test NRC-26 included delayed core heatup to simulate containment failure, and was configured for a smaller 1-inch CL break, and the delayed core heatup in NRC-26 resulted in a heater rod temperature excursion. Test NRC-AP1000-01 was run with a larger DEDVI break without delayed core heatup. The core remained covered during the long-term cooling period of Test NRC-AP1000-01. Both Test NRC-26 and Test NRC-AP1000-01 experienced short periods of CMT refill as a result of condensation-induced pressure drops. A similar test in the ROSA-AP600 facility also investigated a similar scenario. In Test ROSA AP-CL-05, there was no refilling during CMT draining. The difference in ROSA and APEX CMT behavior was attributed to the use of two separate CMT-PBLs (APEX) instead of one (ROSA) and the reduced height scale of APEX (permitting liquid to be drawn through the PBL into the CMTs, which further enhanced condensation).

Test NRC-AP1000-01 simulated a DEDVI break with complete failure of ADS1, 2, and 3. Table C.1 summarizes the facility configuration. This test was defined as a beyond-DBA scenario because of the multiple valve failures. All four ADS4 valves were available and, therefore, this test investigated the ability of the ADS4 system to accomplish system depressurization. The PRHR HX was inactive during this test. The APEX facility models both trains of the AP1000 ADS1, 2, and 3 lines located at the top of the PZR after a flow nozzle that models the scaled choked flow area of the AP1000.

Table C.1 Facility Configuration for Test NRC-AP1000-01

| Component | Configuration |
|---|---|
| ADS1 | Failed Shut |
| ADS2 | Failed Shut |
| ADS3 | Failed Shut |
| ADS4-1 (non-PZR side) | 100% ADS4-1 flow |
| ADS4-2 (PZR-side) | 100% ADS4-2 flow |
| Break | DEDVI Line 1 |

Table C.2 summarizes the sequence of events for Test NRC-AP1000-01. After the break was opened at zero seconds, the PZR, CMTs, and ACC1 immediately began to inject. However, all Side 1 injection flows (ACC1 and CMT1 in Figure C.3), went out the DEDVI Line 1 break. The core collapsed liquid level reached a relative minimum at [ ]$^{a,b,c}$ as shown in Figures C.1 and C.2. The ACC2 injection began at [ ]$^{a,b,c}$ as shown in Figure C.4. The ADS4 valves opened just before the minimum RPV liquid level at around [ ]$^{a,b,c}$.

The RPV two-phase level dropped near the bottom of the HL at around [ ]$^{a,b,c}$; however, as a result of CMT2 injection, the water level in the core began to rise at around [ ]$^{a,b,c}$. At [ ]$^{a,b,c}$ CMT2 refilled as a result of condensation-induced pressure drop. At [ ]$^{a,b,c}$, IRWST injection through DVI line 2 began, and the RPV liquid level began to increase.

The RPV two-phase mixture level remained high throughout the entire test, dropping briefly below the bottom of the HL between [ ]$^{a,b,c}$ as shown in Figure C.5. This high liquid level can also been seen by examining the HL liquid level plots in Figure C.6.

At approximately [ ]$^{a,b,c}$, liquid began to preferentially entrain through the non-PZR side ADS4-1 line as shown in Figure C.7. From about [ ]$^{a,b,c}$ on, the flow quality in the non-PZR ADS4-1 line remained constant at approximately 0.05, while the PZR side ADS4-2 line remained constant at approximately 0.4. The core remained covered during the entire test as shown in Figure C.8.

Table C.2 Sequence of Events for Test NRC-AP1000-01

| Time (s) | Event | a,b,c |
|---|---|---|

a,b,c

Figure C.1 Vessel Wide Range Collapsed Water Level

a,b,c

Figure C.2 Core Upper Half and Lower Half Collapsed Water Levels

a,b,c

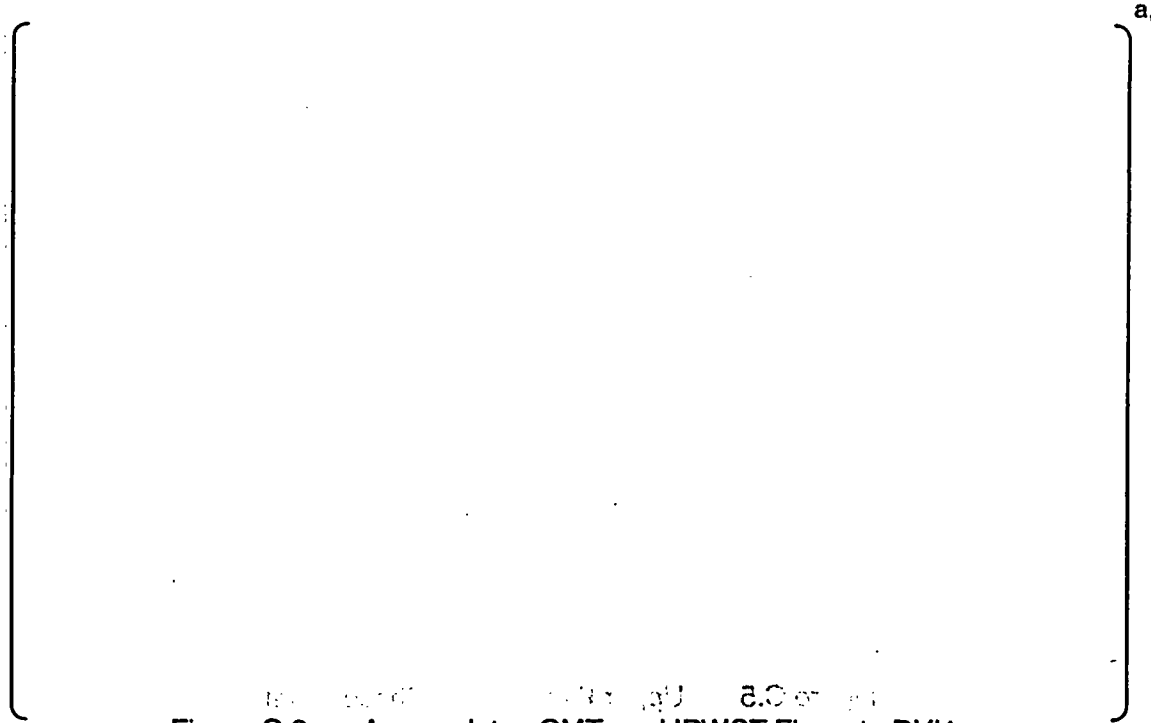

Figure C.3 Accumulator, CMT, and IRWST Flows to DVI1

a,b,c

Figure C.4 Accumulator, CMT, and IRWST Flows to DVI2

a,b,c

Figure C.5 Upper Plenum Two-Phase Level

a,b,c

Figure C.6 Hot Leg Collapsed Water Levels

a,b,c

Figure C.7 ADS4 Flow Qualities

a,b,c

Figure C.8 Core Heater Rod Temperatures

## C.2 NRC-AP1000-02

The objectives of Test NRC-AP1000-02 were to determine system behavior during a loss of shutdown cooling, if the RCS would pressurize sufficiently to prevent IRWST injection, and if CCFL would prevent the PZR from draining. In this test, a loss of RNS cooling was simulated after the reactor had been shutdown for 24 hours. The RCS was at [ ]$^{a,b,c}$ with an initial PZR level of [ ]$^{a,b,c}$. The ADS3 valve was opened (which simulated two trains of ADS1, 2, and 3 in AP1000) venting the RCS to the IRWST. The SG secondary sides were assumed to have been drained for maintenance. The ACCs and CMTs were assumed to be unavailable. One ADS4 valve was failed on demand. The facility configuration for this test is given in Table C.3.

Table C.3 Facility Configuration for Test NRC-AP1000-02

| Component | Configuration |
|---|---|
| ADS1 | Failed Shut |
| ADS2 | Failed Shut |
| ADS3 | Open to vent primary system |
| ADS4-1 (non-PZR side) | 1 out of 2 Failed Open |
| ADS4-2 (PZR-side) | 100% ADS4-2 flow |
| ACCs | Unavailable |
| CMTs | Unavailable |
| RNS Cooling | Unavailable |
| Break | None |

Table C.4 summarizes the sequence of events for this test. The test was started by increasing reactor power to 320 kW. When both HL liquid levels decreased to approximately ½-inch, one IRWST valve and one ADS4 valve were opened after a [ ]$^{a,b,c}$ time delay. ADS4B was opened at around [ ]$^{a,b,c}$ , which caused a rapid depressurization of the primary system and the IRWST began injecting makeup water by [ ]$^{a,b,c}$ as shown in Figure C.9. The sump recirculation valves were opened at [ ]$^{a,b,c}$, as shown by a sharp increase in IRWST injection flow rate, and the facility transitioned into long-term cooling mode.

As the heater rod power was increased in the beginning of the test, the RPV liquid level dropped significantly [ ]$^{a,b,c}$ as water was boiled off and released out of the open ADS3 valve as shown in Figure C.10. After ADS4 actuation, the RPV level increased as IRWST injection was provided to the core. This same trend is shown in Figure C.11, which plots the RPV mixture level. During the entire transient, the core never uncovered, and the mixture level was always above the level of the upper core plate. Figure C.14 plots the core collapsed liquid levels from the lower core plate to the mid-core spacer grid (LDP-109) and from the mid-core spacer grid to the upper-core spacer grid (LDP-110).

Figure C.12 plots the HL levels on the PZR and non-PZR sides of the plant. At around [ ]$^{a,b,c}$, when the HL levels dropped to ½-inch, ADS4B was opened. The HL liquid levels

briefly continued to drop, but quickly turned around as makeup water was provided from the IRWST, and the decrease in pressure caused the RPV mixture level to swell. At no time during the transient were the HLs emptied.

One of the objectives of this test was to determine if the PZR would be able to drain as a result of CCFL. Figure C.13 plots PZR level versus time and shows that the PZR drained slowly from about [ ]$^{a,b,c}$ as primary water was boiled off and the steam exited the open ADS3 valve. When the ADS4B valve was actuated, the PZR quickly drained and remained empty until about [ ]$^{a,b,c}$ when the plant refilled as a result of IRWST injection. Figure C.15 plots core heater rod temperatures, and no high rod temperature excursion was experienced during the entire test.

Table C.4 Sequence of Events for Test NRC-AP1000-02

a,b,c

| Time (s) | Event |
|---|---|
| | |

a,b,c

Figure C.9 IRWST (Lines 1 and 2) Injection Flow Rates

a,b,c

Figure C.10 RPV Collapsed Liquid Level

a,b,c

Figure C.11 RPV Mixture Level

a,b,c

Figure C.12 Hot Leg Collapsed Liquid Levels

a,b,c

Figure C.13 PZR Collapsed Liquid Level

a,b,c

Figure C.14 Core Collapsed Liquid Levels

a,b,c

Figure C.15 RPV Heater Rod Temperatures

## C.3 NRC-AP1000-03

This test simulated a DEDVI DVI line 1 break with two of the four ADS4 valves failed closed (ADS4-2 closed and ADS4-1 opened), with the purpose of investigating a major failure of the ADS system. Both failed ADS4 valves were on the PZR side of the plant. Table C.5 summarizes the facility configuration. This test is similar in intent to NRC-10, which was conducted for AP600 design certification. In NRC-10, failure of three of the four ADS4 valves produced core uncovery and heatup for a 1-inch CL break.

Table C.5 Facility Configuration for Test NRC-AP1000-03

| Component | Configuration |
|---|---|
| ADS1 | Normal actuation |
| ADS2 | Normal actuation |
| ADS3 | Normal actuation |
| ADS4-1 (non-PZR side) | 100% ADS4-2 flow |
| ADS4-2 (PZR side) | Failed Shut |
| Break | DEDVI Line 1 |

Table C.6 summarizes the sequence of events for NRC-AP1000-03. Similar to NRC-AP1000-01, this DEDVI test depressurized quickly, causing a low inventory in the vessel as shown in Figure C.16, indicating that the break (rather than early actuation of the ADS1, 2, and 3 valves) was responsible for the initial rapid depressurization and mass loss. CMT1 began draining out of the DVI line 1 break immediately after the break opened. ADS1, 2, and 3 were opened in sequence from [ ]$^{a,b,c}$, further depressurizing the plant. ACC2 was injecting by [ ]$^{a,b,c}$, while ACC1 and CMT1 emptied by [ ]$^{a,b,c}$. All Side 1 injection flow (ACC1, CMT1, and IRWST Line 1) was lost out of the DEDVI break. At [ ]$^{a,b,c}$, the ADS4-1 valve was opened. Coupled with CMT2 and ACC2 injection, the vessel inventory increased until these two tanks were completely emptied by [ ]$^{a,b,c}$. As shown in Figure C.19, there was a period [ ]$^{a,b,c}$ when there was no injection flow to the core. This delay in IRWST injection was also experienced in NRC-AP600-10 and is attributable to a known scaling distortion related to the reduced IRWST head, which is an artifact of the one-quarter height scaling in APEX and is conservative in nature.

The RPV two-phase water level dropped below the bottom of the HL from [ ]$^{a,b,c}$ as shown in Figure C.20. IRWST injection increased from [ ]$^{a,b,c}$, and the core water level rose to a relative maximum at approximately [ ]$^{a,b,c}$. Then the vessel inventory decreased slowly over time, as shown in Figure C.16, as IRWST injection decreased until emptying at [ ]$^{a,b,c}$. Sump recirculation began at about [ ]$^{a,b,c}$, thus ending the IRWST injection phase, as shown in Figure C.21, and transitioning the plant into long-term cooling mode.

The HL water levels are shown in Figure C.22. HL2 emptied from [ ]$^{a,b,c}$ and refilled from [ ]$^{a,b,c}$ while CMT2 and ACC2 injected water into the RPV. When CMT2 and ACC2 emptied at approximately [ ]$^{a,b,c}$, HL2 was empty from [ ]$^{a,b,c}$. IRWST injection raised the HL levels from [ ]$^{a,b,c}$, but as injection flow decreased, the HL2

liquid level began to decrease until it emptied for the last time at approximately [ ]$^{a,b,c}$. This is the time that IRWST injection ceased and sump recirculation began. Enough water was recirculated through the core that the quality out the ADS4-1 line was not unity (~0.8), as shown in Figure C.23. During this time, the RPV two-phase level was well below the bottom of the HL, as shown in Figure C.20, and a fair amount of water remained in HL1, as shown in Figure C.22. This behavior illustrates the importance of upper plenum and HL entrainment on passive safety system performance.

Figure C.24 depicts the PZR wide range level. After the initial blowdown, substantial PZR injection began at approximately [ ]$^{a,b,c}$ and it ceased to inject water into the primary system at [ ]$^{a,b,c}$.

Several small heater rod temperature spikes are shown in Figure C.25. The first spike at around [ ]$^{a,b,c}$ corresponded to the lowest vessel level experienced during the test, which is shown Figure C.16. This spike occurred when all CMTs and ACCs were empty before IRWST injection flow began. The next significant temperature spike occurs at around [ ]$^{a,b,c}$ when the core water level was low during sump recirculation. However, even though the vessel level was low at certain times during the test, the core still remained covered. Consequently, these temperature spikes were most likely caused by relatively large voids in the core coming into contact with specific thermocouples and do not represent an "average" core temperature, but local "warm spots".

Table C.6 Sequence of Events for Test NRC-AP1000-03

| Time (s) | Event |
|---|---|

a,b,c

a,b,c

Figure C.16 Vessel Wide Range Collapsed Water Level

a,b,c

Figure C.17 Core Upper Half and Lower Half Collapsed Water Levels

a,b,c

Figure C.18 Accumulator, CMT, and IRWST Flows to DVI1

a,b,c

Figure C.19 Accumulator, CMT, and IRWST Flows to DVI2

a,b,c

Figure C.20 RPV Two-Phase Level

a,b,c

Figure C.21 Sump Recirculation Flows

a,b,c

Figure C.22 Hot Leg Collapsed Water Levels

a,b,c

Figure C.23 ADS4-1 (Non-Pressurizer Side) Flow Quality

a,b,c

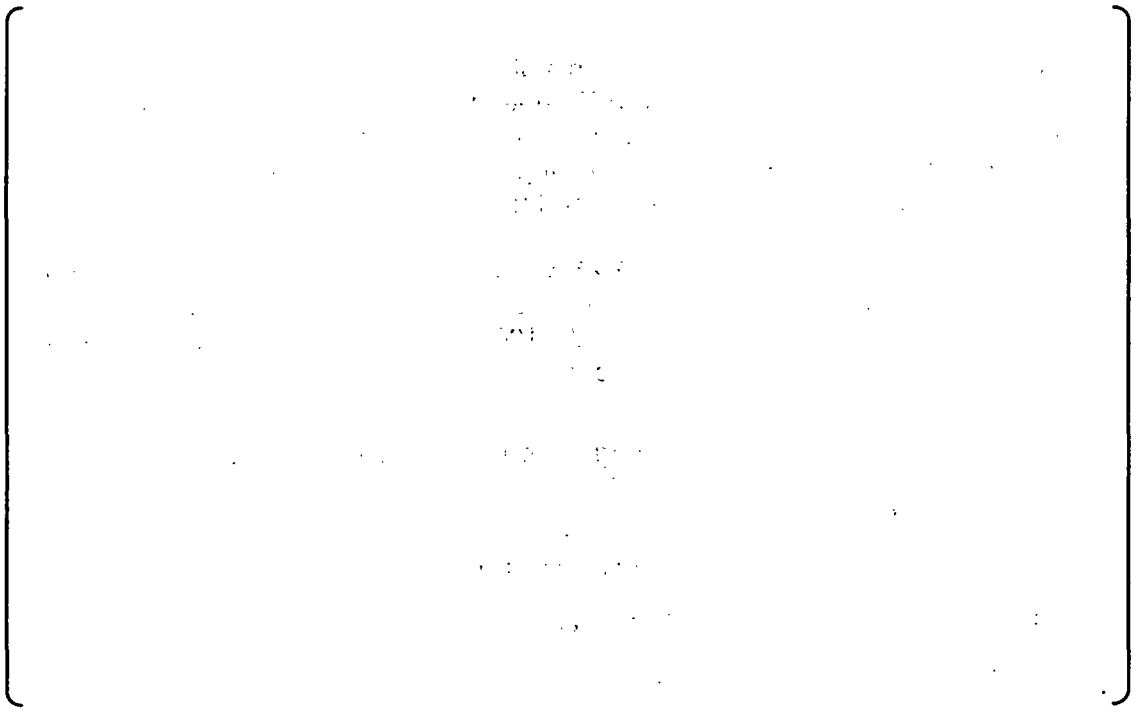

Figure C.24 Pressurizer Wide Range Collapsed Water Level

a,b,c

Figure C.25 Core Heater Rod Temperatures

## C.4 NRC-AP1000-04

Test NRC-AP1000-04 was a beyond-DBA test simulating a 1-inch CL break with one ADS4-1 valve failed shut (50% line flow) on the non-PZR side of the plant. In addition, CMT1, ACC1, sump recirculation line 1, and IRWST injection line 1 were unavailable. Table C.7 summarizes the facility configuration for this test. Upon reaching 30 minutes of steady-state long-term cooling, the primary sump drain valve was opened to simulate a degraded containment sump.

This test was similar in intent to NRC-AP600-27, where a similar break size with a degraded sump was simulated, in part, to determine the impact on long-term cooling as a result of depleting the primary sump inventory. In NRC-AP1000-04 and both AP600 tests, the two-phase level in the core remained above the heater rods.

Table C.7 Facility Configuration for Test NRC-AP1000-04

| Component | Configuration |
|---|---|
| ADS1 | Normal actuation |
| ADS2 | Normal actuation |
| ADS3 | Normal actuation |
| ADS4-1 (non-PZR side) | 50% ADS4-1 flow |
| ADS4-2 (PZR side) | 100% ADS4-2 flow |
| CMT1 | Unavailable |
| ACC1 | Unavailable |
| Sump Recirculation Line 1 | Unavailable |
| IRWST Injection Line 1 | Unavailable |
| Break | 1-inch bottom of CL 4 |

Table C.8 summarizes the sequence of events for NRC-AP1000-04. The break was opened at zero seconds, causing the CMTs to inject immediately and, during the initial blowdown, the RPV vessel inventory dropped to a relative minimum at around [ ]$^{a,b,c}$ as shown in Figures C.26 and C.27. The ACC2 injection began at [ ]$^{a,b,c}$ as shown in Figure C.28. The RPV inventory remained relatively low until around [ ]$^{a,b,c}$ IRWST injection began, and the inventory in the RPV increased to a relative maximum at approximately [ ]$^{a,b,c}$. This was around the same time IRWST injection reached maximum flow as shown in Figure C.28.

At [ ]$^{a,b,c}$ the primary sump drain valve was opened to simulate a degraded sump (ending the IRWST injection phase of the transient), which created an increase in IRWST flow shown in Figure C.28. Primary sump overflow occurred at approximately [ ]$^{a,b,c}$ and water was recirculated from the sump, to the IRWST, through the DVI2 line and into the RPV.

From [ ]$^{a,b,c}$ the two-phase RPV level never dropped below the bottom of the HL and remained high until test termination at [ ]$^{a,b,c}$ as shown in Figure C.29. The HL liquid levels also remained high after the initial plant blowdown as shown in Figure C.30.

High HL and two-phase RPV levels provided an increased amount of water for liquid entrainment out of the ADS4 valves. In Figure C.31, the quality out of ADS4-1 was very low (< 0.04) compared to ADS4-2 quality ([ ]$^{a,b,c}$), illustrating a preference to entrain liquid through the non-PZR side HL. This same preference was also observed in Test NRC-AP1000-01. This preferential entrainment to one side of the plant was unique, but did not raise any safety concerns and this phenomenon is currently being investigated in conjunction with thermal-hydraulic code development and assessment activities.

The PZR began to drain at [ ]$^{a,b,c}$ and emptied by [ ]$^{a,b,c}$ as shown in Figure C.32. Adequate injection was provided by CMT2, ACC2, and the PZR during the initial blowdown to keep the heater rods covered. A 1-inch CL break along with a degraded sump did not challenge the passive safety systems enough to uncover the heater rods. The core remained adequately cooled during the entire test, as shown in Figure C.34.

Table C.8 Sequence of Events for Test NRC-AP1000-04

| Time (s) | Event |
|---|---|

a,b,c

a,b,c

Figure C.26 Vessel Wide Range Collapsed Water Level

a,b,c

Figure C.27 Core Upper Half and lower Half Collapsed Water Levels

a,b,c

Figure C.28 Accumulator, CMT, and IRWST Flows to DVI2

a,b,c

Figure C.29 Upper Plenum Two-Phase Level

a,b,c

Figure C.30 Hot Leg Collapsed Water Levels

a,b,c

Figure C.31 ADS4 Flow Qualities

a,b,c

Figure C.32 Pressurizer Wide Range Collapsed Water Level

a,b,c

Figure C.33 Core Heater Rod Temperatures

## C.5 NRC-AP1000-05

This simulated a double-ended guillotine break of a DEDVI with two of the four ADS4 valves failed closed (ADS4-1 closed and ADS4-2 opened). Both ADS4 valves on the non-PZR side were failed closed. Table C.9 summarizes the facility configuration. This test compliments Test NRC-AP1000-03, in which the only difference was in the location of the valve failure. In NRC-AP1000-03, both failed valves were on the PZR side.

Table C.9 Facility Configuration for Test NRC-AP1000-05

| Component | Configuration |
|---|---|
| ADS1 | Normal actuation |
| ADS2 | Normal actuation |
| ADS3 | Normal actuation |
| ADS4-1 (non-PZR side) | Failed shut |
| ADS4-2 (PZR side) | 100% ADS4-2 flow |
| Break | DEDVI Line 1 |

Table C.10 summarizes the sequence of events for this test. When the break opened at zero seconds, CMT1, CMT2, and ACC2 immediately began to discharge out the break. By [ ]$^{a,b,c}$, CMT1, ACC1, and ACC2 were completely empty. Figures C.36 and C.37 depict the flow from the ACCs, CMTs, and IRWST. The vessel inventory was low from approximately [ ]$^{a,b,c}$.

The vessel inventory increased slightly, as shown in Figure C.38, as CMT2 injection was prolonged, but after CMT2 emptied at [ ]$^{a,b,c}$, no injection water was provided to the core. The RPV water level in the core began to drop at approximately [ ]$^{a,b,c}$ into the test.

With no flow from the IRWST, HL1 emptied at [ ]$^{a,b,c}$ while water continued to be entrained out the ADS4-2 line, as shown in Figure C.40. A significant water level in HL2 was maintained until [ ]$^{a,b,c}$. The flow quality in ADS4-2 throughout most of the test remained fairly low (~0.5), even when the RPV two-phase level dropped below the bottom of the HLs. The minimum level that the two-phase probe can measure is approximately 2 inches above the upper core plate. Thus, the LT-120 measurement could not decrease after it "bottomed" at [ ]$^{a,b,c}$.

By [ ]$^{a,b,c}$ the PZR had still not drained due to CCFL, as shown in Figure C.41, and the heater rods began to uncover. At [ ]$^{a,b,c}$ a heater rod temperature excursion was observed, as shown in Figure 4.9, and the heater rod power was shut off at [ ]$^{a,b,c}$. Immediately after the heater rods were turned off, IRWST injection flow began.

The results of this test illustrate the sensitivity of ADS4 valve failure on core coolability. In this test, IRWST injection never began through DVI Line 2 as water was lost out ADS4-2 as a result of upper head and HL liquid entrainment.

Table C.10 Sequence of Events for Test NRC-AP1000-05

a,b,c

| Time (s) | Event |
|---|---|

a,b,c

Figure C.34 Vessel Wide Range Collapsed Water Level

a,b,c

Figure C.35 Core Upper Half and Lower Half Collapsed Water Levels

a,b,c

Figure C.36 Accumulator, CMT, and IRWST Flows to DVI1

a,b,c

Figure C.37 Accumulator, CMT, and IRWST Flows to DVI2

a,b,c

Figure C.38 Upper Plenum Two-Phase Level

a,b,c

Figure C.39 Hot Leg Collapsed Water Levels

a,b,c

Figure C.40 ADS4-2 (Pressurizer Side) Flow Quality

a,b,c

Figure C.41 Pressurizer Wide Range Collapsed Water Level

a,b,c

Figure C.42 Core Heater Rod Temperatures

## C.6 NRC-AP1000-06

The purpose of this test was to investigate a significant failure of the ADS4 system for a small CL break. It is similar in intent to Test NRC-10, which was conducted for AP600 design certification. In NRC-10, a 1-inch CL break was simulated with three of the four ADS4 valves failed closed. The AP600 test indicated that a failure of three of the four ADS4 valves to open resulted in a significant delay in the start of IRWST injection. The liquid level dropped below the top of the core, and a temperature excursion was observed. This result did not agree with those of the ROSA counterpart, Test AP- CL-07. The difference in the APEX and ROSA results was attributed to the reduced elevation head available for IRWST injection in APEX.

Test NRC-AP1000-06 simulated a 2-inch equivalent diameter break at the bottom of CL4. This was a beyond-DBA test, with two of the four ADS4 valves failed closed. Table C.11 summarizes the facility configuration. Both of the failed valves were on the ADS4-1 line, which connects to the HL without the PZR. The PRHR HX was inactive during this test.

Table C.11 Facility Configuration for Test NRC-AP1000-06

| Component | Configuration |
|---|---|
| ADS1 | Normal actuation |
| ADS2 | Normal actuation |
| ADS3 | Normal actuation |
| ADS4-1 (non-PZR side) | Failed shut |
| ADS4-2 (PZR side) | 100% ADS4-2 flow |
| Break | 2-inch bottom of CL |

Test NRC-AP1000-06 investigated a larger break size than NRC-10, but failed two of the four ADS4 valves. Similar to NRC-10, the water level dropped below the top of the core, and a temperature excursion occurred. Table C.12 summarizes the sequence of events for NRC-AP1000-06. Figure C.43 shows the vessel wide range collapsed water level, which remained above the top of the core until shortly after [ ]$^{a,b,c}$, which is when the ACCs emptied. As the ACC flows decreased, the collapsed water level in the top half of the core decreased rapidly, as shown in Figure C.44. Figures C.45 and C.46 depict the flow from the ACCs, CMTs, and IRWST.

The CMTs both emptied by [ ]$^{a,b,c}$. The system had not depressurized sufficiently to begin IRWST injection, so from this time until the test was terminated at [ ]$^{a,b,c}$, there was no injection flow to the vessel. The two-phase level, shown in Figure C.47, remained above the bottom of the HLs until approximately [ ]$^{a,b,c}$, as indicated by the two-phase level probe (LT-120). The two-phase level continued to decrease, and the upper plenum emptied at [ ]$^{a,b,c}$ (based on LDP-112). The minimum level that the two-phase probe can measure is approximately 2 inches above the upper core plate. Thus, the LT-120 measurement could not decrease after it "bottomed" at [ ]$^{a,b,c}$.

Figure C.48 depicts the HL levels. Of particular interest, is the difference in levels at approximately [ ]$^{a,b,c}$. The HL on the non-PZR side (HL1) emptied shortly before the two-phase level dropped below the bottom of the HLs. A level in the PZR side HL (HL2) remained even after the upper plenum emptied at [ ]$^{a,b,c}$. Figure C.49 depicts the PZR water level, which remained high following ADS4 opening at [ ]$^{a,b,c}$.

Flow quality to the ADS4-2 line, is low ($x < 0.1$) immediately following valve opening at [ ]$^{a,b,c}$ as shown in Figure C.49. The quality increased rapidly from approximately 0.1 to 0.4 shortly after accumulator injection stopped, and then increased again after the CMTs emptied. The quality increased from approximately 0.8 as the two-phase level dropped below the bottom of the HL, and remained less than 0.9 even after the upper plenum became empty at [ ]$^{a,b,c}$.

At [ ]$^{a,b,c}$, a core temperature excursion was observed, as shown in Figure C.51. The core power was manually scrammed. IRWST injection began immediately after to prevent heater rod damage.

Table C.12 Sequence of Events for Test NRC-AP1000-06

a,b,c

| Time (s) | Events |
|---|---|

a,b,c

Figure C.43 Vessel Wide Range Collapsed Water Level

a,b,c

Figure C.44 Core Upper Half and Lower Half Collapsed Water Levels

a,b,c

Figure C.45. Accumulator, CMT, and IRWST Flows to DVI1

a,b,c

FigureC.46 Accumulator, CMT, and IRWST Flows to DVI2

a,b,c

Figure C.47 Upper Plenum Two-Phase Level from Level Transmitter

a,b,c

Figure C.48 Hot Leg Collapsed Water Levels

a,b,c

Figure C.49 ADS4-2 Flow Quality

a,b,c

Figure C.50 Pressurizer Wide Range Collapsed Water Level

a,b,c

Figure C.51 Core Heater Rod Temperatures

## C.7 NRC-AP1000-10

The objective of this test was to obtain thermal-hydraulic data for PRA verification of a simulated AP1000 2-inch CL break off the bottom of CL4. The test was initiated from normal operating temperature and pressure. For this test, ADS1-3 and one of the four ADS4 valves failed to open on the non-PZR side of the plant. In addition, a [ ]$^{a,b,c}$ sharp edge orifice was installed in each SG PORV line. The SG PORVs were allowed to cycle between [ ]$^{a,b,c}$ (open) and [ ]$^{a,b,c}$ (closed) to help remove decay heat during the initial blowdown stage of the transient. The IRWST sump recirculation set point was changed from [ ]$^{a,b,c}$. The test was terminated after 30 minutes of steady-state long-term cooling. Table C.13 shows the facility configuration for this test.

Table C.13 Facility Configuration for Test NRC-AP1000-10

| Component | Configuration |
|---|---|
| ADS1 | Failed shut |
| ADS2 | Failed shut |
| ADS3 | Failed shut |
| ADS4-1 (non-PZR side) | 50% ADS4-1 flow |
| ADS4-2 (PZR side) | 100% ADS4-2 flow |
| Break | 2-inch bottom of CL 4 |

Table C.14 summarizes the sequence of events for this test. The break was initiated at zero seconds, and the CMTs immediately began to drain, as shown in Figures C.52 and C.53. The ACCs began to inject around [ ]$^{a,b,c}$ and, shortly afterward at [ ]$^{a,b,c}$, the ADS4 valves opened. This caused the plant to further depressurize and increased ACC injection flow rates considerably, as shown in Figures C.52 and C.53.

Between [ ]$^{a,b,c}$, there was a noticeable oscillation of IRWST injection flow rate (Figures C.52 and C.53), core liquid level (Figure C.54), and ADS4 line flow qualities (Figure C.59). The RPV pressure was very close to atmospheric by [ ]$^{a,b,c}$ (Figure C.58), and the HLs were almost completely flooded (Figure C.56). This oscillatory behavior is consistent with separate effects experiments run in ATLATS, which investigated the intermittent nature of liquid entrainment from the HLs into the vertical ADS4 lines.

The RPV liquid level reached a maximum around [ ]$^{a,b,c}$, and then began to slowly decrease as the IRWST injection flow rate decreased. Oscillations were experienced again from [ ]$^{a,b,c}$, because the core exit flow returned to saturated conditions as IRWST injection flow was considerably decreased. These RSOs are consistent with previous AP600 testing, and are described in Section 4.1.4 of this report. The plant entered long-term cooling at [ ]$^{a,b,c}$ when the sump recirculation lines were opened. Figure C.60 plots the RPV heater rod temperature and shows that the core remained adequately cooled during the entire test.

Table C.14 Sequence of Events for Test NRC-AP1000-10

| Time (s) | Events |
|---|---|
| | |

a,b,c

a,b,c

Figure C.52 Side 1 Injection Flow Rates (ACC1, CMT1, and IRWST Line 1)

a,b,c

Figure C. 53 Side 2 Injection Flow Rates (ACC2, CMT2, and IRWST Line 2)

a,b,c

Figure C.54 RPV Collapsed Liquid Level

a,b,c

Figure C.55 RPV Mixture Level

a,b,c

Figure C. 56 Hot Leg Collapsed Liquid Levels

a,b,c

Figure C.57 Core Collapsed Liquid Levels

a,b,c

Figure C.58 PZR Wide Range Collapsed Liquid Level

a,b,c

Figure C.59 ADS4 Flow Qualities

a,b,c

Figure C.60 RPV Heater Rod Temperatures

## C.8 NRC-AP1000-11

The objectives of this test were to (1) evaluate long-term PRHR HX operation including heatup of the IRWST to saturated temperature, (2) determine the effect of system behavior caused by ADS1-3 discharge to the saturated liquid inside the IRWST, and (3) determine the effects on long-term cooling caused by the injection of saturated liquid into the RPV from the IRWST.

The control logic was modified to simulate station blackout (loss of all AC power). The core was operated at reduced power (600 kW) and with a modified decay power curve to preserve integrated energy. The SG PORVs were set to cycle between [ ]$^{a,b,c}$. When the SG wide range level decreased to [ ]$^{a,b,c}$, an "S" signal was generated to open CMT injection valves and the PRHR HX outlet valve. The ADS was actuated [ ]$^{a,b,c}$ after initiation of the "S" signal. Table C.15 summarizes the facility configuration for this test.

Table C.15 Facility Configuration for Test NRC-AP1000-11

| Component | Configuration |
|---|---|
| ADS1 | Normal operation |
| ADS2 | Normal operation |
| ADS3 | Normal operation |
| ADS4-1 (non-PZR side) | 50% ADS4-1 flow |
| ADS4-2 (PZR side) | 100% ADS4-2 flow |
| Break | None |

Table C.16 summarizes he sequence of events for this test. The main feed pump was tripped at zero seconds, and the RCP coastdown command was given at 1 sec. For the next [ ]$^{a,b,c}$, the SG PORVs cycled open and closed. The plant slowly depressurized for about [ ]$^{a,b,c}$ as shown in Figure C.61. The CMTs began to inject at a low flow rate around [ ]$^{a,b,c}$ (Figures C.62 and 63).

At [ ]$^{a,b,c}$ ADS1-3 stages began to open, causing a rapid depressurization of the plant (Figure C.61). The ACCs began injecting about [ ]$^{a,b,c}$ later, and CMT injection flow increased significantly. Another jump in the ACC injection flow rate occurred at [ ]$^{a,b,c}$, after ADS4 valve actuation. IRWST injection began by [ ]$^{a,b,c}$, the CMTs and ACCs were emptied, illustrating about a 10-minute overlap in passive safety injection flow.

The RPV collapsed liquid level remained high until ADS actuation, when it dropped just below the top of the core, as shown in Figure C.64. However, the two-phase mixture level remained well above the bottom of the HL throughout the entire test (Figure C.65).

As the SG PORVs cycled open and closed between [ ]$^{a,b,c}$, removing decay heat from the core, the RPV collapsed liquid level decreased (Figure C.64), while the PZR level increased, as shown in Figure C.67, as steam boiled off in the core filled the PZR. At about [ ]$^{a,b,c}$, the PZR was completely filled (Figure C.67) and the primary system began to

pressurize (Figure C.61). At this time, the primary system went "solid" and the RPV liquid level remained constant (Figures C.64 and 65).

The last phase of the transient, sump recirculation cooling, began upon reaching a low level in the IRWST corresponding to the containment sump flood-up elevation. The PRHR HX and CMT operation were capable of removing core decay energy (Figure C.69) during the prolonged operation expected for a station blackout. The ADS1-4 blowdown was not affected by the saturated conditions inside the IRWST.

Table C.14 Sequence of Events for Test NRC-AP1000-11

| Time (s) | Events | a,b,c |
|---|---|---|

a,b,c

Figure C.61 RPV Head Pressure

a,b,c

Figure C.62 Side 1 Safety Injection Flow (ACC1, CMT1, and IRWST Line 1)

a,b,c

Figure C.63 Side 2 Safety Injection Flow (ACC2, CMT2, IRWST Line 2)

a,b,c

Figure C. 64 RPV Collapsed Liquid Level

a,b,c

Figure C.65 RPV Mixture Level

a,b,c

Figure C.66 Hot Leg Collapsed Liquid Levels

Figure C.67 PZR Wide Range Collapsed Liquid Level

a,b,c

Figure C.68 Core Collapsed Liquid Levels

a,b,c

Figure C.69 RPV Heater Rod Temperatures

NRC FORM 335 (9-2004) NRCMD 3.7

U.S. NUCLEAR REGULATORY COMMISSION

# BIBLIOGRAPHIC DATA SHEET

*(See instructions on the reverse)*

1. REPORT NUMBER (Assigned by NRC, Add Vol., Supp., Rev., and Addendum Numbers, if any.)

NUREG-1826

2. TITLE AND SUBTITLE

APEX-AP1000 Confirmatory Testing to Support AP1000 Design Certification (Non-Proprietary)

3. DATE REPORT PUBLISHED

| MONTH | YEAR |
|---|---|
| August | 2005 |

4. FIN OR GRANT NUMBER

5. AUTHOR(S)

K.B. Welter, S.M. Bajorek, J.N. Reyes*, B. Woods*, J. Groome*, J. Hopson*, E. Young*, J. DeNoma*, K. Abel*

6. TYPE OF REPORT

Technical

7. PERIOD COVERED *(Inclusive Dates)*

8. PERFORMING ORGANIZATION - NAME AND ADDRESS *(If NRC, provide Division, Office or Region, U.S. Nuclear Regulatory Commission, and mailing address; if contractor, provide name and mailing address.)*

Division of Systems Analysis and Regulatory Effectiveness
Office of Nuclear Regulatory Research
U.S. Nuclear Regulatory Commission
Washington, DC 20555-0001

*Department of Nuclear Engineering
Institute of Thermal-Hydraulics
Oregon State University
Corvallis, OR 97601

9. SPONSORING ORGANIZATION - NAME AND ADDRESS *(If NRC, type "Same as above"; if contractor, provide NRC Division, Office or Region, U.S. Nuclear Regulatory Commission, and mailing address.)*

Division of Systems Analysis and Regulatory Effectiveness
Office of Nuclear Regulatory Research
U.S. Nuclear Regulatory Commission
Washingon, DC 20555-0001

10. SUPPLEMENTARY NOTES

NRC Project Manager: Gene S. Rhee

11. ABSTRACT *(200 words or less)*

This report summarizes the confirmatory testing performed using the Advanced Plant Experiment (APEX) facility at Oregon State University (OSU). The APEX is a unique thermal-hydraulic integral system test facility, which is used to assess the performance of passive safety systems and was modified to accurately represent the design of the Westinghouse AP1000 advanced passive nuclear reactor. The U.S. Nuclear Regulatory Commission (NRC) sponsored eight beyond-design-basis accident (DBA) tests in the APEX facility, which were successfully completed from June 2003 through July 2004 and are discussed in detail in this report. Those eight beyond-DBA tests investigated scenarios with two or more simultaneous failures of the AP1000 passive safety systems during large- and small-break loss-of-coolant accidents, including station blackout and cold shutdown conditions. The experiments run in APEX-AP1000 confirm significant liquid entrainment and carryover of water to the automatic depressurization system (ADS) during and after actuation of the fourth-stage (ADS4) valves. These processes are important as thermal-hydraulic codes used to analyze the AP1000 design must adequately predict or bound upper plenum and hot leg entrainment. In addition, the tests show that failure of ADS4 valves on the non-pressurizer side of the plant results in a greater delay in in-containment refueling water storage tank (IRWST) injection than failure of ADS4 valves on the pressurizer side of the plant; while failure of two out of four ADS4 valves on the non-pressurizer side of the plant produces low two-phase mixture levels in the reactor vessel during certain simulated vessel injection line and cold leg breaks.

12. KEY WORDS/DESCRIPTORS *(List words or phrases that will assist researchers in locating the report.)*

AP1000
Advanced Plant Experiment (APEX)
thermal hydraulic computer code
design certification
hot leg entrainment
upper plenum entrainment

13. AVAILABILITY STATEMENT

unlimited

14. SECURITY CLASSIFICATION

*(This Page)* unclassified

*(This Report)* unclassified

15. NUMBER OF PAGES

16. PRICE

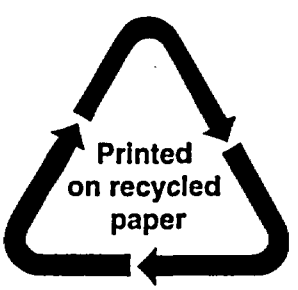


Federal Recycling Program

UNITED STATES
NUCLEAR REGULATORY COMMISSION
WASHINGTON, DC 20555-0001

OFFICIAL BUSINESS